

MATHEMATICAL EXAMINATION OF PULMONARY  
GAS TRANSPORT

A Thesis submitted to

THE UNIVERSITY OF ASTON IN BIRMINGHAM

for the award of the degree of

DOCTOR OF PHILOSOPHY

by

ROBERT JOHN LOUGHNANE, BSc (hons)

May, 1979

23 JAN 1980

244087

612-2162 LOW

# MATHEMATICAL EXAMINATION OF PULMONARY GAS TRANSPORT

Submitted by

ROBERT JOHN LOUGHNANE

for the award of the Degree of Doctor of Philosophy

MAY 1979

---

## SUMMARY

A quantitative mathematical examination of contemporary models of pulmonary gas transport and mixing is presented. This examination involved both a reappraisal of the *boundary conditions* assumed in these models and an exhaustive account of their respective stability and convergence criteria. As a result of this examination a revised single series compartmental mathematical model, derived from physiological data and incorporating revised boundary conditions, is developed to allow for a more faithful simulation of pulmonary gas transport phenomena.

The model is used to demonstrate that the expired "phase III slope" or "alveolar plateau slope" of a tracer gas may give an indication of end expiratory stratified concentration differences in the acinus. The model also allows for a comparison between *rigid* and *compliant* model predictions at low tidal ventilations.

By extending the model to include *parallel* as well as *series* elements it is possible to simulate the combined effects of regional and stratified inhomogeneities upon gas mixing efficiency in both normal and diseased lungs. The influence of regional inequalities in ventilation, regional inequalities in diffusion pathway length and regional inequalities in gas flux (i.e. gas exchange) are studied in various simulated normal and diseased states. In all instances it is shown that such regional inequalities accentuate both the end expiratory concentration gradients (stratified inhomogeneities) and the resulting phase III slope of a respired tracer gas.

Utilising an alternative and more detailed model of the bronchial airways, the predictions of the earlier series and series/parallel models are further verified.

KEY WORDS: PULMONARY GAS TRANSPORT MODELS  
BOUNDARY CONDITIONS  
MATHEMATICAL MODELS  
STRATIFIED INHOMOGENEITY  
REGIONAL INEQUALITIES

CONTENTS

|  |    |
|--|----|
| Summary  |    |
| Declaration  |    |
| Acknowledgements   |    |
| List of Figures  |    |
| 1. Introduction  | 1  |
| 2. Assessment of Contemporary Models   | 8  |
| 2.1 The Physical Models  | 8  |
| 2.2 The Mechanisms of Pulmonary Gas Transport  | 9  |
| 2.3 The Governing Equations  | 11 |
| 2.4 The Assumed Boundary Conditions  | 18 |
| 2.5 Alternative Boundary Conditions  | 23 |
| 2.6 The Numerical Solution Techniques  | 25 |
| 2.7 Discussion   | 44 |
| 3. A Revised Model   | 45 |
| 3.1 The Revised Boundary Conditions  | 45 |
| 3.2 The Total Flux Equation  | 50 |
| 3.3 Simulation of the Single-Breath Washout<br>Test for Gases of Different Diffusivity | 52 |
| 3.4 Simulation of the Single-Breath Washout<br>Test for gases of different solubility  | 54 |
| 3.5 Results for Different Volumetric Flow-Rates  | 57 |
| 3.6 Results for different Pre-inspiratory<br>Lung Volumes                              | 59 |
| 3.7 Breath-Holding Studies   | 60 |
| 3.8 Compliant Model Predictions  | 63 |

|      |  |     |
|------|--|-----|
| 4.   | REGIONAL DIFFERENCES   | 66  |
| 4.1  | A Regional Model   | 67  |
| 4.2  | The Governing Equations  | 70  |
| 4.3  | Boundary Conditions  | 71  |
| 4.4  | Results for Constant Diffusion<br>Pathway Lengths                                  | 74  |
| 4.5  | Results for Variable Diffusion<br>Pathway Lengths                                  | 76  |
| 4.6  | Simulation of "Average Case of Emphysema"  | 78  |
| 4.7  | Simulation of the Single-Breath Washout<br>Test for Gases of Different Diffusivity | 80  |
| 4.8  | Simulation of the Single-Breath Washout<br>Test for Gases of Different Solubility  | 82  |
| 4.9  | Breath-Holding Studies   | 84  |
| 4.10 | Cardiogenic Gas Mixing Effects   | 87  |
| 4.11 | Discussion   |     |
| 5.   | A BRANCHED "PIPE" MODEL  | 92  |
| 5.1  | Model Configuration  | 93  |
| 5.2  | The Governing Equations  | 94  |
| 5.3  | Boundary Conditions  | 95  |
| 5.4  | Comparison of the "Trumpet" and "Pipe"<br>Model Predictions                        | 100 |
| 5.5  | Comparison of the "Regional Trumpet" and<br>"Regional Pathway" Model Predictions   | 101 |
| 5.6  | Discussion   | 105 |

|     |   |     |
|-----|---|-----|
| 6.  | DISCUSSION  | 109 |
| 6.1 | Re-assessment of the Revised Boundary Conditions                    | 109 |
| 6.2 | Results for Non Trumpet/Thumbtack Shaped Models                     | 111 |
| 6.3 | Effects of Considering Negative 'G' Values                          | 113 |
| 6.4 | Bronchial Cross-Section from Lung Gas Washout - The Inverse Problem | 115 |
| 6.5 | Equivalent Asynchronous Emptying                                    | 125 |
| 6.6 | Nitrogen Retention Curves - The Stationary Interface                | 127 |
| 7.  | CONCLUSION  | 134 |
| 8.  | FUTURE WORK   | 138 |
|     | Appendix I  | 140 |
|     | Appendix II   | 143 |
|     | Appendix III  | 146 |
|     | Appendix IV   | 150 |
|     | Appendix V  | 152 |
|     | Appendix VI   | 156 |
|     | Appendix VII  | 160 |
|     | References  | 168 |
|     | Tables  |     |
|     | Figures   |     |

DECLARATION

No part of the work described in this thesis has been submitted in support of an application for another degree or qualification of this or any other University or other institute of learning.

No part of the work described in this thesis has been done in collaboration with any other person.

ACKNOWLEDGEMENTS

The author expresses his sincere thanks to Dr. D. A. Scrimshire for his guidance, supervision and most importantly, his ever increasing *critical* but *valued* assessment of the major contributions of the work.

A further expression of sincere gratitude is also due to Professor R. H. Thornley, Head of the Department of Production Technology and Production Management at Aston for the opportunity of carrying out the work.

Ms. Barbara Drinkwater is also thanked for typing the final manuscript and for not complaining about the lengthy and rather complex equations.

Lastly but by no means leastly, I am indebted to my mother for her encouragement, understanding and above all her continual *prayers* throughout the difficult moments of the work.

LIST OF FIGURES

1. Approximate branching pattern of the human bronchial airways based on Weibel's symmetrical 'Model A'.
2. Total Cross-Sectional Area/Distance relationship based on the "combined airways approximation", i.e. the 'Trumpet' or 'Thumbtack' shaped model.
3. The 'Trumpet' or 'Thumbtack' shaped model corresponding to the data of Hansen and Ampaya (1975)
4. Characteristic times for diffusion and convection in the human lung based on Weibel's symmetrical 'Model A'
5. (a) Elemental segment of the 'trumpet' model  
(b) Division of 'trumpet' model into annular sections for stochastic simulation
6. Normalised 'Flux Curves' obtained from the single series compartmental 'trumpet' model and for the *conventional* boundary conditions ( $D = 0.25 \text{ cm}^2/\text{sec}$  equivalent to  $O_2/N_2$ ).
7. Normalised 'Flux Curves' obtained from the single series compartmental 'trumpet' model and for the *revised* boundary conditions ( $D = 0.25 \text{ cm}^2/\text{sec}$  equivalent to  $O_2/N_2$ )
8. Concentration/Distance profiles obtained from the single series compartmental 'trumpet' model and for the revised boundary conditions ( $D = 0.25 \text{ cm}^2/\text{sec}$  equivalent to  $O_2/N_2$ )
9. A more detailed illustration of the end expiratory concentration/distance profile obtained from the single series compartmental 'trumpet' model and for the revised boundary conditions ( $D = 0.25 \text{ cm}^2/\text{sec}$  equivalent to  $O_2/N_2$ )

10. The Simulated Single-Breath Nitrogen Washout Curves obtained from the single series compartmental 'trumpet' model and for the revised boundary conditions.
11. The end inspiratory input gas concentration/distance profiles for SF<sub>6</sub>/N<sub>2</sub>, Ne/N<sub>2</sub> and He/N<sub>2</sub> obtained from the single series compartmental 'trumpet' model and for the revised boundary conditions.
12. The end expiratory input gas concentration/distance profiles for SF<sub>6</sub>/N<sub>2</sub>, Ne/N<sub>2</sub> and He/N<sub>2</sub> obtained from the single series compartmental 'trumpet' model and for the revised boundary conditions.
13. The simulation single-breath input gas washout curves for SF<sub>6</sub>, Ne and N<sub>2</sub> as obtained from the single series compartmental 'trumpet' model and for the revised boundary conditions.
14. Predicted end inspiratory input gas concentration/distance profiles for a hypothetical soluble tracer gas (D = 0.25 cm<sup>2</sup>/sec, G = +10.0, +25.0, +50.0 mls/sec) as obtained from the single series compartmental lung model and for the revised boundary conditions.
15. Predicted end expiratory input gas concentration/distance profiles for a hypothetical soluble tracer gas (D = 0.25 cm<sup>2</sup>/sec, G = +10.0, +25.0, +50.0 mls/sec) as obtained from the single series compartmental 'trumpet' model and for the revised boundary conditions.

16. Simulated single-breath N<sub>2</sub> washout curves corresponding to a hypothetical soluble tracer gas ( $D = 0.25 \text{ cm}^2/\text{sec}$ ,  $G = +10.0, +25.0, +50.0 \text{ mls/sec}$ ) as obtained from the single series compartmental 'trumpet' model and for the revised boundary conditions.
17. End inspiratory input gas concentration/distance curves for Argon and Nitrous Oxide as derived from the single series compartmental 'trumpet' model and when the revised boundary conditions are holding.
18. End expiratory input gas concentration/distance curves for Argon and Nitrous Oxide as derived from the single series compartmental 'trumpet' model and when the revised boundary conditions are holding
19. Simulated single-breath input gas washout tests for Argon and Nitrous Oxide as obtained from the single series compartmental 'trumpet' model and when the revised boundary conditions are holding.
20. Predicted concentration/distance profiles for a tri-angular wave flow form ( $D = 0.25 \text{ cm}^2/\text{sec}$ ) as derived from the single series compartmental 'trumpet' model and for the revised boundary conditions.
21. Simulated single-breath N<sub>2</sub> washout curve for a tri-angular wave flow form as predicted by the single series compartmental 'trumpet' model and for the revised boundary conditions.

22. Predicted concentration/distance profiles for a sinusoidal wave flow form as predicted by the single series compartmental 'trumpet' model and for the revised boundary conditions ( $D = 0.25 \text{ cm}^2/\text{sec}$ ).
23. Simulated single-breath  $\text{N}_2$  washout curve for a sinusoidal wave flow form as predicted by the single series compartmental 'trumpet' model and when the revised boundary conditions apply.
24. End inspiratory input gas concentration/distance profiles for various pre-inspiratory lung volumes ( $D = 0.25 \text{ cm}^2/\text{sec}$ ) as predicted by the single series compartmental 'trumpet' model and when the revised boundary conditions apply.
25. End expiratory input gas concentration/distance profiles for various pre-inspiratory lung volumes ( $D = 0.25 \text{ cm}^2/\text{sec}$ ) as predicted by the single series 'trumpet' model and when the revised boundary conditions apply.
26. Simulated single-breath  $\text{N}_2$  washout curves for various pre-inspiratory lung volumes as predicted by the single series 'trumpet' model and when the revised boundary conditions apply.
27. End inspiratory input gas concentration profiles ( $D = 0.25 \text{ cm}^2/\text{sec}$ , equivalent to  $\text{O}_2/\text{N}_2$ ) for various breath-holding times (1, 2 and 5 seconds) as predicted by the single series 'trumpet' model and when the revised boundary conditions apply.

28. End expiratory input gas concentration profiles ( $D = 0.25 \text{ cm}^2/\text{sec}$ , equivalent to  $O_2/N_2$ ) for various breath-holding times (1, 2 and 5 seconds) as predicted by the single series 'trumpet' model and when the revised boundary conditions apply.
29. Simulated single-breath  $N_2$  washout curves for various breath-holding times (1, 2 and 5 seconds) as predicted by the single series 'trumpet' model when the revised boundary conditions are holding.
30. Simulated single-breath  $N_2$  washout curves obtained from the *compliant* single series 'trumpet' model and when the revised boundary conditions apply.
31. Simulated single-breath  $N_2$  washout curve obtained from the *compliant* single series 'trumpet' model for a larger tidal ventilation (i.e.  $V_T = 1000 \text{ mls}$ ) and when the revised boundary conditions apply.
32. Schematic representation of the regional lung model (or the series/parallel model).
33. End expiratory concentration/distance profiles for constant diffusion pathway lengths ( $D = 0.25 \text{ cm}^2/\text{sec}$ ) as predicted by the regional 'trumpet' model and for the revised boundary conditions.
34. Simulated single-breath  $N_2$  washout curves for constant diffusion pathway lengths as predicted by the regional 'trumpet' model and for the revised boundary conditions.
35. End expiratory concentration/distance profiles for

variable diffusion pathway lengths ( $D = 0.25 \text{ cm}^2/\text{sec}$ ) as predicted by the regional 'trumpet' model and for the revised boundary conditions.

36. Simulated single-breath  $N_2$  washout curves for variable diffusion pathway lengths as predicted by the regional 'trumpet' model and for the revised boundary conditions.
37. End expiratory concentration/distance profiles for constant diffusion pathway lengths ( $D=0.25 \text{ cm}^2/\text{sec}$ ) and more *marked* regional flow differences as obtained from the regional 'trumpet' model when the revised boundary conditions apply.
38. Simulated single-breath  $N_2$  washout curves for constant diffusion pathway lengths and more *marked* regional flow differences as obtained from the regional 'trumpet' model when the revised boundary conditions apply.
39. End expiratory concentration/distance profiles for variable diffusion pathway lengths and more *marked* regional flow differences as derived from the regional 'trumpet' model when the revised boundary conditions apply.
40. Simulated single-breath  $N_2$  washout curves for variable diffusion pathway lengths and more *marked* regional flow differences as derived from the regional 'trumpet' model when the revised boundary conditions apply.

41. Predicted end expiratory input gas concentration/distance profiles for SF<sub>6</sub>/N<sub>2</sub>, Ne/N<sub>2</sub> and He/N<sub>2</sub> mixtures and for constant diffusion pathway lengths as obtained from the regional 'trumpet' model and when the revised boundary conditions apply.
42. Predicted end expiratory input gas concentration/distance profiles for SF<sub>6</sub>/N<sub>2</sub>, Ne/N<sub>2</sub> and He/N<sub>2</sub> mixtures and for variable diffusion pathway lengths as obtained from the regional 'trumpet' model when the revised boundary conditions are holding.
43. Simulated single-breath input gas washout curves for SF<sub>6</sub>, Ne and He and for constant diffusion pathway lengths as predicted by the regional 'trumpet' model and when the revised boundary conditions are applying.
44. Simulated single-breath input gas washout curves for SF<sub>6</sub>, Ne and He and for variable diffusion pathway lengths as predicted by the regional 'trumpet' model when the revised boundary conditions apply.
45. End expiratory input gas concentration/distance profiles for hypothetical soluble tracer gases (D = 0.25 cm<sup>2</sup>/sec and G = +10.0, +25.0, +50.0 mls/sec) and for various regional flow differences pertaining to the regional 'trumpet' model when the revised boundary conditions are applying.

46. The simulated single-breath  $N_2$  washout curves relative to hypothetical soluble tracer gases ( $D = 0.25 \text{ cm}^2/\text{sec}$ ,  $G = +10.0, +25.0, +50.0 \text{ mls/sec}$ ) and for various regional flow differences pertaining to the regional 'trumpet' model when the revised boundary conditions are applying.
47. Predicted end expiratory input gas concentration /distance profiles for Argon and Nitrous Oxide and for various regional flow differences as obtained from the regional 'trumpet' model when the revised boundary conditions apply.
48. Simulated single-breath input gas washout curves for Argon and Nitrous Oxide and for various regional flow differences as obtained from the regional 'trumpet' model when the revised boundary conditions apply.
49. End expiratory concentration/distance profiles for a hypothetical tracer gas ( $D = 0.25 \text{ cm}^2/\text{sec}$  equivalent to  $O_2/N_2$ ) for 1 second of breath-holding and for various regional flow differences as determined by the regional 'trumpet' model when the revised boundary conditions apply.
50. End expiratory concentration/distance profiles for a hypothetical tracer gas ( $D = 0.25 \text{ cm}^2/\text{sec}$  equivalent to  $O_2/N_2$ ) for 2 seconds of breath-holding and for various regional flow differences as predicted by the regional 'trumpet' model when the revised boundary conditions apply.

51. End expiratory concentration/distance profiles for a hypothetical tracer gas ( $D = 0.25 \text{ cm}^2/\text{sec}$  equivalent to  $\text{O}_2/\text{N}_2$ ) for 5 seconds of breath-holding and for various regional flow differences as predicted by the regional 'trumpet' model when the revised boundary conditions apply.
52. Simulated single-breath  $\text{N}_2$  washout curves corresponding to a hypothetical tracer gas ( $D = 0.25 \text{ cm}^2/\text{sec}$  equivalent to  $\text{O}_2/\text{N}_2$ ) for 1 second of breathholding and for various regional flow differences as predicted by the regional 'trumpet' model when the revised boundary conditions apply.
53. Simulated single-breath  $\text{N}_2$  washout curves corresponding to a hypothetical tracer gas ( $D = 0.25 \text{ cm}^2/\text{sec}$  equivalent to  $\text{O}_2/\text{N}_2$ ) for 2 seconds of breath-holding and for various regional flow differences as predicted by the regional 'trumpet' model when the revised boundary conditions apply.
54. Simulated single-breath  $\text{N}_2$  washout curves corresponding to a hypothetical tracer gas ( $D = 0.25 \text{ cm}^2/\text{sec}$  equivalent to  $\text{O}_2/\text{N}_2$ ) for 5 seconds of breath-holding and for various regional flow differences as predicted by the regional 'trumpet' model when the revised boundary conditions apply.

55. Predicted end expiratory concentration/distance profiles for regional differences in both molecular diffusion coefficient and volumetric flow-rate (simulating the effects of cardiogenic gas mixing) as derived from the regional 'trumpet' model when the revised boundary conditions apply.
56. Simulated single-breath N<sub>2</sub> washout curves for regional differences in both molecular diffusion coefficient and volumetric flow-rate (simulating the effects of cardiogenic gas mixing) as derived from the regional 'trumpet' model when the revised boundary conditions are applying.
57. Discontinuity in the 'trumpet' model shape.
58. Single 'pathway' or 'pipe' model from the mouth to the distal air sacs based on Weibel's 'Model A'
59. A branched 'pathway' or 'pipe' model of the human bronchial airways.
60. Concentration/distance profiles for both the single 'trumpet' and single 'pathway' models when the revised boundary conditions are employed (D = 0.25 cm<sup>2</sup>/sec).
61. Simulated single-breath N<sub>2</sub> washout curves corresponding to both the 'trumpet' and 'pathway' models and when the revised boundary conditions apply.

62. Predicted end expiratory concentration/distance profiles for various regional flow differences as determined by the branched pathway model and when the revised boundary conditions apply.
63. Simulated single-breath N<sub>2</sub> washout curves, for various regional flow differences, predicted by the branched pathway model and when the revised boundary conditions apply.
64. End expiratory input gas concentration/distance profiles for regional differences in both volumetric flow-rate and diffusion pathway length as predicted by the branched pathway model when the revised boundary conditions are applying  
( $D = 0.25 \text{ cm}^2/\text{sec}$ )
65. The simulated single-breath N<sub>2</sub> washout curves for regional differences in both volumetric flow-rate and diffusion pathway length as predicted by the branched pathway model when the revised boundary conditions are applying.
66. Predicted concentration/distance profiles when the effects of Taylor Dispersion are incorporated in the single pathway model and when the revised boundary conditions are applying.
67. Predicted concentration/distance profiles when the effects of Scherer Dispersion are incorporated in the single pathway model and when the revised boundary conditions are applying.

68. Solutions of the pulmonary gas transport equation in non 'trumpet' shaped models and for the conventional boundary conditions.
69. Solutions of the pulmonary gas transport equation in non 'trumpet' shaped models and for the revised boundary conditions.
70. Predicted end inspiratory and end expiratory concentration/distance profiles for a tracer gas having a molecular diffusion coefficient of  $D = 0.25 \text{ cm}^2/\text{sec}$  (equivalent to  $\text{O}_2/\text{N}_2$ ) and for six values of  $G$  (i.e.  $G = -10.0, -25.0, -50.0, +10.0, +25.0, +50.0$ ) relative to the single 'trumpet' model and when the revised boundary conditions are holding.
71. Simulated single-breath input gas washout curves for  $D = 0.25 \text{ cm}^2/\text{sec}$  and  $G = -10.0, -25.0, -50.0, +10.0, +25.0, +50.0 \text{ mls/sec}$  as obtained from the single 'trumpet' model when the revised boundary conditions apply.
72. Simulation of the single-breath  $\text{N}_2$  washout curve obtained by numerical solution of the pulmonary gas transport equation in the single 'trumpet' model and when neglecting mixing during expiration.

73. Total bronchial cross-sectional areas computed from the expired nitrogen washout curves of three normal subjects compared with anatomical data obtained from detailed post-mortem measurements on several human lungs.
74. Effects of axial dispersion (Taylor and Scherer) on the total bronchial cross-sectional areas computed from the expired nitrogen washout curves of three normal subjects.
75. Single-breath  $N_2$  -Retention curve pertaining to the 'perfectly mixed' model of the bronchial airways.
76. Comparison of the single-breath nitrogen retention curves predicted on the basis of the 'perfectly mixed' and the 'imperfectly mixed' 'trumpet' (with revised boundary conditions) models.
77. Simulated single-breath  $N_2$  -Retention curves for various regional flow differences obtained from the regional 'trumpet' model when the revised boundary conditions apply.

## CHAPTER 1

### INTRODUCTION

As a complete mathematical description of the respiratory system as a whole is probably an impossible task, some attempts have been made to analyse its more important characteristics. For example, the present study is concerned with the mathematical examination of pulmonary gas transport and mixing, with the particular aim of answering one question which has given rise to a large number of conflicting results - "is the concentration of an inert inspired tracer gas the same in the series spaces of the lung at the end of expiration?"

Further, since quantitative information concerning the equilibrium of gas molecules within the terminal airway units (or primary lobules) of the human lung is difficult, if not impossible, to obtain from experimental data alone, it has been necessary to simulate the relevant gas mixing processes in lung models replicating the pulmonary airway system in order to shed some light on this problem.

The importance of gaseous diffusion in the process of ventilation has been recognised since the early part of the century. As early as 1917, Krogh and Lindhard observed that, after a single inspiration of a gas, the concentration of the gas in the latter part of the subsequent expiration did not

reach a true plateau but continued to decrease generating the well-known phase III slope. Krogh and Lindhard contended that, while new air is entering the lung, there are always longitudinal concentration differences in the terminal airway units (stratified inhomogeneities) and that these differences are reflected at the mouth during the following expiration.

This view, that stratified inhomogeneity was responsible for the phase III slope was accepted generally until Rauwerda (1946) published the results of his model investigations into the rate of gaseous diffusion. This work was subsidiary to his main purpose, which was the determination of cardiac output, and his approach to the problem of diffusion was the application of analytical mathematical techniques to model situations analogous to those thought to occur within the lung.

He came to the conclusion that diffusion in the lungs was sufficiently rapid as to exclude a measurable concentration gradient within a terminal airways unit one second after the establishment of the gaseous interface. He defined a terminal airways unit as that structure fed by a terminal bronchiole, and hence having a length of 7 mm. As a result of his analysis he concluded that the current explanation of the phase III slope as representing stratified inhomogeneity was incorrect. It was not until some 20 years later that Cumming et al (1966)

criticised Rauwerda's analysis primarily on the assumptions on which he based his model. The major criticism being that the lung cannot be represented by any closed object (cylinder, sphere or cone) 7 mm. in length, because reflection and diffusion from both ends makes mixing very rapid. In fact, Cumming et al (1966) proposing instead several larger versions of Rauwerda's models and employing similar solution techniques demonstrated how stratification could be present at the end of a breath of normal duration.

Both of these previous model analyses have been criticised by La Force and Lewis (1970) on two grounds. First "if the terminal airways are to be treated as a solid figure, the appropriate one is not a cone but a golf tee or a thumbtack". The second criticism is that "the airways are not a solid figure but a succession of dichotomous branches". Thus, La Force and Lewis set out to treat a "dichotomously branched model" having the lengths and cross-sectional areas proposed by the morphometric analysis of Weibel (1963). In addition to this model they also considered a model which takes into account the additional cross-sectional area contributed by the alveoli.

From a geometric point of view the models considered by La Force and Lewis appeared to be more realistic. It is interesting to note, however, that their claim that the analysis was for a "dichotomously branched" model is of little

practical significance since the mathematics used by La Force and Lewis yielded the same results as that for a solid figure of the "thumbtack" shape. In fact, they concluded that the alveolar concentration stratification disappeared in much less than one second and therefore rejected the findings of Cumming et al (1966).

Although these analyses represented the initial steps in analysing gas transport in a geometry approaching that of the lungs, they were inadequate because the effects of convective gas flow were not included.

The inclusion of convective gas flow simultaneous with longitudinal diffusion has recently been considered by several groups of investigators (Cumming et al, 1971; Baker et al, 1974, 1975; Scherer et al, 1972; Pedley 1970; Paiva, 1972, 1973, 1978; Davidson and Fitzgerald, 1974; Davidson, 1975 and Pack et al, 1974, 1977). These models improved on the earlier models in another important way; washout of gas from the lung could be simulated. This was of fundamental importance since, given that any stratification which is obtained reflects in some way that which actually occurs in the lung, there is no way that this will evidence itself in the expired gas concentrations. During expiration following an inspiration of air, for example, gas comparatively rich in oxygen is convected out of the lung, and diffusion continues down existing longitudinal concentration gradients; these gradients will

therefore decrease. That is, Krogh and Lindhards explanation for the phase III slope requires that the longitudinal concentration differences remain significant in the gas during expiration by the time it reaches the mouth.

Although all the above groups of workers have allowed for the important concept of convectional transport they have differed considerably in its' interpretation within the framework of their models. For example, Cumming et al (1971) solved the classic static diffusion equation approximating convective gas flow by allowing successive quanta of flow to enter their model followed by a diffusion period, (100 mls entered after every 150 m/sec diffusion period). Scherer et al (1972), on the other hand, derived a partial differential equation for simultaneous convection and diffusion. More recently Davidson and Fitzgerald (1974) and Davidson (1975) developed a detailed model of a pathway through the branched system of the respiratory region, which when matched onto the one-dimensional "trumpet" model described by Pedley (1970) for the conducting airways, enabled the time course of gas concentrations from the mouth to the pulmonary membrane during a breath to be predicted. Besides allowing for the convective flow of gas and taking some account of the detailed anatomical features in the respiratory region, the pathway model also facilitated for the expansion of the respiratory region during breathing - an important physical process which will be dealt with in more detail in subsequent chapters.

The primary intent of these contemporary model simulations was to examine the existence of concentration stratification (serial gradients) and it's possible contribution to the phase III slope. All of the investigators found that significant concentration gradients exist within the acinus at the end of a normal inspiration but only Cumming et al (1971) observed a resulting 'phase III' slope during expiration.

This thesis serves to reconcile these apparently conflicting conclusions by mathematically examining the above contemporary model analyses. As a result of the detailed examinations, a revised pulmonary gas transport model has been developed capable of simulating results in close agreement with those obtained from normal subjects. Further, by extending this revised model to include parallel as well as series elements it has been possible to infer how certain specific types of pulmonary defects can affect the gas mixing behaviour in the acinar region. By modifying the above revised models appropriately, it has also be possible to estimate how the effects of molecular exchange across the alveolar-capillary membrane influence the approach to gaseous equilibrium. Finally, an improved mathematical description of molecular gas movements consisting of a detailed model pathway from the mouth to the terminal alveolar sacs is presented. The model pathway consists of a succession of uniform cylindrical pipes varying in dimensions according to the morphometric data of Weibel (1963). This improved model has then been used

to examine how micro (rather than macro) changes in both airway calibre and regional gas flow-rate influence gas equilibrium in the acinus. Results obtained from this new model have also proved useful in both testing the predictions and verifying the conclusions of the earlier revised models discussed above.

## CHAPTER 2

### ASSESSMENT OF CONTEMPORARY MODELS

#### 2.1 The Physical Models

The best known and widely used quantitative description of the pulmonary airway system is the so-called Weibel symmetrical 'model A' (Weibel, 1963). Weibel has approximated the complex branching pattern of the bronchial tree by 23 generations of successive dichotomously branching right cylindrical airway tubes (Figure 1). Generation 0 corresponds to the trachea and there are  $2^i$  ( $i = 0, 1 \dots 23$ ) equal elements in generation  $i$ . Generations 17 to 19 correspond to respiratory bronchioles, where walls (lumen) are partially alveolated, and generations 20 to 22 to alveolar ducts where the entire wall is occupied by alveoli. Alveolar sacs (generation 23) end the bronchial tree (see table 1).

The data from Weibel's 'model A' is invariably used to represent the bronchial tree by combining the dimensions of all airways of the same generation number, thereby producing the well known "trumpet" (Paiva, 1972) or "thumbtack" (La Force and Lewis, 1970) shaped function of total cross-sectional area and distance (Figure 2).

With the advent of more powerful morphological measuring techniques, a greater insight into the detailed shape of the "trumpet" model distal to generation 17 (respiratory bronchioles) has been attained (Horsfield et al, 1968, 1971 and Hansen and Ampaya, 1975) (Figure 3). These improved morphometric estimates have been employed more recently to examine the influence of changes in the structural dimensions of the models on the gas mixing behaviour in the acinus (Paiva, 1976 and Mons and Ultman, 1977).

## 2.2 The Mechanisms of Pulmonary Gas Transport

The inspired gas enters the lung through the trachea and passes through some 23 generations of branching to reach the terminal alveolar sacs. The bulk movement of the inspired gas is induced by a pressure gradient and is termed convection. Superimposed on this bulk flow at all times is molecular diffusion due to local concentration gradients. The actual transport of the inspired gas is accomplished by the coupling of these two mechanisms. If inspired gas is a mixture of only two components (as assumed in all contemporary models), then the transport of either component may be described by the binary convective-diffusion equation.

$$\frac{\partial F}{\partial t} + (V \cdot \nabla) F = D \nabla^2 F + R \quad (1)$$

in which  $F$  is the concentration (in, say, mol/litre) of

the component under consideration in the binary system,  $V$  is the velocity vector of the bulk flow,  $\nabla$  is the vector operator "del" (Hildebrand, 1962),  $D$  is the diffusion coefficient between the two components of the gas mixture and  $R$  is the sink or source term in the mass balance equation. Equation (1) is a general equation in the vector form and is valid for any co-ordinate system. The first term on the left hand side of this equation gives the transient change of  $F$  at the position under consideration, the second term represents the convection of this component due to local velocity  $V$  at the same position.

The first term on the right hand side describes the diffusion of the gas under consideration through an indigenous gas in the binary system as characterised by  $D$  whose value depends on the total pressure and the temperature of the mixture, the molecular weights of the two species involved and is almost independent of the composition of the mixture. The last term of the equation represents the rate of production or disappearance usually due to chemical reactions. If no reactions are involved in the mass transport process,  $R \equiv 0$ .

In a healthy subject breathing normally, i.e. 500 cm<sup>3</sup> tidal volume, the inspired air arrives by convection until the 19<sup>th</sup> or 20<sup>th</sup> bronchial generation of Weibel's 'model A'

and attains then, by diffusion the alveolocapillary membrane, where it passes into the blood. This is demonstrated more precisely in Figure 4 in which characteristic times for convection and diffusion have been calculated. The ascending curve ( $t_c$ ) represents the time for the inspired gases to pass through one generation by convection and the descending curve ( $t_d$ ) and equivalent time for the diffusion. The first curve rises very steeply because the lung ends in a "cul-de-sac", and the second varies with the square of the lengths of the different generations.

### 2.3 The Governing Equations

The equations governing the transport (simultaneous convection and diffusion) of gas molecules within the bronchial airways are obtained by applying Ficks Law and the principal of mass balance to an elemental segment of the "trumpet" model shown in figure 2 (see Figure 5).

#### Diffusional Transport

The transport of gas molecules due to diffusion at a distance 'y' from the portal end of the "trumpet" model may be written as:

$$T = - D S \frac{\partial F}{\partial y} \quad (2)$$

where,  $F \equiv F(y, t)$  is the fractional input gas concentration at distance 'y' from the beginning of the model and at time t after the start of the transport process,  $S \equiv S(y)$  is the total cross-sectional area of the airways at distance 'y' from the portal end and D is the binary molecular diffusion coefficient of the input gas/residual gas. From equation (2) and the conservation of mass, it follows that,

$$S \frac{\partial F}{\partial t} = - \frac{\partial T}{\partial y} \quad (3)$$

hence, from equations (2) and (3) we obtain

$$S \frac{\partial F}{\partial t} = - \frac{\partial}{\partial y} \left( D S \frac{\partial F}{\partial y} \right) \quad (4)$$

where t is the time.

In deriving equation (4) all previous investigators have explicitly assumed that the tortuosity resulting from branching does not affect the form of the overall conservation equation for the total gas in the  $n^{\text{th}}$  generation and that any concentration gradients perpendicular to the airway axes (i.e. radial concentration gradients) can be ignored. The latter assumption has been shown to be realistic as judged from a detailed survey of gas diffusion in an alveolar duct (Paiva, 1974).

### Convictional Transport

Equation (4) describes the change in the number of gas molecules in the elemental segment due to diffusion. This number also changes due to the convective airflow which is responsible for the change in lung volume.

$$T = F S v \quad (5)$$

where,  $v$  is the convective velocity of input gas molecules ( $Sv$  is the volumetric gas flow rate). Using equations (3) and (5) it follows that,

$$S \frac{\partial F}{\partial t} = - \frac{\partial}{\partial y} (F S v) \quad (6)$$

Now the general form of the governing gas transport equation (convection-diffusion equation) is obtained by combining the equations (4) and (6) such that,

$$S \frac{\partial F}{\partial t} = \frac{\partial}{\partial y} (D S \frac{\partial F}{\partial y}) - \frac{\partial}{\partial y} (F S v) \quad (7)$$

When discussing solutions of equation (7) it is important to distinguish between two distinctly different types of model, i.e. that of the 'rigid model' and the 'compliant model'.

### Rigid Models

Workers who have employed rigid type models, i.e. (Pedley, 1970; Paiva, 1972, 1973 and Baker et al, 1974, 1975) have further simplified equation (7) by assuming that,

$$S v \equiv \dot{Q} \quad (\text{constant}) \quad (8)$$

This last assumption has caused considerable controversy particularly as regards the correct boundary conditions to employ at the alveolar wall (Scrimshire et al, 1978).

### Compliant Models

On the otherhand, those workers who have developed compliant models such as Scherer et al(1972) and Pack et al (1974,1977) have adopted a different approach in that they have assumed that the incompressible convective flow into and out of the bronchial airways is caused by the expansion and contraction of the alveolar regions. In fact, they considered that the amount of convection  $v(y, t) S(y, t)$  was equal to the total volume change in the airways distal to some base point, i.e.

$$v(y, t) = \frac{1}{S(y, t)} \int_Y^L \frac{\partial S}{\partial t} dy \quad (9)$$

and where  $L$  is the total length of the model.

The expansion and contraction of these models is determined by the functional relation,

$$S(y, t) = S(y) \left[ 1.0 - f(y) b(t) \right] \quad (10)$$

which defines the total cross-sectional area at any point during the breathing cycle in terms of a "flexibility function"  $f(y)$ , and an oscillatory function of time,  $b(t)$ . Since there is a lack of experimental evidence on the precise distribution of lung volume changes (Hughes et al, 1972; Marshall and Holden, 1963) the functional form of  $f(y)$  must remain empirical and the authors assume it to be evenly distributed along the length of their models.

Perhaps the most perplexing problem encountered in developing a compliant lung model is in deciding exactly how the model should expand and contract. For example, should we a priori specify how the volume changes thereby imposing a flow of gas into and out of the bronchial airways such as in the models of Scherer et al (1972) and Pack et al (1977). Or should we impose the flow of gas and allow the model to expand and contract in a way that at least agrees qualitatively with observed behaviour in vivo as experimentally determined by such authors as Hughes et al (1972). Since in all instances a flow of gas must be imposed in order to solve the pulmonary gas transport equation,

it would appear that the latter approach is the more realistic. The mathematical details of such an alternative approach will now be presented and compared with the corresponding contemporary model developments.

Hughes et al (1972) have inferred from their somewhat extensive experimental findings that lung volume varies approximately in proportion to the cube of bronchial distance, i.e.

$$V \propto l^3 \quad (11)$$

$$\therefore V = k l^3 \quad (12)$$

Where  $V$  is the lung volume and  $l$  is the bronchial distance. Let us now define the following,

$$V_1 = \text{Initial lung volume or functional residual capacity} \quad (13)$$

$$V_2 = V_1 + \Delta V_T \quad (14)$$

where,  $\Delta V_T$  is the amount of the tidal volume ( $V_T$ ) that enters the lung model over an infinitesimal time interval  $\Delta t$ .

Then we may write,

$$V_1 = k l_1^3 \quad (15)$$

$$V_2 = k l_2^3 \quad (16)$$

and hence,

$$l_2 = l_1 \left( \frac{V_2}{V_1} \right)^{\frac{1}{3}} \quad (17)$$

If we now let  $a = \left( \frac{V_2}{V_1} \right)^{\frac{1}{3}}$ , then

$$l_2 = a l_1 \quad (18)$$

$$S_2 = a^2 S_1 \quad (19)$$

Thus, as  $\Delta t \rightarrow 0$  equations (18) and (19) imply that,

$$l(t + \Delta t) = [a(t)] l(t) \quad (20)$$

and,

$$S(t + \Delta t) = [a(t)]^2 S(t) \quad (21)$$

Inherent in the derivation of equations (20) and (21) is the fact that the trumpet model simultaneously increases/decreases it's length whilst the volume expands/contracts respectively.

However, previous compliant lung models (Scherer et al, 1972 and Pack et al, 1974, 1977) have only allowed their models to expand and contract but have kept their lengths fixed. It will be shown later (Chapter 3) that these inconsistencies in the physical models can contribute to an artificially rapid approach towards gaseous equilibrium within the acinus.

## 2.4 The Assumed Boundary Conditions

At this stage the general form of the boundary conditions assumed by all previous contemporary workers, employing either a 'rigid' or a 'compliant' "trumpet" shaped model, shall merely be stated and subsequently be assessed in the light of a recent reappraisal (Scrimshire et al, 1978).

### DURING INSPIRATION

$$F(o, t) = 1.0 \quad \text{for} \quad t_1 \leq t \leq \frac{T}{2} \quad (22)$$

and

$$\left. \frac{\partial F}{\partial y} \right|_{y=L} = 0.0 \quad \text{for} \quad t_1 \leq t \leq \frac{T}{2} \quad (23)$$

### DURING EXPIRATION

$$\left. \frac{\partial F}{\partial y} \right|_{y=0} = 0.0 \quad \text{for} \quad \frac{T}{2} < t \leq T \quad (24)$$

and

$$\left. \frac{\partial F}{\partial y} \right|_{y=L} = 0.0 \quad \text{for} \quad \frac{T}{2} < t \leq T \quad (25)$$

Before assessing these boundary conditions it is advantageous to consider the functional form of the total flux equations,  $G(y, t)$  defined as the combination of both convective and diffusive flux contributions, i.e.

$$G(y, t) = S v F - D S \frac{\partial F}{\partial y} \quad (26)$$

### Rigid Models

For rigid models we know that from equations (8) and (26) that,

$$G_R(y, t) = \dot{Q} F - D S \frac{\partial F}{\partial y} \quad (27)$$

Thus,

$$G_R(0, t) = \dot{Q} F \Big|_{y=0} - D S(0) \frac{\partial F}{\partial y} \Big|_{y=0} \quad (28)$$

Since we are assuming that a uniform convective flux (that is uniform flow) of gas enters the model, we do not expect any concentration differences to exist near the model entrance.

In other words, we require that

$$G_R(0, t) = + \dot{Q} F \Big|_{y=0} \quad (29)$$

which implies from equation (28) that

$$\frac{\partial F}{\partial y} \Big|_{y=0} = 0.0 \quad (30)$$

It is thus intuitively obvious that the input gas concentrations at the model entrance must remain constant as defined in equation (22).

Whilst the boundary conditions conventionally assumed for the entry portal of all previously proposed models are easily understood, and represent a reasonable approximation to reality, those specified at the distal end of rigid models are less obvious. The intention is to define a situation which ensures a zero flux of input gas across the alveolar wall,  $y = L$ , thus mimicing the behaviour of an insoluble tracer.

From equation (27) we have that,

$$G_R (L, t) = \pm \dot{Q} F \Big|_{y=L} - D S (L) \frac{\partial F}{\partial y} \Big|_{y=L} \quad (31)$$

and on substituting from equations (23) and (25) into equation (31) we find,

$$G_R (L, t) = + \dot{Q} F \Big|_{y=L}, \text{ for } t_1 \leq t \leq \frac{T}{2} \quad (32)$$

and,

$$G_R (L, t) = - \dot{Q} F \Big|_{y=L}, \text{ for } \frac{T}{2} < t \leq T \quad (33)$$

From a scrutiny of equation (32) it is clear that a finite flux of input gas is being continuously drawn out of the model across the alveolar wall during inspiration, and from equation (33) it can be seen that gas is being similarly drawn into the model during expiration. This is not really surprising since the conservation of mass dictates that, during inspiration in a rigid model, an outflow must occur across the alveolar wall and during expiration a reverse inflow must occur. Such an artifact in rigid models violates the physiological condition of "no flux" at the alveolar wall. Now, during expiration the contribution from diffusive mixing near the model entrance is negligible in comparison to the convective mixing (Paiva, 1972). As a result a relatively uniform convective flux of gas out of the model is anticipated, which may be stated mathematically as,

$$G_R (o, t) = - \dot{Q} F \Big|_{y=0} \quad (34)$$

During expiration, we have from equation (27) that

$$G_R (o, t) = - \dot{Q} F \Big|_{y=0} - D S (o) \frac{\partial F}{\partial y} \Big|_{y=0} \quad (35)$$

Substituting from equation (34) into equation (35) gives

$$\frac{\partial F}{\partial y} \Big|_{y=0} = 0 \quad (36)$$

which also implies that the concentration gradient has smoothed out by the time the mouth is reached (Pedley, 1970). In fact, equations (33) and (34) state that eventually gas is leaving the model at the same rate at which it is being withdrawn through the alveolar wall; hence concentration gradients would not be expected to persist under such conditions. In other words, the artifact caused by the violation of the "no-flux" condition at the alveolar wall would appear to be primarily responsible for the unrealistically rapid approach to gaseous equilibrium.

### Compliant Models

For the compliant models of Scherer et al (1972) and Pack et al (1974, 1977) we have from equations (9) and (26) that

$$G_c(y, t) = \pm \left[ \int_y^L \frac{\partial S}{\partial t} dy \right] F - D S \frac{\partial F}{\partial y} \quad (37)$$

Putting  $y = L$  in equation (37) yields

$$G_c(L, t) = - D S (L) \frac{\partial F}{\partial y} \Big|_{y=L}, \quad t_1 \leq t \leq T \quad (38)$$

In order to ensure that the total flux is zero at the alveolar wall, it is further necessary to specify the boundary condition

$$\left. \frac{\partial F}{\partial y} \right|_{y=0} = 0.0, \text{ as in rigid models.}$$

Since some 95 per cent of lung volume is contained within the terminal generations of the bronchial tree (a linear distance of only 0.6 cms) it is hardly surprising that these compliant models again fail to display any stratified inhomogeneities in the acinar region because of this explicit assumption. On reflection, it is clearly inappropriate to specify the boundary conditions in terms of a fixed concentration gradient at the alveolar wall, since it is the change in concentration gradient immediately adjacent to this point that is the main purpose of the simulations.

## 2.5 Alternative Boundary Conditions

From the above discussions it is evident that a better approximation to the actual conditions within the lungs could be made by ensuring a zero flux of gas at the alveolar wall whilst simultaneously allowing the concentration gradient to be a variable. Applying the former condition, i.e.  $G(L,t) \equiv 0$  to equation (31) yields,

$$0 = + \dot{Q} F \Big|_{y=L} - D S (L) \left. \frac{\partial F}{\partial y} \right|_{y=L} \quad \text{for } t_1 \leq t \leq \frac{T}{2} \quad (39)$$

$$0 = - \dot{Q} F \Big|_{y=L} - D S (L) \frac{\partial F}{\partial y} \Big|_{y=L} \quad \text{for } \frac{T}{2} < t \leq T \quad (40)$$

Rearranging, we obtain

$$\frac{\partial F}{\partial y} \Big|_{y=L} = + \frac{\dot{Q}}{D S (L)} F \Big|_{y=L}, \quad \text{for } t_1 \leq t \leq \frac{T}{2} \quad (41)$$

and,

$$\frac{\partial F}{\partial y} \Big|_{y=L} = - \frac{\dot{Q}}{D S (L)} F \Big|_{y=L}, \quad \text{for } \frac{T}{2} < t \leq T \quad (42)$$

Equations (41) and (42) now represent a true "no-flux" condition.

By adopting boundary conditions identical to those given in equations (41) and (42), it can be shown how significant concentration gradients (stratified inhomogeneities) can exist at end expiration, (a 0.7% difference in input gas concentration between the ends of a single compartmental model). Further, by suitably modifying this analysis it is possible to simulate the corresponding single breath nitrogen washout curve having a 'phase III' slope of 3.42% in agreement with the experimental findings obtained from normal subjects (Mills and Harris, 1965 and Jones, 1967).

The application of the above revised boundary conditions to situations analogous to those thought to occur within the lung will be discussed in more detail in chapters 3 and 4.

## 2.6 The Numerical Solution Techniques

The numerical solution techniques employed by the contemporary workers fall into two main categories, i.e. those workers who have adopted finite difference techniques (Scherer et al (1972); Baker et al (1974, 1975); Pack et al (1974, 1977) and Scrimshire et al (1978)) and those other workers who have resorted to Monte Carlo methods or stochastic simulation (Paiva, 1972, 1973 and Jones and Scrimshire, 1976). In order to determine which of these methods is the most efficient to use when solving the pulmonary gas transport equation, it is necessary to compare their respective stability and convergence criteria.

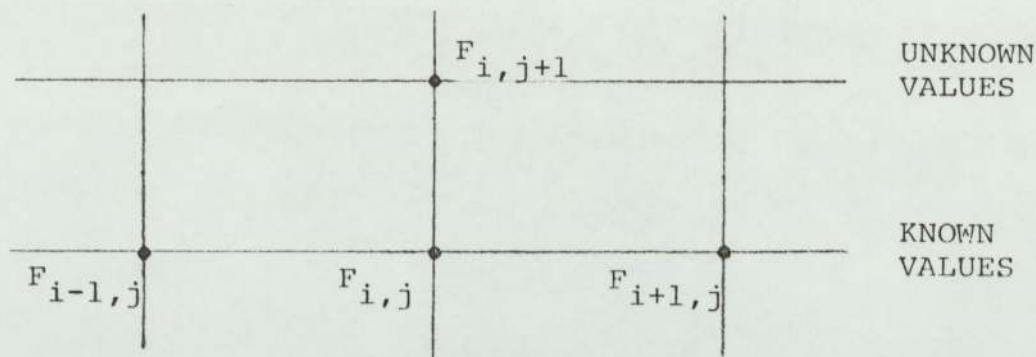
### Finite Difference Schemes

Essentially, two types of finite difference approximation are available, i.e. those of the 'explicit' (direct) and the 'implicit' (indirect) types. The pertinent characteristics of these schemes will now be highlighted and subsequently it will be demonstrated how the explicit scheme is more efficient than its implicit counterpart in the numerical solution of the pulmonary gas transport equation. Further,

a general stability criterion for a 'four point' explicit finite difference approximation to parabolic type systems is derived which will not only be of use in the present situation but also in many other scientific and engineering situations analogous to that of the present case.

### Explicit Methods

The power of the explicit method over that of its implicit counterpart is due mainly to the fact that in the former case the approximate value at any nodal point  $i$  on the  $(j + 1)^{\text{th}}$  time level may be expressed directly in terms of known values on the  $j^{\text{th}}$  time level (see diagram below).



Central (rather than forward or backward) difference approximation of derivatives have been employed due mainly to their higher order of convergence. In fact, both forward and backward differences are accurate to  $O(\Delta y)$  whereas central differences are accurate to  $O(\Delta y^2)$  as has been demonstrated in all standard texts on numerical methods (see for example Smith, 1965). Thus, the most efficient

explicit finite difference approximation of derivatives may be summarised as follows:-

$$\frac{\partial F}{\partial t} = \frac{(F_{i,j+1} - F_{i,j})}{(\Delta t)} \quad (43)$$

$$\frac{\partial F}{\partial y} = \frac{(F_{i+1,j} - F_{i-1,j})}{2 (\Delta y)} \quad (44)$$

$$\frac{\partial^2 F}{\partial y^2} = \frac{(F_{i+1,j} - 2F_{i,j} + F_{i-1,j})}{(\Delta y)^2} \quad (45)$$

On substituting these finite difference approximations into equation (7) we obtain the following,

$$F_{i,j+1} = F_{i,j} + Dr (F_{i+1,j} - 2F_{i,j} + F_{i-1,j}) + K_i r (F_{i+1,j} - F_{i-1,j}) \quad (46)$$

where,

$$K_i = \frac{1}{2} (\Delta y) \left[ \frac{D \partial S_i}{S_i \partial y} - \frac{\dot{Q}}{S_i} \right] \quad (47)$$

and,

$$r = \frac{\Delta t}{(\Delta y)^2}$$

Equation (46) may be further simplified yielding

$$F_{i,j+1} = (D - K_i)r F_{i-1,j} + (1 - 2Dr) F_{i,j} + (D + K_i)r F_{i+1,j} \quad (49)$$

for  $2 \leq i \leq N - 1$  and for  $j = 1, 2, \dots$

In order to ensure that the solutions of the difference equations given in equation (49) converge to the true solution of the pulmonary gas transport equation (7), it has been necessary to derive an appropriate stability criterion. There are basically two main methods of treating stability, i.e. the matrix method and the method of Fourier Series. We will now illustrate these two methods as applied to the system of relations given in equation (49)

#### Stability by the Fourier Series method

This method, developed by von Neumann during World War II, was first discussed in detail by O'Brien et al (1951). It expresses an initial line of errors in terms of a finite Fourier series, and considers the growth of a function that reduces to this series for  $t = 0$  by a 'variables separable' method identical with that commonly used for deriving analytical solutions of partial differential equations. The

Fourier series can be formulated in terms of sines or cosines but the algebra is easier if the complex exponential form is used, i.e. with  $\sum a_n \cos \frac{n\pi y}{l}$  or

$\sum b_n \sin \frac{n\pi y}{l}$  replaced by the equivalent,

$\sum A_n e^{\frac{in\pi y}{l}}$ , where  $i = \sqrt{(-1)}$  and  $l$  is the

interval throughout which the function is defined.

The idea behind this method is to express the errors at the nodal points along  $t = 0$  between  $y = 0$  and  $Nh$ , by  $E(p) = E_p$ ,  $p = 0, 1, \dots, N$ . Then the  $(N + 1)$  equations

$$E_p = \sum_{n=0}^N A_n e^{i\beta n p h}, \quad (p = 0, 1, \dots, N)$$

are sufficient to determine the  $(N + 1)$  unknowns  $A_0, A_1, \dots, A_N$  uniquely, showing that an arbitrary distribution of initial errors can be expressed in terms of this complex exponential form. As our finite difference equations will always be linear, and therefore separate solutions additive, we need only consider the propagation of the error due to a single term, such as  $e^{i\beta p h}$ . The coefficient  $A_n$  is a constant and can be neglected.

To investigate the propagation of this error as  $t$  increases it is necessary to find a solution to the finite-difference equation which reduces to  $e^{i\beta ph}$  when  $t = qk = 0$ . Assume

$$E_{p,q} = e^{i\beta y} e^{\alpha t} = e^{i\beta ph} e^{\alpha qk} = e^{i\beta ph} \zeta^q$$

where  $\zeta = e^{\alpha k}$ , and  $\alpha$ , in general, is a complex constant. This obviously reduces to  $e^{i\beta ph}$  when  $q = 0$ . The error will not increase as  $t$  increases provided

$$|\zeta| \leq 1$$

Letting  $F_{p,q} = e^{i\beta ph} \zeta^q$  in equation (49) yields

$$\begin{aligned} e^{i\beta ph} \zeta^q + 1 &= (D - K_i) r e^{i\beta(p-1)h} \zeta^q + (1 - 2Dr) e^{i\beta ph} \zeta^q \\ &\quad + (D - K_i) r e^{i\beta(p+1)h} \zeta^q \end{aligned} \quad (50)$$

for  $2 \leq i \leq N - 1$  and for  $j = 1, 2, \dots$

Simplifying equation (50) we have that

$$\zeta = (D - K_i) r e^{-i\beta h} + (1 - 2Dr) + (D + K_i) r e^{i\beta h}$$

i.e.

$$(\xi - 1) = -4Dr \sin^2\left(\frac{\beta h}{2}\right) + 4K_i r \sin\left(\frac{\beta h}{2}\right)\cos\left(\frac{\beta h}{2}\right) \quad (51)$$

For stability we require that  $|\xi| \leq 1$ , i.e.

$$r \leq \frac{D}{2 D^2 \sin^2\left(\frac{\beta h}{2}\right) + K_i^2 \cos^2\left(\frac{\beta h}{2}\right)} \quad (52)$$

Two cases now arise

Case 1:  $D > K_i$  and  $\cos^2\left(\frac{\beta h}{2}\right) = 0$  and then

from equation (52) we know that,

$$r \leq \frac{1}{2D} \quad (53)$$

Case 2:  $D < K_i$  and  $\sin^2\left(\frac{\beta h}{2}\right) = 0$  and then we have that,

$$r \leq \frac{D}{2K_i^2} \quad (54)$$

Whilst the Fourier Series method is very powerful it is also rather laborious particularly as regards the present problem. Fortunately, there is an alternative and more rigorous technique which involves matrix algebra.

Matrix Method of Stability

This method expresses the finite-difference equations given in equation (49) in matrix form and examines the eigenvalues of an associated matrix. Before continuing it is necessary to state the following useful theorems on the bounds for eigenvalues, the proofs of which are given in appendix I.

Gerschgorin's Theorem

The modulus of the largest eigenvalue of the square matrix A cannot exceed the largest sum of the moduli of the terms along any row or column.

Brauers Theorem

Let  $P_s$  be the sum of the moduli of the terms along the  $s^{th}$  row excluding the diagonal element  $a_{ss}$ . Then every eigenvalue of A lies inside or on the boundary of at least one of the circles  $|\lambda - a_{ss}| = P_s$ .

The finite-difference equations given in equation (49) together with the initial and conventional boundary conditions given previously, may be written in matrix form as,

$$\begin{bmatrix} F_{1,j+1} \\ F_{2,j+1} \\ \vdots \\ F_{N,j+1} \end{bmatrix} = \begin{bmatrix} 1 & & & \\ (D - K_2)r & (1 - 2Dr) & (D + K_2)r & \\ & & & \\ & & & 2Dr (1 - 2Dr) \end{bmatrix} \begin{bmatrix} F_{1,j} \\ F_{2,j} \\ \vdots \\ F_{N,j} \end{bmatrix}$$



### Stability of General Explicit Methods

Consider the problem of solving the more general linear parabolic partial differential equation with variable coefficients, i.e.

$$\frac{\partial F}{\partial t} = a \frac{\partial^2 F}{\partial y^2} + b \frac{\partial F}{\partial y} + c F + d \quad (55)$$

where  $a$ ,  $b$ ,  $c$  and  $d$  are functions of  $t$  and  $y$  only, and with the more general boundary condition

$$p \frac{\partial F}{\partial y} + q F = v \quad (56)$$

where  $p$ ,  $q$  and  $v$  are functions of  $t$  only.

Now, there is an important class of simulations to linear parabolic equations with variable coefficients for which rigorous sufficient conditions for stepwise stability are easily obtained (see Hildebrand, 1968). In illustration, let us suppose that a 'four-point' formulae has been obtained, for equations (55) and (56) above, in the form,

$$F_{i,j+1} = C_{-1}(i,j)F_{i-1,j} + C_0(i,j)F_{i,j} \\ + C_1(i,j)F_{i+1,j} + d_{i,j} \quad (57)$$

as a consistent simulation, where the coefficients  $C_n(i,j)$  are known functions of  $i$  and  $j$ . We suppose that equation (57)

holds for  $i = 1, 2, \dots, N$  and  $j = 1, 2, \dots$ . The propagated error  $\epsilon_{i,j}$  due to an initial error distribution  $g_i$  is then specified by the relations,

$$\epsilon_{i,j+1} = \sum_{n=-1}^1 C_n(i,j) \epsilon_{i+n,j} \quad (58)$$

and,

$$\epsilon_{i,1} = g_i \quad (59)$$

If the coefficients  $C_{-1}$ ,  $C_0$  and  $C_1$  are non-negative for all relevant values of  $i$  and  $j$ , i.e.

$$C_n(i,j) \geq 0 \quad (n = -1, 0, 1) \quad (60)$$

and if their sum does not exceed unity,

$$\sum_{n=-1}^1 C_n(i,j) \leq 1 \quad (61)$$

then we may deduce from equation (58) the relation

$$\epsilon_{i,j+1} < \sum_{n=-1}^1 C_n(i,j) \left| \epsilon_{i+n,j} \right| < \max_n \left| \epsilon_{i+n,j} \right|$$

$$\text{for } i = 1, 2, \dots, N \text{ and } j = 1, 2, \dots \quad (62)$$

It thus follows that when the conditions (60) and (61) are satisfied for all relevant values of  $i$  and  $j$ , the errors propagated by a single line of initial errors can never exceed

the largest initial error in magnitude, so that the formulation is stable in the stepwise sense. While the conditions (60), (61) and (62) are sufficient for stepwise stability, they may not be necessary, in the sense that the formulation may be stable even though one or more of these conditions is violated.

The power of the above general stability criterion can only be realised when it is applied to an actual physical problem. As it happens, the pulmonary gas transport equation forms an ideal "model example" on which to demonstrate it's wide range of application.

On equating coefficients of equation (49) with those of equation (57) we have that

$$C_{-1} (i,j) = (D - K_i) r \quad (63)$$

$$C_0 (i,j) = (1 - 2Dr) \quad (64)$$

$$C_1 (i,j) = (D + K_i) r \quad (65)$$

and then using equations (60) and (61) we have

$$r \leq \frac{1}{2D} , \quad K_i < D \quad \text{again as previously derived by the Fourier}$$

Series method. It is apparent that this general stability criterion is superior to both that of the Fourier Series method and the matrix method and as such will find wider applications in other scientific and engineering fields.

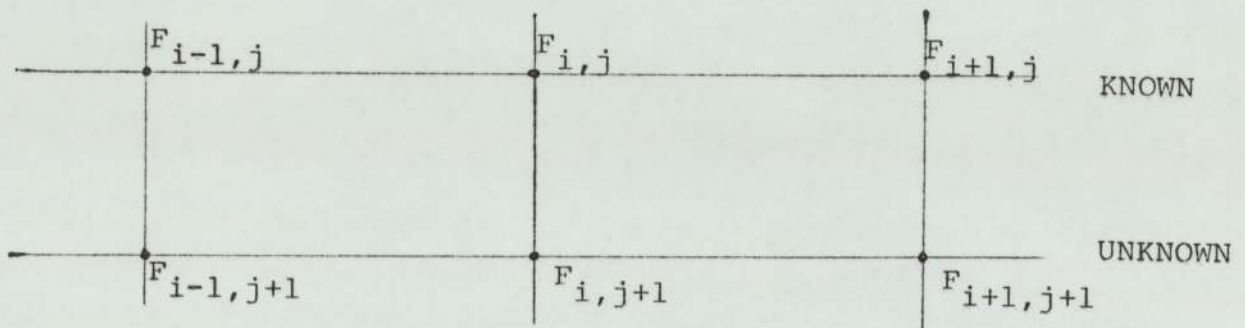
Implicit methods

One of the most powerful and widely used implicit schemes is that of the Crank-Nicolson implicit method. It involves replacing the derivatives  $\frac{\partial F}{\partial Y}$ ,  $\frac{\partial^2 F}{\partial Y^2}$  by the mean of their finite-difference approximations on the  $j^{\text{th}}$  and  $(j + 1)^{\text{th}}$  time levels, i.e.

$$\frac{\partial F}{\partial Y} = \frac{1}{2} \left[ \frac{(F_{i+1,j+1} - F_{i-1,j+1})}{2 (\Delta Y)} + \frac{(F_{i+1,j} - F_{i-1,j})}{2 (\Delta Y)} \right] \quad (66)$$

$$\frac{\partial^2 F}{\partial Y^2} = \frac{1}{2} \left[ \frac{(F_{i+1,j+1} - 2F_{i,j+1} + F_{i-1,j+1})}{(\Delta Y)^2} + \frac{(F_{i+1,j} - 2F_{i,j} + F_{i-1,j})}{(\Delta Y)^2} \right] \quad (67)$$

In this case the approximate value at the  $i^{\text{th}}$  node on the  $(j + 1)^{\text{th}}$  time level depends upon values at both the  $j^{\text{th}}$  and  $(j + 1)^{\text{th}}$  time levels (see diagram).



Hence, it will not be possible to solve the resulting difference equations directly and therefore an indirect technique such as the Gauss elimination method will have to be adopted.



i.e., as

$$(2I - r M_N) F_{j+1} = (2I + r M_N) F_j \quad (69)$$

where

$$M_N = \begin{bmatrix} -2D & (D + K_1) & & & \\ & (D - K_2) & -2D & (D + K_2) & \\ & & & & \\ & & & & (D - K_N) & -2D \end{bmatrix}$$

Equation (69) can also be written in the form

$$(2I - r M_N) F_{j+1} = [4I - (2I - r M_N)] F_j \quad (70)$$

and letting  $B = (2I - r M_N)$  we have

$$B F_{j+1} = (4I - B) F_j \quad (71)$$

giving

$$F_{j+1} = (4B^{-1} - I) F_j \quad (72)$$

The Crank-Nicolson finite-difference equations will be stable when the modulus of every eigenvalue of  $(4B^{-1} - I)$  does not

exceed one, that is, when

$$\left| \frac{4}{\lambda} - 1 \right| \leq 1 \quad (73)$$

where  $\lambda$  is an eigenvalue of B.

Equation (73) implies that  $\lambda \geq 2$ . For the matrix B,  $a_{ss} = 2 + 2Dr$ ,  $\max P_s = 2Dr$ , so Brauer's theorem leads to,

$$\left| \lambda - (2 + 2Dr) \right| \leq 2Dr,$$

or

$$- 2Dr \leq \lambda - 2 - 2Dr \leq 2Dr$$

i.e.

$$2 \leq \lambda \leq 2 + 4Dr$$

proving that the equations are unconditionally stable as  $\lambda \geq 2$  for all values of r.

Although the Crank-Nicolson finite-difference equations are stable for all values of r this does not imply that their solution converges rapidly to the actual solution of the pulmonary gas transport equation. In fact, due to the presence of the convection term in equation (7), the Gaussian elimination method, which is necessary in order to solve the relevant difference equations, requires large

amounts of computing time in order to attain the same degree of accuracy as that achieved with the direct explicit method.

The convergence properties of both the above schemes have been dealt with in an exhaustive manner in appendix III.

### Stochastic Simulation Methods

Stochastic simulation methods have proved to be attractive alternatives to the classical approaches in solving the gas transport equation. The full theoretical description of the stochastic method is given by Cox and Miller (1968) and the first use of stochastic methods for solving the gas transport equation owes much to Paiva, (1972).

The essence of this method is to sub-divide the "trumpet" model of the bronchial tree into annular sections of length  $\Delta y$  as in figure 5b where  $p_n$  and  $q_n$  represent random particle movements and  $a_n$  causes a drift which is equated to gas convection. If we now let  $b_n$  represent the total number of particles in the  $n^{\text{th}}$  annulus and  $F_n$  and  $S_n$  be the gas concentration and total cross-sectional area associated with this annulus then we know that:

$$b_n = F_n \Delta y S_n \quad (74)$$

and for a time change of  $\Delta t$

$$\Delta b_n = \Delta F_n \Delta y S_n \quad (75)$$

It should now be clear that the change in the number of particles in the  $n^{\text{th}}$  annulus in time  $\Delta t$  may be represented as

$$\begin{aligned} \Delta b_n = & b \left[ (n-1) \rightarrow (n) \right] - b \left[ (n) \rightarrow (n-1) \right] \\ & + b \left[ (n+1) \rightarrow (n) \right] - b \left[ (n) \rightarrow (n+1) \right] \end{aligned} \quad (76)$$

Using equations (74) and (75) together with the probabilities given in figure 5b we find that:

$$\begin{aligned} \Delta F_n \Delta y S_n = & \Delta y S_{n-1} F_{n-1} (p_{n-1} + a_{n-1}) - \Delta y F_n S_n (q_n - a_n) \\ & + \Delta y S_{n+1} F_{n+1} (q_{n+1} - a_{n+1}) - \Delta y S_n F_n (p_n + a_n) \end{aligned} \quad (77)$$

which may be rearranged and divided by  $\Delta y \Delta t$  to give

$$\begin{aligned} \frac{\Delta F_n}{\Delta t} = & \frac{1}{\Delta t} \left[ \frac{S_{n-1}}{S_n} F_{n-1} p_{n-1} - F_n q_n + \frac{S_{n+1}}{S_n} F_{n+1} q_{n+1} - F_n p_n \right] \\ & + \frac{1}{S_n \Delta t} \left[ S_{n-1} F_{n-1} a_{n-1} - S_{n+1} F_{n+1} a_{n+1} \right] \end{aligned} \quad (78)$$

If we compare the previous finite difference approximation equation (68) with that of equation (78) we find that stability

is assured provided

$$p_n = \frac{1}{2}, \quad q_n = \frac{S_{n-1}}{S_n}, \quad (\Delta y)^2 = 2D \Delta t \quad (79)$$

$$\text{and } 2 a_n S_n (\Delta y) = \dot{Q} \Delta t$$

For a particular flow ( $\dot{Q}$ ) equation (79) allows a stochastic matrix  $P$  to be constructed. The elements of this stochastic matrix define the probabilities of gas molecules moving between the annular states in time interval  $\Delta t$ . Thus, if  $F_0$  is the column vector of concentrations at zero time and  $F_1$  is the corresponding concentrations at time  $\Delta t$  then

$$F_1 = P F_0 \quad (80)$$

and similarly the end inspiratory concentrations are given by

$$F_m = p^m F_0 \quad (81)$$

where  $T = m (\Delta t)$  is the duration of the inspiratory cycle. A similar procedure will yield the expiratory concentrations with the proviso that the initial expiratory concentrations are identical to the end inspiratory gas concentrations as previously assumed in all model analyses.

It would appear from equation (81) that the technique of stochastic simulation is only a slight variation of the explicit finite difference method. However, on comparing the stability criteria corresponding to these two schemes it is found that this is grossly untrue. The conditions given in equation (79) dictate that small step lengths,  $\Delta y$ , and hence large computing times are necessary in order to obtain a stable and convergent solution.

#### DISCUSSION

The major contributions of the present assessment of contemporary models have been to critically examine

- (i) the assumed boundary conditions
- (ii) the assumed physical models
- (iii) the methods of solving the governing pulmonary gas transport equations, and
- (iv) The stability and convergence of the methods employed in (iii)

Whilst the earlier diffusion type models have already been exhaustively scrutinised by various eminent physiologists (Chang and Farhi, 1973; Piper and Schied, 1971 and Cumming, 1974) the same cannot be said for the more recent simultaneous convection-diffusion model analyses. It is hoped therefore that the present chapter has made some headway in achieving such a general scrutiny.

### CHAPTER 3

#### A REVISED MODEL

The objective of this chapter is to highlight the crucial role played by boundary conditions in influencing the simulation of gaseous transport mechanisms in the bronchial tree. Initially, results are presented pertaining to the *rigid* trumpet single series compartmental model as given in figure 2, however, later in this chapter it is shown how these results compare favourably with the corresponding *compliant* model predictions.

#### 3.1 The Revised Boundary Conditions

It is of value to restate the form of the revised boundary conditions previously derived in chapter 2 as it will subsequently be necessary to examine their stability and convergence within the context of a previously adopted explicit finite difference numerical solution technique (Bush et al, 1977).

The revised boundary conditions may be written in the form:-

$$\left. \frac{\partial F}{\partial y} \right|_{y=L} = + \frac{\dot{Q}}{D S (L)} F \Big|_{y=L}, \quad \text{for } t_1 \leq t \leq \frac{T}{2} \quad (82)$$

and

$$\left. \frac{\partial F}{\partial y} \right|_{y=L} = - \frac{\dot{Q}}{D S (L)} \left. F \right|_{y=L}, \text{ for } \frac{T}{2} < t \leq T \quad (83)$$

where  $t_1$  and  $T$  have been defined previously.

The stability and convergence of the above revised boundary conditions will now be examined in two ways firstly by recourse to the general stability criterion derived in chapter 2 and secondly by the less rigorous Fourier Series method. A third method (the matrix method) is dealt with in detail in appendix II.

Using central difference approximations of derivatives, as derived earlier, equations (82) and (83) become

$$F_{N,j+1} = 2Dr F_{N-1,j} + \left[ 1 - 2Dr + \frac{2r(\Delta y)\dot{Q}}{S_N} + \frac{2K_N r(\Delta y)\dot{Q}}{DS_N} \right] F_{N,j} \quad \dots \dots \dots (84)$$

and

$$F_{N,j+1} = 2Dr F_{N-1,j} + \left[ 1 - 2Dr - \frac{2r(\Delta y)\dot{Q}}{S_N} - \frac{2K_N r(\Delta y)\dot{Q}}{DS_N} \right] F_{N,j} \quad \dots \dots \dots (85)$$

where,

$$K_N = \frac{1}{2} (\Delta y) \left[ \frac{D}{S_N} \frac{\partial S_N}{\partial y} \pm \frac{\dot{Q}}{S_N} \right] \quad (86)$$

Method 1

Now, from the general stability conditions derived earlier in chapter 2 we know that

$$r \leq \frac{1}{2 (D + A_N)} \quad (87)$$

where,

$$A_N = \frac{\dot{Q} (\Delta y)}{D S_N} (K_N + D) \quad (88)$$

Since  $A_N \ll D$ , stability and convergence of the above revised boundary conditions is guaranteed by the relations derived using the Fourier Series method.

Method 2

When the Fourier Series method of stability was applied to equations (84) and (85) it was found that stability and convergence depended upon the value of  $r$  where

$$r = \frac{2 \left[ 4D \sin^2 \left( \frac{\beta h}{2} \right) - B_N \right]}{\left[ 8D (2D - B_N) \sin^2 \left( \frac{\beta h}{2} \right) + B_N^2 \right]} \quad (89)$$

and where

$$B_N = \frac{2 \dot{Q} (D + K_N) (\Delta y)}{DS_N} \quad (90)$$

The expression on the right hand side of equation (89) can be re-written in terms of partial fractions in the form,

$$r = \frac{1}{(2D - B_N)} - \frac{B_N (4D - B_N)}{(2D - B_N)} \left[ \frac{1}{8D(2D - B_N) \sin^2\left(\frac{\beta h}{2}\right) + B_N} \right] \dots\dots\dots (91)$$

For the particular solutions that have so far been given, the values of the physical model parameters were as follows:-

$$\begin{aligned} \Delta y &= 0.02, & S_N &= 26,216.0 \text{ (see Table )} \\ D &= 0.25, & \dot{Q} &= 250 \text{ cm}^3/\text{sec} \end{aligned}$$

Substituting these values into the expression for K we obtain,

$$K \approx 0.0125$$

and hence from equation (90) we know that

$$B_N \approx \frac{10.5}{26,216.0} \ll D \quad (92)$$

Since  $r > 0$ , the expression for  $r$  given in equation (91) will assume a minimum value when  $\sin\left(\frac{\beta h}{2}\right) = 0$

i.e.

$$r_{\min} < \frac{1}{(2D - B_N)} - \frac{B_N (4D - B_N)}{(2D - B_N)^2} \frac{1}{(4D - B_N)^2}$$

$$r_{\min} < \frac{1}{\left(2D - \frac{B_N}{2}\right)} \tag{93}$$

When  $B_N$  is very small (as in the present case where  $B_N \approx 0.0004$ ), equation (93) becomes identical to the relationship derived earlier (see chapter 2). In order to test the validity of this stability criterion equation (7) was solved with the revised "no-flux" boundary conditions and for different values of  $r$  (in fact,  $r = 0.5$  and  $r = 1.0$ ) it was found that the solutions were identical to the sixth decimal place, thus indicating that both a convergent and stable solution was attained. Hence, it is concluded that all of the present and subsequent model predictions are free from numerical artefacts arising from the use of a non-zero concentration gradient at the alveolar wall.

### 3.2 The Total Flux Equation

The total flux at any station within the model is made up of both convection and diffusion flux contributions and is defined as:-

$$G(y,t) = \pm \dot{Q} F(y,t) - D S \frac{\partial F}{\partial y} \quad (94)$$

From this equation we can derive the gaseous flux per unit flow which is defined as

$$\frac{G(y,t)}{\dot{Q}} = \pm F(y,t) - \frac{D S}{\dot{Q}} \frac{\partial F}{\partial y} \quad (95)$$

In order to fully appreciate the physical or physiological significance of the above revised boundary conditions it is only necessary to compare the flux curves (Pack et al, 1977) as plotted in figures 6 and 7. Figure 6 presents results for the conventional type *rigid* model, (Paiva, 1973) and clearly demonstrates the *sink* and *source* effects occurring during inspiration and expiration respectively. However, when the revised boundary conditions are applied it is clear from figure 7 that these artefacts disappear and that a true "no-flux" condition is specified at the alveolar wall,  $y=L$ , throughout the duration of the respiration cycle.

### Concentration/Distance Profiles

The resulting concentration/distance profiles, corresponding to the revised boundary conditions, are shown in figure 8 from which it will be noted that not only are there significant concentration differences in the acinus region at end inspiration, but more importantly, these stratifications persist during expiration. For example, a 0.7 per cent ( $\approx$  5.32 mm Hg) difference in tracer gas concentration exists between the ends of the model at end expiration (see Table 2); 60 per cent of this difference occurring in the acinus. These end expiratory concentration gradient distributions are perhaps more readily discernable in relation to a more refined concentration scale as indicated in figure 9.

### The Single-Breath Nitrogen Washout Test

In order to test the validity of the above revised boundary conditions and to relate the true "no-flux" conditions to know behaviour in vivo it is necessary to modify the above analysis to facilitate a simulation of the single breath nitrogen washout curve by taking,

$$F_{E_{N_2}}(t) = 0.8 \left[ 1.0 - F(o, t - t_1) \right] \quad (96)$$

where  $F_{E_{N_2}}(t)$  is the variation of the nitrogen concentration at the entry of the trachea during the first expiration following a single oxygen inspiration.

The resulting plot of expired nitrogen against volume is given in figure 10 and clearly shows the expected phase III (or alveolar plateau) slope, (see Table 3). On extrapolating this curve to 500 mls expired the observed slope is equivalent to 3.42 per cent, which is reminiscent of the average value for normals obtained experimentally by Mills and Harris (1965) and more recently by Jones (1967).

The only previous analytical work to show a similar finite phase III slope was that of Cumming et al (1971), who produced a 1.1 per cent gradient between 750 mls and 1250 mls expired. These authors, however, did not attempt to simulate *simultaneous* convection and diffusion, but allowed successive quanta of flow to enter their model followed by a diffusion period. Although this "relaxation" technique only provided a crude approximation to the actual process of pulmonary gas transport, it did guarantee that no gas was lost across the alveolar wall. Moreover, by controlling the way in which gas flowed out of their model, a continual fall in fractional concentration at the mouth was ensured, giving rise to the small alveolar slope.

### 3.3 Simulation of the single-breath washout test for Gases of Different Diffusivity

The ability of the present model analysis to discriminate between the behaviour of insoluble tracer gases of differing binary molecular diffusion coefficient will now be examined.

More specifically, it will be shown how gaseous concentration differences (stratified inhomogeneities) existing in the acinar region can be related to expired concentrations measurable at the mouth.

Figures 11 and 12 show the input gas concentrations within the model at end inspiration and end expiration respectively for three tracers having molecular diffusion coefficients of  $0.1 \text{ cm}^2/\text{sec}$ ,  $0.315 \text{ cm}^2/\text{sec}$  and  $0.76 \text{ cm}^2/\text{sec}$  corresponding to  $\text{SF}_6/\text{N}_2$ ,  $\text{Ne}/\text{N}_2$  and  $\text{He}/\text{N}_2$  mixtures. As intuitively expected, it can be seen that at end inspiration the heavier gas ( $\text{SF}_6$ ) has penetrated deeper into the model than that of the lighter gases (Ne or He), and hence it has a greater dead space volume. Furthermore, the heavier gas displays a more marked concentration stratification in the acinar regions. The actual concentration differences between the ends of the model at end expiration are 0.42% for He, 0.6% for Ne, and 1.2% for  $\text{SF}_6$ , with the greatest gradients occurring over the last 0.5 cms of the model length.

The resulting concentrations of the three tracer gases being expired through the "mouth" end of the model are given in figure 13 and show that the heavier the gas, the greater the dead space volume and the greater the alveolar plateau slope. The plateau slopes for the three tracer gases were calculated on the basis of an extrapolation to 500 mls expired and were found to be 2.9% for He, 3.4% for Ne and 4.8% for  $\text{SF}_6$ .

The theoretical results presented in figures 12 and 13 show that the expired "alveolar plateau" slope of a tracer gas does indeed give an indication of end expiratory concentration differences in the acinus. Moreover, the magnitude of the slope and the degree of stratified inhomogeneity, *increase* as the molecular weight of the input gas increases (that is D decreases). Such results concur with the experimental findings of previous workers (Georg et al, 1965; Cumming et al, 1967; Read, 1966; Power, 1969; Sikand et al, 1967; and Kawashiro et al, 1976), who also concluded that gases having lower diffusivities should reach equilibrium more slowly and that the observed expired concentration differences arose as a consequence of similar differences obtaining in the more distal regions of the bronchial tree.

### 3.4 Simulation of the single-breath washout test for gases of different solubility

The particular form of the revised boundary conditions so far encountered ensure that none of the tracer gas escapes, or indeed is reabsorbed through the alveolar wall. As the three gases just considered have very low blood solubilities ( $\text{SF}_6 = 0.0067$ ,  $\text{Ne} = 0.011$ ,  $\text{He} = 0.0098$ ) such an assumption would appear to be a reasonably accurate representation. Nevertheless, it is interesting to speculate how a finite gas flux across the alveolar wall would affect concentration

gradients. Change and Farhi (1973) have already considered such a case in qualitative terms, and have suggested that the gas exchange is likely to increase any stratified inhomogeneities in the acinus. The present model may readily be modified to accommodate a finite gas flux across the alveolar wall by slightly altering the boundary conditions (82) and (83) above. The necessary modification involves changing "G = 0" to "G = k", where k is the amount of input tracer gas (mls/sec) being taken up by the blood flowing in the alveolar capillaries. In fact, equations (82) and (83) become

$$\left. \frac{\partial F}{\partial y} \right|_{y=L} = + \frac{\dot{Q}}{D S (L)} F \Big|_{y=L} - \frac{G}{D S (L)} \quad (97)$$

and,

$$\left. \frac{\partial F}{\partial y} \right|_{y=L} = - \frac{\dot{Q}}{D S (L)} F \Big|_{y=L} - \frac{G}{D S (L)} \quad (98)$$

The effect of applying three values of G (10, 25 and 50 mls/sec) to a hypothetical tracer gas having a diffusion coefficient of 0.25 cm<sup>2</sup>/sec (equivalent to O<sub>2</sub>/N<sub>2</sub>) is shown in figure 14 for end inspiration. It can be seen that the higher the G value, the greater the concentration gradients for the input gas in the acinar region and the lower the alveolar gas concentration. The latter effect is to be

expected since higher values of  $G$  are associated with tracers having a higher blood solubility hence they are being removed from alveolar space at a faster rate by capillary blood.

Figure 15 gives the ensuing end expiratory concentrations within the model. It will be noted that more marked stratified inhomogeneities are associated with tracers having higher blood solubilities, and that these concentration gradients are also reflected at the "mouth" end of the model as is evident from figure 16.

A more realistic illustration of the independent effects of input gas solubility on stratified inhomogeneities may be given by considering the specific gases Argon and Nitrous Oxide because they have very similar diffusion coefficients ( $D = 0.192$  for Ar and  $D = 0.189$  for  $N_2O$ ). Because the solubility of Argon can be considered negligible, a value of zero is assumed for  $G$ . Nitrous Oxide in contrast has a much greater affinity for blood, having a solubility coefficient of 0.465. Using an earlier algebraic gas exchange model (Scrimshire et al, 1973) the value of  $G$  during a normal initial breath of 100%  $N_2O$  is estimated to be approximately 5.5 mls/sec. The results for the two tracer gases are given in figures 17 and 18 and as anticipated, greater end inspiratory and end expiratory input gas concentration gradients exist in the acinus for Nitrous Oxide. Moreover, the actual alveolar concentration level for Nitrous

Oxide is significantly lower than that for Argon for the reason previously discussed. The simulated single-breath input gas washout tests for these two tracer gases are given in figure 19 and demonstrate a significantly greater alveolar plateau slope for Nitrous Oxide again reflecting conditions within the lung.

### 3.5 Results for Different Volumetric Flow-Rates

As yet, only square wave flow-rates have been imposed in order to achieve the required tidal ventilation. Since the precise volumetric flow-rate variation within the bronchial airways is at present unknown (see Schroter and Sudlow, 1969) it is of interest to consider alternative forms of mass movement. Furthermore, the consideration of flow-rates other than that of the square-wave type will provide an alternative means of testing the stability and convergence of the revised boundary conditions.

On resolving equation (7) with both triangular and a sinusoidal wave flow-forms and for the same parameter specifications as previously considered in figures (6) to (19), the results given in figures (20) to (23) were obtained. It is clear from these curves that the only significant changes, in comparison to those earlier simulated results given in figures (6) to (19), are as follows:-

- (i) The concentration/distance profiles for the sinusoidal wave flow-rate oscillate whilst the alveolar tracer gas concentration level continually increases during inspiration
- (ii) The dead space volumes (or phase II) of all tracer gases were slightly greater when the triangular and sinusoidal flow-rates were considered
- (iii) The calculated phase III (alveolar plateau) slopes of all tracer gases compared well with those obtained when a square wave flow-rate was considered. This is more readily demonstrated in table 4.

It is intuitively obvious that the concentration/distance profiles in the conducting airways (where mass movement by convection is dominant) will change in synchrony with the oscillating flow form. However, in the more distal regions this effect is negligible.

The small fluctuations in phase II and phase III values are in agreement with the experimental results of Bashoff et al (1967) and Jones and Glaister (1969). These workers demonstrated that increasing expiratory flow-rate results in small decreases in the dead space volume and alveolar plateau slope.

### 3.6 Results for different Pre-inspiratory Lung Volumes

It is well known that the shape of phase II and the slope of phase III are critically dependent upon the initial lung volume from which the single-breath test was performed (Mills and Harris, 1965; Bashoff et al, 1967; Jones, 1967). The results presented in figures 24 and 25 are for a range of such pre-inspiratory lung volumes, in fact, for lung volumes varying between 2.5 litres and 5.5 litres. The most important observation to be made concerning these results is that both the end expiratory concentration differences and the resulting phase III slopes decrease as the pre-inspiratory lung volume increases (see Table 5).

Since there is a significant variation in functional residual capacity (FRC) between one normal subject and the next, we would not expect to be able to put rigorous bounds on the corresponding change in phase III slope. In fact, Mills and Harris (1965) have indicated that in normals this phase III slope may vary between 2% - 4%.

It should be noted that the results given in figures 24 and 25 and Table 5 are typical of those obtained with various flow-forms and diffusivities.

### 3.7 Breath-Holding Studies

In almost all single-breath determinations, whether they be obtained from normal or abnormal subjects, a finite breath-holding time is unavoidably incurred due mainly to the inability of the subject under consideration to perform an instantaneous reversal of flow. This is particularly true in the case of chronic bronchitics and emphysematics who find difficulty in performing even the simplest respiratory manoeuvres. Thus, it is necessary and interesting to speculate how a finite breath-holding time will influence both the approach towards gaseous equilibrium and the observed phase III slope of a respired tracer gas.

At the outset it was necessary to modify the existing analysis in the following way:-

#### INSPIRATION

$$F(o, t) = 1.0, \text{ for } t_1 \leq t \leq \frac{T}{2} \quad (99)$$

$$\left. \frac{\partial F}{\partial y} \right|_{y=L} = + \frac{\dot{Q}}{D S (L)} \left. F \right|_{y=L}, \quad t_1 \leq t \leq \frac{T}{2} \quad (100)$$

BREATH-HOLDING

$$\left. \frac{\partial F}{\partial y} \right|_{y=0} = 0.0, \quad \text{for } \frac{T}{2} < t \leq T_B \quad (101)$$

$$\left. \frac{\partial F}{\partial y} \right|_{y=L} = 0.0, \quad \text{for } \frac{T}{2} < t \leq T_B \quad (102)$$

EXPIRATION

$$\left. \frac{\partial F}{\partial y} \right|_{y=0} = 0.0, \quad \text{for } T_B < t \leq T \quad (103)$$

$$\left. \frac{\partial F}{\partial y} \right|_{y=L} = \frac{\dot{Q}}{D S (L)} \left. F \right|_{y=L}, \quad T_B < t \leq T \quad (104)$$

where  $T_B$  is the duration of breath-holding.

The boundary conditions holding during breath-holding are obtained from equations (82) and (83) with  $\dot{Q} \equiv 0$  (i.e. no convective flow of gas through the "mouth end" of the model).

When the gas transport equation was solved with the above boundary conditions and for various breath-holding times, the results presented in figures 27, 28 and 29 and table 7 were obtained. The figures give results corresponding to 1, 2 and 5 seconds breath-holding respectively. As breath-holding proceeds two major effects were noticed, i.e.

- (i) The appearance of the phase II (concentration transition) occurred earlier indicating a significant reduction in dead space volume
- (ii) The slope of phase III (alveolar plateau) was significantly reduced.

These two "effects" may be more readily examined by reference to the results in Table 7.

The above two observations have already been verified experimentally by Georg et al (1965), Cumming et al (1967) and Power (1969). Further, the actual concentration points detailed in table 7 can be related to similar experimentally tabulated results of Cumming et al (1967).

The reasons for the rapid decrease in phase II and phase III values are two-fold:-

- (a) During breath-holding the dead space gas and the alveolar gas will have time to reach an

equilibrium concentration and therefore any stratified inhomogeneities existing in the acinus will have been abolished.

- (b) Since  $\dot{Q} \equiv 0$  during breath-holding the alveolar wall boundary condition reduces to the conventionally assumed condition as given in equation (102). Thus, all previous arguments apply suggesting that any concentration gradients will be eventually obliterated.

### 3.8 Compliant Model Predictions

The results presented so far have been based upon a rigid physical model, hence it was necessary to impose a gaseous flow to simulate inspiration and expiration. In reality, breathing is brought about by the expansion and contraction of the respiratory regions of the lung, however, in order to follow these movements exactly it would be necessary to solve the appropriate hydrodynamic equations. Such additional complexity is considered unnecessary in view of the fact that the results obtained from variable volume models (for example, Pack et al, 1977) do not differ significantly from those obtained from rigid models at low tidal volumes (for example, Paiva, 1973) which are similar to that so far considered in this chapter. However, when it becomes

necessary to simulate larger tidal ventilations some account must be taken of lung expansion (Davidson, 1975, 1977).

The geometrical boundaries of the trumpet model were allowed to expand and contract in accordance with the relation derived by Hughes et al (1972), i.e. lung volume varied proportional to the cube of the bronchial distance. On solving the pulmonary gas transport equation, whilst simultaneously allowing for such lung expansion the results given in figure 30 and table 8 were obtained. These results are for a square-wave flow rate ( $\dot{Q} \equiv 250 \text{ cm}^2/\text{sec}$ ) and a tidal volume of 500 mls. Clearly, there is very good agreement between the "rigid" and "compliant" model predictions for these specific values of the respiratory parameters. The only effect of considering rigid rather than variable volume models (at low tidal volume) would appear to be that input gas concentrations are slightly underestimated a point also noted by Paiva (1978).

Perhaps the greatest significance to the clinician is the ability of the variable volume model to allow for larger tidal ventilations and subsequent larger expirations. This is an important improvement in the model development since Bashoff et al (1967) have indicated that there are basically two main forms of the single-breath test, i.e.

- (i) Inspiration of a small tidal volume ( $V_T \approx 500$  mls) from the level of F.R.C. and subsequent expiration to the resting expiratory level
  
- (ii) Inspiration of a larger tidal volume ( $V_T \approx 1000$  mls) from the level of F.R.C. and then expiration of about 2 litres.

The latter form (ii) is usually used in estimating the slope of the phase III. In fact, the value taken for this slope is the difference in expired gas concentration between 750 mls and 1,250 mls expired.

On carrying out a single-breath nitrogen washout test identical to that described in (ii) above, the results demonstrated in figure 31 and table 9 were obtained. As expected, the longer duration of the expiratory cycle reduces both the end expiratory concentration stratifications and the phase III slope. Table 9 gives a detailed description of these concentration differences.

## CHAPTER 4

### REGIONAL DIFFERENCES

One has only got to consider the complex branching pattern of the bronchial airways (Weibel, Model B, 1963; Horsfield and Cumming, 1968 and Horsfield et al, 1971) to realise the limitations of the single series compartmental models in providing a realistic simulation of molecular gas movements. This situation is even more pronounced in many cases of chronic obstructive lung disease (C.O.L.D.) (Horsfield et al, 1973 and Demedts et al, 1976) and as such there is a need for an improved physical model representation.

Further, in many forms of pulmonary disease, the pattern of regional ventilation and blood flow distributions may be greatly altered from the normal. For example, investigations using  $Xe^{133}$  as a tracer gas have shown very considerable regional abnormalities of function in vivo, as revealed by impairment of both ventilation and perfusion, in numerous subjects diagnosed as having pulmonary emphysema. In certain subjects it has been clearly demonstrated that most of the tidal volume goes to zones, or possibly lobes, of the lung in which the structure is relatively preserved, but which represent only a small fraction of the total lung volume (Bentivoglio et al, 1963). The latter findings again emphasise the need for an improved model description.

#### 4.1 A REGIONAL MODEL

The basic form of such an improved physical model consists of an upper airways compartment in *series* with two *parallel* compartments as shown diagrammatically in figure 28. The choice of two parallel compartments was taken solely for ease of illustration, but the model can be extended to include any number of such parallel compartments *vide infra*.

#### Regional Inhomogeneities

In order to assess the effects of regional inhomogeneities upon the efficiency of pulmonary gas transport and mixing it is necessary to specify which particular model parameters are varying and exactly what type of inhomogeneity they are simulating. In fact, only three specific types of regional inhomogeneity have been considered.

- (a) Regional inequalities of volumetric flow-rate
- (b) Regional variations in compartmental volume
- (c) Regional differences in diffusion pathway length

In cases (a) and (b), only single parameter variations occur, whereas, in case (c) multiple variations are necessary. For the changes required for type (c) it was found necessary to utilise the empirical relationship derived by Hughes et al (1972) which states that lung volume varies proportional to the cube of the bronchial length.



Let  $\dot{Q}_i$  ( $i = 1, 2$ ) be the regional volumetric flow-rates down the parallel compartments and  $V_i$  ( $i = 1, 2$ ) their corresponding volumes, then in mathematical terms the above three types of regional inhomogeneity may be stated in the form:-

$$(a) \quad \dot{Q}_1 \neq \dot{Q}_2 \quad \text{and} \quad V_1 = V_2$$

$$(b) \quad \dot{Q}_1 = \dot{Q}_2 \quad \text{and} \quad V_1 \neq V_2$$

$$(c) \quad V_1 \neq V_2 \quad \text{and} \quad l_1 \neq l_2 \quad \text{where } l_1 \quad \text{and } l_2 \\ \text{are the lengths of the parallel compartments.}$$

Since,

$$V \propto l^3 \tag{i}$$

$$\text{i.e. } V = k l^3 \tag{ii}$$

we may now write

$$V_1 = k l_1^3 \quad , \quad V_2 = k l_2^3 \tag{iii}$$

and from (iii) we can derive

$$l_2 = l_1 \left( \frac{V_2}{V_1} \right)^{\frac{1}{3}} = a l_1 \tag{iv}$$

which implies that,

$$S_2 = a^2 S_1 \tag{v}$$

Further, in each of cases (a), (b) and (c) the parallel compartments *expand* and *contract* to accommodate their relative inspired and expired fractions of the total tidal volume. In order to simulate the compliant characteristics of these parallel compartments, it was again necessary to make recourse to the empirical findings of Hughes et al (1972).

Thus, at time  $t = 0$  the cross-sectional area/distance distributions for the parallel compartments are given by,

$$S_i \equiv S_i (y_i, t), \quad i = 1, 2 \quad (\text{vi})$$

where the data for the  $S_i$  ( $i = 1, 2$ ) have been obtained from a modified version of Weibel's Model A;  $y_i$  is the distance variable corresponding to compartment  $i$  ( $i = 1, 2$ ) respectively. During the subsequent time interval  $\Delta t$ ,  $\dot{Q}_i \Delta t$  ( $i = 1, 2$ ) of gas enters these parallel compartments causing an increase in volume (and hence also  $S_i$ ) according to the relations previously outlined in (iv) and (v) above, i.e.

$$S_i (y_i, t + \Delta t) = a_i^2 S_i (y_i, t), \quad i = 1, 2 \quad (\text{vii})$$

where,

$$a_i = \frac{(V_i + \dot{Q}_i \Delta t)^{1/3}}{V_i}, \quad i = 1, 2 \quad (\text{viii})$$

Equations (vii) and (viii) yield an efficient iteration procedure governing the *expansion* and subsequent *contraction* of the parallel compartments (i.e. respiratory regions). It is important to note that coupled with equations (vii) and (viii) we also have,

$$y_i (t + \Delta t) = a_i y_i (t) , \quad i = 1,2 \quad (ix)$$

indicating that the diffusion pathway lengths are continually increasing during inspiration and similarly decreasing during expiration in line with the suggestion proposed by Chang and Farhi (1973). However, it should also be noted that similar solutions to the governing gas transport equations are obtained when equation (x) is employed,

$$y_i (t + \Delta t) = y_i (t) , \quad i = 1,2 \quad (x)$$

#### 4.2 THE GOVERNING EQUATIONS

The equations governing the transport of gaseous species into and out of the *compliant* model illustrated in figure 32 may be written as:-

$$\frac{\partial F_i}{\partial t} = D \frac{\partial^2 F_i}{\partial y_i^2} + \frac{1}{S_i} \frac{\partial S_i}{\partial y_i} \frac{\partial F_i}{\partial y_i} - \frac{\dot{Q}_i}{S_i} \frac{\partial F_i}{\partial y_i} \quad (105)$$

$$(i = 0, 1 \text{ and } 2)$$

and  $i = 0$  refers to the upper airways compartment;  $F_i \equiv F_i(y_i, t)$  is the fractional concentration of input tracer gas at distance  $y_i$  from the portal end of compartment  $i$  and at time  $t$  after the start of the respiratory manoeuvre;  $S_i \equiv S_i(y_i, t)$  is the total cross-sectional area/distance distribution relative to compartment  $i$  and at time  $t$  during its expansion/contraction cycle;  $y_i$  is the distance variable associated with compartment  $i$  and  $D$  is the binary molecular diffusion coefficient between the inspired and residual gases.

The solution of equation (105) in the model configuration shown in figure (32) requires the specification of appropriate initial and boundary conditions.

#### 4.3 BOUNDARY CONDITIONS

The initial and boundary conditions employed in the present chapter are almost identical to those used in the last chapter, the only difference being that in this chapter it is necessary to specify a further *internal* boundary condition at the junction of the *series* and *parallel* compartments (branch point A in figure (32) ).

Inspiratory Cycle

We assume a constant flow of input gas through the "mouth end" of the model which implies that,

$$F_o (0, t) = 1.0 \text{ for } t_1 \leq t \leq \frac{T}{2} \quad (106)$$

At point A we must have a continuity relationship which implies that,

$$F_{oA} = F_{iA} \text{ , } i = 1,2 \text{ for } t_1 \leq t \leq \frac{T}{2} \quad (107)$$

At the alveolar walls of the parallel compartments we again must impose "zero flux" conditions when considering the transport of insoluble tracer gases. The total flux of gas at any point in the model and at time t is given by:-

$$G_i (y_i, t) = \dot{Q}_i F_i (y_i, t) - D S_i \frac{\partial F_i}{\partial y_i} \text{ , } i = 1,2 \quad (108)$$

$$(0 \leq t \leq T)$$

Putting  $G_i (L_i, t) = 0$ ,  $i = 1,2$  (where  $L_i$  refers to the length of compartment i) gives,

$$\left. \frac{\partial F_i}{\partial y_i} \right|_{y_i=L_i} = \frac{\dot{Q}_i}{D S_i (L_i)} \left. F_i \right|_{y_i=L_i} \text{ , } t_1 \leq t \leq \frac{T}{2} \quad (109)$$

$y_i=L_i \text{ , } i = 1,2$

Expiratory Cycle

During expiration the contribution from diffusive mixing at the portal end of the model is considered negligible in comparison to the convective mixing (Paiva, 1972), hence we have that,

$$\left. \frac{\partial F_o}{\partial y_o} \right|_{y=0} = 0 \quad \text{for } \frac{T}{2} < t \leq T \quad (110)$$

The "no flux" conditions at the alveolar walls,  $y_i=L_i$  again yields from (108) above:-

$$\left. \frac{\partial F_i}{\partial y_i} \right|_{y_i=L_i} = - \frac{\dot{Q}_i}{D S_i (L_i)} F_i \Big|_{y_i=L_i}, \quad \frac{T}{2} < t \leq T \quad (111)$$

$i = 1, 2$

The single most important boundary condition relating the influence of regional inequalities to the corresponding expired gas concentrations at the mouth, is the condition holding at branch point A (see figure 32). In fact, this condition assumes the form,

$$F_{OA} = \frac{(\dot{Q}_1 F_{1A} + \dot{Q}_2 F_{2A})}{(\dot{Q}_1 + \dot{Q}_2)} = \frac{\sum_{i=1}^2 \dot{Q}_i F_{iA}}{\sum_{i=1}^2 \dot{Q}_i} \quad (112)$$

and in the general case of n parallel compartments we obviously would have,

$$F_{OA} = \frac{\sum_{i=1}^n \dot{Q}_i F_{iA}}{\sum_{i=1}^n \dot{Q}_i} \quad (113)$$

It is through the interaction of equations (111) and (112) that the *combined* effects of *regional* and *stratified* inhomogeneities can be studied with the present lung model.

#### 4.4 RESULTS FOR CONSTANT DIFFUSION PATHWAY LENGTHS

The solutions to equation (105) for constant diffusion pathway lengths (i.e.  $y_1 \equiv y_2$ ) and for the prescribed initial and boundary conditions are presented in figures (33) and (34). In each case, results are given for two positions of the nodal branch point A, that is in generation 17 (solid line) and generation 14 (dotted line), however, other positions may also be considered as will be discussed later.

It is clear from table 10 and figures 33 (a to c) that the higher the regional flow differences, the greater the end expiratory acinar concentration gradients irrespective of the position of the nodal point A. The largest concentration gradients

(stratified inhomogeneities) occurred when point A was in the region of the respiratory bronchioles (see table 10) in agreement with the current trend of experimental predictions (Engel et al, 1973; Sikand et al, 1966, 1976 and Kawashiro et al, 1976). It should also be noted that in the regions adjacent to the branch point A significant 'local' stratification is present and that this will also contribute to the subsequent expired concentration curve at the mouth. On closer examination of table 10 and figures 33 (d to f) it is found that similar *increases* in concentration gradient are observed for *constant* regional flows  $\dot{Q}_i$  ( $i = 1,2$ ), consequent upon *decreases* in the regional compartmental volumes  $V_i$  ( $i = 1,2$ ). Such results were also noted by Young and Martin (1966) and Tsunoda et al (1972).

The sensitivity of the single-breath nitrogen washout curve to such independent  $\dot{Q}_i$  ( $i = 1,2$ ) and  $V_i$  ( $i = 1,2$ ) variations is clearly demonstrated in figures 34 (a to f) and a detailed breakdown of the results can be found in table 10. Essentially three observations are noted on closely scrutinising these curves, i.e.

- (i) the phase III slope (alveolar plateau) *increases* as either the regional flow-differences *increase* or as the regional volumes  $V_i$  ( $i = 1,2$ ) *decrease* (when the  $\dot{Q}_i$  ( $i = 1,2$ ) remain constant).
- (ii) the *steeper* phase III slopes occur when nodal point A is situated in the more distal airways reflecting the corresponding *steeper* concentration gradients.

- (iii) the phase III (concentration transition) appears later (reflecting a greater dead space volume) when nodal point A is situated in the more distal airways.

The first observation above indicates that regional inequalities in ventilation produce the *increased* end expiratory concentration gradients (stratified inhomogeneities) and correspondingly *increased* phase III slopes. Hence, even without considering the added effects of diffusion pathway length variation we have already established useful criterion for distinguishing between the gas mixing behaviour in diseased lungs.

#### 4.5 RESULTS FOR VARIABLE DIFFUSION PATHWAY LENGTHS

As already mentioned in the opening paragraph of this chapter, the structure of the human bronchial tree is certainly not symmetrical as assumed in Weibel's Model A (1963) but significant *regional differences* in diffusion pathway length occur within both the normal and diseased lungs. For example, Horsfield and Cumming (1968) and Horsfield et al (1971) have concluded from their somewhat extensive morphometric analyses that within the respiratory lobules the distribution of pathway lengths varies from 2 mm to 9 mm and on extrapolating this result to the lung as a whole, they have suggested that total pathway lengths may vary as much as from 7.5 cms to 21.5 cms.

The implications of the above findings upon the efficiency of pulmonary gas transport and mixing have not, as yet, been considered due mainly to the nature of the previously assumed physical models of the pulmonary airways (i.e. the single series 'trumpet' or 'thumbtack' models). What is really required is a lung model that will allow for regional differences in diffusion pathway length and lung volume simultaneous with regional inequalities in ventilation distribution, such as that outlined in figure 32.

The results illustrated in figures 35 (a to f) show how the added effect of variable diffusion pathway lengths influence gas mixing efficiency in the acinus. It is clear that in all cases considered, there are significantly greater stratified concentration differences when the diffusion pathway length is varied simultaneous with increased regional flow-differences. The magnitude of such differences can be computed from tables 10 and 11, and in some cases amount to as much as a 50% increase in gradient, irrespective of the position of the nodal point A. The degree of the concentration gradient adjacent to the nodal point A has also increased in the present case (i.e. 'local' stratification has increased) and the extent of these increases may also be judged by scrutinising the corresponding single-breath nitrogen washout curves as given in figures 36 (a to f).

On comparing the single-breath nitrogen washout curves given in figures 34 (a to f) and 36 (a to f) (corresponding to

'constant' and 'variable' diffusion pathway lengths, respectively) one cannot fail to observe the following major differences:-

- (a) The phase III slopes presented in figures 36 (a to f) are *substantially greater* than their corresponding counterparts given in figures 34 (a to f) (see table 11), reflecting the already observed *greater differences* in end expiratory concentration gradient.
  
- (b) In all cases considered, the appearance of the concentration transition (phase II) is slightly delayed in the latter curves (figures 36 (a to f) ) indicating that transit time distribution may well influence dead space determination in patients with chronic lung disorders.

#### 4.6 SIMULATION OF "AVERAGE CASE OF EMPHYSEMA"

A further group of simulations were carried out in order to demonstrate how the present regional model could predict results in agreement with known experimental findings. More specifically, the "average case of emphysema" as quoted by Briscoe and Cournand (1959) was analysed. Briscoe and Cournand (1959) have indicated that in an "average case of emphysema" 66 per cent of the lung volume is ventilated by only 10 per cent of the alveolar ventilation which may readily

be incorporated within the framework of the existing lung model analysis by taking  $V_1:V_2 = 1:2$  with  $\dot{Q}_1:\dot{Q}_2 = 9:1$ . The actual parameter variations considered are detailed in table 12 where once again both constant and variable diffusion pathway lengths have been considered.

The results given in figures 37 (a to f) and 39 (a to f) again demonstrates those features already observed in figures 33 (a to f) and 35 (a to f) (i.e. *increased* end expiratory stratifications for corresponding *increases* in the regional flow differences. On singling out those average cases of emphysema as discussed above, it is found from table 12 that these end expiratory concentration stratifications may vary between 1.25% and 3.0%.

The single-breath nitrogen washout curves corresponding to this latter group of simulations are presented in figures 38 (a to f) and 40 (a to f) and clearly demonstrate those features previously noted in (a) and (b) above (see section 4.5). On scrutinising table 12 it is found that in those cases in which 66% of the lung volume is ventilated by 90% of the inspired tidal volume, the phase III slope varies between 7.74% and 13.47% which compares favourably with known experimental findings obtained from patients with C.O.L.D. (chronic obstructive lung disease) and pulmonary emphysema by Demedts et al (1976). In fact, Demedts et al (1976) have indicated that in patients with severe forms of C.O.L.D. with emphysema (group D in their paper) the phase III slope varies between 8.0% and 13.0% in close agreement with the present theoretical predictions.

4.7 Simulation of the Single-Breath Washout Test  
for gases of different diffusivity

It is of interest to compare the present 'regional' model predictions with the corresponding single 'series' compartmental model simulations given in the last chapter. In particular, attention will be focused on the relations between the end expiratory acinar input gas concentration gradients and the subsequent expired concentrations measured at the mouth.

Figures 41 (a to f) and 42 (a to f) show the input gas concentrations within the present 'regional' model (for the same regional inhomogeneities as considered in section 4.5) at end expiration for three tracers having molecular diffusion coefficients of  $0.1 \text{ cm}^2/\text{sec}$ ,  $0.315 \text{ cm}^2/\text{sec}$  and  $0.76 \text{ cm}^2/\text{sec}$  corresponding to  $\text{SF}_6/\text{N}_2$ ,  $\text{Ne}/\text{N}_2$  and  $\text{He}/\text{N}_2$  mixtures. As intuitively expected, it can be seen that in each case the heavier gas displays a more marked concentration stratification in the acinus reaffirming the results already given in section 3.3. The actual magnitudes of these concentration differences can be found by reference to table 13.

The resulting concentrations of the three tracer gases being expired through the "mouth" end of the present regional model are given in figures 43 (a to f) and 44 (a to f) and show that (independent of the type of regional inequality considered) the heavier the gas the greater the dead space volume and the greater the phase III slope (see table 13). Again, these

latter results bear out the predictions given previously in chapter 3 (section 3.3).

Apart from the major observations detailed above, it is also important to note the following 'secondary features' arising from a close inspection of all curves given in figures 41 to 44 (a to f):-

- (i) For all the tracer gases considered the greatest concentration gradients *always* occur when nodal point A is situated in the more distal airways (respiratory bronchioles)
- (ii) For all the tracer gases considered more marked concentration differences were observed when the diffusion pathway lengths varied simultaneous with the regional inequalities in flow and volume
- (iii) The 'local' stratification adjacent to branch point A was in all cases greatest for the heaviest tracer gas
- (iv) The phase III slopes of all tracer gases considered were steepest when the diffusion pathway lengths varied simultaneously with the regional inequalities in flow and volume reflecting the corresponding steeper concentration gradients noted in (ii) above.

- (v) In all cases considered there is greatest delay in the appearance of the concentration transition (phase II) for the heaviest tracer gas.

#### 4.8 Simulation of the Single Breath Washout Test for gases of different Solubility

In order to compare the '*series*' and '*parallel*' model simulations for the transport and mixing of gases of different *solubility* it is necessary to formulate appropriate boundary conditions (similar to those specified in equations (96) and (97) which will allow for a specific finite flux of gas to be taken up by the blood flowing in the alveolar capillaries. Clearly, these modified boundary conditions will assume the following form:-

$$\left. \frac{\partial F_i}{\partial y_i} \right|_{y_i=L_i} = + \frac{\dot{Q}_i}{D S_i (L_i)} F_i \Big|_{y_i=L_i} - \frac{G_i}{D S_i (L_i)} \quad (114)$$

$$\text{for } 0 \leq t \leq \frac{T}{2}, \quad i = 1, 2$$

and,

$$\left. \frac{\partial F_i}{\partial y_i} \right|_{y_i=L_i} = - \frac{\dot{Q}_i}{D S_i (L_i)} F_i \Big|_{y_i=L_i} - \frac{G_i}{D S_i (L_i)} \quad (115)$$

$$\text{for } \frac{T}{2} < t \leq T, \quad i = 1, 2$$

where,

$$G \equiv G_1 + G_2 \quad (116)$$

The solutions to equation (105) corresponding to the above boundary conditions (i.e. equations (114) and (115) ), and for various combinations of  $\dot{Q}_i$  and  $G_i$  ( $i = 1,2$ ) are presented in figures 45 (a to f) and 46 (a to f). These figures are for a hypothetical gas having a diffusion coefficient of  $0.25 \text{ cm}^2/\text{sec}$  (equivalent to  $\text{O}_2/\text{N}_2$ ). The actual values of  $G_i$  ( $i = 1,2$ ) and  $\dot{Q}_i$  ( $i = 1,2$ ) considered can be found by reference to table 15. On examining these curves it is clear that the higher the  $G_i$  ( $i = 1,2$ ) value, the greater the steeper the concentration gradients for the input gas in the acinus and the lower the alveolar gas concentration level in agreement with the results already presented in figure 14 (chapter 3). It should again be noted that apart from these main observations, the 'secondary features' outlined in the last section reapply in the case of the present simulations (i.e. points (i) to (v) ).

On modifying the existing 'regional' model analysis slightly to allow for the simulation of the tracer gases Argon and Nitrous Oxide, the results presented in figures 47 (a to f) and 48 (a to f) were obtained. As anticipated, greater end expiratory input gas concentration gradients exist in the acinus for Nitrous Oxide (this is more readily apparent from figures

47 (a to f)). Similarly, the single-breath input gas washout tests for these two tracer gases given in figures 48 (a to f) demonstrate a significantly greater phase III slope for Nitrous Oxide again reflecting conditions within the lung and concurring with the results given in section 3.4 (last chapter).

#### 4.9 Breath-Holding Studies

It has already been mentioned in section 3.7 that chronic bronchitics and emphysematics find difficulty in performing even the simplest routine respiratory maneuvres. By means of the existing 'regional' lung model analysis, it is possible to predict how a finite breath-holding time will interfere with the combined effects of *regional* and *stratified* inhomogeneities upon both the rate of approach towards gaseous equilibrium within the acinus and the phase III slope of the resulting single-breath nitrogen washout curves.

In order to allow for a finite breath-holding time the following modifications to the model equations were necessary.

#### INSPIRATION

$$F_o(0, t) = 1.0, \quad t_1 \leq t \leq \frac{T}{2} \quad (117)$$

$$F_{iA} \equiv F_{oA}, \quad t_1 \leq t \leq \frac{T}{2} \quad (118)$$

$$i = 1, 2$$

$$\left. \frac{\partial F_i}{\partial Y_i} \right|_{Y_i=L_i} = + \frac{Q_i}{D S_i (L_i)} \left. F_i \right|_{Y_i=L_i}, \quad t_1 \leq t \leq \frac{T}{2} \quad (119)$$

$i = 1, 2$

BREATH-HOLDING

$$\left. \frac{\partial F_o}{\partial Y_o} \right|_{Y_o=0} = 0.0, \quad \frac{T}{2} < t \leq T_B \quad (120)$$

$$F_{iA} \equiv F_{oA}, \quad \frac{T}{2} < t \leq T_B \quad (121)$$

$i = 1, 2$

$$\left. \frac{\partial F_i}{\partial Y_i} \right|_{Y_i=L_i} = 0.0, \quad \frac{T}{2} < t \leq T_B \quad (122)$$

$i = 1, 2$

EXPIRATION

$$\left. \frac{\partial F_o}{\partial Y_o} \right|_{Y_o=0} = 0.0, \quad T_B < t \leq T \quad (123)$$

$$F_{OA} = \frac{(\dot{Q}_1 F_{1A} + \dot{Q}_2 F_{2A})}{(\dot{Q}_1 + \dot{Q}_2)}, \quad T_B < t \leq T \quad (124)$$

$$\left. \frac{\partial F_i}{\partial y_i} \right|_{y_i=L_i} = - \frac{\dot{Q}_i}{D S_i (L_i)} \left. F_i \right|_{y_i=L_i}, \quad T_B < t \leq T \quad (125)$$

$i = 1, 2$

On carrying out the above modifications and resolving the governing pulmonary gas transport equation (105), the results given in figures 49 (a to f) through to 54 (a to f) (for a value of  $D = 0.25 \text{ cm}^2/\text{sec}$  equivalent to  $O_2/N_2$ ) were obtained. The values assumed by the physical model parameters for these latter simulations are detailed in table 16 along with a quantitative assessment of the actual predicted concentration gradients.

One may summarise *all* the results presented in figures 49 to 54 by noting the following three important features:-

- (a) For all cases considered, the end expiratory input gas concentration gradients *decrease* as the duration of breath-holding *increases*

- (b) For all the cases considered in (a) above, the corresponding phase III slopes of the single-breath nitrogen washout curves similarly *decrease* as the time of breath-holding *increases*
- (c) As breath-holding time *increases* the concentration transition (phase II) appears *earlier* in the expirate reflecting a significant *reduction* in dead space volume

All of the above three features are more marked in the present cases (i.e. when large regional inequalities in flow and volume are present), than in the *series* model simulations presented in the last chapter (section 3.7). It should also be borne in mind that the features noted in (a), (b) and (c) above are common to all tracer gases considered (i.e. SF<sub>6</sub>, Ne and He).

#### 4.10 Cardiogenic Gas Mixing Effects

Engel et al (1973) have demonstrated *marked* differences in gas mixing behaviour between *in vitro* and *post mortem* studies on canine lungs. In fact, they have suggested that the effects of heartbeat may be such as to enhance the approach towards gaseous equilibrium, amounting to as much as a four-fold increase in the value of the molecular diffusion coefficient in certain regional lung areas. This type of empirical

finding is well suited to simulation within the framework of the existing 'regional' lung model analysis, the revised governing equation now being:-

$$\frac{\partial F_i}{\partial t} = D_i \frac{\partial^2 F_i}{\partial y_i^2} + \frac{1}{S_i} \frac{S_i}{y_i} \frac{\partial F_i}{\partial y_i} - \frac{\dot{Q}_i}{S_i} \frac{\partial F_i}{\partial y_i} \quad (126)$$

$$i = 1, 2$$

where all model parameters are as described previously and  $D_i$  ( $i = 1, 2$ ) are the regional variations in the molecular diffusion coefficient due to the action of the heart.

The form of the revised boundary conditions at the alveolar walls  $y_i = L_i$  ( $i = 1, 2$ ) become:-

$$\left. \frac{\partial F_i}{\partial y_i} \right|_{y_i=L_i} = \frac{\dot{Q}_i}{D_i S_i (L_i)} \left. F_i \right|_{y_i=L_i}, \quad i = 1, 2 \quad (127)$$

The solutions to equation (105) for various values of  $D_i$ ,  $\dot{Q}_i$  and  $S_i$  ( $i = 1, 2$ ) are given in figures 55 (a to f) and 56 (a to f) and the detailed concentration values are also given in table 17. Clearly, the major factors to emerge from this latter group of model simulations may be detailed in the following manner:-

- (i) the 'overall' concentration stratification in the acinus is significantly reduced when the effects of cardiogenic gas mixing are involved.
  
- (ii) In line with (i) the phase III slopes have also been reduced indicating that there is some sort of direct relationship between the end expiratory input gas concentrations and the subsequent expired concentration curves at the mouth.
  
- (iii) The concentration transition (phase II) appears slightly later for the case of the present simulations in contrast to the larger dead space volume variations observed for breath-holding studies.

#### 4.11 DISCUSSION

The major contribution of the present chapter has been to present an exhaustive study of the combined effects of *regional* and *stratified* inhomogeneities within the context of a "multiple pathway" pulmonary gas transport model. That this "multiple pathway" model was a natural and necessary extension of the single *series* compartmental model analyses becomes self evident on perusing through any of the current review papers in the literature (Puper and Scheid, 1971; Cumming, 1974 and Pedley, 1977).

In essence, the most important finding of this chapter has been to show how, under a wide range of simulatory conditions, regional inequalities in ventilation and volume can increase *significantly* both the end expiratory acinar concentration gradients and the resulting phase III slopes of a tracer gas. Further, on examining the results in more detail, it has also been possible to differentiate between the effects of, on the one hand geometric (diffusion pathway length) variations, and on the other hand, regional inequalities in volumetric gas flow-rate, upon the efficiency of gas transport and mixing within the acinus. This *distinct* difference between 'geometric' and 'ventilatory' inequalities is most important to a full understanding of how gas mixes within the more distal regions of diseased lungs. The initial hypotheses put forward by Horsfield and Cumming (1967, 1968) and Cumming (1974) concerning

the influence of asymmetrical bronchial tree characteristics upon the gas mixing process have been put on a quantitative basis in this chapter and subsequently shown to have a substantial 'effect'.

Finally, whilst the experimental evidence purporting to support the existence of *sequential* or *asynchronous* lung emptying is well documented in the literature (Fowler, 1949; Roos et al, 1955; Sandquist et al, 1959; Shephard, 1956; Young et al, 1963, 1966; Read, 1966; Sikand et al, 1966; Milic Emili et al, 1966; Dollfuss et al, 1967; Engel et al, 1979, Mills and Harris, 1965; Bashoff et al, 1967; Hughes et al, 1968; Sutherland et al, 1968; Robertson et al, 1969 and Tsunodo et al, 1972), the present chapter has demonstrated that, nevertheless, significant phase III slopes can be produced without recourse to such *temporal* lung emptying patterns.

CHAPTER 5

A BRANCHED "PIPE" MODEL

Traditionally, models used to simulate gas transport within the lung have been based on a single one-dimensional form which represents the bronchial tree such as those presented in chapters 3 and 4 of this thesis. Now, although these "trumpet" type models can lead to a reasonably accurate description of molecular gas movements within a regular monotonically increasing branching airway system, they are nevertheless, deficient in that they are unable to account for sudden abrupt changes in terminal airways structure as indicated, for example, in the experimental findings of Hansen and Ampaya (1975). This deficiency is due mainly to the fact that the previous "trumpet" models were not considering a particular airway but rather a combination of all such airways leading in some cases to an unrealistic physical situation (see figure 57).

The obvious way to overcome this problem is to consider a particular pathway through the bronchial airways resembling as close as possible the actual geometric configuration. This is not an easy task as the tortuosity of the airways causes complex flow formations within each particular pathway (Schroter and Sudlow, 1969). It has therefore been

necessary to ignore the tortuosity of the actual airway system and consider instead a direct pathway from the mouth to the distal air sacs (figure 58).

It is the intention of the present chapter to develop such a branched "pipe" (or pathway) model in order to obtain greater insight into the rate of approach towards gaseous equilibrium within the more distal regions of both normal and diseased lungs. In particular, this detailed pathway model will prove extremely useful in testing the predictions and verifying the conclusions of the contemporary "trumpet" type lung models developed in the previous two chapters.

### 5.1 Model Configuration

The basic form of the single pathway model (or "pipe" model) consists of a succession of right cylindrical airway pipes arranged in order of decreasing size, the dimensions of which are derived from a modified version of Weibel's Model A (Weibel, 1963) and are given in table 18. The general form of the model configuration employed in the present chapter is detailed in figure 59 and represents a detailed dual branched pathway from the carina to the distal air sacs. Clearly, this model may be extended to include any number of such branched pathways through the respiratory region *vide infra*.

## 5.2 The Governing Equations

On applying Fick's law and the conservation of mass to any of the cylindrical pipes shown in figure 60 we obtain the following set of partial differential equations describing the transport of gaseous molecules into and out of the model:-

$$\frac{\partial F_i}{\partial t} = D_i \frac{\partial^2 F_i}{\partial y_i^2} - V_i \frac{\partial F_i}{\partial y_i}, \quad i = 0, 23 \quad (128)$$

where  $F_i \equiv F_i(y_i, t)$  is the fractional concentration of input gas at distance  $y_i$  from the portal end of the relevant tube  $i$  and at time  $t$  after the start of the respiratory manoeuvre;  $V_i$  is the convective velocity of gas molecules down tube  $i$  and remains constant throughout the length of each tube and  $D_i$  is the effective diffusion coefficient with respect to tube  $i$  and assumes the value of the binary molecular diffusion coefficient in the respiratory region ( $i > 17$ ).

### 5.3 Boundary Conditions

#### Inspiratory Cycle

The inspiratory boundary conditions associated with each tube may be stated as follows:-

$$F_0 (0, t) = 1.0 \quad \text{for } t_1 \leq t \leq \frac{T}{2} \quad (129)$$

$$F_i (0, t) = F_{i-1} (L_{i-1}, t), \quad 0 < i \leq 23 \quad (130)$$

$$\text{for } t_1 \leq t \leq \frac{T}{2}$$

where  $L_i$  is the length of tube  $i$

$$F_i (y_i, 0) = 0, \quad \text{for } 0 \leq i \leq 23 \quad (131)$$

and

$$F_i (\alpha, t) = 0, \quad \text{for } 0 \leq i \leq 22 \quad (132)$$

$$t_1 \leq t \leq \frac{T}{2}$$

The revised boundary conditions (discussed in chapters 2 and 3) hold at the alveolar wall of the most distal pipe i.e.

$$\left. \frac{\partial F_{23}}{\partial y_{23}} \right|_{y_{23}=L_{23}} = \frac{V_{23}}{D_{23}} \left. F \right|_{y_{23}=L_{23}} \quad (133)$$

$$\text{for } t_1 \leq t \leq \frac{T}{2}$$

Taking the Laplace Transform of both sides of equation (128) yields

$$D_i \frac{d^2 F_i}{dy_i^2} - V_i \frac{dF_i}{dy_i} - p F_i = 0 \quad (134)$$

$$\text{for } 0 \leq i \leq 22$$

and where, of course,

$$F_i = \int_0^\alpha e^{-pt} F_i(y_i, t) dt \quad (135)$$

The general solution of equation (134) may be written in the form,

$$F_i = A_i \exp \left[ \frac{V_i + \sqrt{V_i^2 + 4pD_i}}{2D_i} y_i \right] + B_i \exp \left[ \frac{V_i - \sqrt{V_i^2 + 4pD_i}}{2D_i} y_i \right] \quad (136)$$

Employing the boundary conditions given in equations (129) to (133) above, we find that

$$A_i = 0, \quad 0 \leq i \leq 2 \quad (137)$$

and

$$B_0 = \frac{1}{P}, \quad B_i = \frac{F_{i-1}(0, t)}{P}, \quad 1 \leq i \leq 22 \quad (138)$$

i.e.

$$F_0 = \frac{1}{P} \exp \left[ \frac{V_0 - \sqrt{V_0^2 + 4pD_0}}{2D_0} \right] Y_0 \quad (139)$$

and,

$$F_i = \frac{F_{i-1}(0, t)}{P} \exp \left[ \frac{V_i - \sqrt{V_i^2 + 4pD_i}}{2D_i} \right] Y_i \quad (140)$$

$$1 \leq i \leq 22$$

Hence,

$$F_0(y_0, t) = \int^{-1} \frac{1}{P} \exp \left[ \frac{V_0 - \sqrt{V_0^2 + 4pD_0}}{2D_0} \right] Y_0 \quad (141)$$

and

$$F_i (y_i, t) = \int^{-1} \frac{F_{i-1}(0, t)}{P} \exp \left[ \frac{V_i - \sqrt{V_i^2 + 4pD_i}}{2D_i} y_i \right] y_i \quad (142)$$

for  $1 \leq i \leq 2_2$

On performing the inverse Laplace Transforms detailed in equations (141) and (142) above (see appendix V), we obtain the following:

$$F_0 (y_0, t) = \frac{1}{2} \left[ \operatorname{erfc} \left\{ \frac{y_0 - V_0 t}{(4D_0 t)^{\frac{1}{2}}} \right\} + \exp \left\{ \frac{y_0 V_0}{D_0} \right\} \operatorname{erfc} \left\{ \frac{y_0 + V_0 t}{(4D_0 t)^{\frac{1}{2}}} \right\} \right] \quad (143)$$

for  $t_1 \leq t \leq \frac{T}{2}$

and in a similar fashion we have

$$F_i (y_i, t) = \frac{1}{2} F_{i-1} (0, t) \left[ \operatorname{erfc} \left\{ \frac{y_i - V_i t}{(4D_i t)^{\frac{1}{2}}} \right\} + \exp \left\{ \frac{y_i V_i}{D_i} \right\} \operatorname{erfc} \left\{ \frac{y_i + V_i t}{(4D_i t)^{\frac{1}{2}}} \right\} \right] \quad (144)$$

for  $1 \leq i \leq 2_2$

The input gas concentrations down the last tube of the model pathway are calculated using a previously derived explicit finite difference solution technique (Scrimshire et al, 1978) and the relevant boundary conditions.

### Expiratory Cycle

Due to the nature of the boundary conditions holding during expiration (in the present model configuration) it was not possible to obtain an exact analytical solution to the governing pulmonary gas transport equations. Thus, it was again necessary to resort to a previously derived numerical solution technique (Scrimshire et al, 1978). The application of this technique within the context of the present branched "pipe" model configuration is outlined in appendix VI.

The boundary conditions applying during expiration may be stated in the form:-

$$\left. \frac{\partial F_o}{\partial y_o} \right|_{y_o=0} = 0 \quad \text{for} \quad \frac{T}{2} < t \leq T \quad (145)$$

$$F_i(0, t) = F_{i-1}(L_{i-1}, t), \quad 1 \leq i \leq 22 \quad (146)$$

$$\text{for} \quad \frac{T}{2} < t \leq T$$

and once again the revised boundary conditions hold at the distal alveolar wall of the last pipe, i.e.

$$\left. \frac{\partial F_{23}}{\partial Y_{23}} \right|_{Y_{23}=L_{23}} = - \frac{V_{23}}{D_{23}} F_{23} \left. \right|_{Y_{23}=L_{23}} \quad (147)$$

$$\text{for } \frac{T}{2} < t \leq T$$

#### 5.4 Comparison of the "trumpet" and "pipe"

##### Model predictions

It is of interest to compare the predictions of the contemporary "trumpet" (single series compartmental) type lung models developed in chapter 3 with those of the present single "pipe" (single pathway) models in order to test the accuracy of the "combined airways" approximation. Figure 61 clearly demonstrates that the input gas penetrates further into the model when the present "pipe" configuration is employed. Further, there are greater end inspiratory and end expiratory concentration gradients within the pipe model. However, the most important feature to note on closely scrutinising the curves given in figure 61 is the fact that the "combined airways" approximation affords a realistic simulation of pulmonary gas transport (see also appendix VII).

The resulting single-breath nitrogen washout curves corresponding to both the "trumpet" and the "pipe" models are compared in figure 62 and indicate slightly increased phase III values for the existing "pipe" model configuration accounting for the corresponding small differences in stratified inhomogeneity already observed (see table 19).

#### 5.5 Comparison of the regional "trumpet" and regional "pathway" model predictions

The real impetus behind the present "branched pathway" model development was not just to simulate behaviour in the normal state but to estimate the influence of small airways disease upon the rate of approach to gaseous equilibrium in the acinus. Thus, the original model configuration was extended to include a *dual* pathway through the respiratory region beginning at generation 17 (nodal point A in figure 59) and ending at the terminal air sacs (gen. 23). The choice of a *dual* pathway was taken solely for ease of illustration, but the model can be extended to include any number of such regional pathways, *vide infra*.

Solutions to equation (128) in the model configuration of figure 59 are presented in figures 62 (a to f) and for the specific  $\dot{Q}_i$  ( $i = 1, 2$ ) and  $V_i$  ( $i = 1, 2$ ) values detailed in table 20. It is clear from these curves that greater end

expiratory acinar input gas concentration gradients are associated with more *marked* regional flow differences. For example, when  $\dot{Q}_1/\dot{Q}_2 = 125.0/125.0$  and  $V_1/V_2 = 3.0/3.0$  the end expiratory input gas concentration gradient is 0.44%, whereas, when  $\dot{Q}_1/\dot{Q}_2 = 125.0/125.0$  and  $V_1/V_2 = 1.0/4.0$  this gradient increases to 0.99%.

It should also be noted that in the region adjacent to the branch point significant 'local' stratification is present and this will also contribute to the subsequent expired concentration curve at the mouth. The sensitivity of the single-breath nitrogen washout curve to such  $\dot{Q}_i/V_i$  ( $i = 1,2$ ) variations is clearly demonstrated in figures 63 (a to f). Essentially two observations are noted on closely scrutinising these curves, i.e.

- (i) *steeper* phase III slopes are associated with more *marked* regional flow differences reflecting the already observed *steeper* stratified concentration gradients (see table 20). For example, when  $\dot{Q}_1/\dot{Q}_2 = 125.0/125.0$  and  $V_1/V_2 = 3/3$  the phase III slope was only 2.51% (on extrapolating to 500 mls expired), whereas, when  $\dot{Q}_1/\dot{Q}_2 = 125.0/125.0$  and  $V_1/V_2 = 1.0/4.0$  the corresponding phase III slope was 6.72% (see table 20).

- (ii) the phase III (concentration transition) appears slightly later (reflecting a small increase in dead space volume) for more *marked* regional flow differences.

Please note that the above observations ( (i) and (ii)) were also noted in the last chapter (figures 33 to 40).

Although the model given in figure 59 is certainly an improvement over that of the 'single pathway' analyses it still fails to take into account the known assymetrical bronchial pathway length characteristics. However, these characteristics are readily amenable to simulation within the framework of the existing branched model (similar in many respects to the variable diffusion pathway length model of the last chapter). On re-solving equation (128) when taking these assymetrical characteristics into account the results given in figures 64 (a to f) were obtained. Closely scrutinising these curves and comparing them with those previously given in figures 62 (a to f), it can be seen that, in all cases considered, there are greater end expiratory input gas concentration differences when the diffusion pathway length varies simultaneous with more *marked* regional flow differences. For example, on singling out those cases cited earlier, it is found that when  $\dot{Q}_1/\dot{Q}_2 = 125.0/125.0$  and  $V_1/V_2 = 1.5/4.0$  the end expiratory concentration gradient is 0.7% whilst with  $\dot{Q}_1/\dot{Q}_2 = 200.0/50.0$  and  $V_1/V_2 = 1.5/3.5$

the corresponding value is 1.48% which amounts to as much as a 50% increase in gradient. Once again the degree of the concentration gradient adjacent to the nodal point A has also increased.

Comparing the single-breath nitrogen washout curves given in figures 63 (a to f) and 65 (a to f) (corresponding to 'constant' and 'variable' branched pathways respectively) the following major differences will be noted:-

- (a) the phase III slopes given in figures 65 (a to f) are, in all instances, substantially greater than those given in figures 63 (a to f) (see table 20) reflecting the already observed greater differences in concentration gradient
- (b) in all cases the appearance of the concentration transition (phase II) is slightly delayed in the latter curves (figures 65 (a to f) ).

The above two observations were also noted in chapter 4 and quantify the predictions of Horsfield and Cumming (1967, 1968) and Cumming (1974) that the assymetry of the human bronchial tree may well influence the gas mixing behaviour in the acinus.

## 5.6 DISCUSSION

The present 'branched pathway' analysis of gas transport through the bronchial airways departs from the traditional modelling approach in that a detailed pathway from the carina to the distal air sacs has been considered. The results obtained when using such a model and when employing a somewhat modified form of the revised boundary conditions (as presented in chapters 3 and 4) agree *very closely* with the predictions of contemporary "trumpet" model analyses. Further, the corresponding *very close* alignment of results as obtained from the regional "trumpet" and regional "pathway" (or 'pipe') model analyses strongly supports the accuracy of the underlying physical model approximation common to all contemporary derivations namely, that of the 'combined airways' approximation.

All the results thus far presented (i.e. those of chapters 3, 4 and 5) have been for a constant value of the molecular diffusion coefficient ( $D = 0.25 \text{ cm}^2/\text{sec}$  for  $\text{O}_2/\text{N}_2$ ;  $D = 0.76 \text{ cm}^2/\text{sec}$  for  $\text{He}/\text{N}_2$ ;  $D = 0.315 \text{ cm}^2/\text{sec}$  for  $\text{Ne}/\text{N}_2$ ;  $D = 0.1 \text{ cm}^2/\text{sec}$  for  $\text{SF}_6/\text{N}_2$  and  $D = 0.192 \text{ cm}^2/\text{sec}$  for  $\text{Ar}/\text{N}_2$ ). Whilst this latter approximation is acceptable for the more distal airway units (where the convective flow of gas is so low as to exclude any dispersion effects) the same cannot be said for the larger airways where complex flow formations are known to occur (Schroter and Sudlow, 1969).

It has been generally accepted that longitudinal gas dispersion can be characterised by molecular diffusion in the alveolar ducts and sacs. Longitudinal dispersion in the upper airways (first few generations) is about three orders of magnitude greater. However, the relevant role of difference physical dispersive factors is not well known and, until recently, the Taylor-Aris equation (Taylor, 1953; Aris, 1956) for axial dispersion of a gas in fully developed laminar flow (mean velocity  $v$ ) in a circular pipe (radius  $d$ , length  $L$ ) was used, i.e.

$$D_{\text{eff}} = D_{\text{mol}} + \frac{d^2 v^2}{48D} \quad (148)$$

More recently, Scherer et al (1975) have obtained empirical equations for axial dispersion of a gas flowing through a five generation glass model of the upper bronchial airways. These authors found that the effective diffusion coefficient ( $D_{\text{eff}}$ ) was given by,

$$D_{\text{eff}} = D_{\text{mol}} + 1.08 v d \quad (149)$$

for inspiration, and

$$D_{\text{eff}} = D_{\text{mol}} + 0.37 d v \quad (150)$$

for expiration.  $D_{\text{mol}}$  is the molecular diffusion coefficient,

$v$  the mean axial velocity of gas molecules and  $d$  the airway diameter of the relevant generation.

Solutions of equation (128) have been analysed when the effective diffusion coefficient assumed the following form:-

$$D_i = D_{mol} + \frac{d_i^2 v_i^2}{48 D_{mol}}, \quad t_1 \leq t \leq T \quad (151)$$

and

$$D_i = D_{mol} + 1.08 d_i v_i, \quad t_1 \leq t \leq \frac{T}{2} \quad (152)$$

$$D_i = D_{mol} + 0.37 d_i v_i, \quad \frac{T}{2} < t \leq T \quad (153)$$

and where  $d_i$  is the diameter of generation  $i$ .

The calculations indicated that the *net* effect of *axial dispersion* is *small*, and that molecular diffusion remains the decisive factor in limiting gas transport through the lung. Closer inspection of the 'single pathway' model calculations clarifies why this happens. Differences in the concentration profiles produced by axial dispersion are only apparent (see figures 66 and 67) during early inspiration

( $t < 0.8$  secs in a 4.0 secs breath) and early expiration ( $t = 2.0$  to  $t = 2.4$  secs). During early inspiration the concentration profile traverses those airways where axial dispersion is high ( $Z < 12$ ). Here the axial diffusion can be very large at peak flows (e.g. 200 times the molecular diffusivity) but at such times the fast flow quickly convects away the concentration differential through which the diffusion becomes effective.

In particular, the Taylor diffusivity (proportional to the flow velocity squared) becomes negligible relative to the molecular diffusion beyond the 12<sup>th</sup> generation owing to the lower flow velocity in the smaller airways (see Pack et al, 1977). Once the concentration differential passes the 12<sup>th</sup> generation only the molecular diffusion is effective. These latter results confirm the experimental findings of Horsfield et al (1977) and Worth et al (1977) who concluded that axial dispersion has little or no effect upon the rate of gaseous mixing of the normal respiratory gases in vivo.

## CHAPTER 6

### DISCUSSION

Having developed suitable revised models of pulmonary gas transport and mixing and subsequently compared their predictions with contemporary model findings it is now necessary to re-examine the revised boundary conditions in the light of these comparisons. The present chapter therefore addresses itself to a reassessment of all the results so far presented in chapters 3, 4 and 5.

#### 6.1 Reassessment of the Revised Boundary Conditions

The major criticism levelled at the contemporary "trumpet" model analyses, as discussed in chapter 2, was concerned with the boundary conditions imposed at the distal ends of such models. In fact, two independent explanations why the conventionally assumed boundary conditions caused a rapid equilibration of input gas concentrations during early expiration were put forward, namely

- (i) In order to ensure that the total flux was zero at the alveolar wall, it was necessary to specify the boundary condition  $\left. \frac{\partial F}{\partial y} \right|_{y=L} = 0.0$  in both *rigid* and

*compliant* "trumpet" models. However, since some

95 per cent of the lung volume is contained within the terminal generations of the bronchial tree (a linear distance of only 0.2 cms) it was hardly suprising that the contemporary models failed to display any stratified inhomogeneities in the acinar region because of this explicit assumption. Further, it was clearly inappropriate to specify the boundary condition in terms of a *fixed* concentration gradient at the alveolar wall, since it was the change in concentration gradient immediately adjacent to this alveolar wall that was the main purpose of the contemporary model simulations.

(ii) The imposition of the *zero gradient*  $\left. \frac{\partial F}{\partial y} \right|_{y=L} = 0.0$

boundary condition at the distal end of *rigid* models (Baker et al, 1974; Paiva, 1973 and Pedley, 1970) did not specify a true *no flux* condition for the transport of insoluble tracer gases. The *artefact* caused by the violation of this required no-flux condition at the alveolar wall (i.e. the "sink" and "source" effects) was then held responsible for the unrealistically rapid approach to gaseous equilibrium.

Ideally, it would be most advantageous to know which of the above two physical phenomena has the more dominant influence upon the phase III slope of the single-breath nitrogen

washout curve. Having stated the objective in this manner it is now necessary to examine in some detail each of the above possibilities.

## 6.2 Results for non "trumpet"/"thumbtack" models

It is interesting to speculate how physical model geometries other than those of the usual "trumpet" or "thumbtack" shape will influence the rate of approach towards gaseous equilibrium within the acinus. Clearly, these results will indicate whether the second explanation given above is specific to the case of the "trumpet" shape or applies to all geometrical boundaries.

The actual model geometries considered may be described mathematically as follows:-

$$S(y) = a_n y^n + b_n, \quad 0 \leq y \leq L \quad (154)$$

subject to the conditions,

$$S(0) = S_0 \quad (155)$$

and

$$\int_0^L S(y) dy = V_L \quad (156)$$

where,  $S_0$  is the total cross-sectional area of the portal end of the respective model and  $V_L$  is the lung volume (F.R.C.).

Thus, in more precise terms  $S(y)$  may be written in the form,

$$S(y) = \frac{(n+1)(V_L - L S_0)}{L^{n+1}} y^n + S_0 \quad (157)$$

The solutions of the pulmonary gas transport equation in which  $S(y)$  follows the functional forms given in equation (157) (for values of  $n = 1, 2, 3, 4, 5$  and  $6$ ) and for both the conventional and revised boundary conditions are given in figures 68 and 69.

On comparing both the end inspiratory and end expiratory concentration/distance profiles corresponding to each of the conventional and revised model predictions it becomes apparent that although the *artefact* caused by the violation of the "no flux" condition does have an "effect" on the shape of these profiles, it is not as significant as when the "trumpet" model configuration is employed.

The variable determining how influential the violation of the "no flux" condition can be in determining the rate of approach towards gaseous equilibrium within the acinus is not  $S(y)$

but  $\frac{dS}{dy} = S'(y)$ , i.e.

$$S'(y) = \frac{n(n+1)(V_L - LS_O)}{L^{n+1}} y^{n-1} \quad (158)$$

Now,

$$S'(L) = \frac{n(n+1)(V_L - LS_O)}{L^2} \quad (159)$$

and since  $\frac{(V_L - LS_O)}{L^2}$  is a constant common to all model simulations we know that as  $n$  increases  $S'(L)$  increases and hence the violation of the "no flux" condition has a more pronounced effect.

### 6.3 Effects of considering negative 'G' values

What is now really required is a means of separating, in the present analysis, the *dynamic* influence of gas flux from the more *static* influence of the geometrical boundaries of the model. This may best be achieved by allowing for both positive and negative values of 'G' in the model simulations and observing the change, if any, in the resulting end expiratory concentration gradients, and the subsequent phase III slopes of the corresponding single-breath nitrogen washout curves.

The end inspiratory and end expiratory concentration/distance profiles for a tracer gas having a molecular diffusion coefficient of  $D = 0.25 \text{ cm}^2/\text{sec}$  (equal to  $\text{O}_2/\text{N}_2$ ) and for six values of  $G$  (i.e.  $G = -10.0, -25.0, -50.0, +10.0, +25.0, +50.0$ ) are given in figure 70. Now, on closely scrutinising these figures it will be noticed that, even for the most negative value of  $G$ , significant concentration differences (stratified inhomogeneities) exist in the acinus at end expiration (see table 21). Hence, although the "no flux" condition has been violated there are, nevertheless, significant stratified inhomogeneities in the distal regions due to the fact that the concentration gradient at the alveolar wall has not been fixed (see equation (98) ) but has been allowed to vary in such a manner as to account for the variations in 'G'.

These latter findings are more readily discernable by reference to the corresponding single-breath nitrogen washout curves shown in figure 71. The phase III slopes of all curves in these figures remain significant for all the values of  $G$  considered (see table 21). It should be noted at this stage that the above observations were common to *all tracer gas simulations* (i.e.  $\text{SF}_6, \text{He}, \text{Ne}, \text{etc.}$ )

Combining the results given in the last section with the present findings it should now be obvious that the true explanation for the failure of the contemporary model

analyses in predicting a significant phase III slope was due to the fact that the concentration gradient at the alveolar wall was being *fixed* (i.e. explanation (i) ).

#### 6.4 Bronchial Cross-Section from Lung Gas Washout - The Inverse Problem

A further means of discriminating between the above two explanations (i.e. (i) and (ii) ) is to approach the problem from an alternative and perhaps more attractive way. By utilising certain known characteristics of the airway mixing process it is possible to obtain an equation relating total bronchial tree cross-sectional area to the washout nitrogen concentration, and then subsequently infer from this relation the type of boundary condition likely to hold at the distal ends of the "trumpet" models.

Numerical solution of the pulmonary gas transport equation (equation (7) ) has revealed two important characteristics of the gas mixing process in the airways.

The first is the presence of an almost stationary state

(  $\frac{\partial F}{\partial t} \approx 0$  ) for the concentration profile near the end of a steady flow inspiration of  $O_2$  for breathing frequencies less than about  $40 \text{ min}^{-1}$ , (Scherer et al, 1972; Paiva, 1973;

Pack et al, 1977; Paiva et al, 1976 and Scrimshire et al, 1978). This stationary state has also been demonstrated experimentally during the inspiration of oxygen by direct sampling of gas from bronchioles (Engel et al, 1973).

The second characteristic of gas mixing detected by numerical simulation is the relatively small amount of mixing during expiration compared to that during inspiration. This is demonstrated in figure 72, which shows the concentration of nitrogen which would be expired at the mouth following inspiration of a single breath of oxygen as calculated by numerical solution of equation (7). Comparison of the curves obtained by including or neglecting mixing during expiration indicates that the effect of mixing during expiration is small, leading to a shift of the curve to the left by less than 5% of the inspired tidal volume. The computations shown in figure 72 were done assuming  $D$  equal to the molecular diffusivity, since previous work (Pack et al, 1977; Chang, 1976 and Scrimshire et al, 1978) has shown that the effect of convective dispersion on the shape of the  $N_2$  washout curve is small. It appears, therefore, that nitrogen can be considered to be convected out of the lung during expiration in the single-breath nitrogen washout test without significant additional mixing with the inspired oxygen. This fact suggests that, to a good approximation, the nitrogen concentration profile washed out during expiration, if expressed as a function of expired,

volume, represents the stationary nitrogen concentration profile in the airways at the end of inspiration as a function of cumulative airway volume.

It is now possible to utilise these characteristics of the airway mixing process to obtain an equation relating total bronchial tree cross-section to the washout nitrogen concentration profile.

Consider a single breath of oxygen inhaled into a lung initially containing a constant  $N_2$  concentration. Assuming that a stationary state exists at the end of inspiration and that the resulting nitrogen concentration gradient is *convected* out of the lung during expiration *without* further mixing, the nitrogen profile to be convected out is given as a solution of the equation,

$$v \frac{\partial F}{\partial y} = \frac{1}{S} \frac{\partial}{\partial y} (D S \frac{\partial F}{\partial y}) \quad (160)$$

where  $v$  is the gas velocity at the end of inspiration.

Introducing the transformation from linear distance  $y$  to cumulative airway volume  $V(y)$  (Butler, 1974):-

$$V(y) = \int_0^y S(\xi) d\xi \quad (161)$$

Equation (160) becomes,

$$\dot{V} \frac{dF}{dV} = \frac{d}{dV} (D S^2 \frac{dF}{dV}) \quad (162)$$

Where  $\dot{V}(t) = Sv$  is the volume flow rate at any instant over the total airway cross-section. Assuming  $\dot{V}$  to be constant during inspiration and integrating equation (162) once gives,

$$\dot{V} F - D S^2 \frac{dF}{dV} = \text{constant} \quad (163)$$

Equation (163) represents the total  $N_2$  flux ( $\text{cm}^3/\text{sec}$ ) at any point in the airway model during the stationary state. This flux must be equal to zero, since at the mouth, where pure  $O_2$  is being inspired  $F_{N_2} = 0$  and  $dF_{N_2}/dV = 0$ . Equation (163) with the constant equal to zero states that the stationary state present in the airways at the end of inspiration represents a *balance* between  $N_2$  being *convected* down the bronchial tree towards the distal alveoli and  $N_2$  tending to *diffuse* up the bronchial tree towards the mouth due to the concentration gradient (Scherer and Pack, 1977). Setting the constant in equation (163) equal to zero and rearranging gives an equation for determining total airway cross-section  $S(V)$ .

$$S = \sqrt{\left(\frac{\dot{V}}{D}\right) \left(\frac{F}{dF/dV}\right)} \quad (164)$$

Since there is no effective mixing during expiration,  $F(V)$  and  $dF/dV$  can be obtained directly from the  $N_2$  washout curve measured at the mouth during expiration.

Equation (164) has been derived using the transformation given by equation (161), where  $V$  represents the cumulative airway volume into the lung. In applying equation (164) to the expired nitrogen concentration profile, the tacit assumption is made that the first 1.5 litres of gas expired in the single breath  $N_2$  washout test represents gas which, at the end of inspiration, was contained in the airways and not in the alveoli (Scherer and Pack, 1977).

Figure 73 shows total bronchial cross-sectional areas which were computed from the expired nitrogen washout curves of three normal subjects compared with anatomical data obtained from detailed measurement post-mortem on several human lungs (see again Scherer and Pack, 1977). Agreement in shape and order of magnitude between computed and anatomical curves is reasonably good above 400 mls expired.

In calculating the total bronchial area from the nitrogen washout data, equation (164) was used, cardiogenic oscillations were neglected, and  $D$  was set equal to the molecular diffusivity ( $D_{mol}$ ) of nitrogen in oxygen. The single breath tests were carried out with a relatively constant inspired flow-rate ( $\dot{V}$  in equation (164)). To achieve this, the actual

inspired flow-rate, as measured by a pneumotachograph, was demonstrated to the subject on an oscilloscope along with a constant signal which was set at the desired flow-rate. Subjects practised keeping their flow-rate constant before definitive measurements were made. However, the expired flow-rate was not controlled. The total volume of oxygen inspired by the subject was measured and, from knowledge of this and their measured residual volume, the lung volume at end inspiration was calculated. This allowed the computed areas to be corrected to the same lung volume at which the anatomical measurements were made (4.8 L), assuming that total bronchial cross-sectional area is proportional to total lung volume to the 2/3 power (Hughes et al, 1972). For the curves presented in figure 73, the correction was small, being less than 8% in each case.

In using equation (164) to compute airway cross-section from an experimental washout curve, the question arises as to what functional form to use for  $D$ , the effective diffusivity. Different forms of effective diffusivity have been used in modelling mass transport in the airways to account for the gas mixing related to the combined actions of convection and axial and radial diffusion (Pack et al, 1977 and Scrimshire et al, 1978). Scherer et al (1975) obtained an effective diffusivity from measurements in a physical model of the airways, i.e.

$$D = D_{\text{mol}} + 1.08 v d \quad (165)$$

whereas others (Pack et al, 1977; Chang, 1976 and Scrimshire et al, 1978) have used the formulation of Taylor (1953) for steady laminar flow:-

$$D = D_{\text{mol}} + \frac{v^2 d^2}{192 D_{\text{mol}}} \quad (166)$$

The effects of employing these different values of D in equation (164) is shown in figure 74. In these cases, v was set equal to  $\dot{V}/S$  and d was assigned the constant value of 0.05 cms, which is typical of the diameter of airway generations at and beyond generation 17 according to measured anatomical data. The rationale for using this value for d is that the *stationary* N<sub>2</sub> profile at end inspiration is located in this region of the airway structure. The change in computed area resulting from employing the above values of effective diffusivity (equations (165) and (166) ) is seen to be very small.

The fact that equation (164) gives a good estimate of S(V) implies that the *slope* of the *alveolar plateau* is due largely to *diffusion gradients* in the distal airways rather than to a distribution of transit times from well-mixed compartments emptying in parallel. This can be demonstrated more rigorously in the following way:-

From equation (161) we have that

$$\frac{dF_{N_2}}{dy} = S \frac{dF_{N_2}}{dV} \quad (167)$$

and since all of the experimental curves yield significant phase III slopes, then  $\frac{dF_{N_2}}{dV} > 0$  and similarly  $\frac{dF_{N_2}}{dy} > 0$

indicating that diffusion gradients *must* be present in the acinar region and *must* subsequently contribute to the expired phase III slope.

Conversely, if we use the contemporary model predictions, i.e. that  $dF/dV = 0$  and substitute into equation (164) of the present chapter we find that  $S = \infty$  violating the inherent assumption, of all models, i.e. that of finite geometrical boundaries. Thus, the fact that a sloping phase III has not been observed in most of the contemporary model simulations could well be due to the fact that the *boundary conditions* usually used, i.e. impermeability or  $\left. \frac{\partial F}{\partial y} \right|_{y=L} = 0.0$  at the alveolar wall of the single path model, *force* the alveolar plateau to be almost *flat* in the alveolar region.

The assumptions necessary for equation (164) to hold for the single-breath  $N_2$  washout test should be kept in mind. They are: (a) that the multiple pathways can be adequately described by the average single series "trumpet" pathway model; (b) that a stationary state exists at the end of

inspiration, representing a *balance* between the *forward* convection of nitrogen down the bronchial tree and the *backward* diffusion of nitrogen from the alveolar region up the bronchial tree towards the mouth; (c) that the resulting concentration profile is convected out of the lung during expiration with very little further mixing; and (d) that the first 1.5 litres of gas expired were contained in airways at the end of inspiration rather than in the alveoli.

Assumption (a) has been used by several authors (Scherer et al, 1972; Paiva, 1973; Baker et al, 1974; Pack et al, 1977 and Scrimshire et al, 1978) in deriving equation (160). It represents a considerable simplification of the multipath bronchial geometry, but has yielded much new and *valuable insight* into the airway convection-diffusion process.

Assumption (b) has been confirmed experimentally (Engel et al, 1973) and numerically (Paiva, 1973 and Paiva et al, 1976) for certain regions of the bronchial tree. Numerical studies (Paiva, 1973 and Paiva et al, 1976) indicate, however, that if the inspiratory flow is not perfectly steady, then a quasi-steady state is not established for the nitrogen concentration profile closest to the mouth. In this region, nitrogen continues to diffuse back towards the mouth faster than convection can carry it forward. This results in a decrease in  $dF/dV$  below the value consistent with a stationary state. The resulting

increase in  $S(V)$  as computed from equation (164) probably explains the lack of agreement between the computed curves and anatomical data for expired volumes of less than 0.4 litres (see figure 73). Additional numerical studies using equation (164) will provide further information on this point and will enable a correction to the computed area curve for a volume of less than 0.4 litres to be developed.

Assumption (c) is suggested by the numerical computations shown in figure 72 and by some physiological studies (Bouhuys, 1974) which show that the shape of the single breath  $N_2$  washout curve is insensitive to the expiratory flow rate. Gas dispersion measurements in a physical model of the upper bronchial generations (Scherer et al, 1975) have also shown less gas mixing (by a factor of 1/3) during expiration compared to inspiration. Additional gas mixing on expiration would tend to flatten the alveolar plateau, which would lead, on using equation (164), to an overestimate of peripheral airway total cross-section.

Assumption (d) is difficult to justify directly, since the sequence of emptying of lung structures is not known. It can be inferred, however, from known anatomical measurements that the cumulative airway volume, neglecting the alveoli, is about 1.6 litres at 75% of total lung inflation. The agreement in order of magnitude shown in figure 71 between the computed total bronchial area and that from anatomic measurements suggests that assumption (d) is reasonably correct.

\* Weibel

Summarising the above information it may be said that the relationship between total bronchial cross-sectional area and cumulative airway volume given by equation (164) represents the end result of combining recent evidence from both numerical and experimental studies on gas mixing in the lung. Instead of solving the governing pulmonary gas transport equation (equation (7) ) by specifying  $S(y)$  and boundary and initial conditions (as done in chapters 3, 4 and 5), one uses the "solution" of the equation which is provided by the measured expired nitrogen concentration profile to calculate  $S(V)$  (i.e. the *inverse problem*). This method of determining bronchial area may be especially useful in obtaining information about the smaller, more peripheral airways where many pathological processes first appear (Scherer and Pack, 1977).

#### 6.5 Equivalent Asynchronous Emptying

The question now arises as to the *uniqueness* of the results presented in chapters 4 and 5, i.e. could *equivalent* results be produced without recourse to the revised boundary conditions. This question is best answered by means of a simple mathematical analysis.

Considering again the form of the parallel "trumpet" model given in figure 32 only the following two situations are worthy of some attention, namely

- (1) When the regional volumetric flow-rates down the parallel compartments are constant (i.e. not time varying) and the revised boundary conditions hold at the distal alveolar walls, then the internal boundary condition holding at nodal point A assumes the form,

$$\frac{\dot{Q}_1 F_1(t) + \dot{Q}_2 F_2(t)}{(\dot{Q}_1 + \dot{Q}_2)} \quad (168)$$

- (2) When the conventionally assumed boundary conditions are holding at the distal alveolar walls of the parallel compartments, then in order to achieve an *equivalent* concentration/time variation to that given in equation (168) it is necessary to vary the regional flow-rates such that the internal boundary condition holding at nodal point A becomes

$$\frac{\dot{Q}_1(t) F_1 + \dot{Q}_2(t) F_2}{\dot{Q}_1(t) + \dot{Q}_2(t)} \quad (169)$$

In effect, equations (168) and (169) define an *equivalence relationship* between the revised regional model of chapter 4 and a hypothetical (but deterministic) *complete mix* asynchronous model. Such asynchronous emptying lung models have already been examined by Young et al (1963); Young and Martin (1966) and Tsunoda et al (1972).

Extending the above development to the general case of n parallel compartments it should now be obvious that the following form of *equivelance* relation obtains at nodal point A:-

$$\frac{\sum_{i=1}^n \dot{Q}_i F_i (t)}{\sum_{i=1}^n \dot{Q}_i} = \frac{\sum_{i=1}^n \dot{Q}_i (t) F_i}{\sum_{i=1}^n \dot{Q}_i (t)} \quad (170)$$

It would appear from the above considerations that the revised boundary conditions initially given in chapter 2 not only provide for a more realistic simulation of pulmonary gas transport and mixing but also allow for a *link* between *series* and *parallel* model predictions.

### 6.6 Nitrogen Retention Test - "Stationary Interface"

The single-breath nitrogen retention curve is obtained by plotting the expired nitrogen volume against the total expired volume of gas at any particular time t during a single-breath expiratory maneouvre.

If a single-breath of oxygen of defined size enters a lung of known volume and is then perfectly mixed it is simple to predict the volume of nitrogen which would be recovered in an expirate of any given size, namely:-

If  $V_L$  is the initial lung volume,  
and  $V_{DS}$  is the assumed anatomical dead space volume,  
and  $V_T$  is the tidal volume entering the lung,  
then the concentration of nitrogen at the end of inspiration  
in "alveolar air" will be,  $C_1$ , where

$$C_1 = \frac{V_L + (V_T - V_{DS})}{V_L} \times C_0 \quad (171)$$

Since the oxygen is perfectly mixed we know that the amount  
of nitrogen expired will be constant (see figure 75) and  
is given by,

$$C_1 \times (V_T - V_{DS}) = V_{N_2} \quad (172)$$

where  $V_E(t)$  is the total volume of gas expired after time  $t$ .  
Note that we are assuming an 80%/20%  $N_2/O_2$  mixture in the  
above derivation.

In the more general case of incomplete diffusive mixing  
(such as the cases considered in chapters 3, 4 and 5) we have  
the following situation:-

Let  $F_{N_2}(t)$  represent the theoretical "trumpet" model expired  
nitrogen concentration at time  $t$  and let  $\dot{Q}(t)$  be the  
corresponding rate of flow at the same instant in time. Then

the expired nitrogen volume at this particular time  $t$  will be given by

$$V_{N_2} = \int_0^t \dot{Q}(t) F_{N_2}(t) dt \quad (173)$$

and, of course

$$V_E = \int_0^t \dot{Q}(t) dt \quad (174)$$

By comparing the single-breath nitrogen retention curves predicted on the basis of the perfectly mixed model (see figure 76) and the imperfectly mixed "trumpet" model we can determine the effectiveness of gas mixing in terms of a *percentage deficiency* for both normal and diseased subjects. This percentage deficiency in gas mixing after an expired tidal volume of  $V_T$ , is defined as,

$$\frac{C_1 \times V_E(t) - \int_0^t \dot{Q}(t) F_{N_2}(t)}{V_T} \quad (175)$$

and the normal value is about 20% which may rise to 75% in advanced disease.

After suitably modifying the "series" and "parallel" trumpet model analyses to allow for the simulation of the single breath nitrogen retention curve, the results given in figure 77 were obtained. These results are for a simulated normal (see chapter 3) and a simulated "average case of emphysema", (see chapter 4) and are compared with the "ideal" instantaneously mixed model predictions. On examining table 22, it will be found that the predicted *percentage deficiencies* in these cases are 19.66% for the normal and 29.4% for the "average case of emphysema" in very good agreement with the expected values. These differences in the percentage deficiencies may be explained in the following way:- as the inspired gas traverses the bronchi it's linear velocity falls progressively as the bronchial cross section increases. Somewhere in the region of the respiratory bronchioles the velocity due to mass flow becomes equal to the velocity due to diffusion down a concentration gradient so that beyond this point mass flow ceases and gas molecules are transported solely by diffusion.

At this point there exists an *interface* between the gas being inspired and that in the alveoli which remains in a fixed position so long as the inspired flow rate is constant. This has been designated the stationary interface position (Paiva, 1978). As new molecules of inspired gas arrive at the *stationary interface* they enter it and diffuse through it,

so changing the distal airways concentration but not affecting the position of the interface in the airways, so long as the inspired flow rate remains constant. It is possible to determine the exact location of this stationary interface point within the bronchial airways by making some simple assumptions.

Considering once again the governing pulmonary gas transport equation, i.e.

$$\frac{\partial F}{\partial y} = D \left[ \frac{\partial^2 F}{\partial y^2} + \frac{1}{S} \frac{\partial S}{\partial y} \frac{\partial F}{\partial y} \right] - \frac{\dot{Q}}{S} \frac{\partial F}{\partial y} \quad (176)$$

we know that at the stationary interface point the gradient of input gas concentration is a maximum:-

$$\left. \frac{\partial F}{\partial y} \right|_{y=a} \quad \text{is maximum} \quad (177)$$

where 'y = a' is the actual location of the stationary interface point. It should now be obvious that what we are actually searching for is in fact the point of inflexion which leads to the additional constraint of

$$\left. \frac{\partial^2 F}{\partial y^2} \right|_{y=a} = 0 \quad (178)$$

Substituting equations (177) and (178) into equation (176) yields,

$$\left. \frac{\partial F}{\partial t} \right|_{y=a} = \left\{ \frac{D}{S} \frac{\partial S}{\partial y} - \frac{\dot{Q}}{S} \right\} \left. \frac{\partial F}{\partial y} \right|_{y=a} \quad (179)$$

Finally, once the stationary interface point is reached there is no appreciable concentration change with time implying that to a first approximation

$$\left. \frac{\partial F}{\partial t} \right|_{y=a} = 0$$

Hence, equation (179) becomes

$$\left\{ \frac{D}{S} \frac{\partial S}{\partial y} - \frac{\dot{Q}}{S} \right\} \left. \frac{\partial F}{\partial y} \right|_{y=a} = 0 \quad (180)$$

and therefore

$$\left. \frac{\partial S}{\partial y} \right|_{y=a} = \frac{\dot{Q}}{D} \quad (181)$$

Equation (181) demonstrates clearly that the position of the stationary interface point depends solely upon  $S$ ,  $\dot{Q}$  and  $D$ .

It is intuitively obvious that the idea of a *single* stationary interface point may be extended to the more general case of a *distribution* of such stationary interface points (such as would obtain within an n compartmental "trumpet" model). The location of these points will depend mainly upon the regional flow-rates  $\dot{Q}_i$  ( $i = 1$  to  $n$ ) and of course the diffusion pathway lengths  $l_i$  ( $i = 1$  to  $n$ ). Thus, equation (181) will now become,

$$\left. \frac{\partial S_i}{\partial y_i} \right|_{y_i = a_i} = \frac{\dot{Q}_i}{D}, \quad i = 1 \text{ to } n \quad (182)$$

where,  $a_i$ , are the actual locations of the stationary interface points within each of the parallel "trumpet" configurations.

Now, the differences in the percentage deficiencies noted in table 22 may be related to corresponding differences in gas mixing behaviour distal to the relevant stationary interface points. In fact, it has already been demonstrated in chapters 3 and 4 that the greatest concentration drop occurs over that region distal to the stationary interface point (equivalent to nodal point A in the regional lung model).

CHAPTER 7

CONCLUSION

The present mathematical examination of pulmonary gas transport has considered the following:-

- (I) A critical assessment of the contemporary physical models
- (II) A reappraisal of the *boundary conditions* assumed in these contemporary physical models
- (III) A detailed examination of the numerical solution techniques employed by contemporary workers in solving the governing pulmonary gas transport equations
- (IV) A corresponding detailed examination of the *stability* and *convergence* criteria associated with the numerical solution techniques dealt with in (III) above
- (V) An extension of the *variable gradient* boundary condition at the distal end of the "trumpet" model to allow for a *finite flux* of gas across the alveolar membrane, thereby simulating gas exchange.

- (VI) An extension of the single *series* "trumpet" model to include *parallel* compartments
- (VII) The *combined* effects of *regional* and *stratified* inhomogeneities upon pulmonary gas transport and mixing in both normal and diseased lungs.
- (VIII) The development of an *assymetrical* "series-parallel" "trumpet" model to allow for the simulation of varying diffusion pathway length characteristics
- (IX) The development of the "pipe" (or branched pathway) model to test the accuracy of the "trumpet" model predictions.

Having now detailed the mathematical improvements made to the contemporary gas transport model analyses, it is next required to state any conclusions drawn, based on these improved model predictions, i.e.

- (1) A true "no flux" condition *is specified* by means of the revised boundary conditions
- (2) The phase III slope (alveolar plateau slope) appears to be due to failure of the input gas to reach equilibrium during the expiratory cycle, and may be related directly to the *variable gradient* boundary conditions holding at the alveolar wall of the trumpet model.

- (3) Increased phase III slopes are associated with heavier tracer gases and consequently increased stratified inhomogeneities.
- (4) Gases of higher solubility display both a more marked concentration stratification and an increased phase III slope
- (5) *Rigid* and *compliant* model predictions for *low* tidal ventilations are virtually identical
- (6) Regional inequalities of ventilation cause an increase in end expiratory stratified inhomogeneities together with a corresponding increased phase III slope
- (7) Simultaneous regional inequalities in ventilation and gas flux *further* increase the end expiratory concentration gradients and the subsequent phase III slope
- (8) Regional differences in diffusion pathway length can cause slight differences in the dead space volume (i.e. the appearance of phase II)
- (9) Regional differences in diffusion pathway length increase the end expiratory acinar input gas concentration differences over and above those observed in (6) above

- (10) The concentration gradients adjacent to nodal point A (i.e. local stratifications) increase for similar increases in either ventilation inequality or diffusion pathway length variation
  
- (11) The single "branched pathway" model verifies the accuracy of the single series "trumpet" model predictions
  
- (12) The multiple "branched pathway" model verified the accuracy of the multiple compartment "trumpet" model predictions

CHAPTER 8

FUTURE WORK

The most important area of future work must be the extension of the proposed *series* and *parallel* models to allow for more realistic estimates of the uptake of a soluble tracer gas during a single-breath manoeuvre (i.e. a more realistic simulation of the effects of gas exchange across the alveolar membrane). This type of development is of *paramount* importance in the case of the regional model as it will allow for a quantitative analysis of both the *independent* and *combined* effects of ventilation ( $\dot{Q}_i$ ) and perfusion ( $G_i$ ) inequalities upon gas mixing efficiency within the acinus region of both normal and diseased lungs.

Having carried out the extensions to the models discussed above it should then be possible to simulate the important phenomena of *carbon dioxide retention*, by forcing  $G_i$  to assume negative values.

Another area demanding immediate investigation is that of the recovery of bronchial cross-sectional area distributions from single-breath washout data. Clearly, there will be a corresponding demand for more detailed experimental results in this area. In particular, there is a growing need for

some type of classification of each of the phase I, phase II and phase III slopes of single-breath washout curves recovered from patients with chronic lung disorders.

In the long term it now appears plausible that a combined lung mechanics/gas transport model will be developed. Such a model would provide greater insight into the influence of regional differences in compliance upon gas mixing behaviour within the more distal lung regions.

APPENDIX I

Gerschgorin's Theorem

The modulus of the largest eigenvalue of the square matrix A cannot exceed the largest sum of the moduli of the terms along any row or column.

Proof

Let  $\lambda_i$  be an eigenvalue of the  $N \times N$  matrix A, and  $x_i$  the corresponding eigenvector with components  $V_1, V_2, \dots, V_n$ .

Then the equation

$$A x_i = \lambda_i x_i$$

in detail, is

$$a_{1,1} V_1 + a_{1,2} V_2 + \dots + a_{1,n} V_n = \lambda_i V_1$$

$$a_{2,1} V_1 + a_{2,2} V_2 + \dots + a_{2,n} V_n = \lambda_i V_2$$

$$a_{n,1} V_1 + a_{n,2} V_2 + \dots + a_{n,n} V_n = \lambda_i V_n$$

Let  $V_s$  be the largest in modulus of  $V_1, V_2, \dots, V_n$ .

Select the  $s^{\text{th}}$  equation and divide by  $V_s$ , giving

$$\lambda_i = a_{s,1} \left(\frac{V_1}{V_s}\right) + a_{s,2} \left(\frac{V_2}{V_s}\right) + \dots + a_{s,n} \left(\frac{V_n}{V_s}\right)$$

Therefore,

$$|\lambda_i| \leq |a_{s,1}| + |a_{s,2}| + \dots + |a_{s,n}|$$

Since the eigenvalues of the transpose of A are the same as those of A the theorem is also true for columns.

Brauer's Theorem

Let  $P_s$  be the sum of the moduli of the terms along the  $s^{\text{th}}$  row excluding the diagonal element  $a_{s,s}$ . Then every eigenvalue of A lies inside or on the boundary of at least one of the circles  $|\lambda - a_{s,s}| = P_s$

Proof

By the previous proof

$$\lambda_i = a_{s,1} \left(\frac{V_1}{V_s}\right) + a_{s,2} \left(\frac{V_1}{V_s}\right) + \dots + a_{s,s} + \dots + a_{s,n} \left(\frac{V_n}{V_s}\right)$$

Hence,

$$\begin{aligned} \left| \lambda_i - a_{s,s} \right| &= \left| a_{s,1} \left( \frac{V_1}{V_s} \right) + a_{s,2} \left( \frac{V_2}{V_s} \right) + \dots + a_{s,n} \left( \frac{V_n}{V_s} \right) \right| \\ &\leq \left| a_{s,1} \right| + \left| a_{s,2} \right| + \dots + \left| a_{s,n} \right| \\ &= P_s \end{aligned}$$

Which completes the proof.

APPENDIX II

Gauss's Elimination Method

When there are  $N - 1$  internal mesh points along each time row the Crank-Nicolson equations can be written very generally as

$$b_1U_1 - c_1U_2 = d_1$$

$$- a_2U_1 + b_2U_2 - c_2U_3 = d_2$$

$$- a_iU_{i-1} + b_iU_i - c_iU_{i+1} = d_i$$

$$- a_{N-1}U_{N-2} + b_{N-1}U_{N-1} = d_{N-1}$$

where the a's, b's, c's and d's are known. The first equation can be used to eliminate  $U_1$  from the second equation, the new second equation used to eliminate  $U_2$  from the third equation and so on, until finally, the new last but one equation can be used to eliminate  $U_{N-2}$  from the last equation, giving one equation with only one unknown,  $U_{N-1}$ . The unknowns  $U_{N-2}$ ,  $U_{N-3}$  .....  $U_2$ ,  $U_1$  can then be found in turn by back-substitution. Noting that the coefficient c in each new equation is the same as in the corresponding old equation, assume that the following stage of the eliminations has been reached,

$$\alpha_{i-1} U_{i-1} - c_{i-1} U_i = S_{i-1}$$

$$- a_i U_{i-1} + b_i U_i - c_i U_{i+1} = d_i$$

where  $\alpha_1 = b_1$ ,  $S_1 = d_1$

Eliminating  $U_{i-1}$  leads to

$$b_i - \frac{a_i c_{i-1}}{\alpha_{i-1}} U_i - c_i U_{i+1} = d_i + \frac{a_i S_{i-1}}{\alpha_{i-1}}$$

$$\text{i.e. } \alpha_i U_i - c_i U_{i+1} = S_i \quad (\text{a})$$

where

$$\alpha_i = b_i - \frac{a_i c_{i-1}}{\alpha_{i-1}} \quad \text{and } S_i = d_i + \frac{a_i S_{i-1}}{\alpha_{i-1}} \quad (i = 2, 3 \dots)$$

The last pair of simultaneous equations are

$$\alpha_{N-2} U_{N-2} - c_{N-2} U_{N-1} = S_{N-2}$$

and

$$- a_{N-1} U_{N-2} + b_{N-1} U_{N-1} = d_{N-1}$$

Elimination of  $U_{N-2}$  gives

$$(b_{N-1} - \frac{a_{N-1} c_{N-2}}{\alpha_{N-2}}) U_{N-1} = d_{N-1} + \frac{a_{N-1} S_{N-2}}{\alpha_{N-2}}$$

i.e.

$$\alpha_{N-1} U_{N-1} = S_{N-1} \tag{b}$$

Equations (a) and (b) show that the solution can be calculated from

$$U_{N-1} = \frac{S_{N-1}}{\alpha_{N-1}}$$

$$U_i = \frac{1}{\alpha_i} (S_i + c_i U_{i+1}) \quad (i = N-2, N-3 \dots, 1)$$

where the  $\alpha$ 's and  $S$ 's are given recursively by

$$\alpha_1 = b_1, \quad \alpha_i = b_i - \frac{a_i}{\alpha_{i-1}} c_{i-1}$$

$$S_1 = d_1, \quad S_i = d_i + \frac{a_i}{\alpha_{i-1}} S_{i-1} \quad (i = 2, 3 \dots N-1)$$

In many problems  $\alpha_i$  and  $a_i / \alpha_{i-1}$  are independent of time and need only be calculated once, irrespective of the number of time steps.

APPENDIX III

Analytical Treatment of Convergence

Let  $F$  represent the *exact* solution of the pulmonary gas transport equation and  $F'$  the *exact* solution of the difference equations used to approximate this parabolic partial differential equation. Then the finite-difference solution is said to be *convergent* when  $F'$  tends to  $F$  as  $\delta y$  and  $\delta t$  both tend to zero.

Now,

$$e_{i,j} = F_{i,j} - F'_{i,j} \quad (i)$$

and the pulmonary gas transport equation is:-

$$F_{i,j+1} = (D - K_i) r F'_{i-1,j} + (1 - 2Dr)F'_{i,j} + (D + K_i) r F'_{i+1,j} \quad (ii)$$

Substituting from (i) into (ii) yields

$$e_{i,j+1} = (D - k_i)r e_{i-1,j} + (1 - 2Dr)e_{i,j} + (D + K_i)r e_{i+1,j} + (F_{i,j+1} - F_{i,j}) - r \left[ D (F_{i+1,j} - 2F_{i,j} + F_{i-1,j}) - K_i (F_{i+1,j} - F_{i-1,j}) \right] \quad (iii)$$

From (iii) we can see that the *total error* is due to two sources, i.e.

(a) stability, and (b) convergence

Stability has already been dealt with in chapter 2 and it is now only necessary to show that the remaining terms in (iii) vanish as  $\Delta y \rightarrow 0$  and  $\Delta t \rightarrow 0$ .

Expanding  $F_{i,j+1}$ ,  $F_{i+1,j}$  and  $F_{i-1,j}$  by means of a

Taylor series and using the Mean Value theorem, we have

$$F_{i,j+1} = F_{i,j} + k \frac{\partial F_{i,j}}{\partial t} (y, t + \mu_1 k) \quad (\text{iv})$$

$$F_{i+1,j} = F_{i,j} + h \frac{\partial F_{i,j}}{\partial y} + \frac{h^2}{2} \frac{\partial^2 F_{i,j}}{\partial y^2} (y + \mu_2 h, t) \quad (\text{v})$$

$$F_{i-1,j} = F_{i,j} - h \frac{\partial F_{i,j}}{\partial y} + \frac{h^2}{2} \frac{\partial^2 F_{i,j}}{\partial y^2} (y - \mu_3 h, t) \quad (\text{vi})$$

where  $h = \Delta y$ ,  $k = \Delta t$ ,  $0 < \mu_1 < 1$ ,

$0 < \mu_2 < 1$  and  $0 < \mu_3 < 1$ .

The expression for convergence error is

$$\begin{aligned}
 - r \left[ D (F_{i+1,j} - 2F_{i,j} + F_{i-1,j}) - K_i (F_{i+1,j} - F_{i-1,j}) \right] \\
 + (F_{i,j+1} - F_{i,j}) \qquad \qquad \qquad \text{(vii)}
 \end{aligned}$$

Substituting from equations (iv) (v) and (vi) into equation (vii) we obtain the following:-

$$\text{Convergence error} = k \frac{\partial F_{i,j}}{\partial t} (y, t + \mu_1 k)$$

$$- r \left[ D h^2 \frac{\partial^2 F_{i,j}}{\partial y^2} (y + \mu_4 h, t) - K_i h^2 \frac{\partial F_{i,j}}{\partial y} \right] \qquad \qquad \qquad \text{(viii)}$$

with  $-1 < \mu_4 < 1$

However,

$$r h^2 = k \qquad \qquad \qquad \text{(ix)}$$

hence,

$$\text{Convergence Error} = k \left[ \frac{\partial F_{i,j}}{\partial t} (y, t + \mu_1 k) - D \frac{\partial^2 F_{i,j}}{\partial y^2} (y + \mu_4 h, t) + K_i \frac{\partial F_{i,j}}{\partial y} (y, t) \right]$$

Now, in the limit as  $\Delta y \rightarrow 0$  and  $\Delta t \rightarrow 0$  (i.e.  $h \rightarrow 0$  and  $k \rightarrow 0$ ) the convergence error will tend to the partial differential equation itself and will therefore tend to zero. In other words, mesh refinement gives convergence.

The actual estimation of the convergence error is more difficult for particular  $h$  and  $k$  values, since estimates for the higher derivatives are not known. Therefore the usual process is that of mesh refining where the mesh size is reduced until two successive mesh sizes give the same results, but it was still necessary to show theoretically that convergence will occur since Fox and Mayer (1968) have indicated that there are pathological (mathematically speaking) cases where the assumption that mesh refining alone will show convergence may be dangerous.

It was demonstrated in chapter 3 that the revised model predictions were convergent by means of such a "mesh refinement technique".

APPENDIX IV

This appendix demonstrates how the matrix method of stability can easily deal with our revised boundary conditions (or for that matter any general derivative boundary conditions).

From chapter 2 we know that the total finite difference approximation to the pulmonary gas transport equation may be written in *matrix form* as:-

$$\begin{bmatrix} F_{2,j+1} \\ F_{3,j+1} \\ \\ F_{N-1,j+1} \\ F_{N,j+1} \end{bmatrix} = \begin{bmatrix} (1 - 2Dr) & (D + K_2)r & & & \\ (D - K_3)r & (1 - 2Dr) & (D + K_3)r & & \\ & & & & \\ & & (D - K_{N-1})r & (1 - 2Dr) & (D + K_{N-1})r \\ & & & 2Dr & D - 2Dr(1 - A_N) \end{bmatrix} \begin{bmatrix} F_{2,j} \\ F_{3,j} \\ \\ F_{N-1,j} \\ F_{N,j} \end{bmatrix} + \begin{bmatrix} 0 \\ 0 \\ 0 \\ \frac{-2DA_N}{\dot{Q}} \\ Gr \end{bmatrix}$$

As each compartment of the last column vector is a constant the matrix determining the propagation of the error is,



APPENDIX V

Consider the following inverse Laplace Transform:-

$$F(y, t) = \mathcal{L}^{-1} \frac{1}{P} \exp \left[ \left\{ \frac{v - \sqrt{v^2 + 4pD}}{2D} \right\} y \right] \quad (i)$$

before we can perform this inverse we need two further results, i.e.

$$\mathcal{L}^{-1} \exp (- y \sqrt{p}) = \frac{y}{2 \sqrt{\pi t^3}} \exp \left( - \frac{y^2}{4t} \right) \quad (ii)$$

and,

$$\int_0^t \mathcal{L}^{-1} F dt = \mathcal{L}^{-1} \frac{1}{P} F \quad (iii)$$

Thus, using the results given in (ii) and (iii) equation (i) becomes

$$F(y, t) = \frac{y}{2 \sqrt{\pi D}} \int_0^t s^{-\frac{3}{2}} \exp \left\{ - \frac{1}{4Ds} (y - v s)^2 \right\} ds \quad (iv)$$

We will now show how the R.H.S. of equation (iv) can be derived from the following integrals:-

$$I_1 = \int_{\frac{(y-VS)}{(4DS)^{\frac{1}{2}}} }^{\infty} e^{-z^2} dz \quad \text{and} \quad I_2 = \int_{\frac{(y+VS)}{(4DS)^{\frac{1}{2}}} }^{\infty} e^{-z^2} dz \quad (v)$$

Letting

$$z'^2 = z^2 - \frac{Vy}{D} \quad \text{in} \quad I_2$$

then,

$$z' dz' = z dz$$

$$dz = \frac{z'}{\sqrt{z'^2 + \frac{Vy}{D}}} dz'$$

Thus,  $I_2$  becomes

$$I_2 = \int_{\frac{(y-VS)}{(4DS)^{\frac{1}{2}}} }^{\infty} \frac{z'}{\sqrt{z'^2 + \frac{Vy}{D}}} e^{-z'^2} e^{-\frac{Vy}{D}} dz \quad (vi)$$

From equations (v) and (vi) we know that

$$I_1 + e^{\frac{Vy}{D}} I_2 = \int_{\frac{(y-Vs)^{\frac{1}{2}}}{(4DS)^{\frac{1}{2}}} }^{\infty} \left\{ 1 + \frac{z}{\sqrt{z^2 + \frac{Vy}{D}}} \right\} e^{-z^2} dz \quad (\text{vii})$$

Now let

$$z = \frac{(y - Vu)}{(4DU)^{\frac{1}{2}}} \quad \text{in (vii)}$$

then,

$$dz = -\frac{1}{4} \frac{1}{\sqrt{D}} (y + Vu) U^{-\frac{3}{2}} du$$

and,

$$1 + \frac{z}{\sqrt{z^2 + \frac{Vy}{D}}} = \frac{2y}{(y + Vu)}$$

Hence,

$$I_1 + e^{\frac{Vy}{D}} I_2 = \frac{y}{2\sqrt{D}} \int_0^t s^{-\frac{3}{2}} \exp - \left\{ \frac{1}{4DS} (y - Vs)^2 \right\} ds \quad (\text{viii})$$

Comparing equations (iv) and (viii) we have

$$F(y, t) = \frac{1}{\sqrt{\pi}} (I_1 + e^{\frac{Vy}{D}} I_2) \quad (\text{ix})$$

But

$$I_1 = \frac{\sqrt{\pi}}{2} \operatorname{erfc} \left( \frac{y - Vt}{(4Dt)^{\frac{1}{2}}} \right), \quad I_2 = \frac{\sqrt{\pi}}{2} \operatorname{erfc} \left( \frac{y + Vt}{(4Dt)^{\frac{1}{2}}} \right)$$

Thus,

$$F(y, t) = \frac{1}{2} \left[ \operatorname{erfc} \left( \frac{y - Vt}{(4Dt)^{\frac{1}{2}}} \right) + \exp \left( \frac{Vy}{D} \right) \operatorname{erfc} \left( \frac{y + Vt}{(4Dt)^{\frac{1}{2}}} \right) \right] \quad (\text{x})$$

Values of the function erf and erfc are tabulated in Handbook of Mathematical Functions (Dover, 1965) edited by Abramowitz and Stegund.

APPENDIX VI

Since exact analytical solutions to the governing "pipe" model gas transport equations cannot be found for the expiratory cycle, a suitable numerical solution technique must be employed. Such a solution technique has been detailed elsewhere (Scrimshire et al, 1978); however, we shall now indicate how it can be applied in the present situation.

The general form of the governing gas transport equation down tube  $i$  is:-

$$\frac{\partial F_i}{\partial t} = D_i \frac{\partial^2 F_i}{\partial Y_i^2} + V_i \frac{\partial F_i}{\partial Y_i} \quad (i)$$

Using the following central difference approximation of derivatives,

$$\frac{\partial F}{\partial t} = \frac{(F_{i,j+1} - F_{i,j})}{(\Delta t)}, \quad (ii)$$

$$\frac{\partial F}{\partial Y} = \frac{(F_{i+1,j} - F_{i-1,j})}{2 (\Delta Y)}, \quad (iii)$$

and

$$\frac{\partial^2 F}{\partial Y^2} = \frac{(F_{i+1,j} - 2F_{i,j} + F_{i-1,j})}{(\Delta Y)^2} \quad (iv)$$

and substituting into equation (i) we have

$$\frac{(F^n_{i,j+1} - F^n_{i,j})}{(\Delta t)} = D_n \frac{(F^n_{i+1,j} - 2F^n_{i,j} + F^n_{i-1,j})}{(\Delta y_n)^2} + V_n \frac{(F^n_{i+1,j} - F^n_{i-1,j})}{2(\Delta y_n)} \quad (v)$$

Simplifying equation (v) yeilds

$$F^n_{i,j+1} = (D_n + K_n) r_n F^n_{i+1,j} + (1 - 2D_n r_n) F^n_{i,j} + (D_n - K_n) r_n F^n_{i-1,j} \quad (vi)$$

where,

$$K_n = \frac{1}{2} V_n (\Delta y_n) \quad (vii)$$

Equations (vi) and (vii) hold for  $0 \leq n \leq 23$  and for  $i > 0$ ; when  $i = 0$  we have from boundary condition (145)

$$\frac{(F^0_{2,j} - F^0_{0,j})}{2(\Delta y_0)} = 0 \quad (viii)$$

$$\text{i.e. } F^0_{2,j} = F^0_{0,j} \quad (ix)$$

From equation (vi) we know that,

$$F^{\circ}_{1,j+1} = (D_o + K_o)r_o F^{\circ}_{2,j} + (1 - 2D_o r_o)F^{\circ}_{1,j} + (D_o - K_o)r_o F^{\circ}_{o,j} \quad (x)$$

Substituting from equation (ix) into equation (x) we find,

$$F^{\circ}_{1,j+1} = F^{\circ}_{1,j} + 2D_o r_o (F^{\circ}_{2,j} - F^{\circ}_{o,j}) \quad (xi)$$

Similarly at the distal end of the last tube we have from boundary condition (14.7) that

$$\frac{(F^{23}_{m+1,j} - F^{23}_{m-1,j})}{2(\Delta Y_{23})} = - \frac{V_{23}}{D_{23}} F^{23}_{m,j} \quad (xii)$$

i.e.

$$F^{23}_{m+1,j} = F^{23}_{m-1,j} - \frac{2V_{23}}{D_{23}} (\Delta Y_{23}) F^{23}_{m,j} \quad (xiii)$$

Putting  $i = m$  in equation (vi) yields,

$$F^{23}_{m,j+1} = (D_{23} + K_{23})r_{23}F^{23}_{m+1,j} + (1 - 2D_{23}r_{23})F^{23}_{m,j} + (D_{23} - K_{23})r_{23}F^{23}_{m-1,j} \quad (xiv)$$

Substituting from equation (xiii) into equation (xiv) gives,

$$F_{m,j+1}^{23} = 2D_{23}r_{23}F_{m-1,j}^{23} + \left\{ 1 - 2D_{23}r_{23} - \frac{2V_{23}}{D_{23}} (\Delta Y_{23}) \right\} F_{m,j}^{23} \quad (\text{xv})$$

Stability and convergence of the above schemes are guaranteed so long as, in each case, the following conditions are satisfied (Hildebrand, 1968):-

$$r_n < \frac{1}{2D_n} \quad \text{and} \quad r_n < \frac{D_n}{2K_n^2} \quad (\text{xvi})$$

Care must be exercised in choosing the  $\Delta y_n$  such that the conditions given in equations (xvi) are not violated.

APPENDIX VII

Comparison of the derivations of the governing "trumpet"  
and "pipe" model gas transport equations

Because of the geometrical complexity of the airways, most authors have assumed a one-dimensional lung model based upon the depth of the airways for the discussion of gas transport. In this model, the airways are regarded as a variable (trumpet shaped) cross-sectional channel along which the gas moves in and out. The depth of the airways is then equivalent to the distance measuring along the channel from its entrance. It is also assumed in this model that the gas velocity and concentration are uniform over all airways at a given airway depth so that the mathematical equation which describes the gas transport involves only the mean gas velocity and the molecular diffusion coefficient of the gas.

For the purpose of derivation only we are assuming a lung model based on Weibel's (1963) 'Model A', although the mathematical theory may equally well be applied to any lung model consisting of a symmetric and dichotomous branching system of airways.

Owing to the symmetrical nature of the lung model, we know that the inspired gas molecules may traverse any one of  $2^{23}$  distinct pathways in order to reach the terminal air sacs. Thus, by deriving an equation for the mass conservation of the gas in a typical pathway we may easily extend the result to the general case of obtaining an equation of gas transport in all airways.

The following notation will be used throughout the theory:-

$i$  represents a typical pathway ( $1 \leq i \leq 2^{23}$ )

$F_i(y,t)$  is the gas concentration in the  $i^{\text{th}}$  pathway at location  $y$  and time  $t$

$S_i(y,t)$  is the cross-sectional area of the  $i^{\text{th}}$  pathway at location  $y$  and time  $t$

$G_i(y,t)$  is the mass flux of the gas due to the bulk gas motion and molecular diffusion per unit cross-sectional area of the  $i^{\text{th}}$  pathway

$V_i(y,t)$  is the gas velocity in the  $i^{\text{th}}$  pathway

$D$  is the molecular diffusion coefficient

$A_i(y,t)$  is the net loss rate due to chemical reactions and transverse diffusion from the  $i^{\text{th}}$  pathway to surrounding pathways and airway surfaces per unit length.

We may note immediately that

$$G_i(y,t) = V_i(y,t) F_i(y,t) - D \frac{\partial F_i}{\partial y} \quad (i)$$

Conservation of mass

Let us consider an element of the  $i^{\text{th}}$  pathway with a length  $\Delta y$ . Then the increase in the mass (or concentration) of the gas in the element during a time interval  $\Delta t$  must be equal to the net mass flux into the element minus the loss during the same period. Mathematically, this corresponds to the following relation:-

$$\begin{aligned} & F_i(y,t + \Delta t) S_i(y,t + \Delta t)\Delta y - F_i(y,t)S_i(y,t)\Delta y \\ &= S_i(y,t)G_i(y,t)\Delta t - S_i(y + \Delta y,t) G_i(y + \Delta y,t)\Delta t \\ &\quad - A_i(y,t)\Delta y \Delta t \end{aligned} \quad (ii)$$

Dividing equation (ii) by  $\Delta y \Delta t$  and letting  $\Delta y \rightarrow 0$ ,  $\Delta t \rightarrow 0$ , we obtain in the limit,

$$\frac{\partial}{\partial t} (F_i S_i) = - \frac{\partial}{\partial y} (G_i S_i) - A_i \quad (iii)$$

Substituting equation (i) into equation (iii) and simplifying we have

$$\frac{\partial}{\partial t} (F_i S_i) + \frac{\partial}{\partial y} (F_i V_i S_i) = D \frac{\partial}{\partial y} \left( S_i \frac{\partial F_i}{\partial y} \right) - A_i \quad (\text{iv})$$

In the particular case of our "pipe" model derivation we also have that

$$S_i V_i \equiv \text{constant} \quad (\text{v})$$

and hence equation (iv) simplifies to

$$\frac{\partial F_i}{\partial t} = D \frac{\partial^2 F_i}{\partial y^2} - V_i \frac{\partial F_i}{\partial y} \quad (\text{vi})$$

However, in order to proceed to the corresponding "trumpet" model equation the following identities are required, i.e.

$$S(y, t) = \sum_{i=1}^m S_i \quad (\text{vii})$$

$$F(y, t) = \frac{1}{S} \sum_{i=1}^m F_i S_i \quad (\text{viii})$$

$$V(y, t) = \frac{1}{S} \sum_{i=1}^m V_i S_i \quad (\text{ix})$$

$$A(y, t) = \sum_{i=1}^m A_i \quad (\text{x})$$

where  $m = 2^{2^3}$  (when using Weibel's Model A)

Taking the summation of both sides of equation (iv) from  $i = 1$  to  $m$  yields,

$$\begin{aligned} \frac{\partial}{\partial t} (\bar{F} S) + \frac{\partial}{\partial y} (S \bar{V} \bar{F}) + \sum_{i=1}^m \frac{\partial}{\partial y} (S_i \bar{V} F'_i) + \sum_{i=1}^m \frac{\partial}{\partial y} (S_i \bar{F} V'_i) \\ + \sum_{i=1}^m \frac{\partial}{\partial y} (S_i F'_i V'_i) = D \frac{\partial}{\partial y} (S \frac{\partial \bar{F}}{\partial y}) + D \frac{\partial}{\partial y} \left\{ \sum_{i=1}^m S_i \frac{\partial F'_i}{\partial y} \right\} - A \end{aligned}$$

..... (xi)

Now,

$$F_i = \bar{F} + F'_i$$

thus

$$\sum_{i=1}^m F_i S_i = \sum_{i=1}^m \bar{F} S_i + \sum_{i=1}^m F'_i S_i \tag{xii}$$

But,

$$\sum_{i=1}^m F_i S_i \equiv \sum_{i=1}^m \bar{F} S_i \implies \sum_{i=1}^m F'_i S_i \equiv 0$$

and similarly we may say that,

$$\sum_{i=1}^m F_i' S_i \equiv 0$$

Hence, equation (xi) becomes

$$\begin{aligned} \frac{\partial}{\partial t} (F S) + \frac{\partial}{\partial y} (S \bar{V} \bar{F}) + \frac{\partial}{\partial y} (S \overline{V'F'}) \\ = D \frac{\partial}{\partial y} (S \frac{\partial \bar{F}}{\partial y} + S \frac{\partial \overline{F'}}{\partial y}) - A \end{aligned} \quad \text{(xiii)}$$

where

$$\overline{V'F'} = \frac{1}{S} \sum_{i=1}^m S_i F_i' V_i'$$

and

$$\frac{\partial \overline{F'}}{\partial y} = \frac{1}{S} \sum_{i=1}^m S_i \frac{\partial F_i'}{\partial y} \quad \text{(xiv)}$$

It may easily be shown that  $\frac{\partial \overline{F'}}{\partial y} = 0$  and we express  $\overline{V'F'}$  in the following form,

$$\overline{V'F'} = - D' \frac{\partial \bar{F}}{\partial y} \quad \text{(xv)}$$

where  $D'$  is an apparent diffusion coefficient and may be related to the Taylor Diffusion (Taylor, 1953).

We may now write equation (xiii) in the more familiar form, i.e.

$$\frac{\partial}{\partial t} (\bar{F} S) = \frac{\partial}{\partial y} (D_{\text{eff}} S \frac{\partial \bar{F}}{\partial y}) - \frac{\partial}{\partial y} (S \bar{V} \bar{F}) - A \quad (\text{xvi})$$

where,

$$D_{\text{eff}} = D + D'$$

$$D' = - \overline{V'F'} \left( \frac{\partial \bar{F}}{\partial y} \right)^{-1}$$

When considering  $N_2 - O_2$  diffusion in the human lung we have an inert gas  $N_2$ , of low solubility and thus  $A$  is negligible.

The standard notation used by almost all previous workers has been the following:-

$$F = \bar{F}, \quad \bar{V} S \equiv \dot{Q} \equiv \text{constant}$$

Equation (xvi) now becomes

$$\frac{\partial F}{\partial t} = D \left[ \frac{\partial^2 F}{\partial y^2} + \frac{1}{S} \frac{\partial S}{\partial y} \frac{\partial F}{\partial y} \right] - \frac{\dot{Q}}{S} \frac{\partial F}{\partial y} \quad (\text{xvii})$$

where,  $F$  is the 'over-all' mean fractional concentration of gas in the airways situated at distance  $y$  from the origin of the 'combined airways' or "trumpet" shaped model, and at time  $t$ .

$\dot{Q}$  is the mean mass flow-rate of gas occurring throughout the model.

$S$  is the total cross-sectional area of all the airways situated at distance  $y$  from the origin of the model.

It should now be clear why there are slight differences between the "trumpet" and "pipe" model predictions given in chapters 3, 4 and 5.

REFERENCES

ABRAMOWITZ and STEGUND (1965) Handbook of Mathematical Functions, Dover.

ARIS, R. (1956) On the dispersion of a solute in a fluid flowing through a tube. Proc. Roy. Soc. (London) A 235: 67-77.

BAKER, L., R. RHOADES and J. ULTMAN (1974) Simultaneous gas flow and diffusion in a symmetric airway system: a mathematical model. Respir. Physiol. 21: 119-138

BAKER, L. G., J. S. ULTMAN and R. A. RHOADES (1975) Characterisation of lung geometry from the single-breath nitrogen washout test. Comp. Biomed. Res. 8: 254-266

BASHOFF, M. A., R. H. INGRAM and D. P. SCHILDER (1967) Effect of expiratory flow rate on the nitrogen concentration versus volume relationship. J. Appl. Physiol. 23: 895-901

BENTIVOGLIO, L. G., F. BEEREL, P. B. STEWART, A. C. BRYAN, W. C. BALL and D. V. BATES (1963) Studies of regional ventilation and perfusion in pulmonary emphysema using Xenon<sup>133</sup>. Am. Rev. Respir. Diseases 88: 315

BOUHUYS, A. (1974) Breathing Physiology, Environment and Lung Disease. Grune and Stratton, New York.

BRISCOE, W. A. and A. COURNAND (1962) The degree of variation of blood perfusion and of ventilation within the emphysematous lung, and some related considerations (1962) In: Ciba Foundation Symposium on Pulmonary Structure and Function. J and A Churchill Ltd., London.

BUSH, A. W., M. A. PINNEY and J. R. WALLIS (1977) A mathematical model of the production of ammonium sulphate aerosol under an elevated temperature inversion in Cleveland County. In: Proceedings of the International Conference on Applied Numerical Modelling (University of Southampton), pp 309-318

BUTLER, J. (1974) PhD Thesis, Department of Physics, Harvard University, Cambridge.

CHANG, H. K. and L. E. FARHI (1973) On mathematical analysis of gas transport in the lung. *Respir. Physiol.* 18: 370-385

COX, D. R. and H. D. MILLER (1968) The theory of stochastic processes. London: Methuen

CUMMING, G., J. CRANK, K. HORSFIELD and I. PARKER (1966) Gaseous diffusion in the airways of the human lung. *Respir. Physiol.* 1: 58-74

CUMMING, G., K. HORSFIELD, J. G. JONES and D. C. F. MUIR (1967) The influence of gaseous diffusion on the alveolar plateau at different lung volumes. *Respir. Physiol.* 2: 386-398

CUMMING, G., K. HORSFIELD and S. B. PRESTON (1971) Diffusion equilibrium in the lungs examined by nodal analysis. *Respir. Physiol.* 12: 324-345

CUMMING, G. (1974) Alveolar Ventilation: Recent Model Analysis. In: International Review of Science. Vol. 2 *Respir. Physiol.* pp 139-166

DAVIDSON, M. R. and J. M. FITZGERALD (1974) Transport of  $O_2$  along a Model Pathway through the Respiratory Region of the Lung. Bull. Math. Biol. 36: 275-303

DAVIDSON, M. R. (1975) Lung Gas Mixing during Expiration Following an Inspiration of Air. Bull. Math. Biol. 37: 113-126

DAVIDSON, M. R. (1977) The influence of gas exchange on lung gas concentrations during air breathing. Bull. Math. Biol. 39: 73-86

DEMEDTS, M., M. DE ROO, J. COSEMANS, L. BILIET and K. P. VAN DE WOESTIJNE (1976) Xenon and nitrogen single-breath washout curves in patients with airway obstruction J. Appl. Physiol. 41: 185-190

DOLLFUSS, R. E., J. MILIC-EMILI and D. V. BATES (1967) Regional ventilation of the lung studied with boluses of  $Xe^{133}$ . Respir. Physiol. 2: 234-246

ENGEL, L. A., L. WOOD, G. UTZ and P. T. MACKLEM (1973) Gas mixing during inspiration. J. Appl. Physiol. 35: 18-24

ENGEL, L. A., M. PAIVA, D. I. M. SIEGLER and Y. FUKUCHI (1979) Dual tracer single-breath studies of gas transport in the lung. Respir. Physiol. 36: 103-119

FOWLER, W. S. (1949) Lung function studies, III. Uneven pulmonary ventilation in normal subjects and in patients with pulmonary disease. J. Appl. Physiol. 2: 283-299

FOX, L. and D. F. MAYERS (1968) Computing methods for scientists and engineers. Oxford, Clarendon.

- GEORG, J., N. A. LASSEN, K. MELLEMGAAARD and A. VINTHER (1965) Diffusion in the gas phase of the lungs in normal and emphysematous subjects. Clin. Sci. 29: 525-532
- HANSEN, J. E. and E. P. AMPAYA (1975) Human air space shapes, sizes, areas and volumes. J. Appl. Physiol. 38: 990-995
- HILDEBRAND, F. B. (1962) Advanced Calculus for Applications. Englewood Cliffs, Prentice Hall
- HILDEBRAND, F. B. (1968) Finite-Difference Equations and Simulations. New Jersey, Prentice-Hall
- HORSFIELD, K. and G. CUMMING (1968) Morphology of the bronchial tree in man. J. Appl. Physiol. 24: 373-383
- HORSFIELD, K., G. DART, D. E. OLSON, G. F. FILLEY and G. CUMMING (1971) Models of the human bronchial tree. J. Appl. Physiol. 31: 207-217
- HORSFIELD, K., D. H. BARER and G. CUMMING (1973) Centrilobular Emphysema Studied with a mathematical model Scand. J. Respr. Dis. 54: 53-64
- HORSFIELD, K., A. DAVIES and G. CUMMING (1977) Role of conducting airways in partial separation of inhaled gas mixtures. J. Appl. Physiol. 43: 391-396
- HUGHES, J. M. B., J. B. GLAZIER, J. E. MALONEY and J. B. WEST (1968) Effect of lung volume on the distribution of pulmonary blood flow in man. Respir. Physiol. 4: 58-72
- HUGHES, J. M. B., F. G. HOPPIN and J. MEAD (1972) Effect of lung inflation on bronchial length and diameter in excised lungs. J. Appl. Physiol. 32: 25-35

JONES, J. G. (1967) The effect of perinspiratory lung volume on the result of the single-breath O<sub>2</sub> test  
Respir. Physiol. 2: 375-385

JONES, J. G. and S. W. CLARKE (1969) The effect of expiratory flow rate on regional lung emptying  
Clin. Sci. 37: 343-356

JONES, T. J. and D. A. SCRIMSHIRE (1976) Simulation of gas transport mechanisms in the human lung  
In: Applications of Electronics in Medicine, IERE Conference Proceedings No. 34, pp 153-160

KAWASHIRO, T., R. S. SIKAND, F. ADARO, H. TAKAHASHI and J. PIIPER (1976) Study of intrapulmonary gas mixing in man by simultaneous washout of helium and sulphur hexafluoride. Respir. Physiol. 28: 261-275

KROGH, A. and J. LINDHARD (1917) On the average composition of the alveolar air and its variation during the inspiratory cycle. J. Physiol. (London) 47: 431-445

LA FORCE, R. C. and B. M. LEWIS (1970) Diffusional transport in the human lung. J. Appl. Physiol. 28: 291-298

MARSHALL, R. and W. S. HOLDEN (1963) Changes in calibre of the smaller airways in man. Thorax 18: 54-58

MILIC-EMILI, J., J. A. M. HENDERSON, M. B. DOLOVICH, D. TROP and P. KANEKO (1966) Regional distribution of inspired gas in the lung. J. Appl. Physiol. 21: 749-759

MILLS, R. J. and P. HARRIS (1965) Factors influencing the concentration of expired nitrogen after a single breath of oxygen. J. Appl. Physiol. 20: 103-109

- MON and ULTMAN (1976) Gas diffusion in an assymetrical model of the bronchial airways. Bull. Math. Biol. 38: 161-191
- O'BRIEN, G., M. A. HYMAN and S. KAPLAN (1951) A study of the numerical solution of partial differential equations J. Math. Phys. 29: 223-251
- PACK, A., D. I. MURRAY-SMITH, R. J. MILLS, M. B. HOOPER and J. C. TAYLOR (1974) Application of mathematical models in respiratory medicine. Bull.Inst.Math.Applica. 10: 20-26
- PACK, A., M. B. HOOPER, W. NIXON and J. C. TAYLOR (1977) A computational model of pulmonary gas transport incorporating effective diffusion. Respir. Physiol. 29: 101-124
- PAIVA, M. (1972) Computation of the boundary conditions for diffusion in the human lung. Computers Biomed.Res. 5: 585-595
- PAIVA, M. (1973) Gas transport in the human lung J. Appl. Physiol. 35: 401-410
- PAIVA, M., L. M. LACQUET and L. P. VAN DER LINDEN (1976) Gas transport in a model derived from the anatomical data of Hansen and Ampaya. J. Appl. Physiol. 41: 115-119
- PAIVA, M. (1974) Gaseous diffusion in an alveolar duct. Comp. Biomed. Res. 7: 533-543
- PAIVA, M. (1978) Hypotheses underlying a continuous analysis of gas transport in a lung model. In: Bull. Inst. Math. Applics. Vol 14, pp 17-21

- PEDLEY, T. J. (1970) A theory for gas mixing in a simple model of the lung. In: Fluid Dynamics of Blood Circulation and Respiratory Flow, AGARD Conference Proceedings, No. 65
- PIIPER, J. and P. SCHEID (1971) RESPIRATION: ALVEOLAR GAS EXCHANGE. In: Annual Review of Physiology pp 131-154
- POWER, G. (1969) Gaseous diffusion between airways and alveoli in the human lung. J.Appl.Physiol. 27: 701-709
- RAUWERDA, P. E. (1946) Unequal Ventilation of Different Parts of the lung and the Determination of Cardiac Output (thesis). Groningen, The Netherlands, University of Groningen.
- READ, J. (1966a) Alveolar populations contributing to expired gas tension plateaus. J. Appl. Physiol. 21: 1511-1520
- READ, J. (1966b) Stratification of ventilation and blood flow in the normal human lung. J.Appl.Physiol. 21: 1521-1531
- ROBERTSON, P.C., N. R. ANTHONISEN and W. R. D. ROSS (1969) Effect of inspiratory flow rates on regional distribution of inspired gas. J. Appl. Physiol. 26: 438-443
- ROOS, A., H. DAHLSTROM and J. P. MURPHY (1955) Distribution of inspired air in the lungs. J. Appl. Physiol. 7: 645-659
- SANDQUIST, L., and I. KJELLMER (1968) Normal values for the single breath N<sub>2</sub> elimination test in different age groups. Scand. J. Clin. Invest. 12: 131-135
- SCHERER, P. W., L. H. SHENDALMAN and N. M. GREENE (1972) Simultaneous diffusion and convection in single-breath lung washout. Bull.Math.Biophysics. 34: 393-412

- SCHERER, P. W., L. H. SHENDALMAN, N. M. GREENE and A. BOUHUYS (1975) Measurement of axial diffusivities in a model of the bronchial airways. *J. Appl. Physiol.* 38: 719-723
- SCHERER, P. W. and A. I. PACK (1977) Bronchial Cross-Section from Lung Gas Washout. *J. Bio-engineering*, 1: 347-356
- SCHROTER, R. C. and M. F. SUDLOW (1969) Flow patterns in models of the human bronchial airways. *Respir. Physiol.* 7: 341-355
- SCRIMSHIRE, D. A. and P. J. TOMLIN (1973) Gas exchange during the initial stages of  $N_2O$  uptake and elimination in a lung model. *J. Appl. Physiol.* 34: 775-789
- SCRIMSHIRE, D. A., R. J. LOUGHNANE and T. J. JONES (1978) A reappraisal of boundary conditions assumed in pulmonary gas transport models. *Respir. Physiol.* 35: 317-334
- SCRIMSHIRE, D. A., P. J. TOMLIN and R. A. ETHERIDGE (1973) Computer simulation of gas exchange in human lungs. *J. Appl. Physiol.* 34: 687-696
- SHEPHARD, R. J. (1956) Assessment of ventilatory efficiency by the single breath technique. *J. Physiol. (Lond)* 134: 630-649
- SIKAND, R., P. CERRETELLI and L.E. FARHI (1966) Effects of  $\dot{V}_A$  and  $\dot{V}_A/\dot{Q}$  distribution and of time on the alveolar plateau. *J. Appl. Physiol.* 21: 1331-1337
- SIKAND, R., H. MAGNUSSEN, P. SCHEID and J. PIIPER (1976) Convective and diffusive gas mixing in human lungs: Experiments and model analysis. *J. Appl. Physiol.* 40: 362-371

SMITH, G. D. (1965) Numerical Solution of Partial Differential Equations. London, Oxford University Press.

SUTHERLAND, P.W., F. KATSURA and J. MILIC-EMILI (1968) Previous volume history of the lung and regional distribution of gas. J. Appl. Physiol. 25: 566-574

TAYLOR, G. I. (1953) Dispersion of soluble matter in solvent flowing through a tube  
Proc. Roy. Soc. (London) A219: 186-203

TAYLOR, G. I. (1954) The dispersion of matter in turbulent flow through a pipe. Proc. Roy. Soc. (London) A223: 446-468

TSUNODA, S., A. C. YOUNG and C. J. MARTIN (1972) Emptying pattern of lung compartments in normal man. J. Appl. Physiol. 32: 644-649

WEIBEL, E. R. (1963) Morphometry of the Human Lung. Berlin, Springer.

WORTH, H., F. ADARO and J. PIIPER (1977) Penetration of inhaled He and SF<sub>6</sub> into alveolar space at low tidal volumes. J. Appl. Physiol. 43: 403-408

YOUNG, A. C., C. J. MARTIN and W. R. PAGE (1963) Effect of expiratory flow patterns on lung emptying. J. Appl. Physiol. 18: 47-50

Table 1

---

| z  | l    | S        |
|----|------|----------|
| 10 | 0.39 | 9.80     |
| 11 | 0.33 | 14.33    |
| 12 | 0.28 | 21.05    |
| 13 | 0.23 | 32.53    |
| 14 | 0.20 | 50.73    |
| 15 | 0.17 | 82.60    |
| 16 | 0.14 | 131.60   |
| 17 | 0.12 | 242.18   |
| 18 | 0.10 | 522.00   |
| 19 | 0.08 | 1307.00  |
| 20 | 0.07 | 2946.00  |
| 21 | 0.06 | 5510.00  |
| 22 | 0.05 | 15328.00 |
| 23 | 0.04 | 26216.00 |

---

Weibel's Model A with the data scaled such that the FRC corresponds to that of an average normal lung (3.0 litres) where,

z is the generation number

l is the generation length in cm

S is the total cross-sectional area in  $\text{cm}^2$

Table 2

|                       | Distance<br>y (cm) | Fractional Gas<br>Conventional (a) | Concentration<br>Revised (b) |
|-----------------------|--------------------|------------------------------------|------------------------------|
| Conducting<br>Airways | 0.00               | 0.178040                           | 0.155106                     |
|                       | 0.33               | "                                  | 0.154794                     |
|                       | 0.61               | "                                  | 0.154409                     |
|                       | 0.84               | "                                  | 0.153931                     |
|                       | 1.04               | "                                  | 0.153351                     |
|                       | 1.22               | "                                  | 0.152709                     |
| Acinar<br>Region      | 1.36               | "                                  | 0.151825                     |
|                       | 1.48               | "                                  | 0.151004                     |
|                       | 1.58               | "                                  | 0.150414                     |
|                       | 1.66               | "                                  | 0.149832                     |
|                       | 1.73               | "                                  | 0.149280                     |
|                       | 1.79               | "                                  | 0.148725                     |
|                       | 1.84               | "                                  | 0.148510                     |
| 1.88                  | 0.178040           | 0.148296                           |                              |

The table gives the end expiration input gas concentration against distance down the model for (a) the conventional and (b) the revised boundary conditions. It will be noted that no concentration differences are apparent when the conventional boundary conditions apply, whereas with the revised boundary conditions significant gradients exist throughout the model. Specifically, a 0.42% difference in fractional gas concentration (representing 60% of the total predicted gradient) is evident in the acinar region.

Table 3

---

| Expired<br>Volume (ml) | Nitrogen Concentration |             |
|------------------------|------------------------|-------------|
|                        | Conventional (a)       | Revised (b) |
| 25.0                   | 0.000000               | 0.000000    |
| 50.0                   | 0.000000               | 0.000000    |
| 60.0                   | 0.000000               | 0.000000    |
| 75.0                   | 0.041709               | 0.041047    |
| 100.0                  | 0.385600               | 0.378557    |
| 125.0                  | 0.572455               | 0.561785    |
| 150.0                  | 0.632282               | 0.621552    |
| 175.0                  | 0.650133               | 0.640789    |
| 200.0                  | 0.655388               | 0.647882    |
| 225.0                  | 0.656929               | 0.651382    |
| 250.0                  | 0.657513               | 0.653808    |
| 275.0                  | 0.657564               | 0.655901    |
| 300.0                  | 0.657568               | 0.657879    |
| 325.0                  | 0.657568               | 0.659804    |
| 350.0                  | 0.657568               | 0.661695    |
| 375.0                  | 0.657568               | 0.663559    |
| 400.0                  | 0.657568               | 0.665397    |
| 425.0                  | 0.657568               | 0.667210    |
| 450.0                  | 0.657568               | 0.668999    |
| 475.0                  | 0.657568               | 0.670763    |
| 500.0                  | 0.657568               | 0.672504    |

---

The table gives the expired nitrogen concentrations at the beginning of the trachea for (a) the conventional and (b) the revised boundary conditions. It will be noted that the alveolar plateau has zero gradient when the conventional boundary conditions apply, whereas with the revised boundary conditions a significant plateau slope of the order of 1.87% over the terminal 250 ml expired i.e. 3.74% on extrapolating to 500 ml expired.

TABLE 4

Comparison of single-breath N<sub>2</sub> washout concentrations for square, triangular and sinusoidal wave flow-rates.

| <u>T<sub>E</sub></u> | <u>SQUARE</u> | <u>TRIANGULAR</u> | <u>SINUSOIDAL</u> |
|----------------------|---------------|-------------------|-------------------|
| 2.1                  | 0.000000      | 0.000000          | 0.000000          |
| 2.2                  | 0.000000      | 0.000000          | 0.000000          |
| 2.3                  | 0.041047      | 0.187008          | 0.001577          |
| 2.4                  | 0.378557      | 0.560900          | 0.081669          |
| 2.5                  | 0.561785      | 0.636096          | 0.351281          |
| 2.6                  | 0.621582      | 0.652229          | 0.544129          |
| 2.7                  | 0.640789      | 0.657830          | 0.613815          |
| 2.8                  | 0.647882      | 0.661267          | 0.633886          |
| 2.9                  | 0.651382      | 0.664082          | 0.640351          |
| 3.0                  | 0.653808      | 0.666585          | 0.643865          |
| 3.1                  | 0.655901      | 0.668847          | 0.646928          |
| 3.2                  | 0.657879      | 0.670893          | 0.649988          |
| 3.3                  | 0.659804      | 0.672736          | 0.653057          |
| 3.4                  | 0.661695      | 0.674384          | 0.656065          |
| 3.5                  | 0.663559      | 0.675845          | 0.658936          |
| 3.6                  | 0.665397      | 0.677124          | 0.661602          |
| 3.7                  | 0.667210      | 0.678228          | 0.664005          |
| 3.8                  | 0.668999      | 0.679157          | 0.666096          |
| 3.9                  | 0.670732      | 0.679915          | 0.667832          |
| 4.0                  | 0.672504      | 0.680500          | 0.669174          |

T<sub>E</sub> corresponds to the expiration time

TABLE 5

Relation between the end expiratory concentration gradients (stratified inhomogeneities) and the pre-inspiratory lung volume.

| <u>F R C (LITRES)</u> | <u><math>\Delta F_{O_2}</math></u> |
|-----------------------|------------------------------------|
| 3.0                   | 0.70%                              |
| 3.5                   | 0.65%                              |
| 4.0                   | 0.59%                              |
| 4.5                   | 0.51%                              |
| 5.0                   | 0.48%                              |

$\Delta F_{O_2}$  corresponds to the computed end expiratory input gas concentration differences between the ends of the model (in this case, for a hypothetical gas having a molecular diffusion coefficient of  $0.25 \text{ cm}^2/\text{sec}$  equivalent to  $O_2/N_2$ )

TABLE 6

Variation of PHASE III slope with pre-inspiratory lung volume.

| <u>F R C (LITRES)</u> | <u><math>\Delta N_2</math></u> |
|-----------------------|--------------------------------|
| 3.0                   | 3.74%                          |
| 3.5                   | 3.00%                          |
| 4.0                   | 2.50%                          |
| 4.5                   | 2.15%                          |
| 5.0                   | 1.89%                          |

$\Delta N_2$  corresponds to the computed phase III slope and is obtained on extrapolating the single-breath  $N_2$  washout curves to 500 mls expired.

TABLE 7

Relation between the phase II (dead space volume), Phase III (alveolar plateau slope) and the breath-holding time.

| <u>BREATH-HOLDING TIME</u> | <u>PHASE II</u> | <u>PHASE III</u> |
|----------------------------|-----------------|------------------|
| 1.0 SECONDS                | 100 mls         | 2.1%             |
| 2.0 SECONDS                | 90 mls          | 1.05%            |
| 5.0 SECONDS                | 65 mls          | 0.03%            |

It is clear from this table that both the dead space volume and the alveolar plateau slope decrease rapidly for increasing breath-holding times.

TABLE 8

Comparison of the *rigid* and *compliant* model predictions.

| <u>EXP. VOL</u> | <u>RIGID</u> | <u>COMPLIANT</u> |
|-----------------|--------------|------------------|
| 25.0            | 0.000000     | 0.000000         |
| 50.0            | 0.000000     | 0.000000         |
| 60.0            | 0.000000     | 0.000000         |
| 75.0            | 0.041047     | 0.020755         |
| 100.0           | 0.378557     | 0.310366         |
| 125.0           | 0.561785     | 0.529923         |
| 150.0           | 0.621552     | 0.615770         |
| 175.0           | 0.640789     | 0.646508         |
| 200.0           | 0.647882     | 0.657929         |
| 225.0           | 0.651382     | 0.662818         |
| 250.0           | 0.653808     | 0.665529         |
| 275.0           | 0.655901     | 0.667515         |
| 300.0           | 0.657879     | 0.669260         |
| 325.0           | 0.659804     | 0.670921         |
| 350.0           | 0.661695     | 0.672550         |
| 375.0           | 0.663559     | 0.674163         |
| 400.0           | 0.665317     | 0.675766         |
| 425.0           | 0.667210     | 0.677361         |
| 450.0           | 0.668999     | 0.678947         |
| 475.0           | 0.670763     | 0.680526         |
| 500.0           | 0.672504     | 0.682096         |

RIGID corresponds to the model with a *fixed* trumpet volume.

COMPLIANT corresponds to the model with a *variable* trumpet volume.

TABLE 9

The simulated single-breath  $N_2$  washout concentrations obtained from the compliant lung model and for a tidal volume of 1000 mls (i.e.  $V_T = 1$  litre)

| <u>EXP. VOL</u> | <u>F<sub>N<sub>2</sub></sub></u> |
|-----------------|----------------------------------|
| 50.0            | 0.059976                         |
| 100.0           | 0.386778                         |
| 150.0           | 0.495857                         |
| 200.0           | 0.524327                         |
| 250.0           | 0.534947                         |
| 300.0           | 0.541702                         |
| 350.0           | 0.547603                         |
| 400.0           | 0.553287                         |
| 450.0           | 0.558889                         |
| 500.0           | 0.564434                         |
| 550.0           | 0.569927                         |
| 600.0           | 0.575371                         |
| 650.0           | 0.580764                         |
| 700.0           | 0.586106                         |
| 750.0           | 0.591397                         |
| 800.0           | 0.596636                         |
| 850.0           | 0.601824                         |
| 900.0           | 0.606961                         |
| 950.0           | 0.612044                         |
| 1000.0          | 0.617076                         |

Where  $F_{N_2}$  corresponds to the expired nitrogen concentration at the mouth.

CONSTANT DIFFUSION PATHWAY LENGTHS

Nodal Point A in Generation 17

| $\dot{Q}_1$ (mls/sec) | $\dot{Q}_2$ (mls/sec) | $V_1$ (litres) | $V_2$ (litres) | $\Delta F_{1,0_2}$ (%) | $\Delta F_{2,0_2}$ (%) | $\Delta F_{N_2}$ (%) |
|-----------------------|-----------------------|----------------|----------------|------------------------|------------------------|----------------------|
| 125.0                 | 125.0                 | 3.0            | 3.0            | 0.21                   | 0.21                   | 2.46                 |
| 200.0                 | 50.0                  | 3.0            | 3.0            | 0.44                   | 0.11                   | 3.64                 |
| 225.0                 | 25.0                  | 3.0            | 3.0            | 0.57                   | 0.06                   | 4.50                 |
| 125.0                 | 125.0                 | 1.5            | 1.5            | 0.40                   | 0.40                   | 5.54                 |
| 125.0                 | 125.0                 | 1.0            | 3.0            | 0.69                   | 0.23                   | 6.55                 |
| 125.0                 | 125.0                 | 1.0            | 4.0            | 0.70                   | 0.21                   | 6.55                 |

Nodal Point A in Generation 14

|       |       |     |     |       |       |      |
|-------|-------|-----|-----|-------|-------|------|
| 125.0 | 125.0 | 3.0 | 3.0 | 0.145 | 0.145 | 1.72 |
| 200.0 | 50.0  | 3.0 | 3.0 | 0.33  | 0.10  | 2.49 |
| 225.0 | 25.0  | 3.0 | 3.0 | 0.45  | 0.05  | 3.08 |
| 125.0 | 125.0 | 1.5 | 1.5 | 0.285 | 0.285 | 3.78 |
| 125.0 | 125.0 | 1.0 | 3.0 | 0.66  | 0.23  | 6.05 |
| 125.0 | 125.0 | 1.0 | 4.0 | 0.70  | 0.19  | 6.25 |

where,  $\Delta F_{1,0_2}$  (%) = end expiratory concentration gradient down compartment i, i = 1, 2

$\Delta F_{N_2}$  (%) = phase III slope calculated on the basis of an extrapolation to 500 mls expired

Nodal Point A in Generation 17

| $\dot{Q}_1$ (mls/sec) | $\dot{Q}_2$ (mls/sec) | $V_1$ (litres) | $V_2$ (litres) | $\Delta F_{10_2}$ (%) | $\Delta F_{20_2}$ (%) | $\Delta F_{N_2}$ (%) |
|-----------------------|-----------------------|----------------|----------------|-----------------------|-----------------------|----------------------|
| 125.0                 | 125.0                 | 1.5            | 4.0            | 0.46                  | 0.19                  | 4.64                 |
| 125.0                 | 125.0                 | 1.5            | 3.5            | 0.48                  | 0.20                  | 4.72                 |
| 125.0                 | 125.0                 | 1.5            | 1.5            | 0.485                 | 0.485                 | 6.98                 |
| 200.0                 | 50.0                  | 1.5            | 4.5            | 1.02                  | 0.33                  | 10.51                |
| 200.0                 | 50.0                  | 1.5            | 4.0            | 0.98                  | 0.38                  | 10.73                |
| 200.0                 | 50.0                  | 1.5            | 3.5            | 0.96                  | 0.44                  | 10.65                |

Nodal Point A in Generation 14

|       |       |     |     |      |      |      |
|-------|-------|-----|-----|------|------|------|
| 125.0 | 125.0 | 1.5 | 4.0 | 0.36 | 0.14 | 3.08 |
| 125.0 | 125.0 | 1.5 | 3.5 | 0.35 | 0.16 | 3.29 |
| 125.0 | 125.0 | 1.5 | 1.5 | 0.27 | 0.27 | 3.85 |
| 200.0 | 50.0  | 1.5 | 4.5 | 0.91 | 0.26 | 8.53 |
| 200.0 | 50.0  | 1.5 | 4.0 | 0.90 | 0.28 | 8.46 |
| 200.0 | 50.0  | 1.5 | 3.5 | 0.89 | 0.31 | 8.41 |

CONSTANT DIFFUSION PATHWAY LENGTHSNodal Point A in Generation 17

| $\dot{Q}_1$ (mls/sec) | $\dot{Q}_2$ (mls/sec) | $V_1$ (litres) | $V_2$ (litres) | $\Delta F_{10_2}$ (%) | $\Delta F_{20_2}$ (%) | $\Delta F_{N_2}$ (%) |
|-----------------------|-----------------------|----------------|----------------|-----------------------|-----------------------|----------------------|
| 225.0                 | 25.0                  | 2.0            | 4.0            | 0.84                  | 0.41                  | 7.74                 |
| 225.0                 | 25.0                  | 1.5            | 3.0            | 0.96                  | 0.48                  | 11.76                |
| 225.0                 | 25.0                  | 1.0            | 4.0            | 2.4                   | 0.6                   | 21.98                |
| 225.0                 | 25.0                  | 1.0            | 3.0            | 2.25                  | 0.75                  | 21.22                |
| 225.0                 | 25.0                  | 1.5            | 4.5            | 1.13                  | 0.375                 | 11.80                |
| 225.0                 | 25.0                  | 1.25           | 3.75           | 1.5                   | 0.5                   | 15.56                |

| $\dot{Q}_1$ (mls/sec) | $\dot{Q}_2$ (mls/sec) | $V_1$ (litres) | $V_2$ (litres) | $\Delta F_{10_2}$ (%) | $\Delta F_{20_2}$ (%) | $\Delta F_{N_2}$ (%) |
|-----------------------|-----------------------|----------------|----------------|-----------------------|-----------------------|----------------------|
| 225.0                 | 25.0                  | 2.0            | 4.0            | 0.89                  | 0.46                  | 8.60                 |
| 225.0                 | 25.0                  | 1.5            | 3.0            | 1.28                  | 0.71                  | 13.47                |
| 225.0                 | 25.0                  | 1.0            | 4.0            | 2.92                  | 0.73                  | 24.85                |
| 225.0                 | 25.0                  | 1.0            | 3.0            | 2.71                  | 0.94                  | 23.75                |
| 225.0                 | 25.0                  | 1.5            | 4.5            | 1.35                  | 0.64                  | 13.50                |
| 225.0                 | 25.0                  | 1.25           | 3.75           | 1.76                  | 0.64                  | 17.83                |

VARIABLE DIFFUSION PATHWAY LENGTHS

The end expiratory concentration differences for the three tracers gases SF<sub>6</sub>, Ne and He

Nodal Point A in Generation 17

CONSTANT DIFFUSION PATHWAY LENGTHS

| $\dot{Q}_1$ (mls/sec) | $\dot{Q}_2$ (mls/sec) | $V_1$ (litres) | $V_2$ (litres) | $\Delta F_1 SF_6$ | $\Delta F_2 SF_6$ | $\Delta F_1 Ne$ | $\Delta F_2 Ne$ | $\Delta F_1 He$ | $\Delta F_2 He$ |
|-----------------------|-----------------------|----------------|----------------|-------------------|-------------------|-----------------|-----------------|-----------------|-----------------|
| 225.0                 | 25.0                  | 2.0            | 4.0            | 1.01              | 0.62              | 0.77            | 0.36            | 0.61            | 0.22            |
| 225.0                 | 25.0                  | 1.5            | 3.0            | 1.25              | 0.71              | 0.86            | 0.42            | 0.64            | 0.28            |
| 225.0                 | 25.0                  | 1.0            | 4.0            | 2.91              | 0.95              | 2.01            | 0.51            | 1.25            | 0.40            |
| 225.0                 | 25.0                  | 1.0            | 3.0            | 2.71              | 0.93              | 1.84            | 0.63            | 1.11            | 0.51            |
| 225.0                 | 25.0                  | 1.5            | 4.5            | 1.63              | 0.85              | 0.83            | 0.24            | 0.62            | 0.15            |
| 225.0                 | 25.0                  | 1.25           | 3.75           | 2.12              | 1.02              | 1.21            | 0.40            | 0.93            | 0.29            |

VARIABLE DIFFUSION PATHWAY LENGTHS

|       |      |      |      |      |      |      |      |      |      |
|-------|------|------|------|------|------|------|------|------|------|
| 225.0 | 25.0 | 2.0  | 4.0  | 1.06 | 0.67 | 0.82 | 0.41 | 0.66 | 0.27 |
| 225.0 | 25.0 | 1.5  | 3.0  | 1.30 | 0.76 | 0.91 | 0.47 | 0.69 | 0.33 |
| 225.0 | 25.0 | 1.0  | 4.0  | 2.96 | 1.00 | 2.06 | 0.56 | 1.80 | 0.45 |
| 225.0 | 25.0 | 1.0  | 3.0  | 2.76 | 0.98 | 1.89 | 0.68 | 1.66 | 0.56 |
| 225.0 | 25.0 | 1.5  | 4.5  | 1.68 | 0.90 | 0.88 | 0.29 | 0.67 | 0.20 |
| 225.0 | 25.0 | 1.25 | 3.75 | 2.17 | 1.07 | 1.26 | 0.45 | 0.98 | 0.34 |

where,  $\Delta F_{ix}$  = end expiratory acinar concentration gradient of input gas X down compartment

$i, i = 1, 2.$

computed phase III slopes for the three tracers SF<sub>6</sub>, Ne and He

Nodal Point A in Generation 17

CONSTANT DIFFUSION PATHWAY LENGTHS

| $\dot{Q}_1$ (mls/sec) | $\dot{Q}_2$ (mls/sec) | $V_1$ (litres) | $V_2$ (litres) | $\Delta F_{SF_6}$ | $\Delta F_{Ne}$ | $\Delta F_{He}$ |
|-----------------------|-----------------------|----------------|----------------|-------------------|-----------------|-----------------|
| 225.0                 | 25.0                  | 2.0            | 4.0            | 10.52             | 6.23            | 5.6             |
| 225.0                 | 25.0                  | 1.5            | 3.0            | 14.21             | 9.62            | 7.23            |
| 225.0                 | 25.0                  | 1.0            | 4.0            | 25.02             | 19.50           | 17.35           |
| 225.0                 | 25.0                  | 1.0            | 3.0            | 24.56             | 19.31           | 17.12           |
| 225.0                 | 25.0                  | 1.5            | 4.5            | 13.82             | 10.01           | 8.76            |
| 225.0                 | 25.0                  | 1.25           | 3.75           | 19.04             | 14.22           | 11.33           |

VARIABLE DIFFUSION PATHWAY LENGTHS

|       |      |      |      |       |       |       |
|-------|------|------|------|-------|-------|-------|
| 225.0 | 25.0 | 2.0  | 4.0  | 11.33 | 7.56  | 6.49  |
| 225.0 | 25.0 | 1.5  | 3.0  | 16.32 | 11.51 | 9.03  |
| 225.0 | 25.0 | 1.0  | 4.0  | 28.02 | 22.50 | 20.35 |
| 225.0 | 25.0 | 1.0  | 3.0  | 27.56 | 22.31 | 20.12 |
| 225.0 | 25.0 | 1.5  | 4.5  | 15.52 | 11.71 | 10.46 |
| 225.0 | 25.0 | 1.25 | 3.75 | 21.24 | 16.51 | 13.56 |

where,  $\Delta F_X$  is the phase III slope for tracer gas X based on an extrapolation to 500 mls expired

Data for the parallel model soluble tracer gas simulations

Nodal Point A in Generation 17

CONSTANT DIFFUSION PATHWAY LENGTHS ( $\dot{Q}_1, \dot{Q}_2, V_1$  and  $V_2$  as in tables 13 and 14)

| $G_1$ | $G_2$ | $G_3$ | $\Delta F_{10_2}$ | $\Delta F_{20_2}$ | $\Delta F_{30_2}$ | $\Delta F_{1N_2}$ | $\Delta F_{2N_2}$ | $\Delta F_{3N_2}$ |
|-------|-------|-------|-------------------|-------------------|-------------------|-------------------|-------------------|-------------------|
| 10    | 25    | 50    | 1.51              | 2.14              | 3.14              | 8.98              | 10.85             | 12.90             |
| 10    | 25    | 50    | 1.75              | 2.40              | 3.40              | 13.03             | 14.91             | 17.21             |
| 10    | 25    | 50    | 3.50              | 4.25              | 5.25              | 24.12             | 26.00             | 28.75             |
| 10    | 25    | 50    | 3.48              | 4.20              | 5.20              | 24.40             | 26.35             | 29.25             |
| 10    | 25    | 50    | 1.98              | 2.68              | 3.68              | 13.05             | 15.00             | 17.75             |
| 10    | 25    | 50    | 2.49              | 3.19              | 4.19              | 17.75             | 19.13             | 22.00             |

where,  $G_i = \sum_{j=1}^2 G_{ij}$  and  $i = 1$  to  $3$ , also  $G_{i1} : G_{i2} = 9 : 1$

$$\Delta F_{iO_2} = \sum_{j=1}^2 \Delta F_{ijO_2} \quad \text{and } i = 1 \text{ to } 3$$

Regional 'trumpet' model predictions during breath-holding

Nodal Point A in Generation 17

CONSTANT DIFFUSION PATHWAY LENGTHS ( $\dot{Q}_1$ ,  $\dot{Q}_2$ ,  $V_1$  and  $V_2$  as in tables 13, 14 and 15)

| BREATH-HOLDING TIME (SECS) |   | $\Delta F_{10_2}$ | $\Delta F_{20_2}$ | $\Delta F_{50_2}$ | $\Delta F_{1N_2}$ | $\Delta F_{2N_2}$ | $\Delta F_{5N_2}$ |
|----------------------------|---|-------------------|-------------------|-------------------|-------------------|-------------------|-------------------|
| 1                          | 2 | 1.01              | 0.88              | 0.31              | 5.98              | 3.93              | 1.02              |
| 1                          | 2 | 1.22              | 0.98              | 0.43              | 9.00              | 6.98              | 3.03              |
| 1                          | 2 | 2.65              | 2.03              | 0.92              | 19.03             | 15.71             | 9.34              |
| 1                          | 2 | 2.59              | 1.99              | 0.89              | 18.91             | 15.52             | 9.02              |
| 1                          | 2 | 1.19              | 0.91              | 0.38              | 8.84              | 6.666             | 2.89              |
| 1                          | 2 | 1.72              | 1.43              | 0.61              | 12.99             | 9.81              | 3.55              |

where,  $\Delta F_{iO_2}$  and  $\Delta F_{iN_2}$  correspond to the end expiratory concentration gradients and resulting phase III slopes following 1 second, 2 seconds and 5 seconds of breath-holding respectively (i.e.  $i = 1, 2$  and 5).

Regional 'trumpet' model predictions for variations in the value of D (simulating cardiogenic gas mixing)

Nodal Point A in Generation 17

CONSTANT DIFFUSION PATHWAY LENGTHS ( $\dot{Q}_1$ ,  $\dot{Q}_2$ ,  $V_1$  and  $V_2$  as in tables 13, 14 and 15)

| $D_1$ (cm <sup>2</sup> /sec) | $D_2$ (cm <sup>2</sup> /sec) | $\Delta F_{10_2}$ | $\Delta F_{20_2}$ | $\Delta F_{N_2}$ |
|------------------------------|------------------------------|-------------------|-------------------|------------------|
| 1.0                          | 0.25                         | 0.35              | 0.41              | 4.34             |
| 1.0                          | 0.25                         | 0.46              | 0.48              | 7.26             |
| 1.0                          | 0.25                         | 1.23              | 0.60              | 12.12            |
| 1.0                          | 0.25                         | 1.01              | 0.75              | 12.03            |
| 1.0                          | 0.25                         | 0.51              | 0.375             | 7.28             |
| 1.0                          | 0.25                         | 0.62              | 0.50              | 10.05            |

Where,  $D_i$  is the value of the molecular diffusion coefficient relative to compartment i and  $\Delta F_{iO_2}$  are the end expiratory concentration gradients down compartment i. Finally,  $\Delta F_{N_2}$  is the computed phase III slope calculated on the bases of an extrapolation to 500 mls expired.

TABLE 18

Data for the "pipe" (or "pathway") model.

| <u>i</u> | <u>y<sub>i</sub> (cm)</u> | <u>S<sub>i</sub> (cm<sup>2</sup>)</u> |
|----------|---------------------------|---------------------------------------|
| 0        | 12.00                     | 2.54                                  |
| 1        | 4.76                      | 1.165                                 |
| 2        | 1.90                      | 1.5325                                |
| 3        | 0.76                      | 1.25                                  |
| 4        | 1.27                      | 0.155                                 |
| 5        | 1.07                      | 0.0972                                |
| 6        | 0.90                      | 0.0619                                |
| 7        | 0.76                      | 0.0398                                |
| 8        | 0.64                      | 0.0271                                |
| 9        | 0.54                      | 0.0187                                |
| 10       | 0.39                      | 0.0096                                |
| 11       | 0.33                      | 0.0070                                |
| 12       | 0.28                      | 0.0051                                |
| 13       | 0.23                      | 0.0040                                |
| 14       | 0.20                      | 0.0031                                |
| 15       | 0.17                      | 0.0025                                |
| 16       | 0.14                      | 0.0020                                |
| 17       | 0.12                      | 0.0018                                |
| 18       | 0.10                      | 0.0020                                |
| 19       | 0.08                      | 0.0024                                |
| 20       | 0.07                      | 0.0028                                |
| 21       | 0.06                      | 0.0026                                |
| 22       | 0.05                      | 0.0036                                |
| 23       | 0.04                      | 0.0031                                |

where,  $y_i$  is the length of the  $i^{\text{th}}$  "pipe" of the "pathway", and  $S_i$  is the cross-sectional area of the  $i^{\text{th}}$  "pipe" of this pathway.

TABLE 19

Comparison of "trumpet" and "pipe" model predictions.

|         | <u><math>\Delta F_{O_2}</math></u> | <u><math>\Delta F_{N_2}</math></u> |
|---------|------------------------------------|------------------------------------|
| TRUMPET | 0.7%                               | 3.74%                              |
| PIPE    | 0.74%                              | 3.96%                              |

where,  $\Delta F_{O_2}$  is the end expiratory input gas concentration gradient and  $\Delta F_{N_2}$  the corresponding phase III slope based on an extrapolation to 500 mls expired.

| $\dot{Q}_1$ (mls/sec) | $\dot{Q}_2$ (mls/sec) | $V_1$ litres | $V_2$ litres | $\Delta F_{10_2}$ (%) | $\Delta F_{20_2}$ (%) | $\Delta F_{N_2}$ (%) |
|-----------------------|-----------------------|--------------|--------------|-----------------------|-----------------------|----------------------|
| 125.0                 | 125.0                 | 3.0          | 3.0          | 0.22                  | 0.22                  | 2.51                 |
| 200.0                 | 50.0                  | 3.0          | 3.0          | 0.48                  | 0.12                  | 3.78                 |
| 225.0                 | 25.0                  | 3.0          | 3.0          | 0.62                  | 0.09                  | 4.75                 |
| 125.0                 | 125.0                 | 1.5          | 1.5          | 0.43                  | 0.43                  | 5.82                 |
| 125.0                 | 125.0                 | 1.0          | 3.0          | 0.72                  | 0.27                  | 6.56                 |
| 125.0                 | 125.0                 | 1.0          | 4.0          | 0.74                  | 0.23                  | 6.72                 |

VARIABLE DIFFUSION PATHWAY LENGTHS

|       |       |     |     |      |      |       |
|-------|-------|-----|-----|------|------|-------|
| 125.0 | 125.0 | 1.5 | 4.0 | 0.49 | 0.21 | 4.72  |
| 125.0 | 125.0 | 1.5 | 3.5 | 0.51 | 0.22 | 4.84  |
| 125.0 | 125.0 | 1.5 | 1.5 | 0.50 | 0.50 | 7.20  |
| 200.0 | 50.0  | 1.5 | 4.5 | 1.08 | 0.36 | 10.75 |
| 200.0 | 50.0  | 1.5 | 4.0 | 1.04 | 0.39 | 11.05 |
| 200.0 | 50.0  | 1.5 | 3.5 | 1.02 | 0.46 | 10.87 |

TABLE 21

| <u>G</u> | <u><math>\Delta F_{O_2}</math></u> | <u><math>\Delta F_{N_2}</math></u> |
|----------|------------------------------------|------------------------------------|
| -50.0    | 0.15%                              | 0.79%                              |
| -25.0    | 0.41%                              | 2.20%                              |
| -10.0    | 0.57%                              | 3.04%                              |
| +10.0    | 0.79%                              | 4.17%                              |
| +25.0    | 0.95%                              | 5.02%                              |
| +50.0    | 1.21%                              | 6.43%                              |

where,  $\Delta F_{O_2}$  is the end expiratory input gas concentration gradient within the model and  $\Delta F_{N_2}$  is the corresponding phase III slope based on an extrapolation to 500 mls expired.

TABLE 22

Predicted *percentage deficiencies* for a simulated normal and for a simulated "average case of emphysema".

|                                  | <u>PERCENTAGE DEFICIENCY</u> |
|----------------------------------|------------------------------|
| <u>NORMAL</u>                    | 19.66%                       |
| <u>AVERAGE CASE OF EMPHYSEMA</u> | 29.46%                       |

FIGURE 1

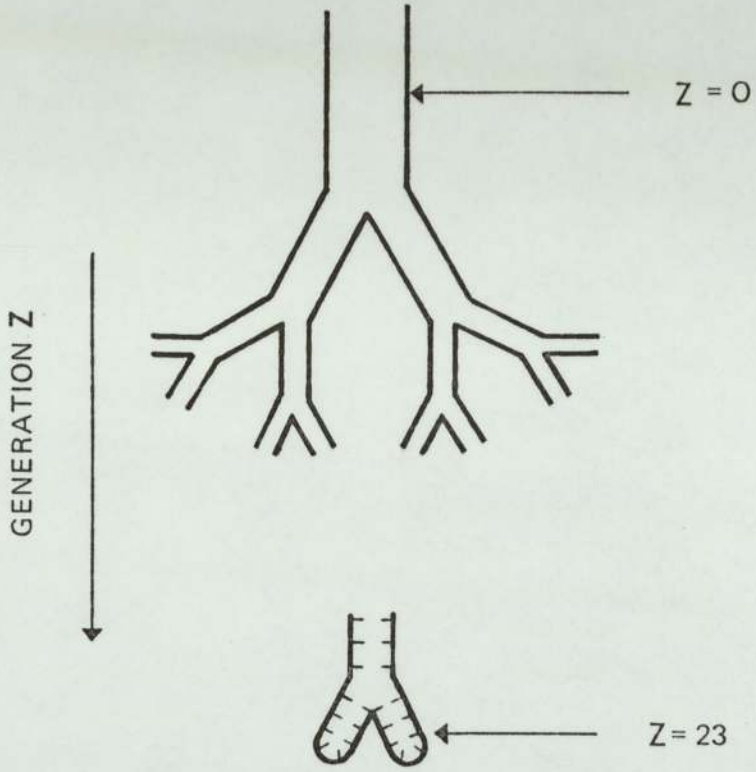


FIGURE 2

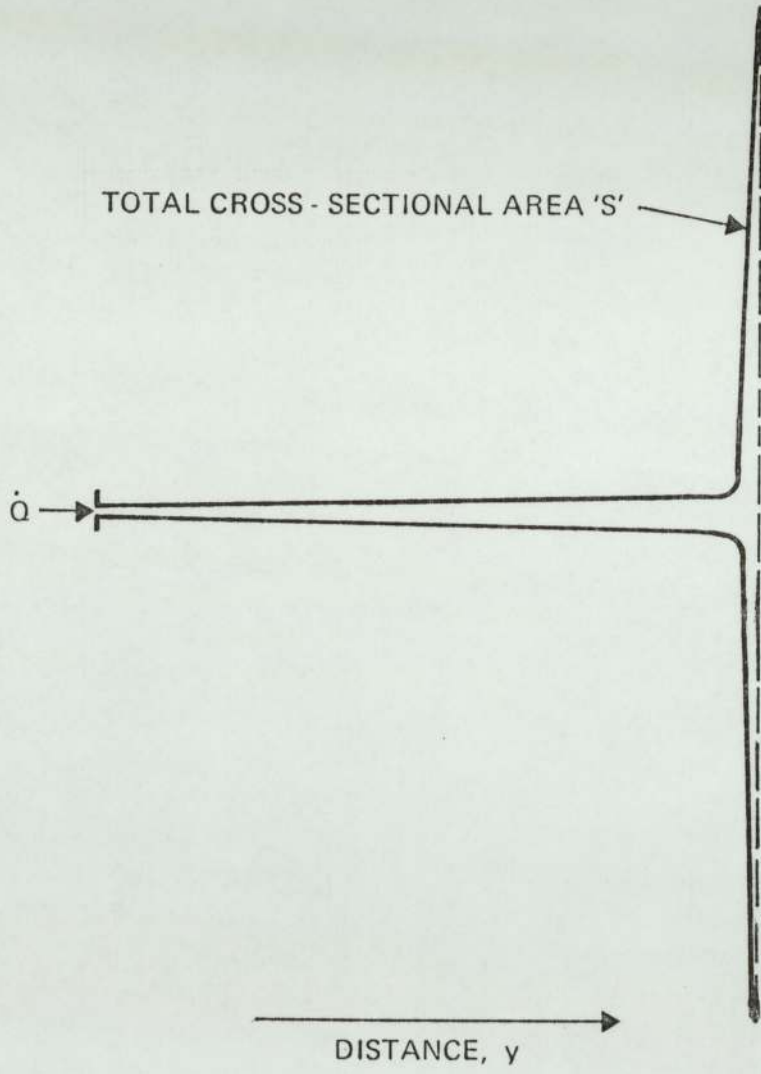
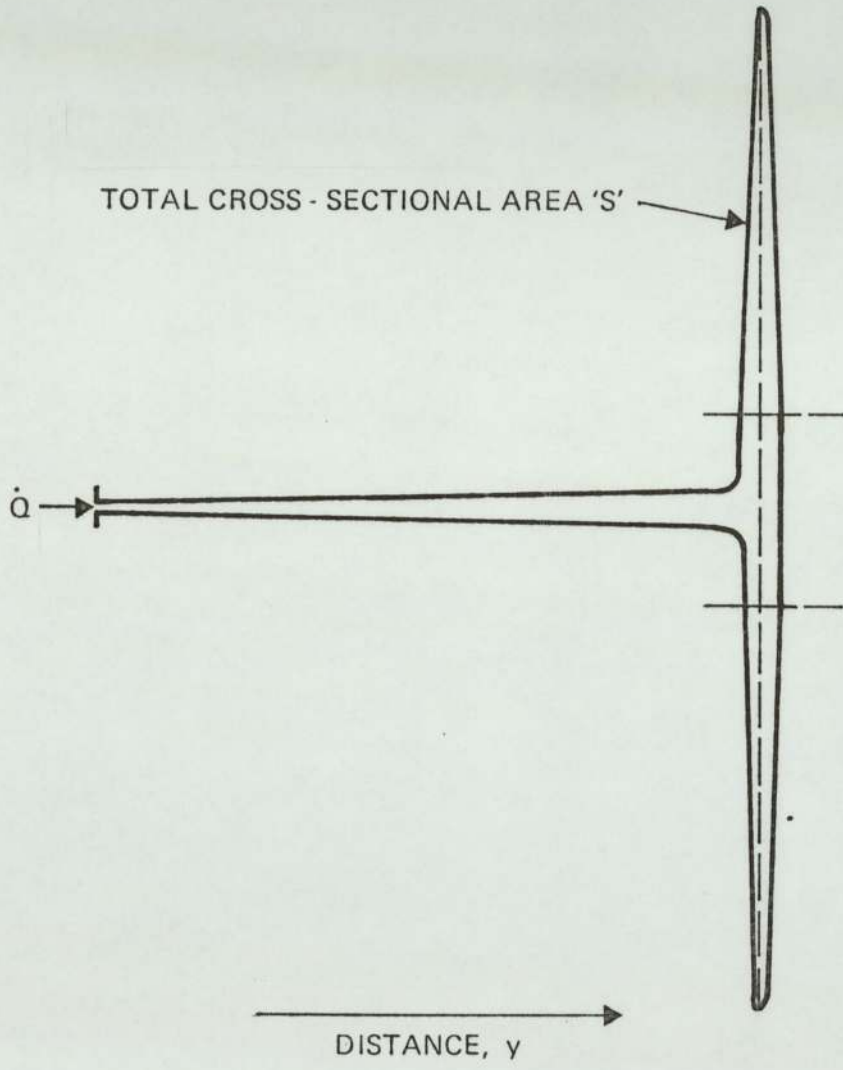


FIGURE 3



INVERSE CHARACTERISTIC TIMES FOR DIFFUSION  
AND CONVECTION

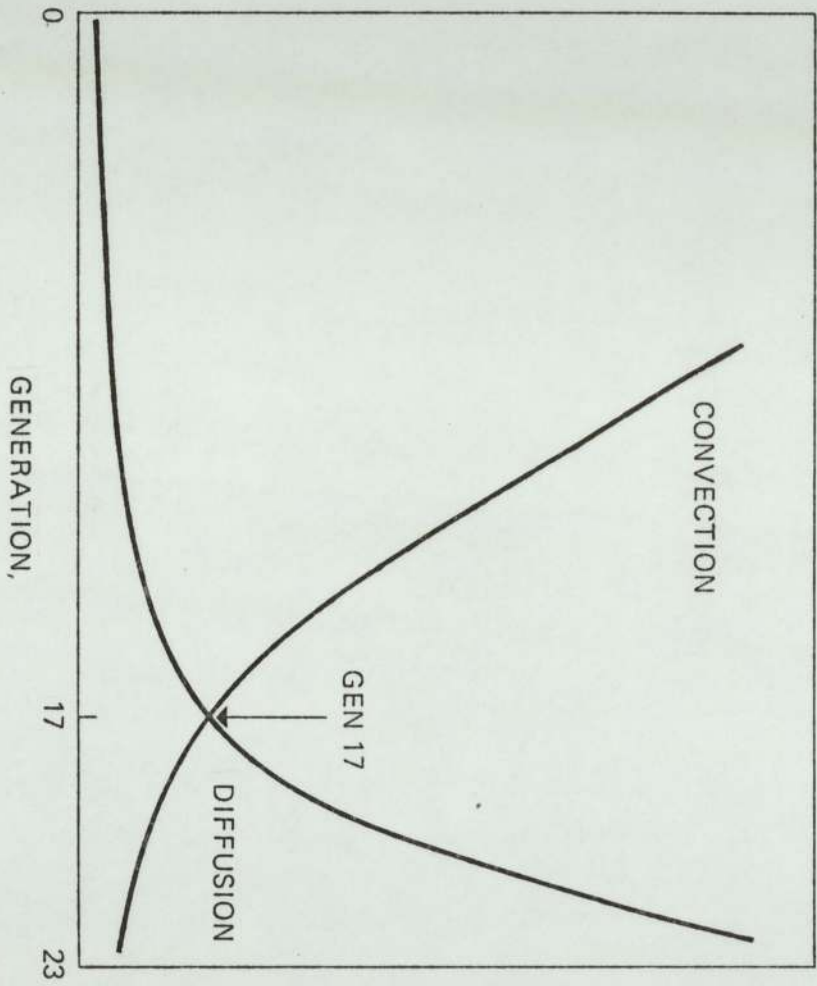
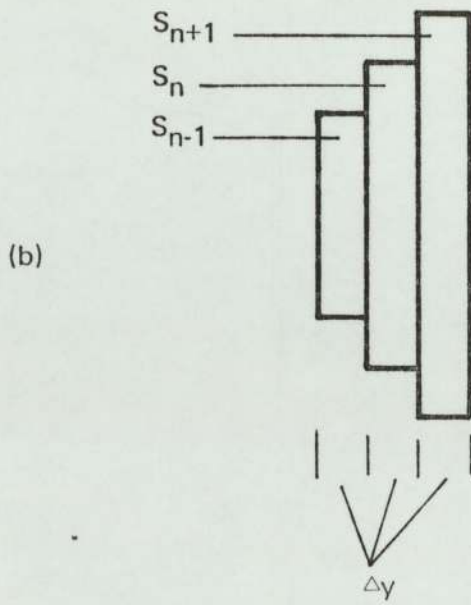
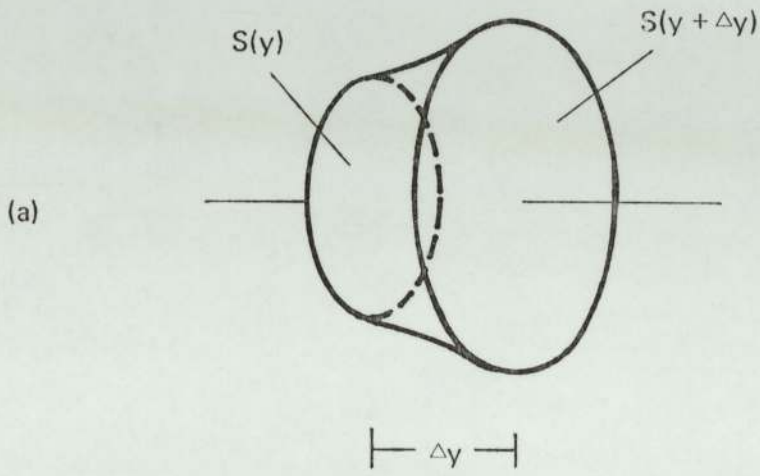


FIGURE 4

FIGURE 5



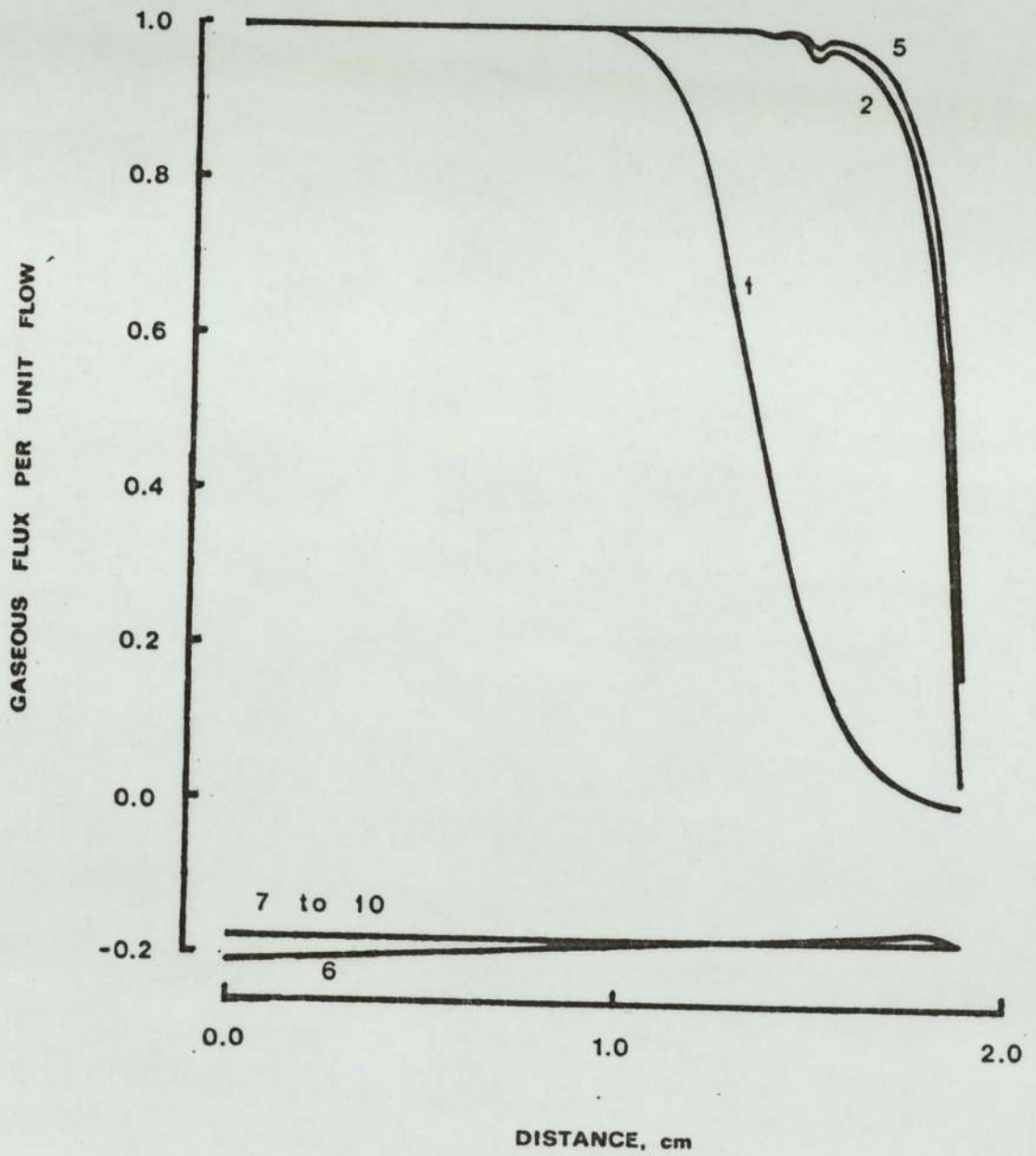


FIGURE 6

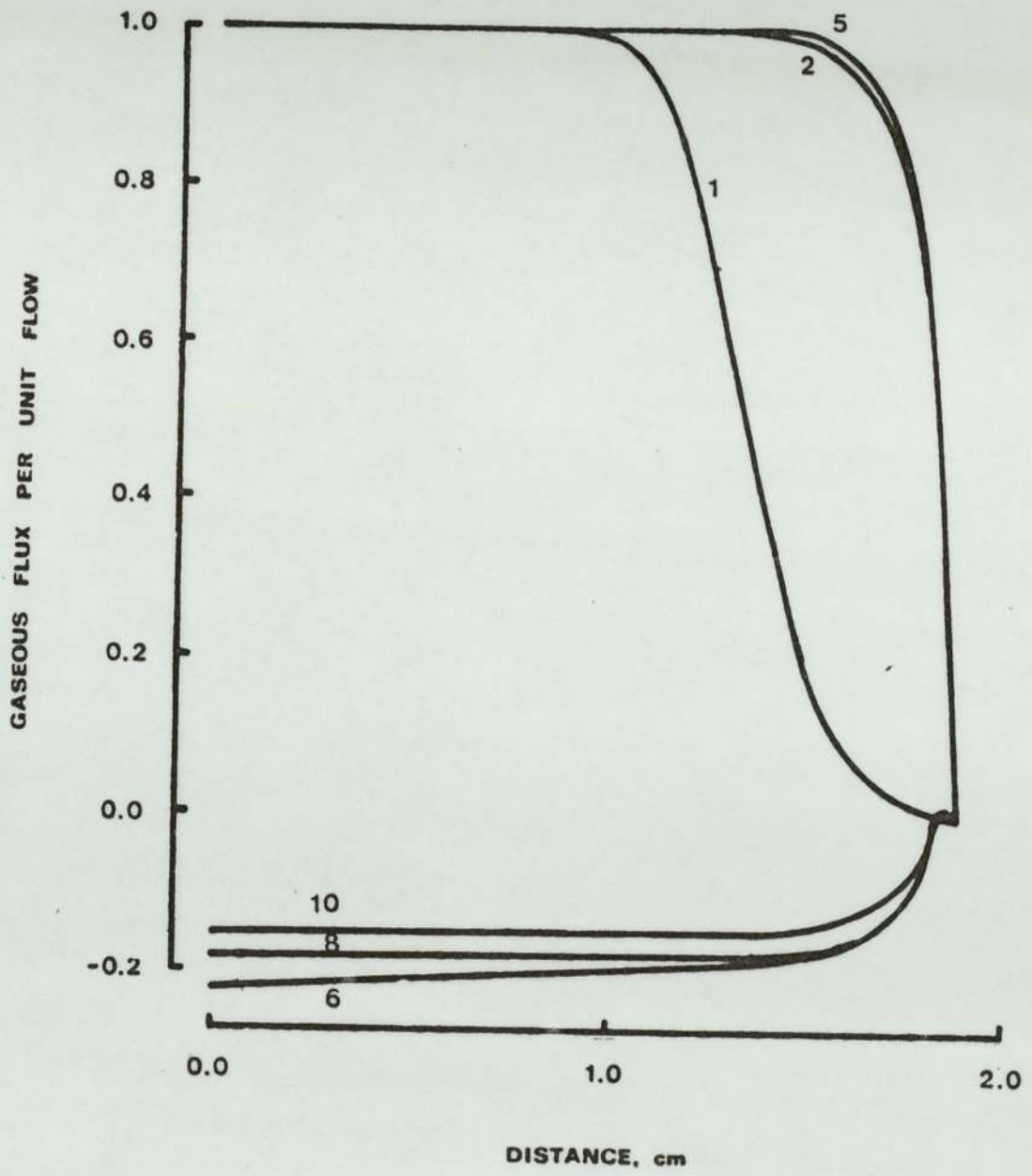


FIGURE 7

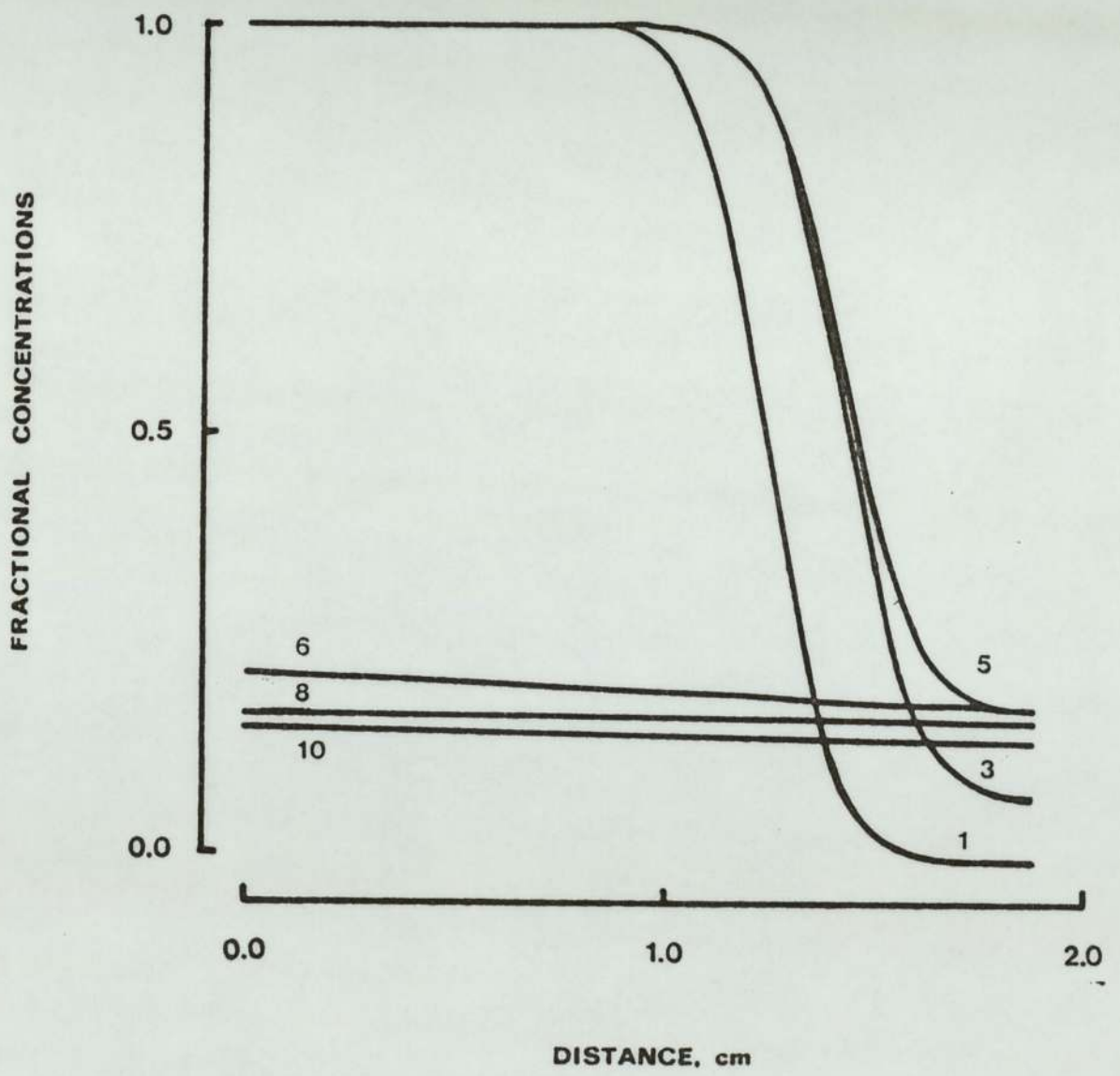


FIGURE 8

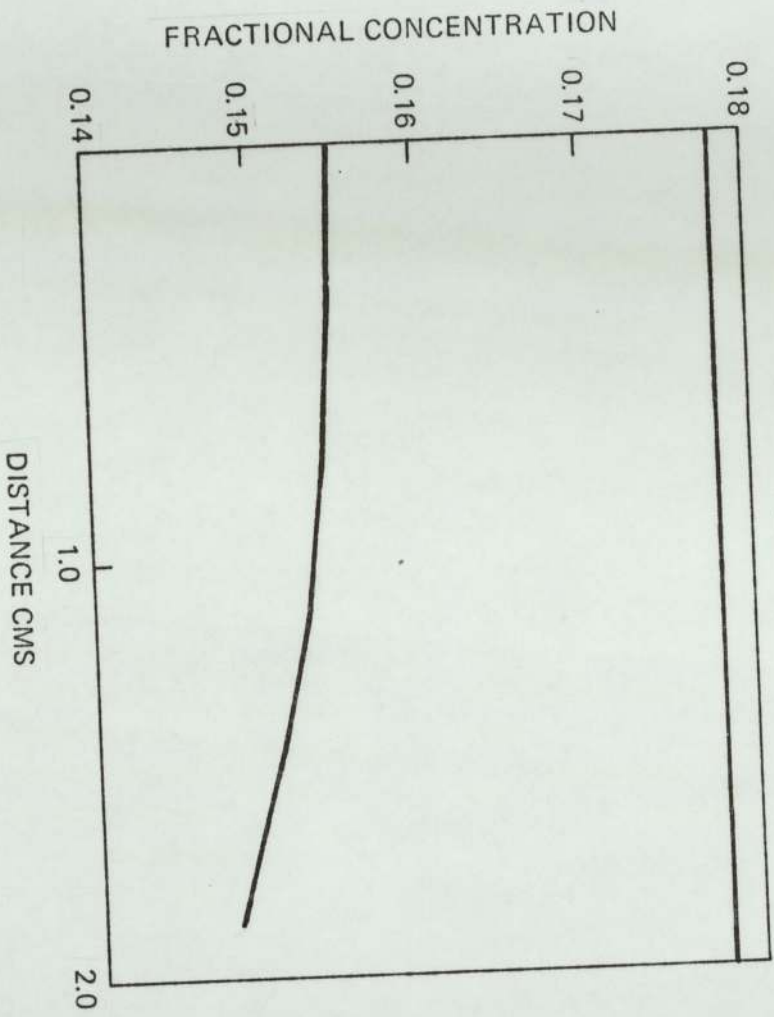
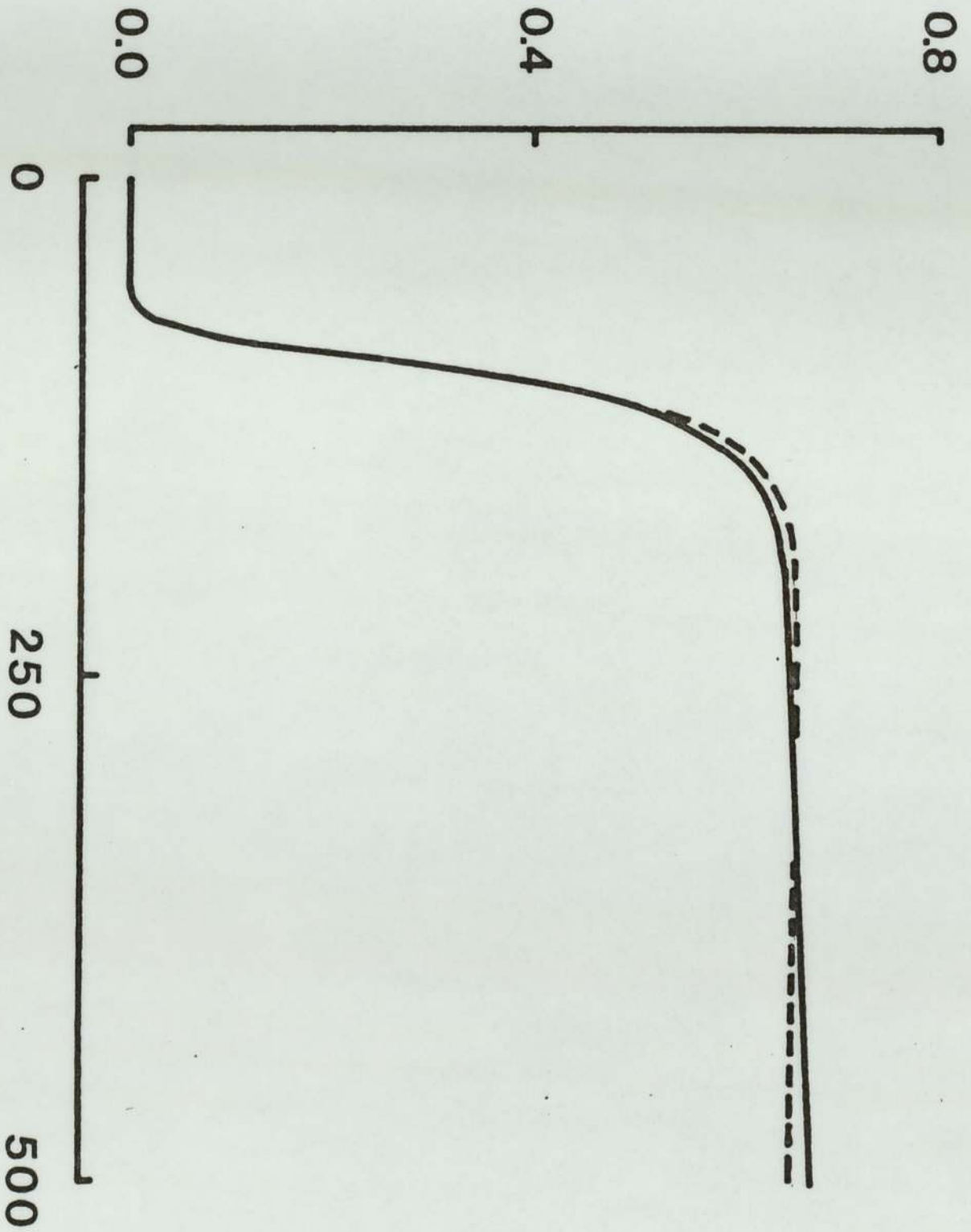


FIGURE 9

# NITROGEN CONCENTRATION



EXPERIMENTAL DATA

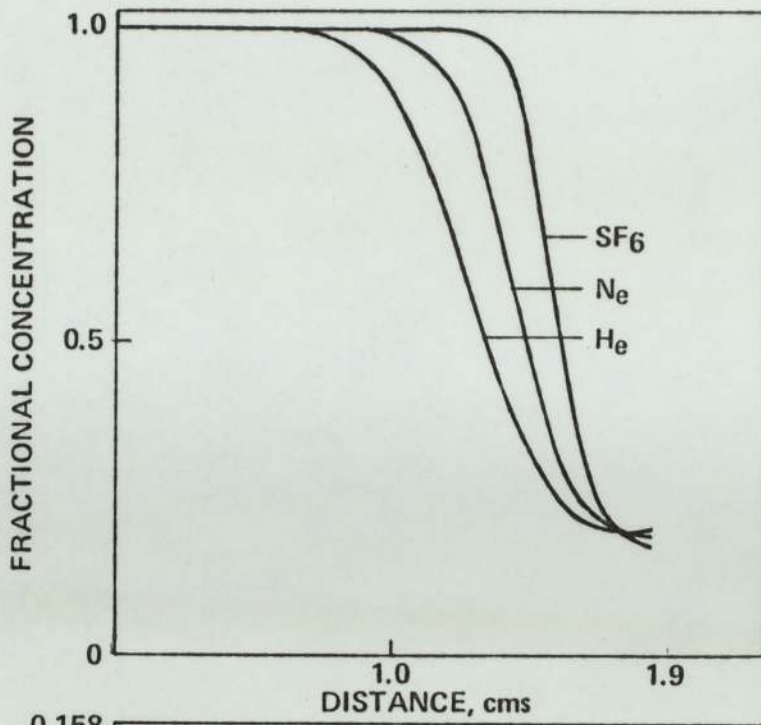


FIGURE 11

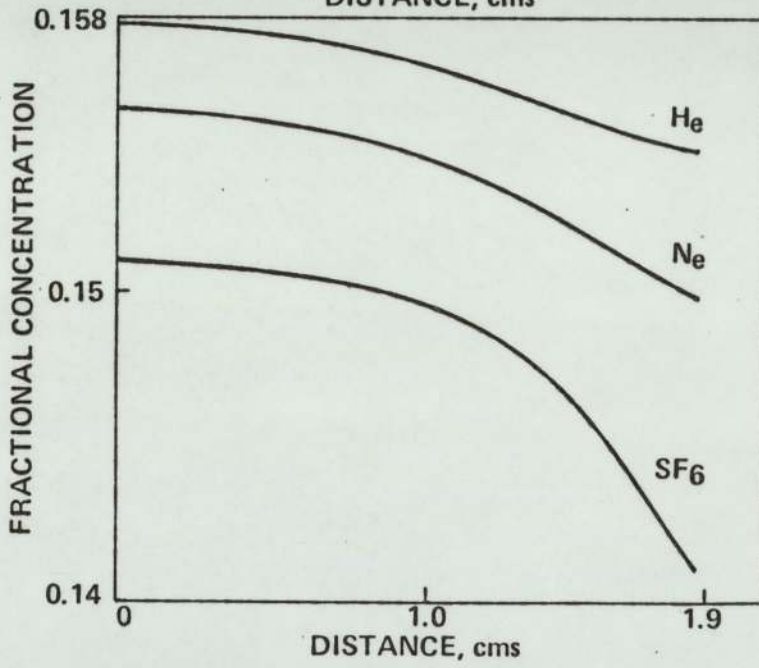


FIGURE 12

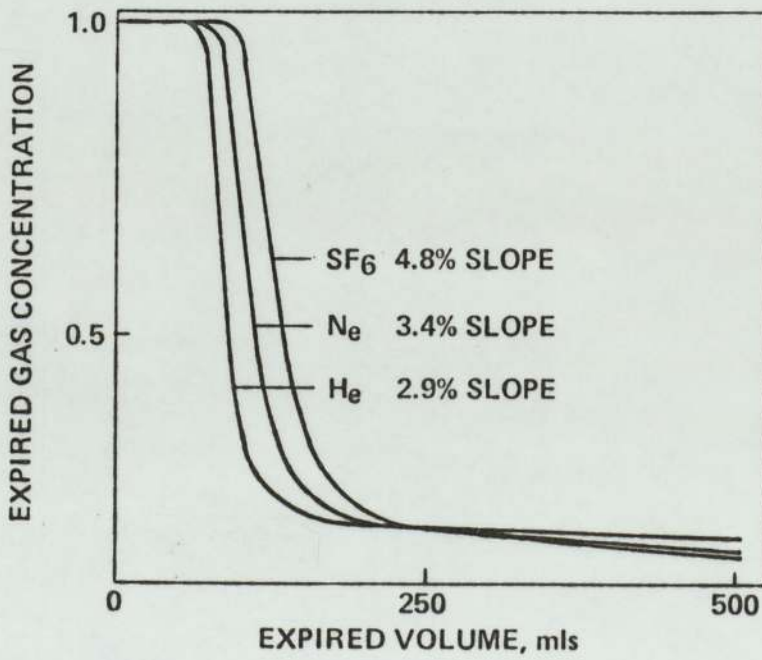


FIGURE 13

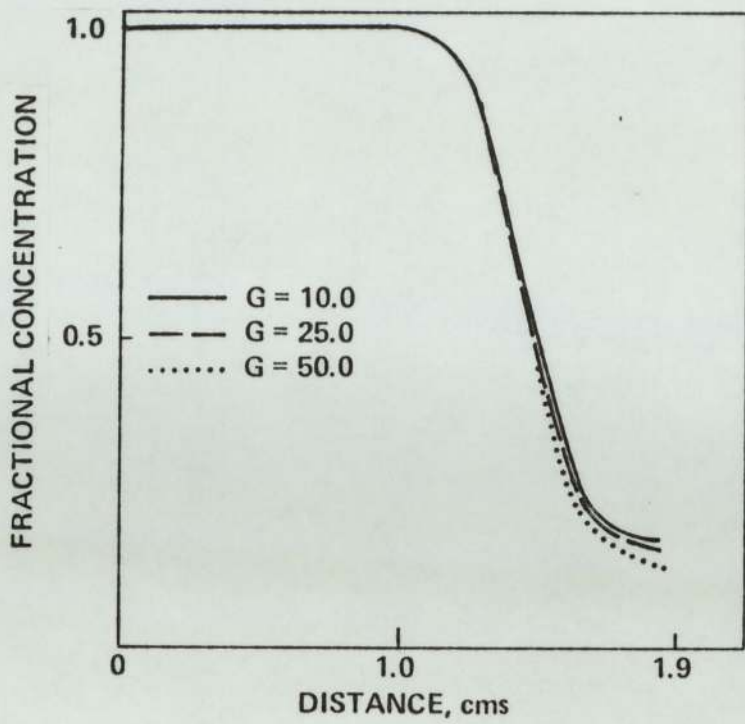


FIGURE 14

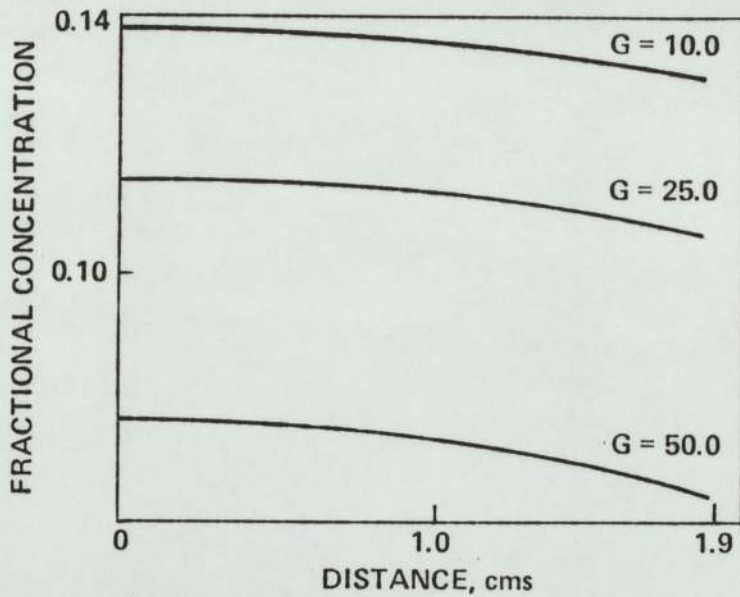


FIGURE 15

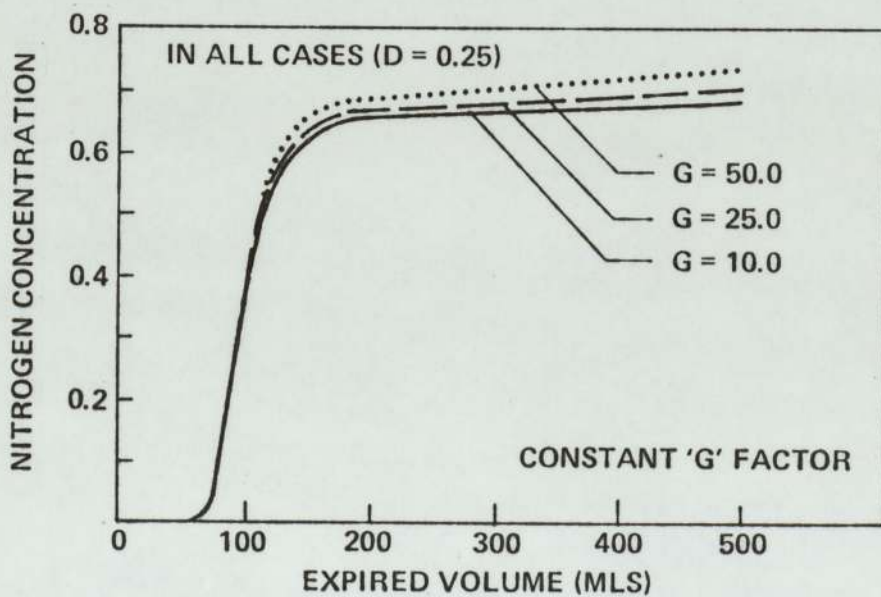


FIGURE 16

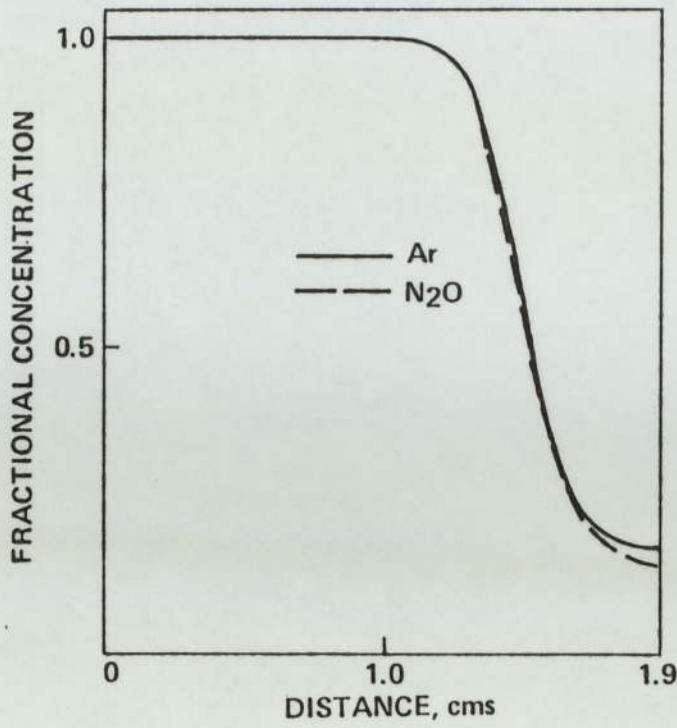


FIGURE 17

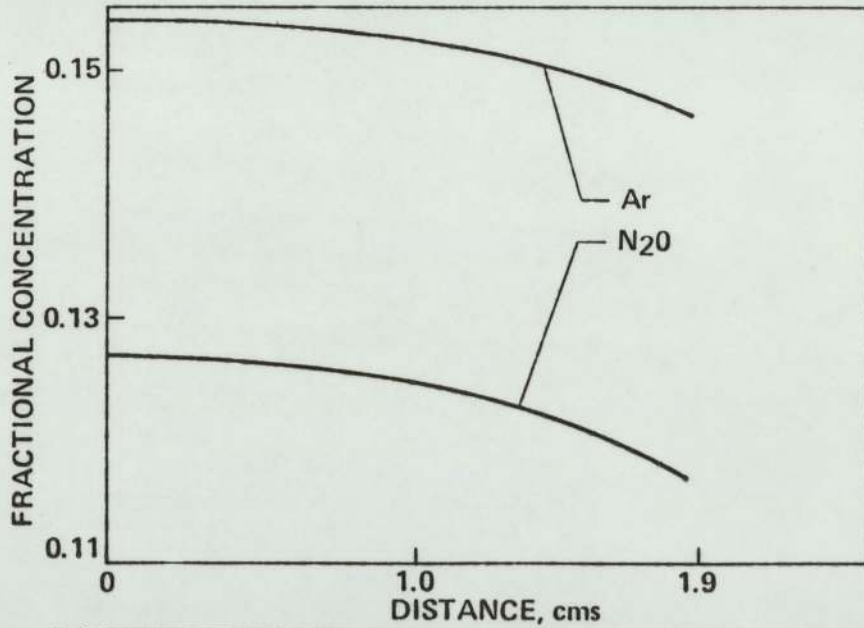


FIGURE 18

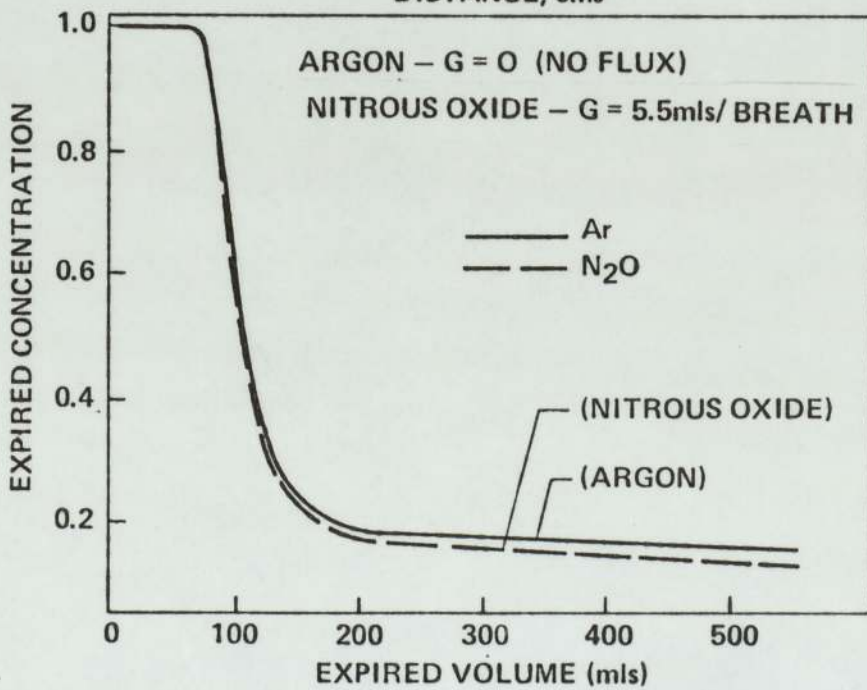
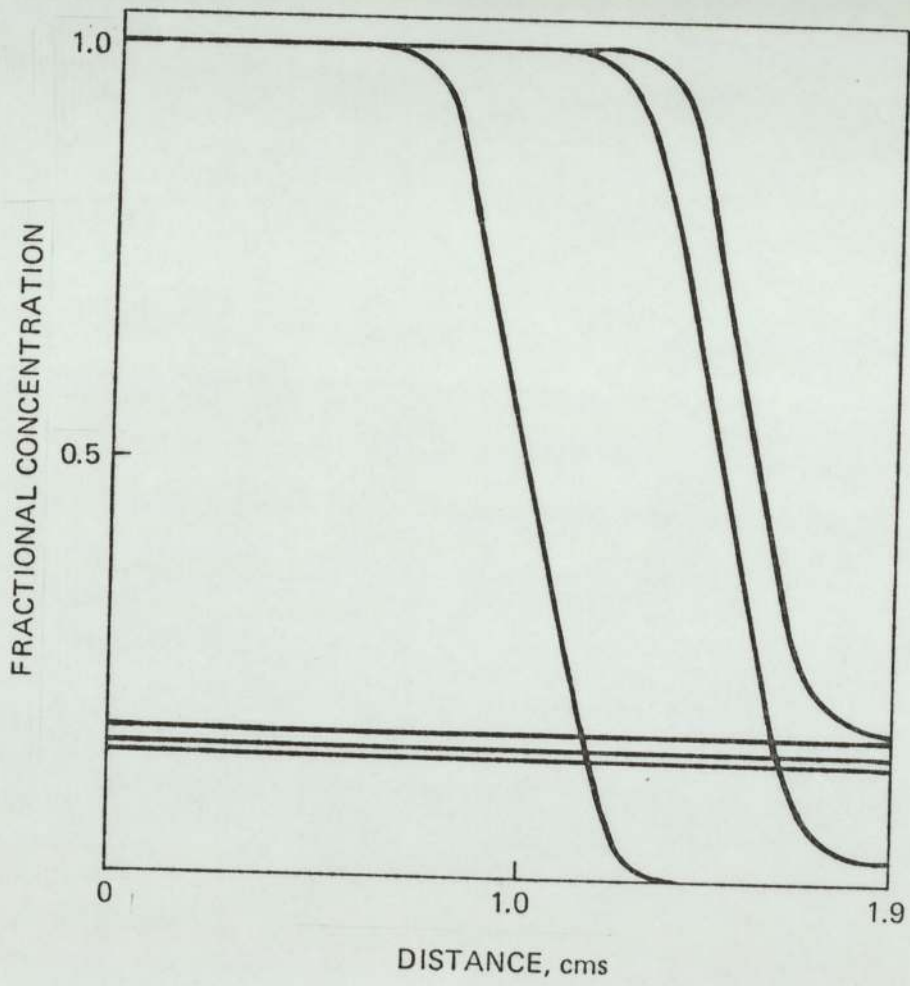


FIGURE 19

FIGURE 20



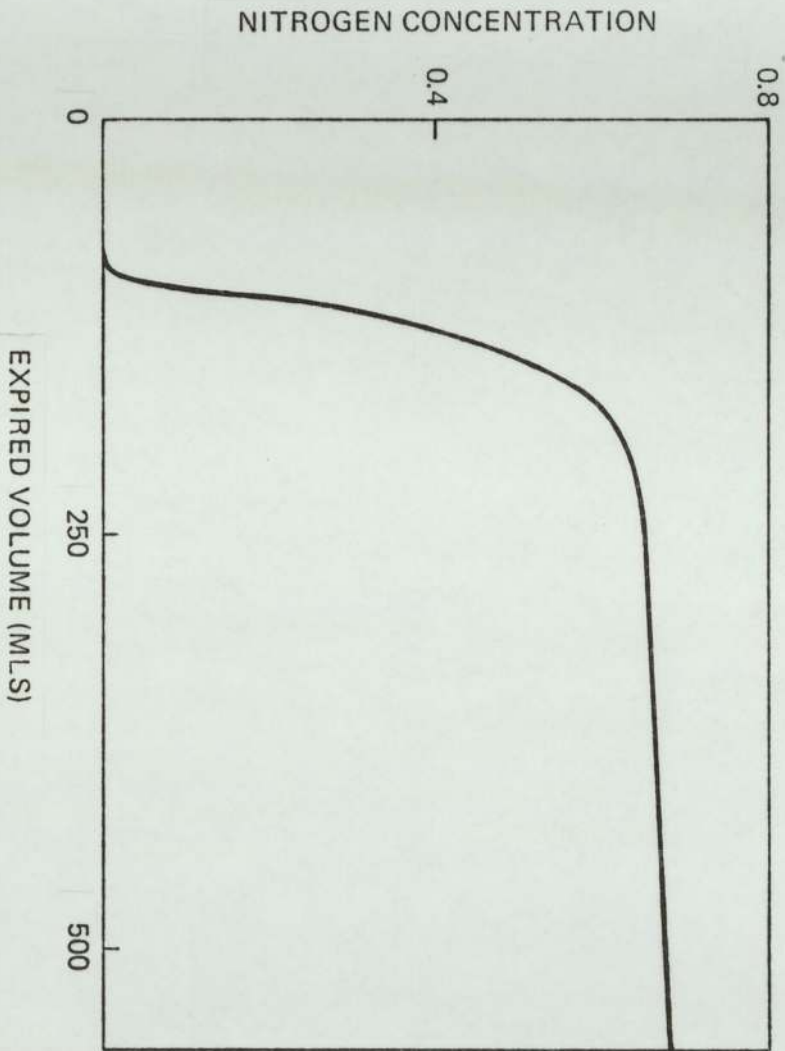
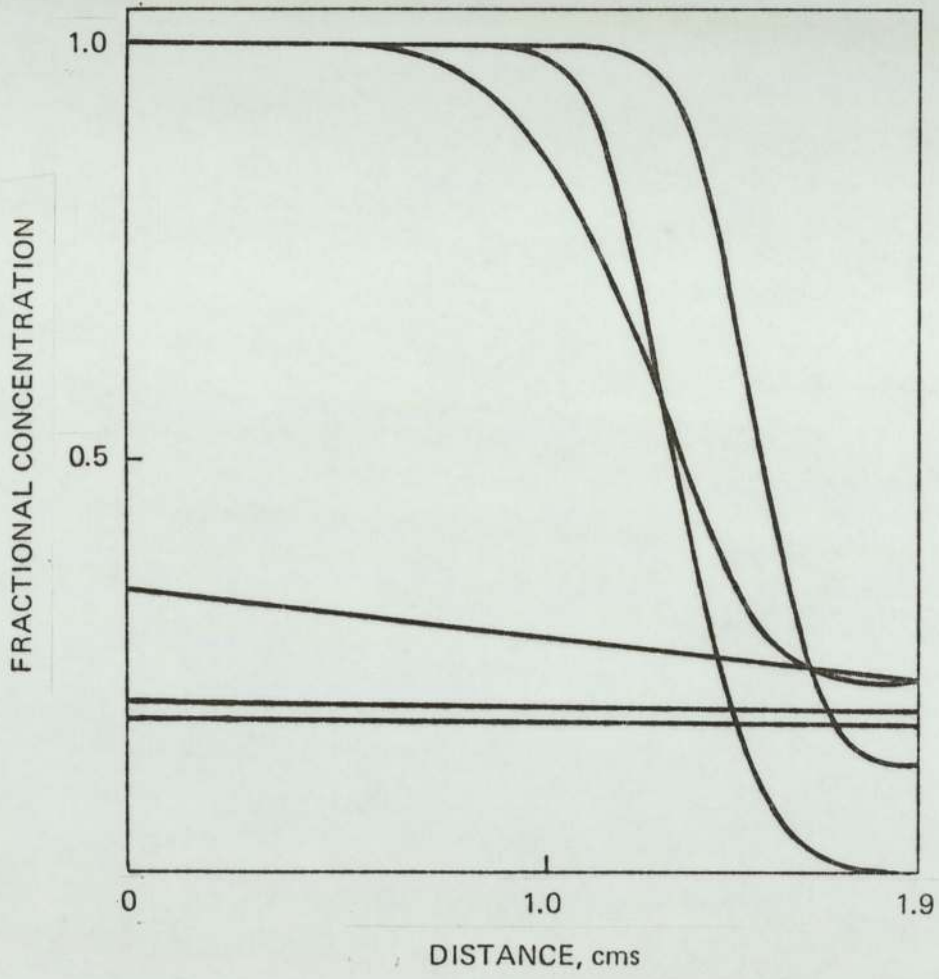


FIGURE 21

FIGURE 22



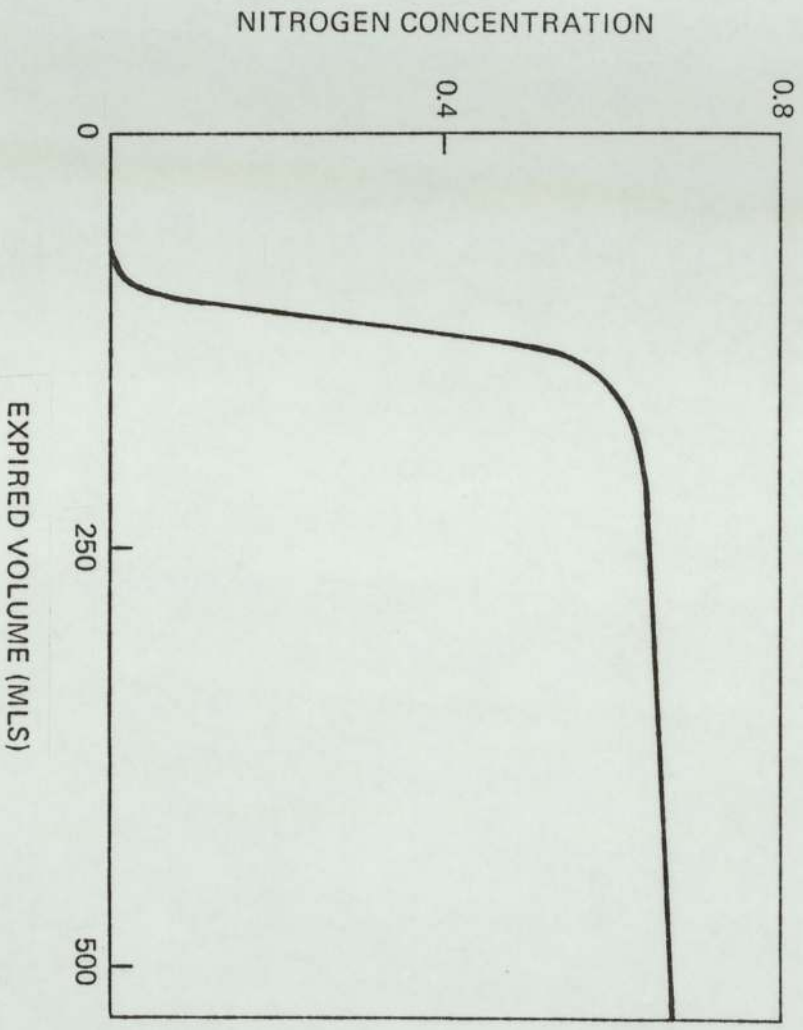
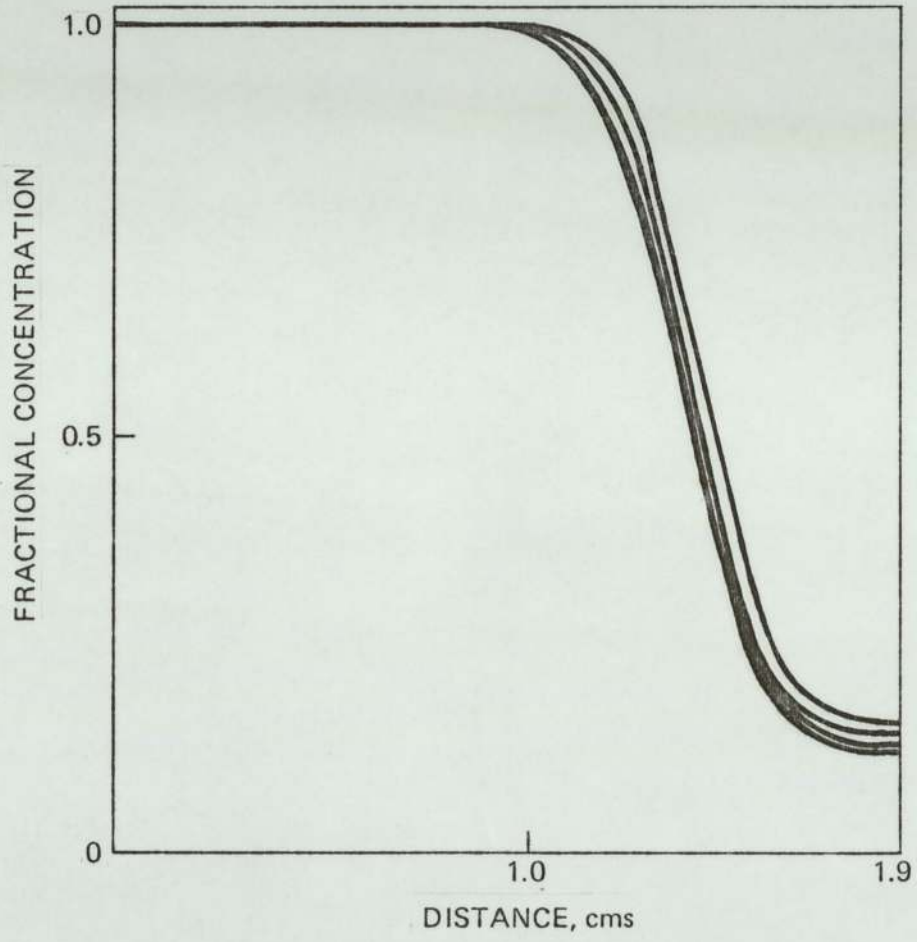


FIGURE 23

FIGURE 24



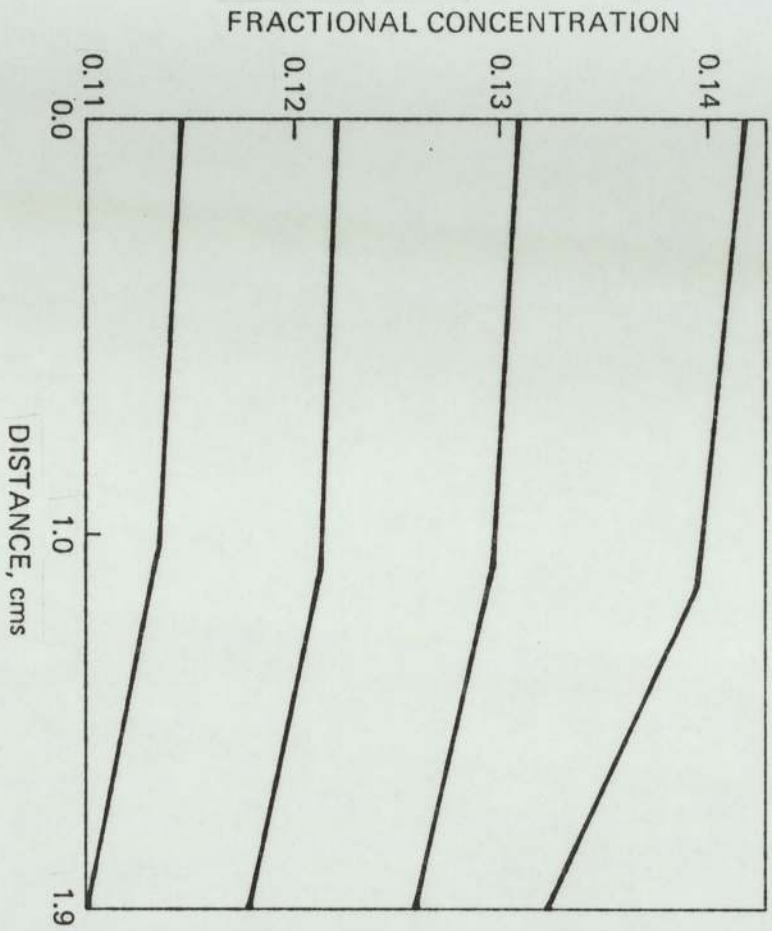


FIGURE 25

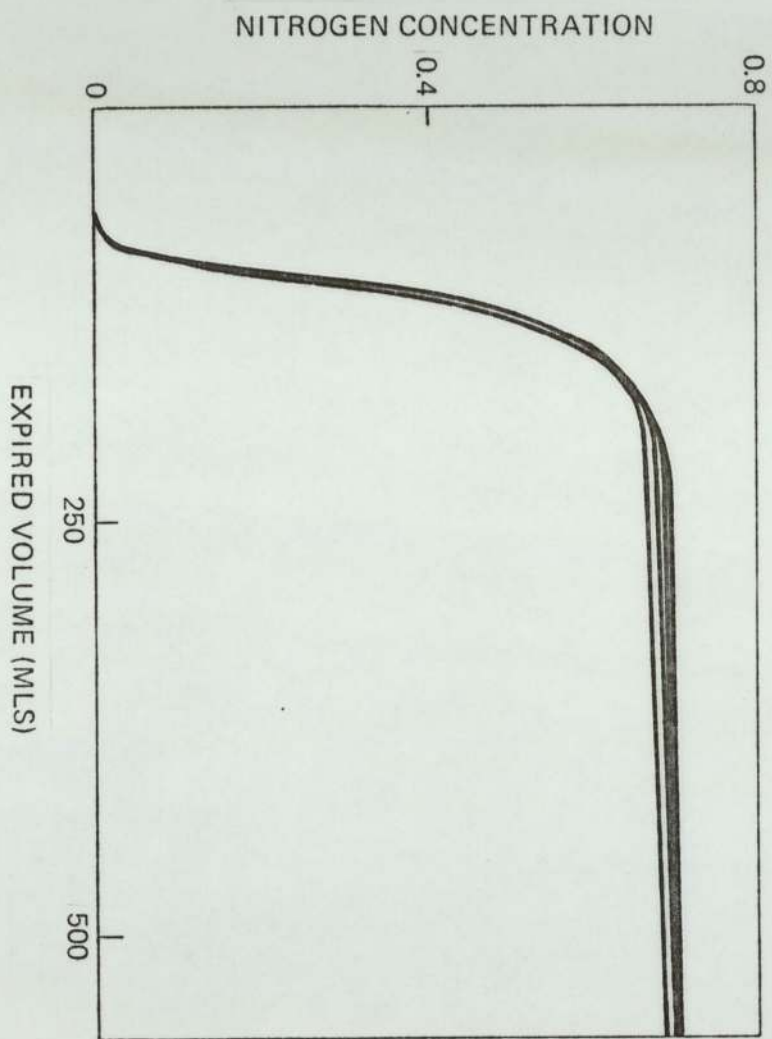
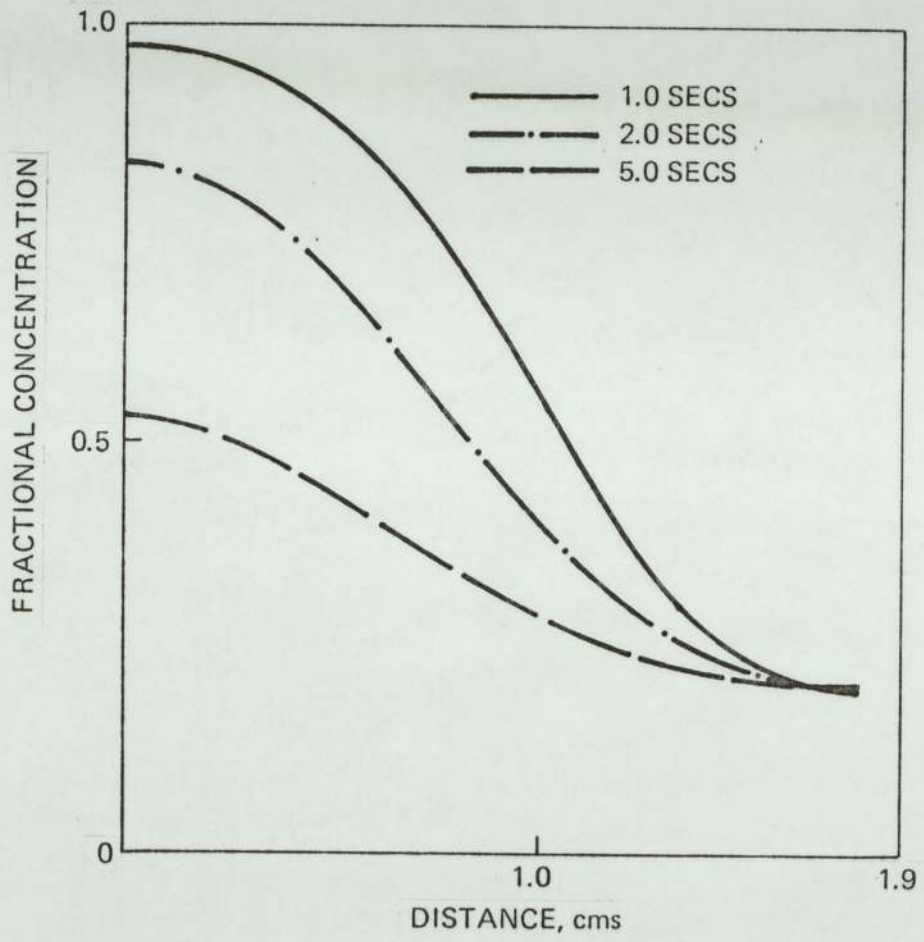


FIGURE 26

FIGURE 27



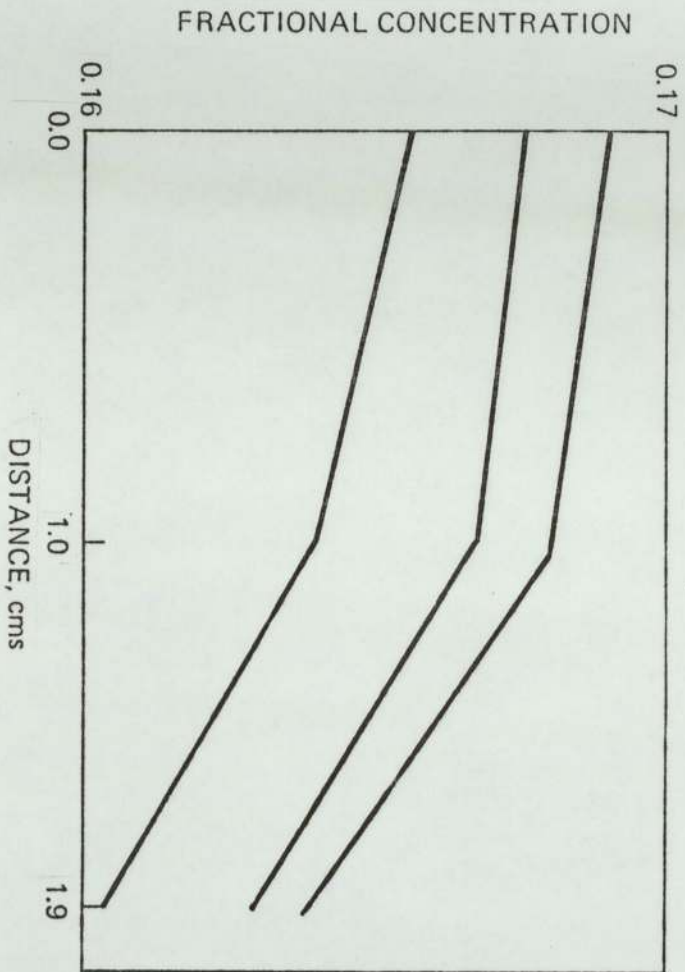
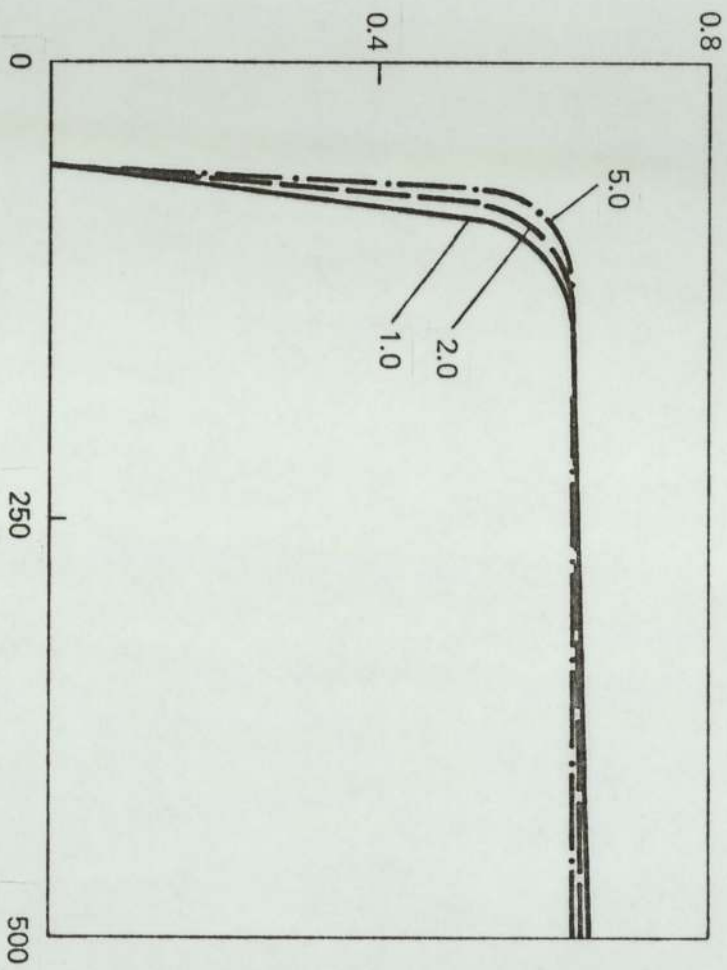


FIGURE 28

FIGURE 29  
BREATH - HOLDING STUDIES



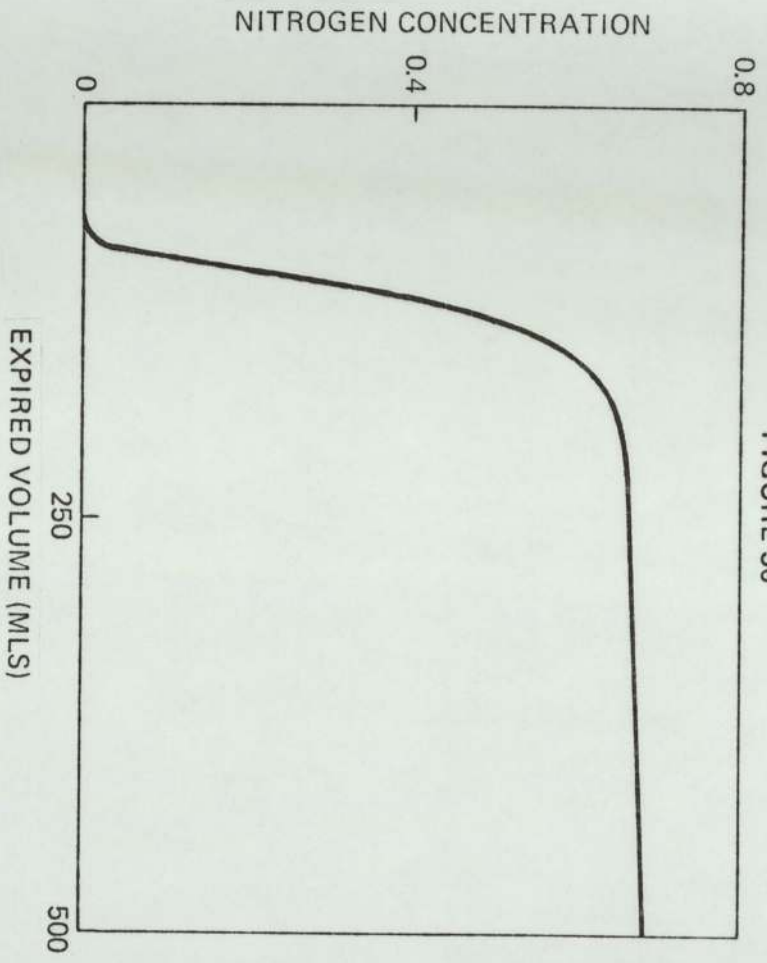


FIGURE 30

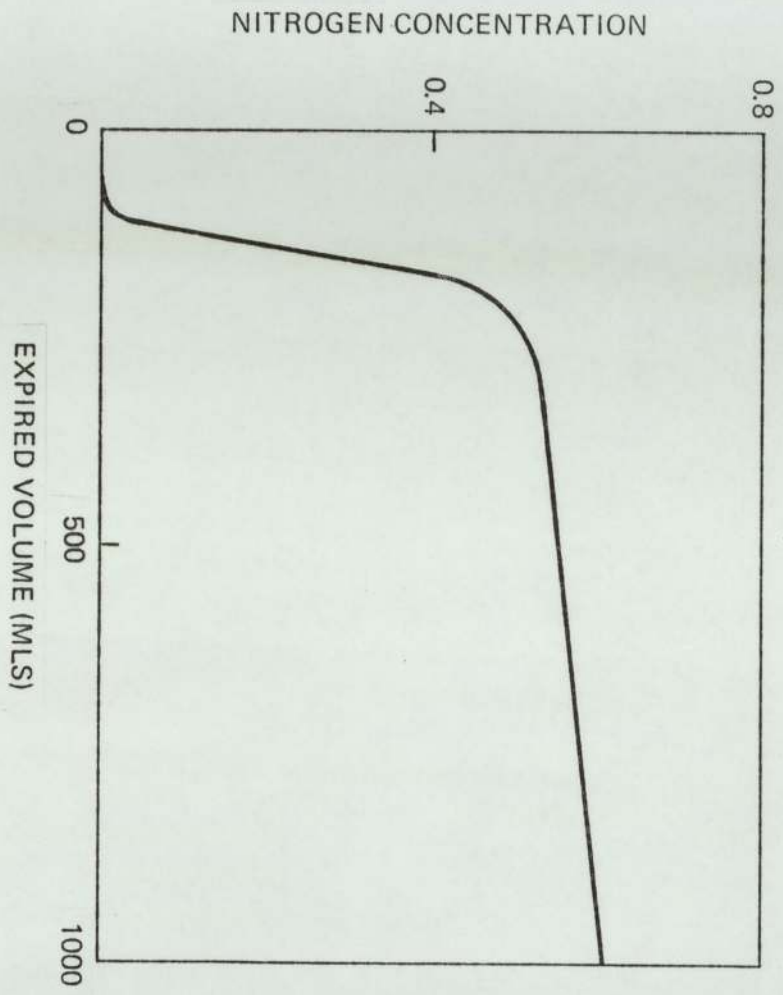


FIGURE 31

SCHEMA OF MODEL WITH NODAL POINT A IN GENERATION 17

FIGURE 32

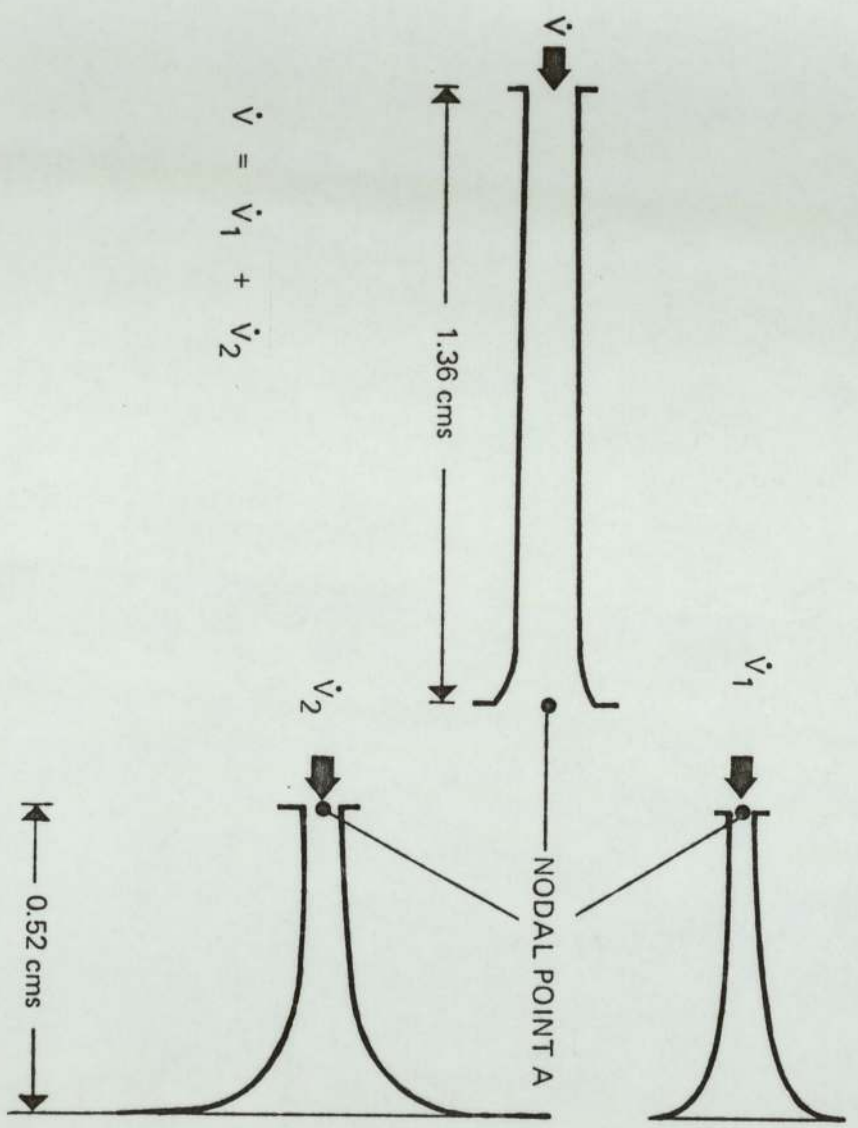


FIGURE 33

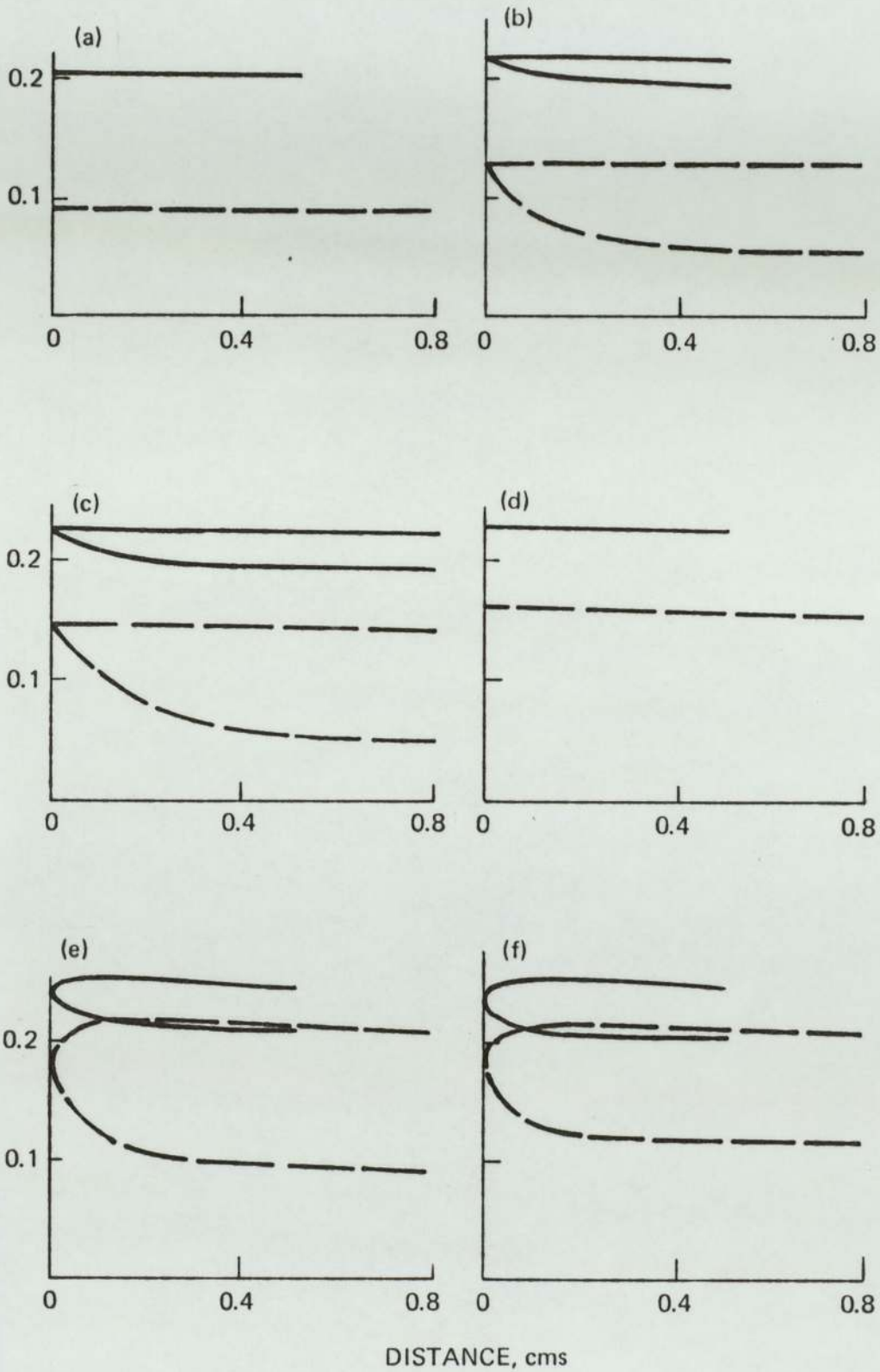


FIGURE 34

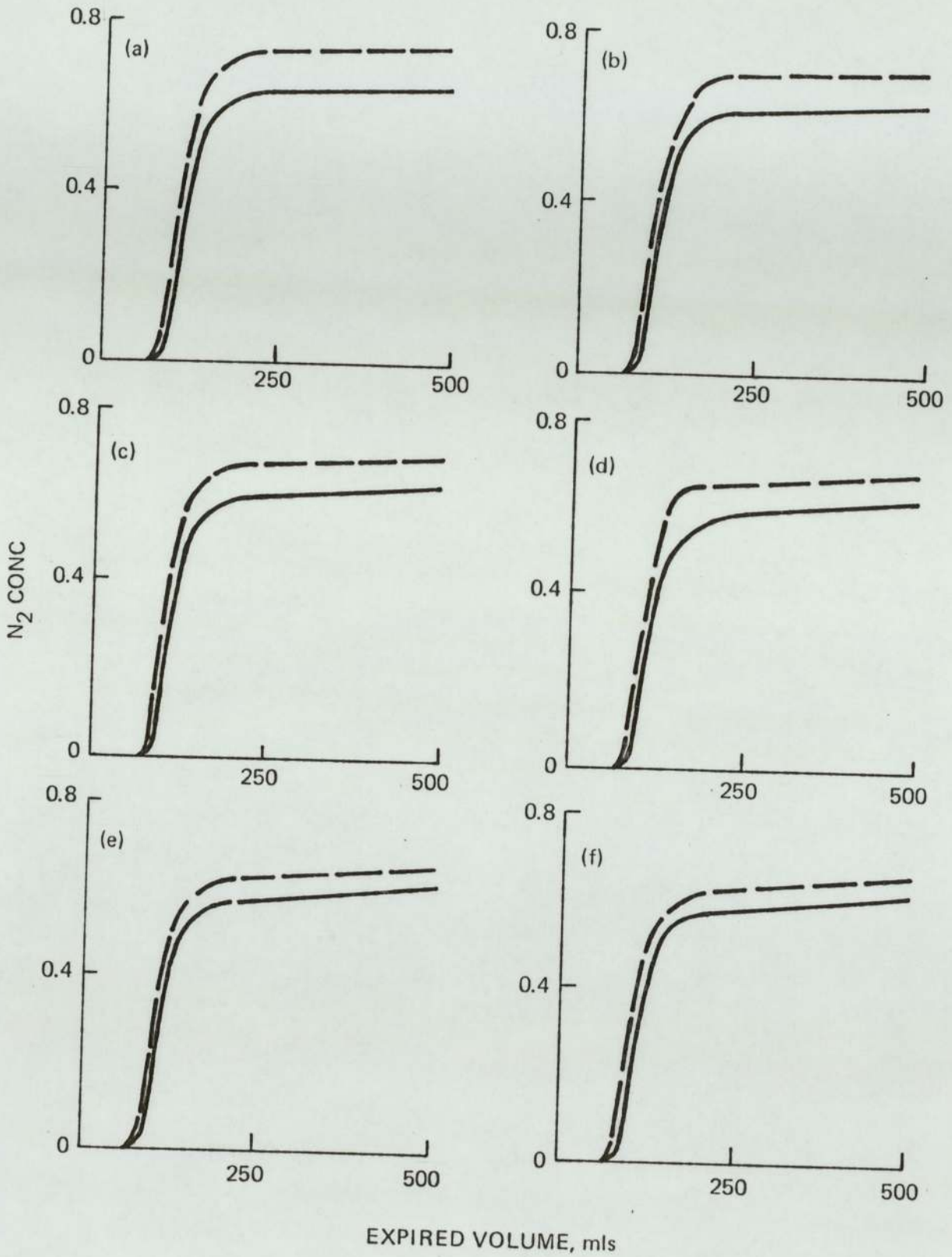


FIGURE 3.5

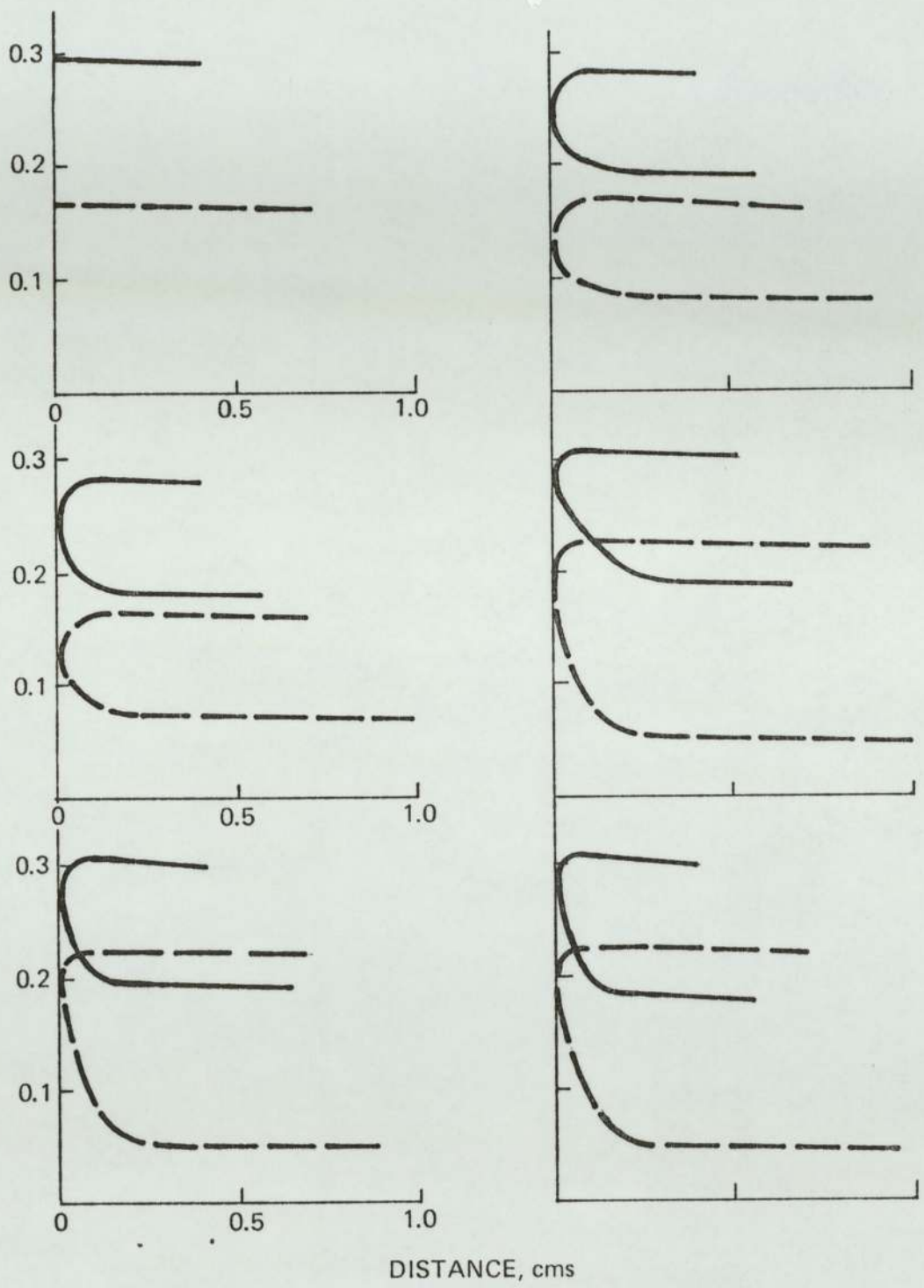


FIGURE 36

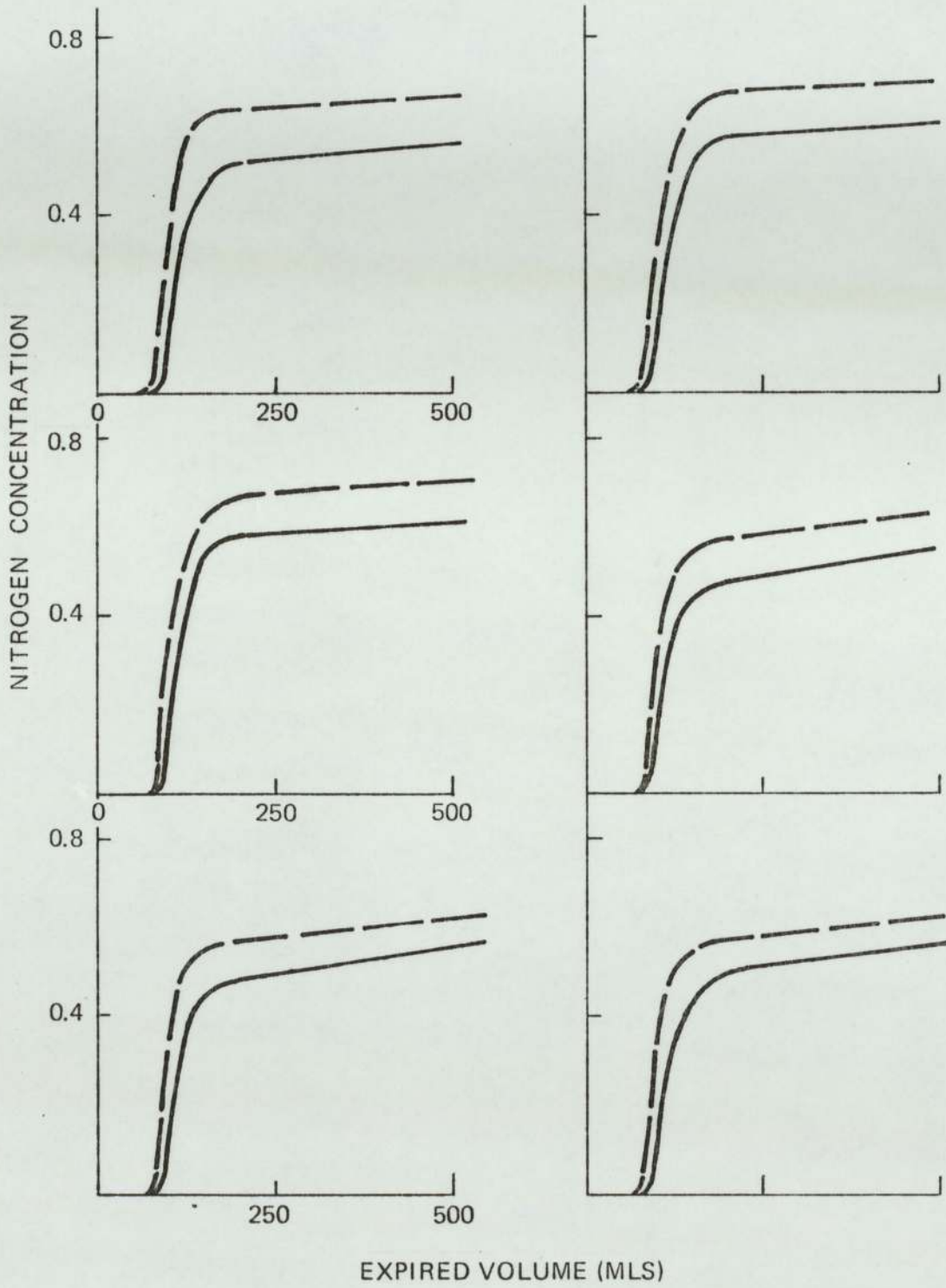


FIGURE 37

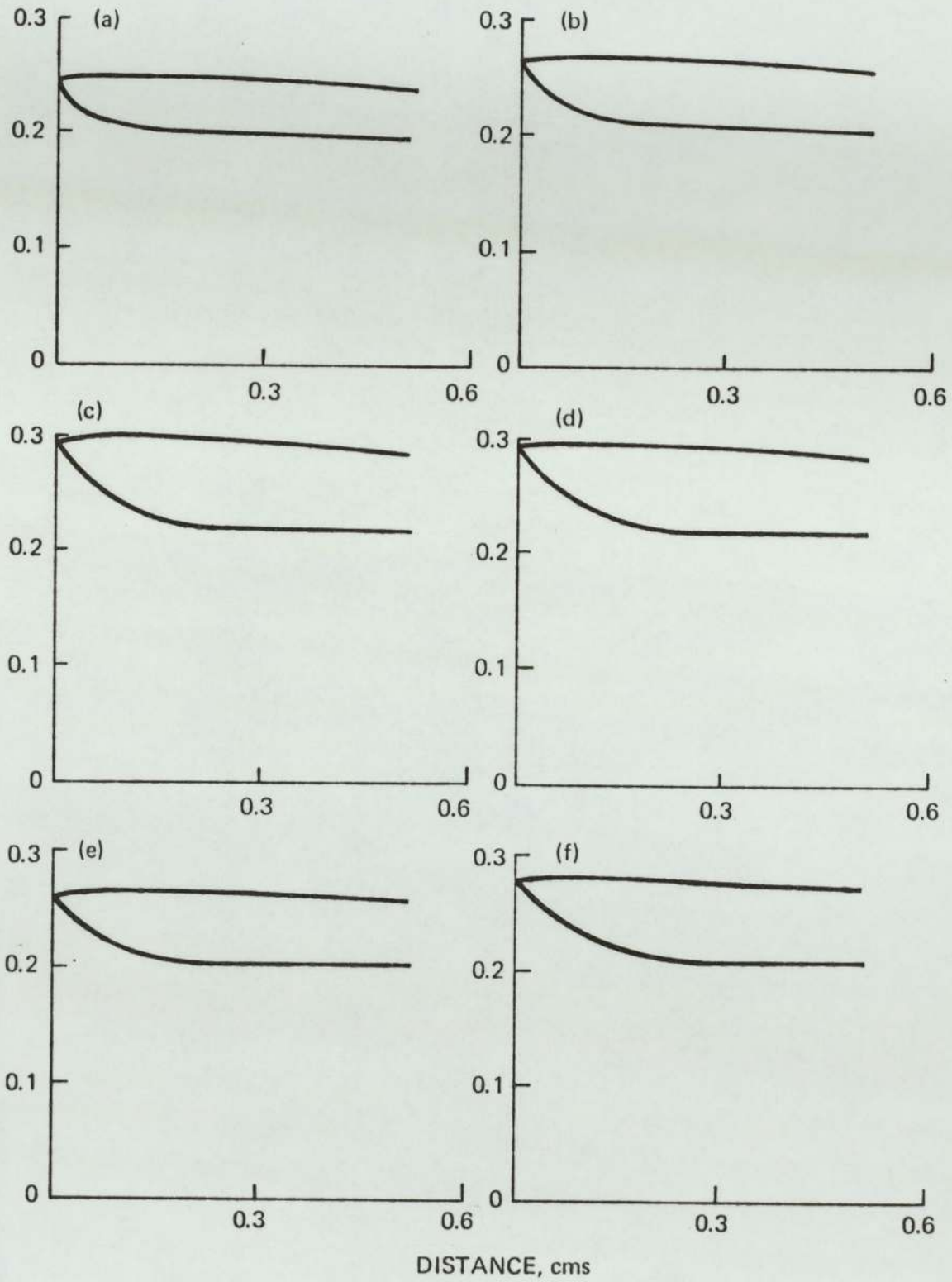


FIGURE 38

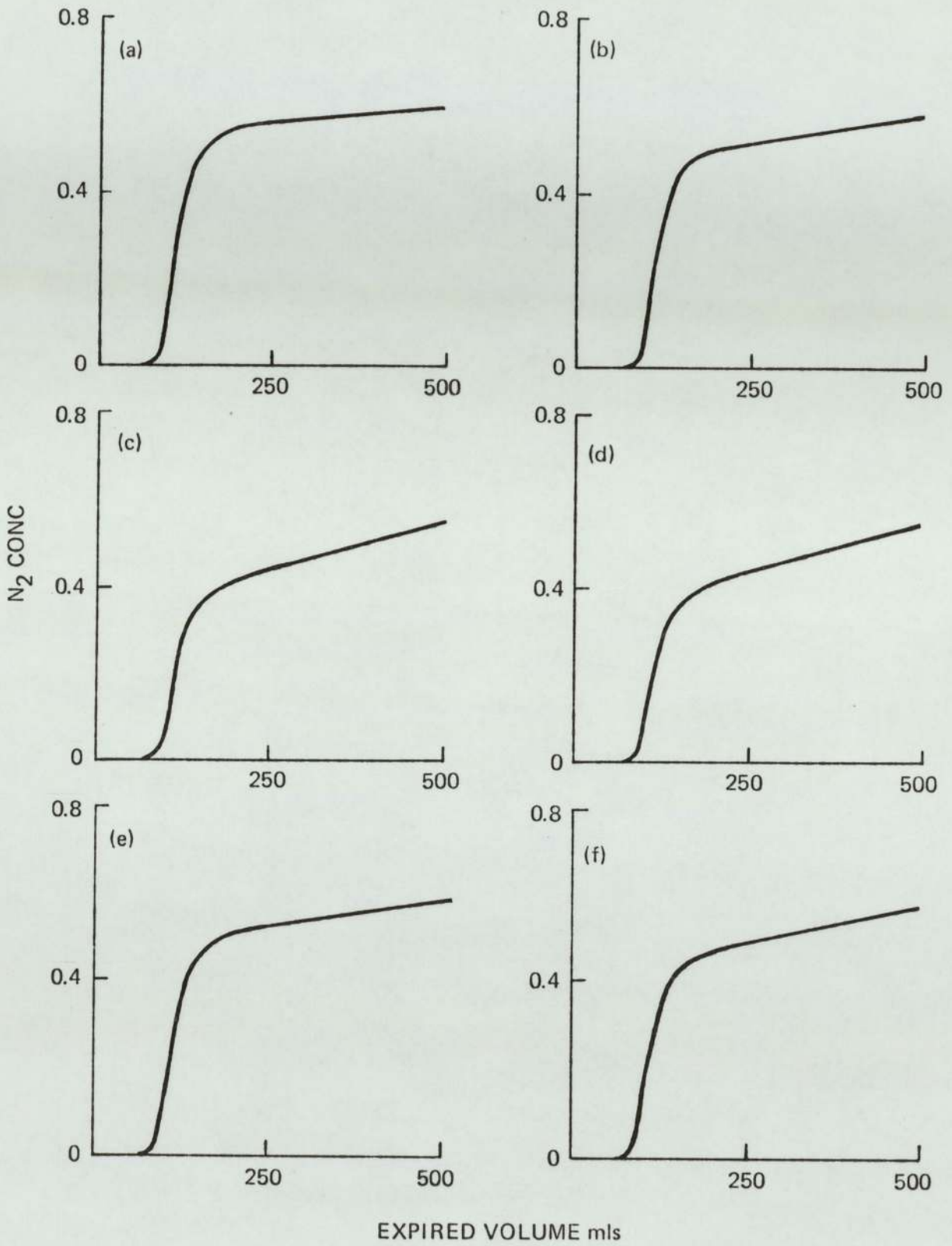


FIGURE 39

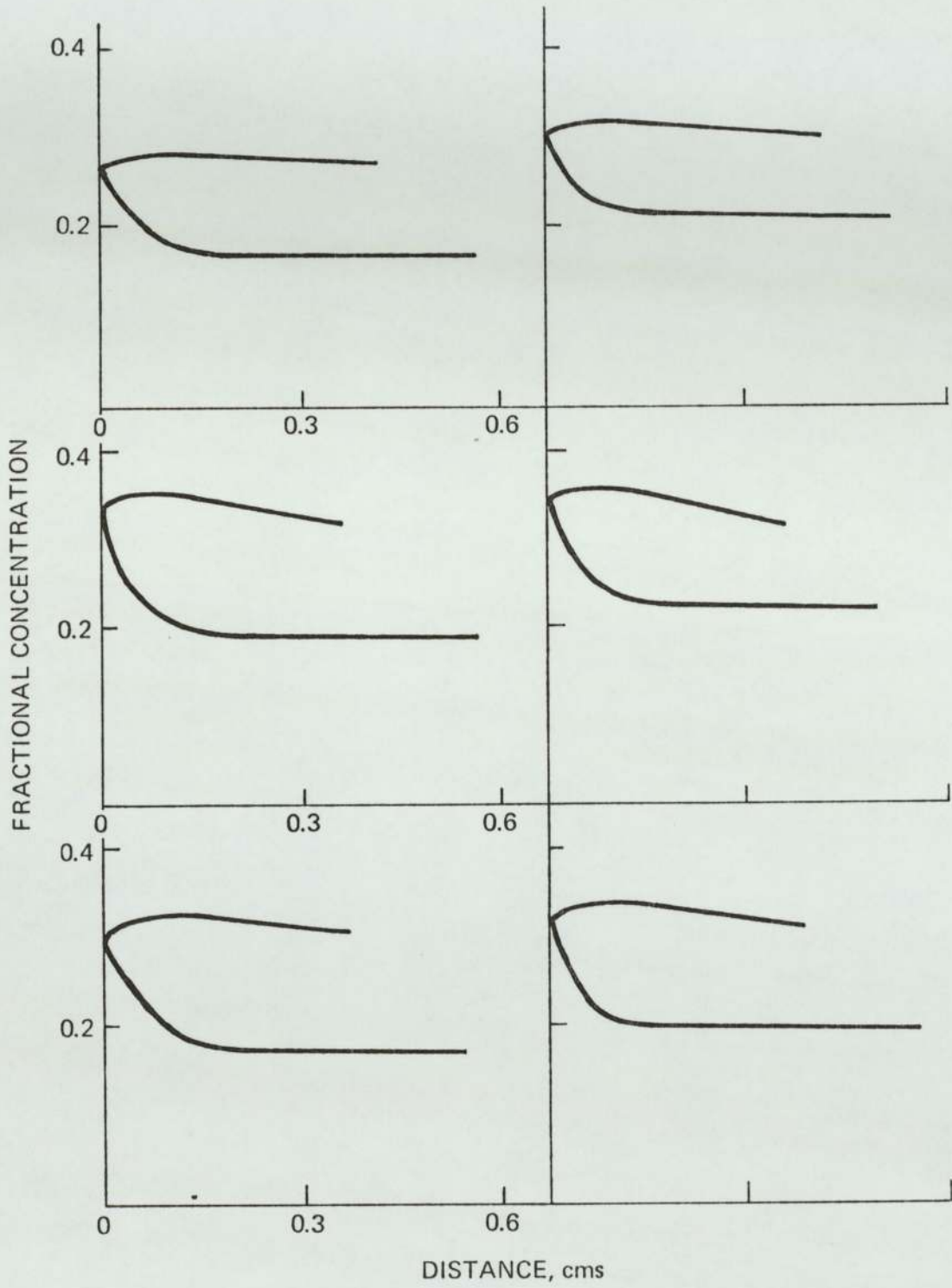


FIGURE 40

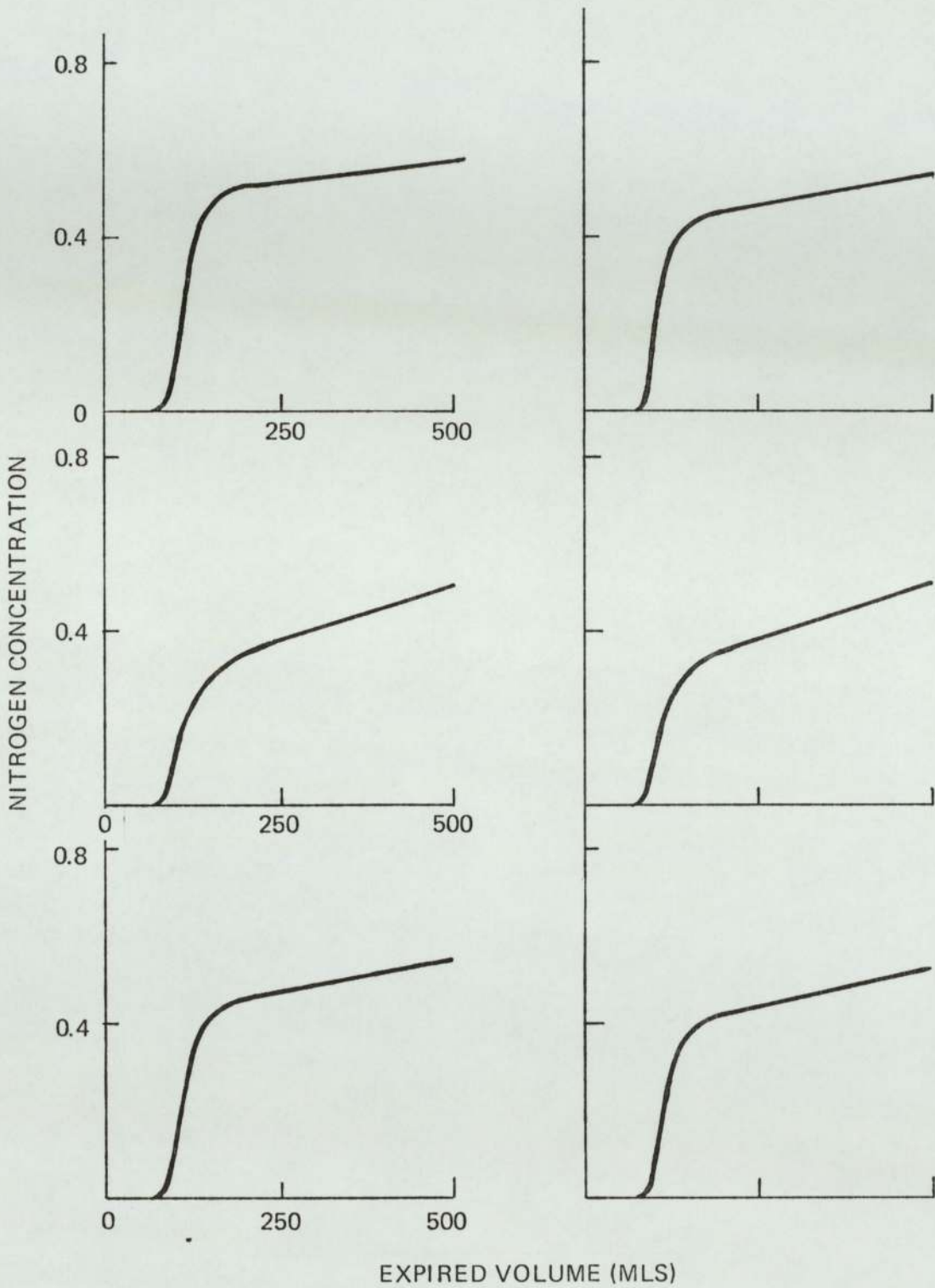


FIGURE 41

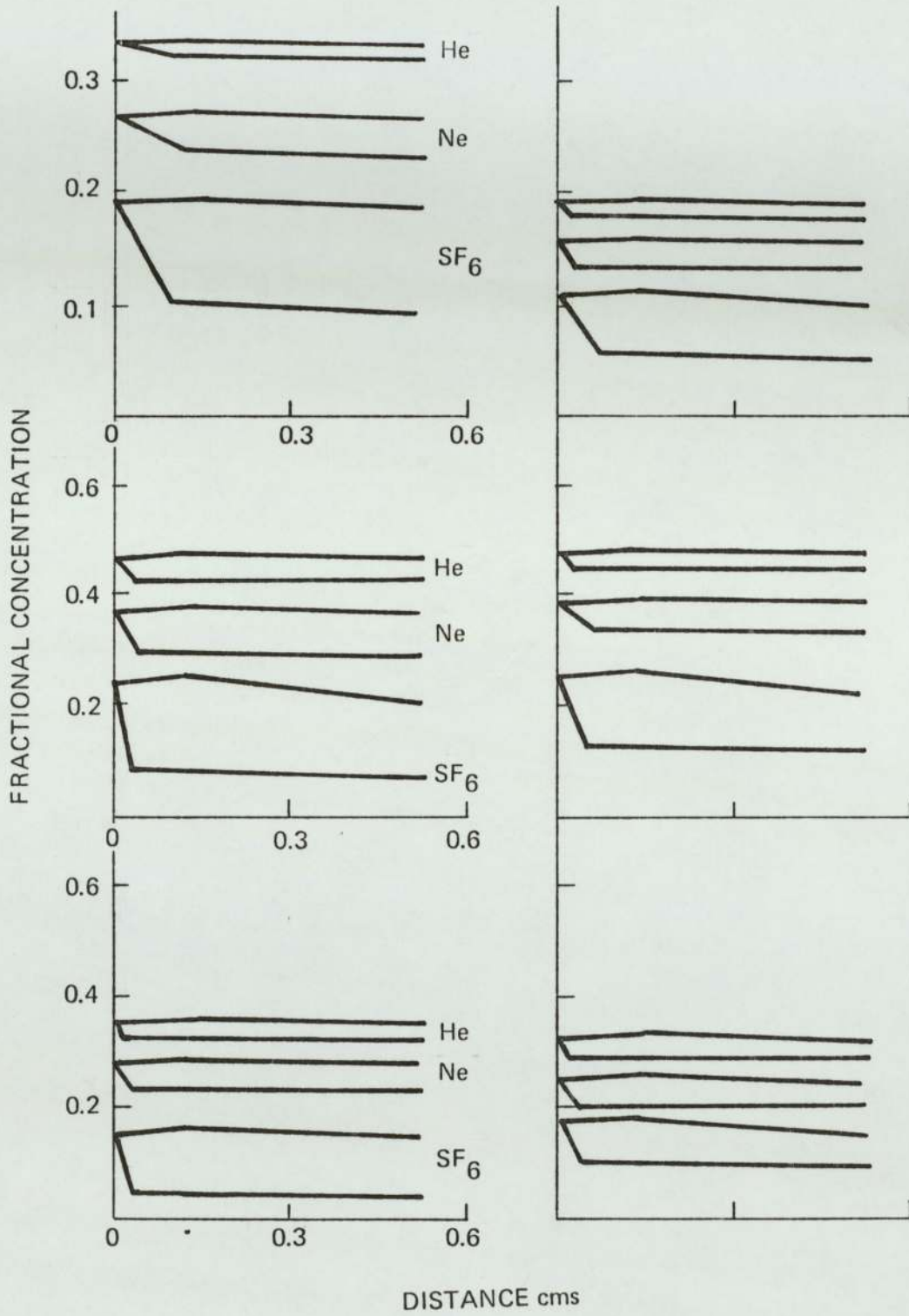


FIGURE 42

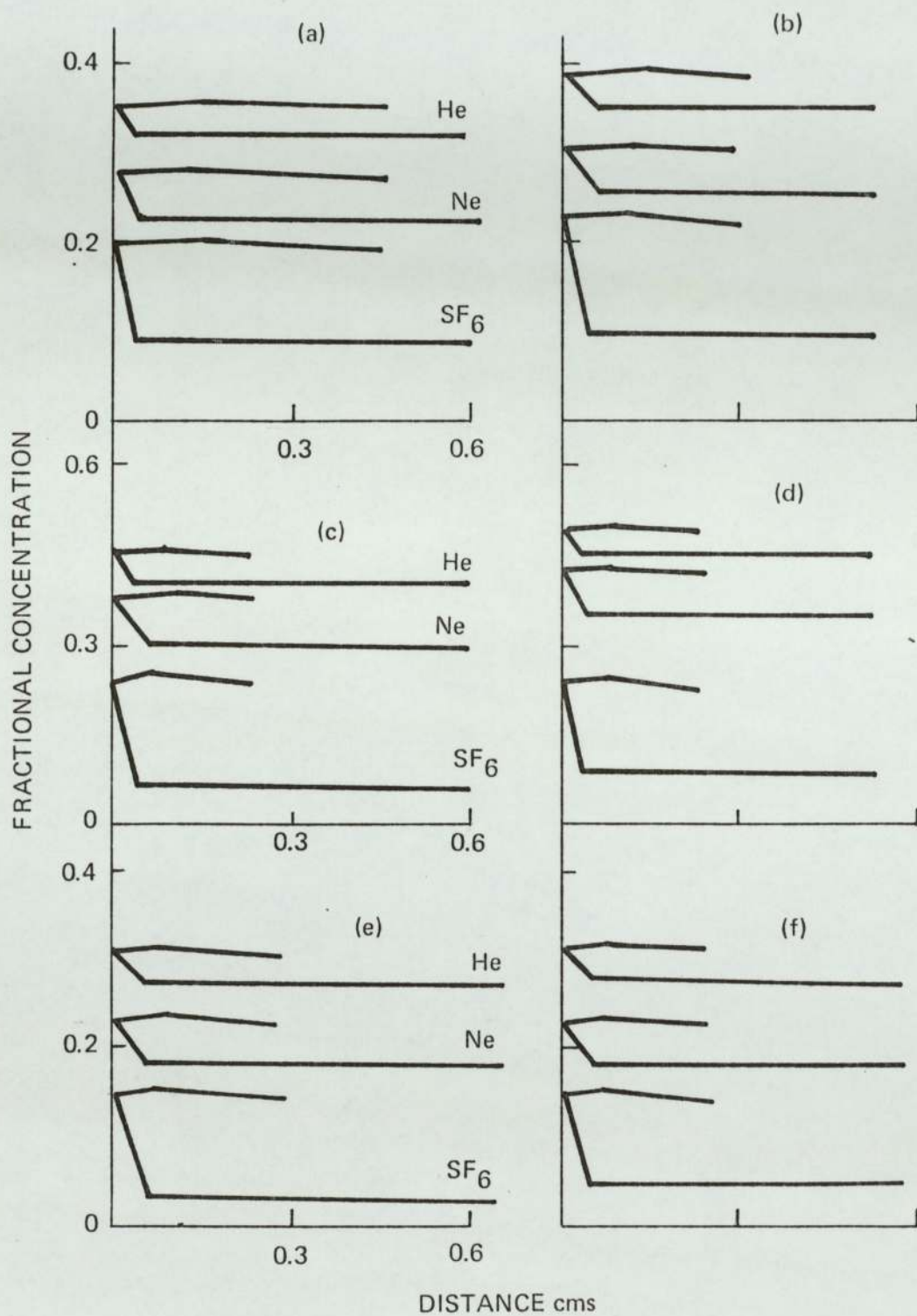




FIGURE 44

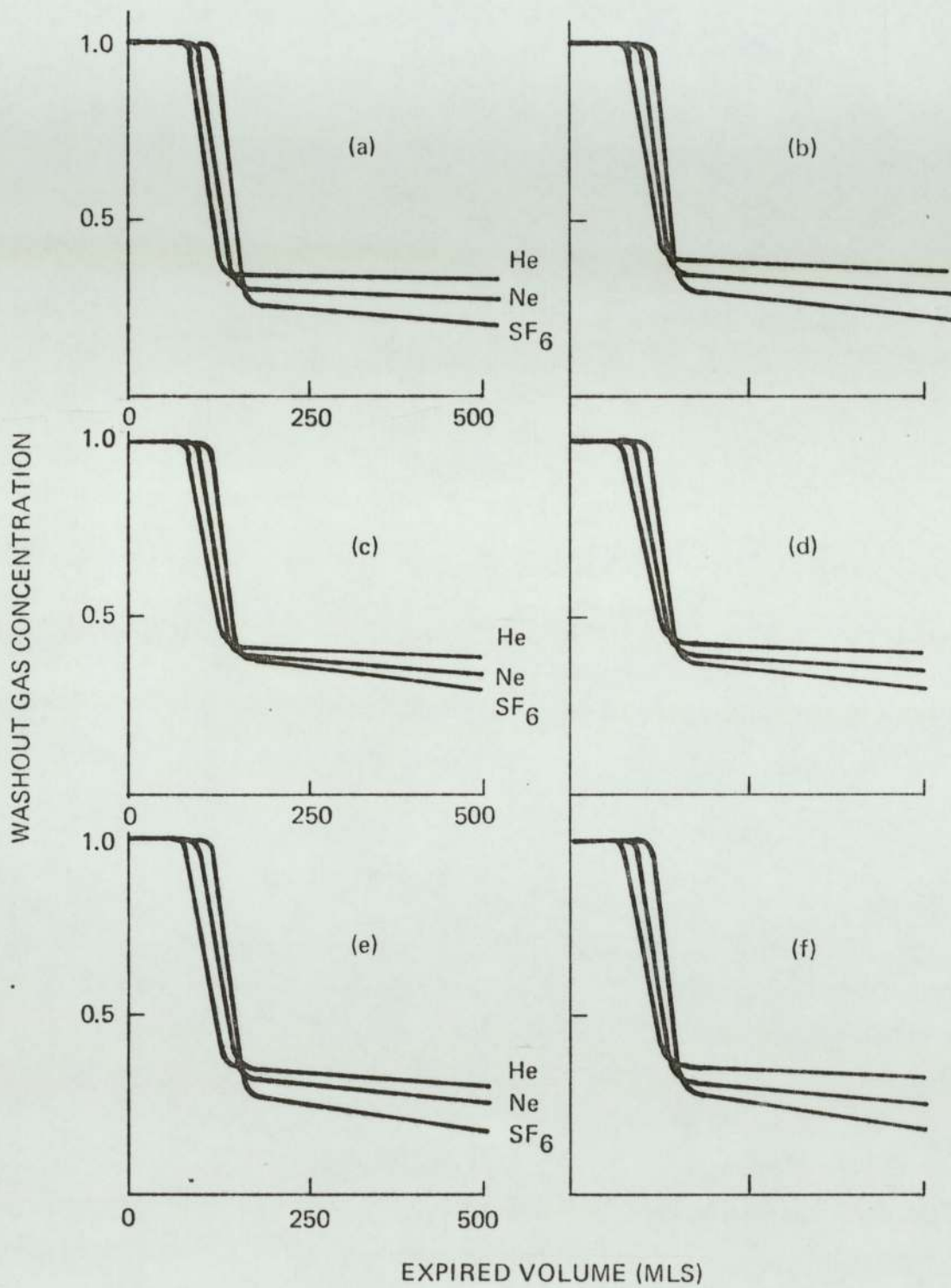


FIGURE 45

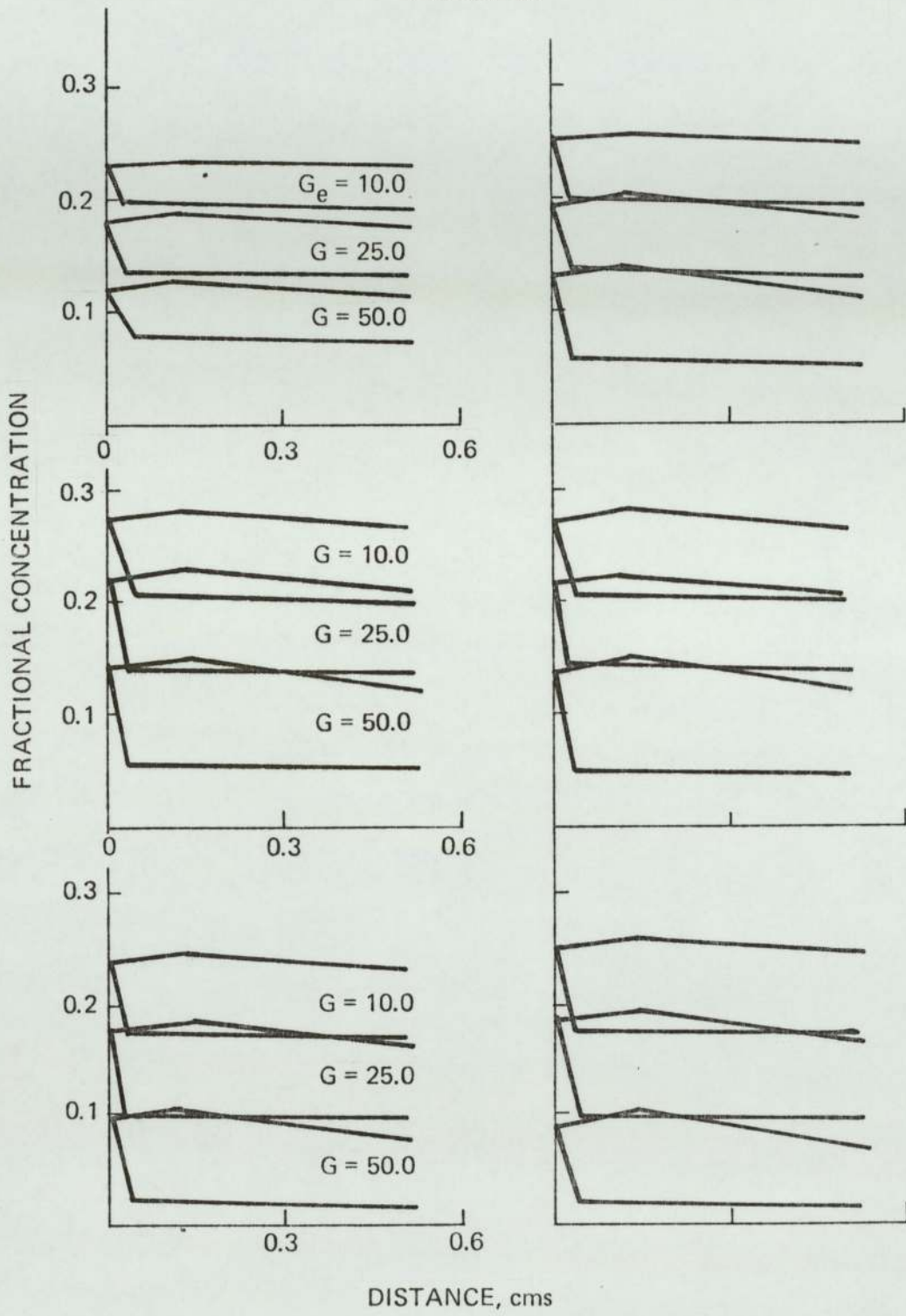


FIGURE 46

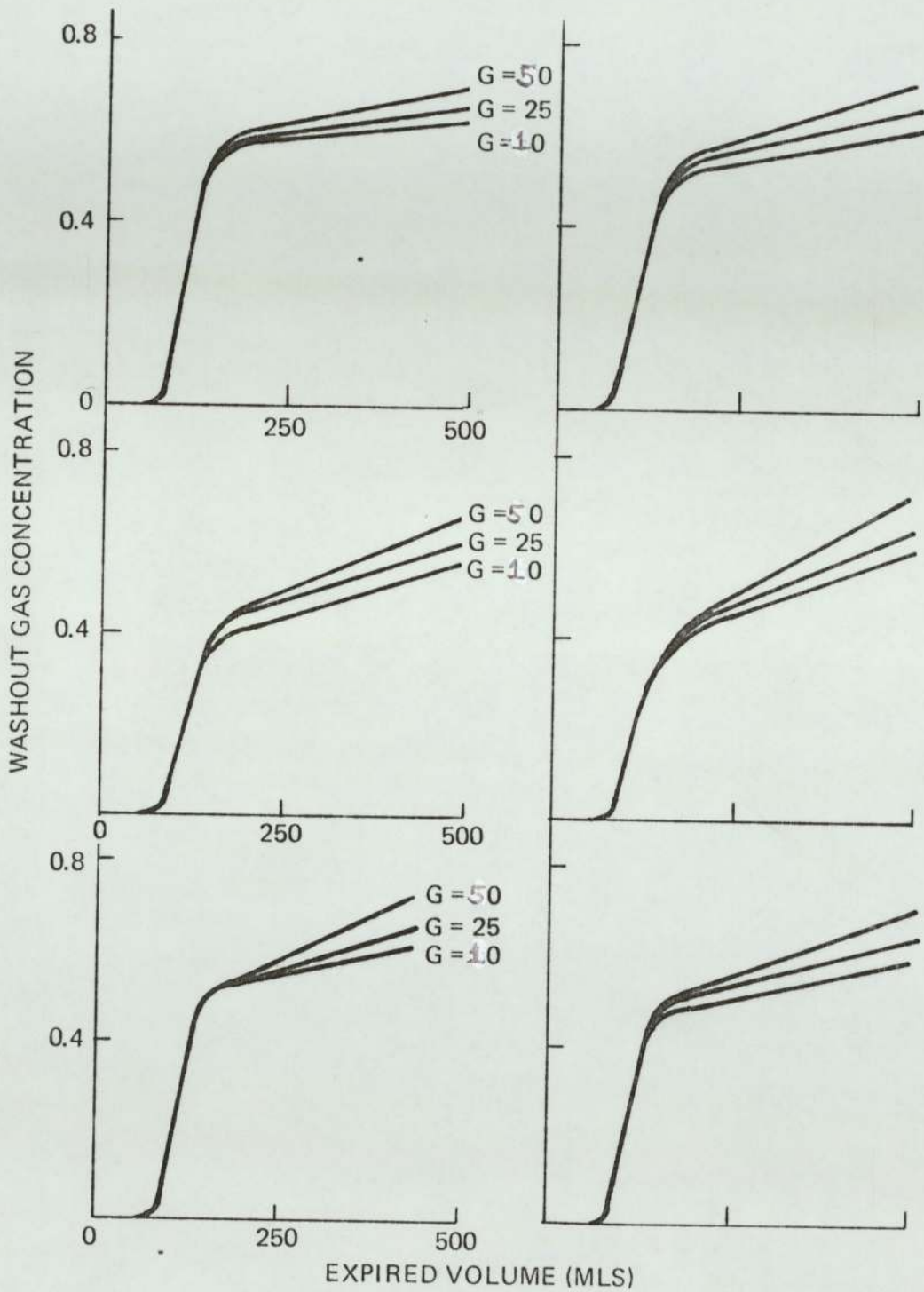


FIGURE 47

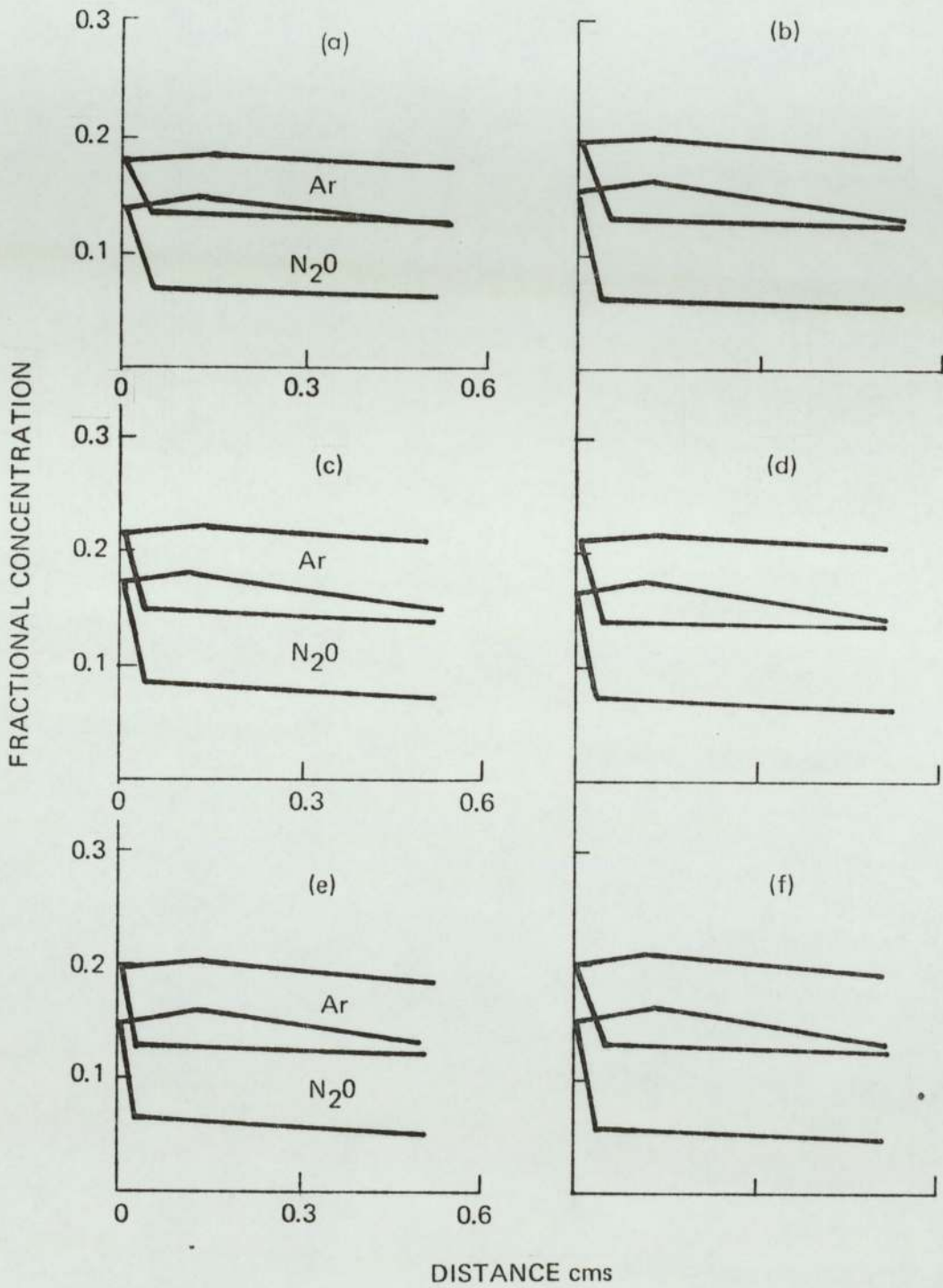


FIGURE 48

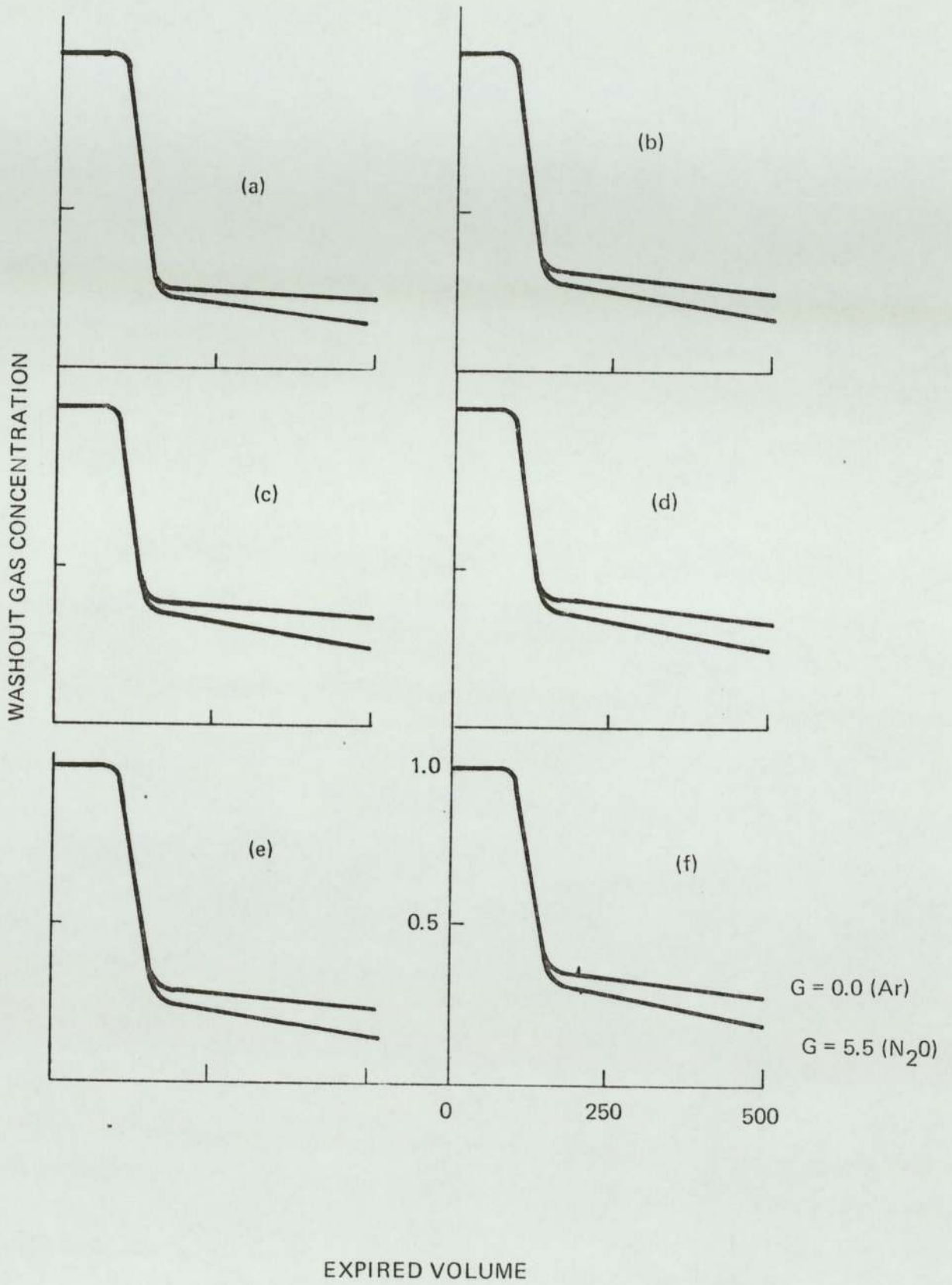


FIGURE 49

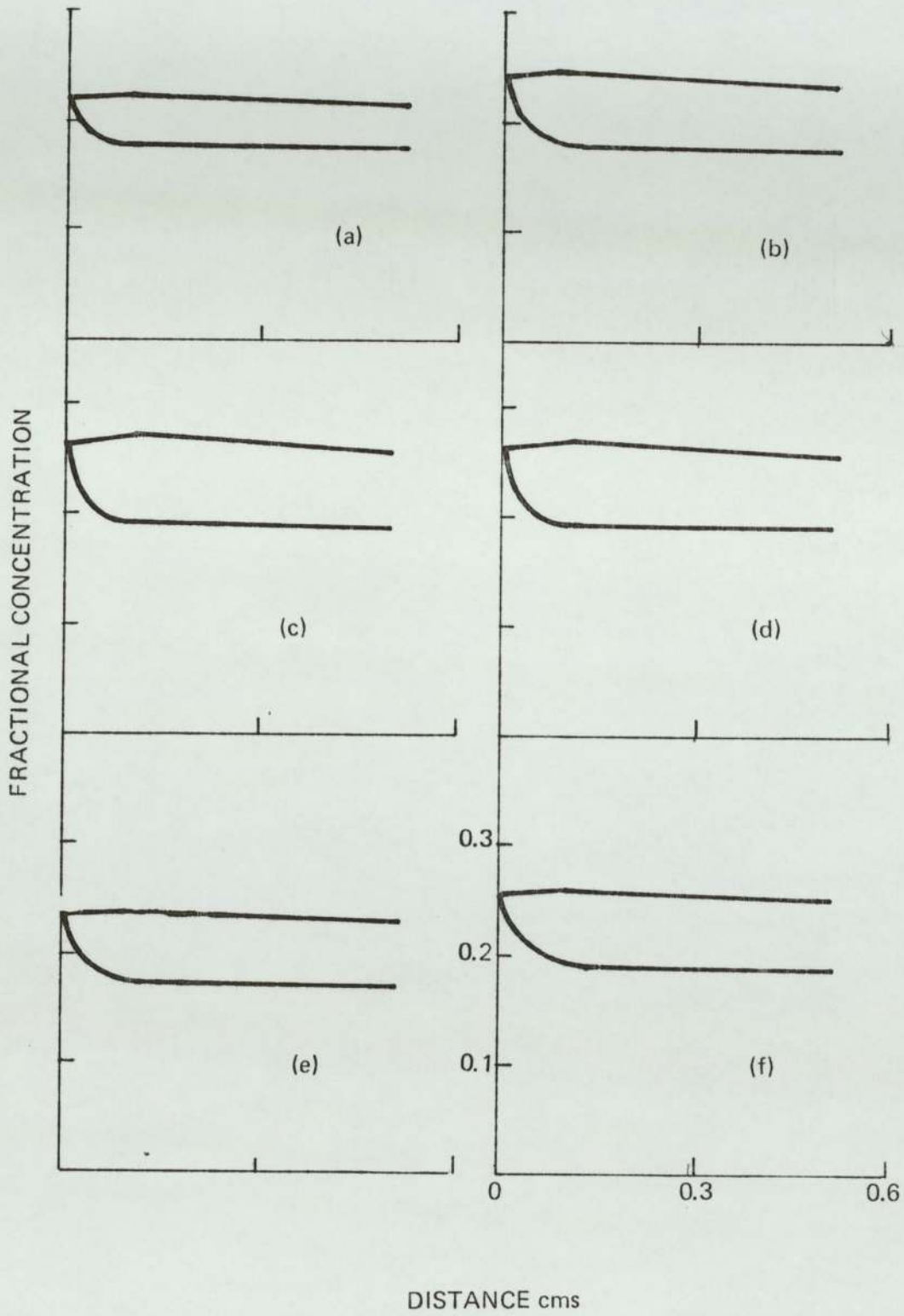


FIGURE 50

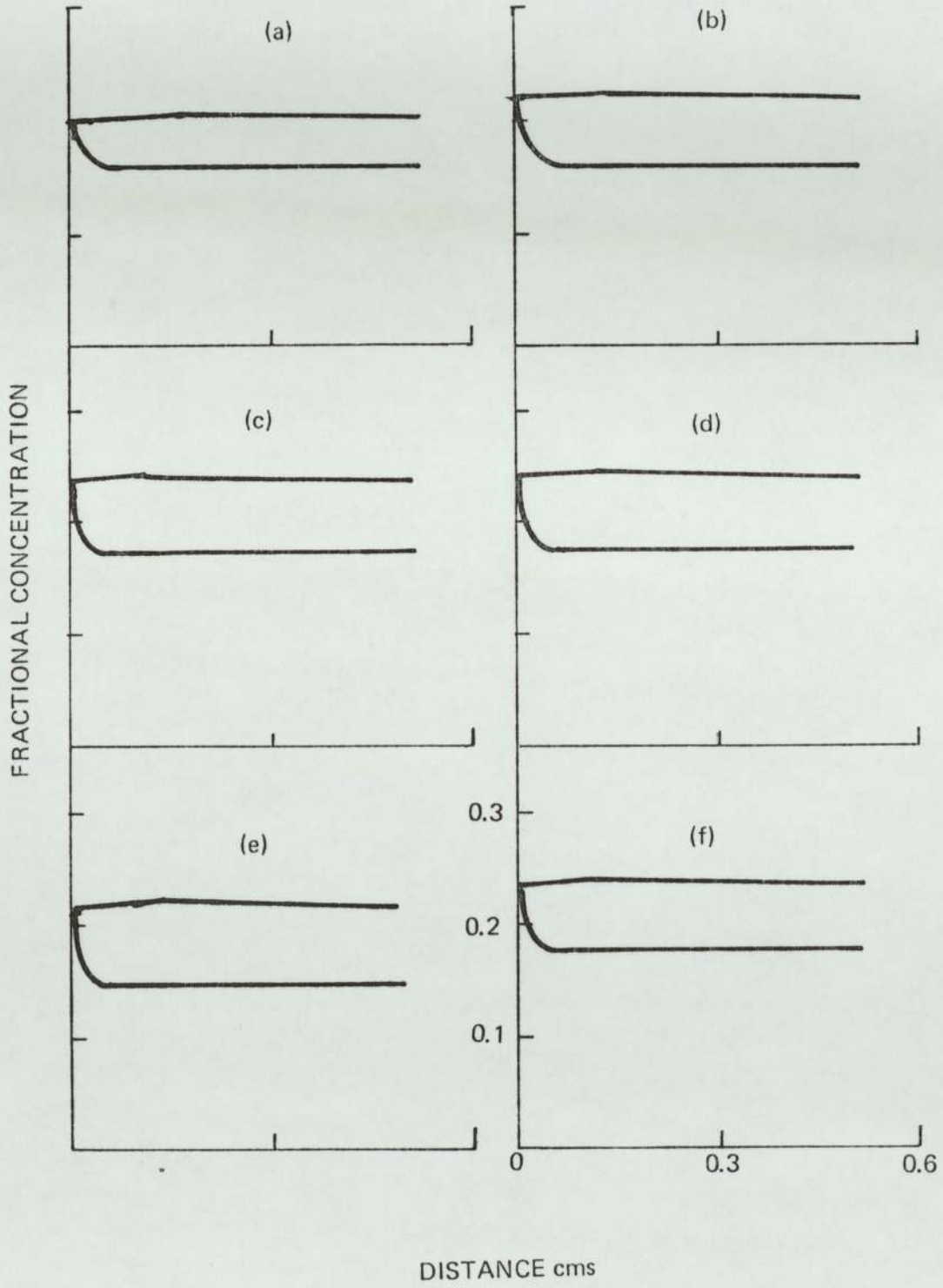


FIGURE 51

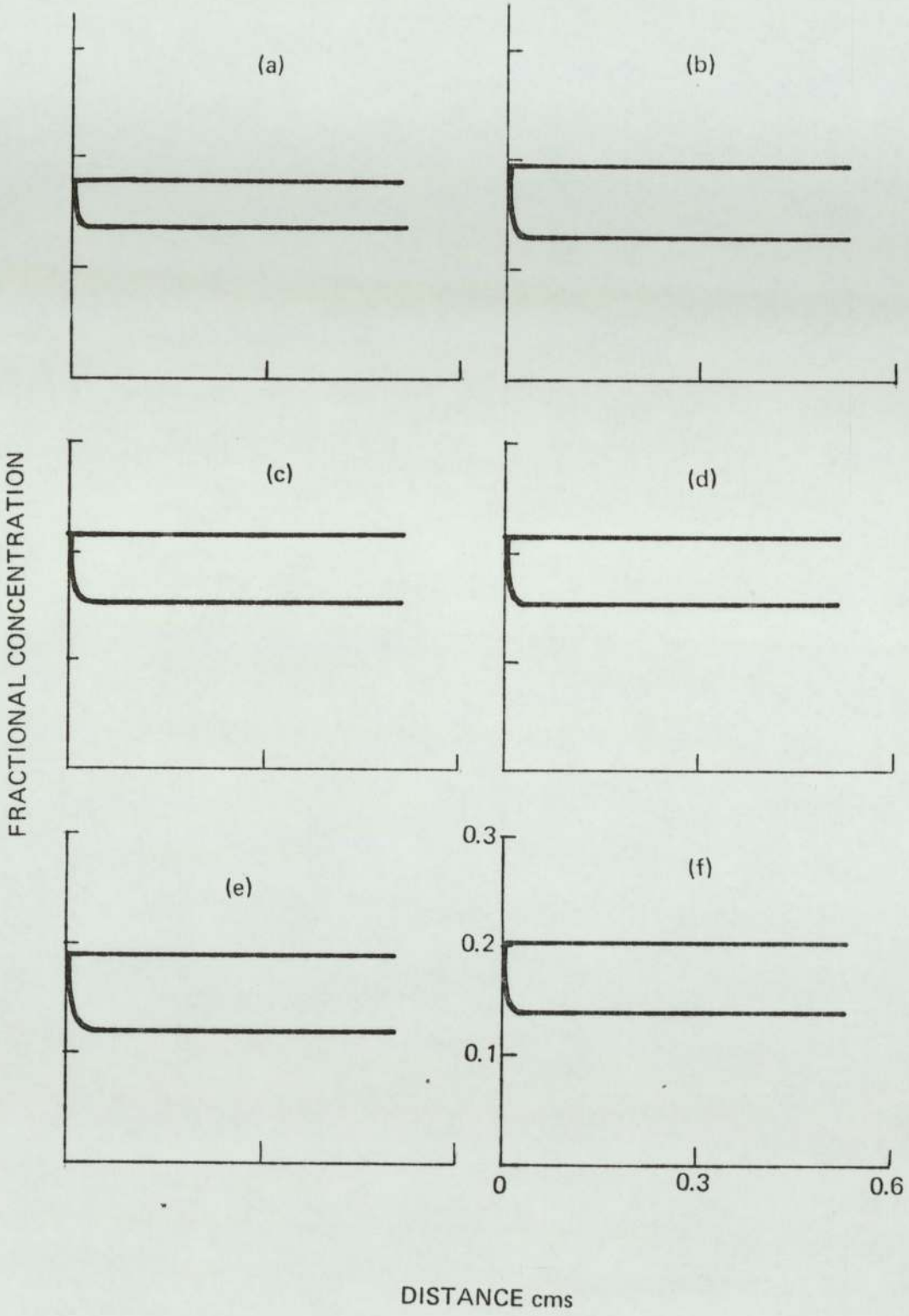


FIGURE 52

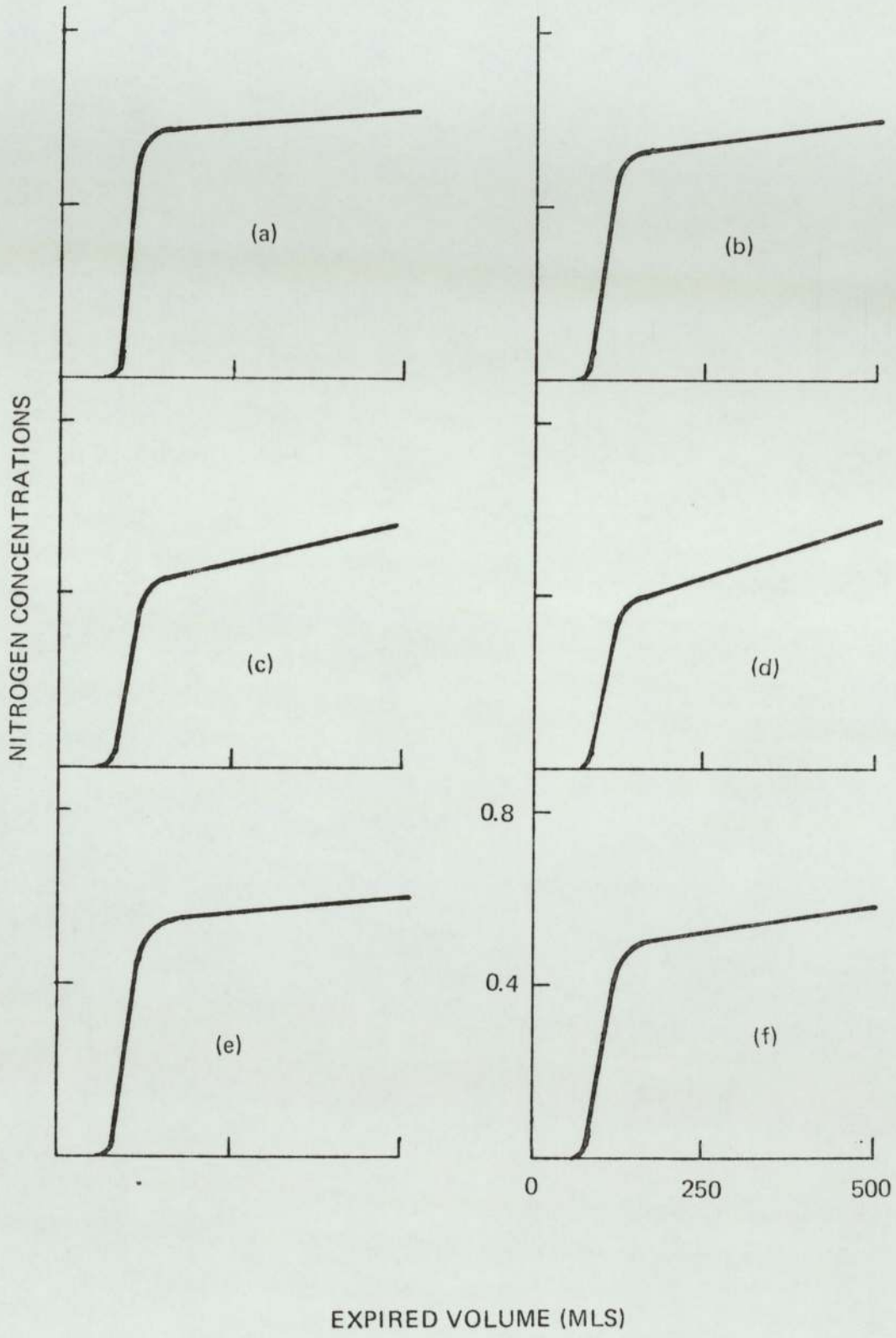


FIGURE 53

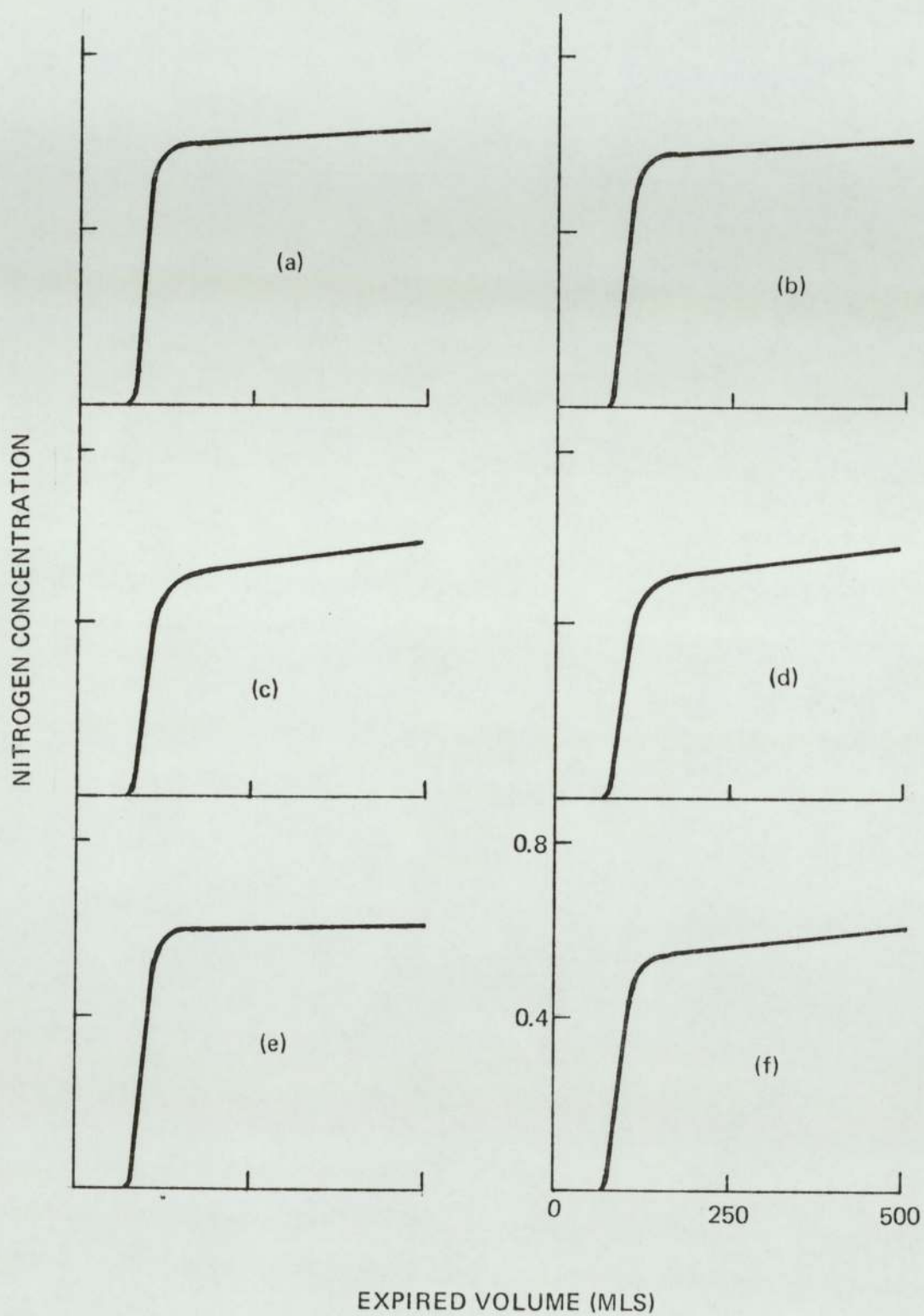


FIGURE 54

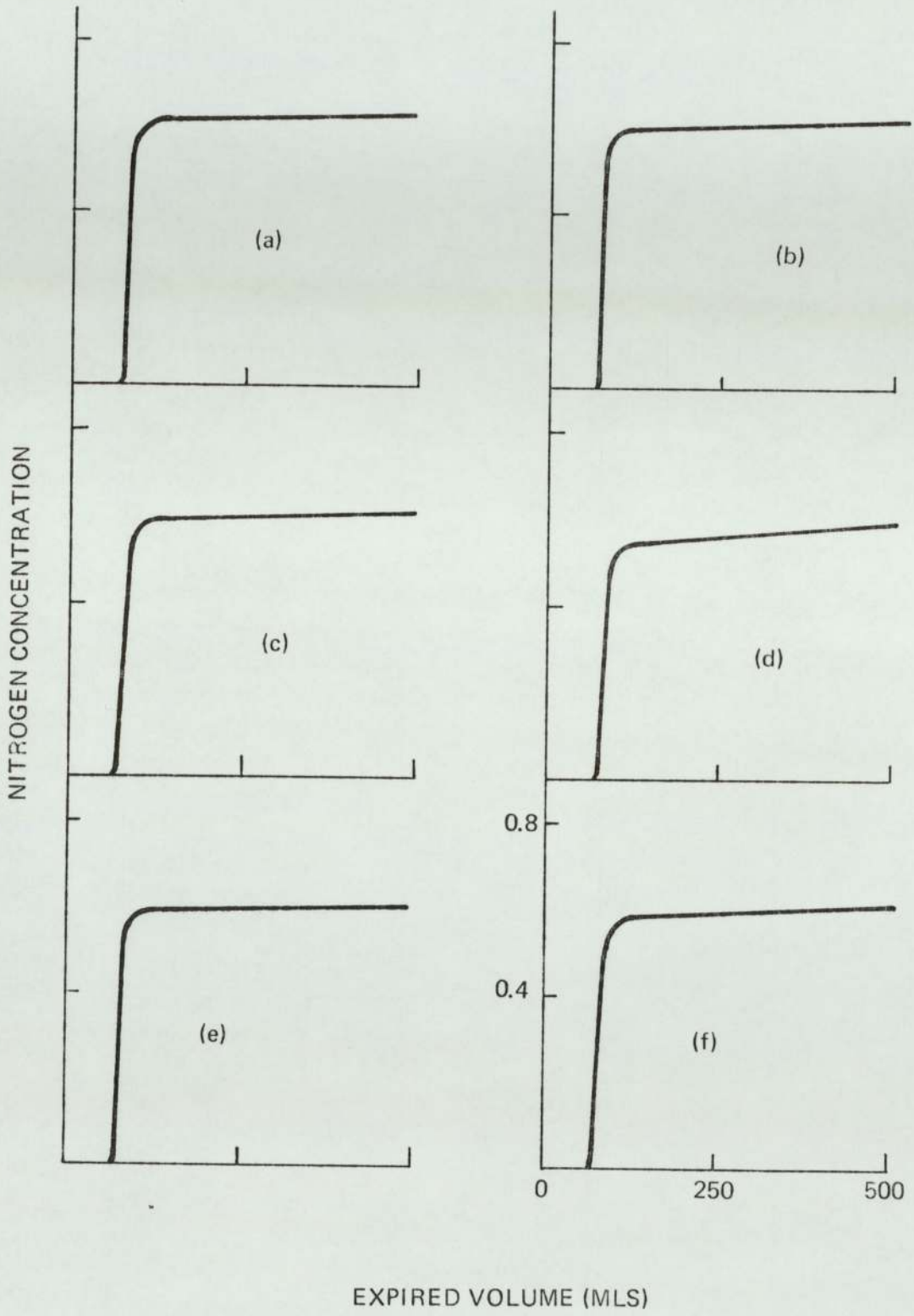


FIGURE 55

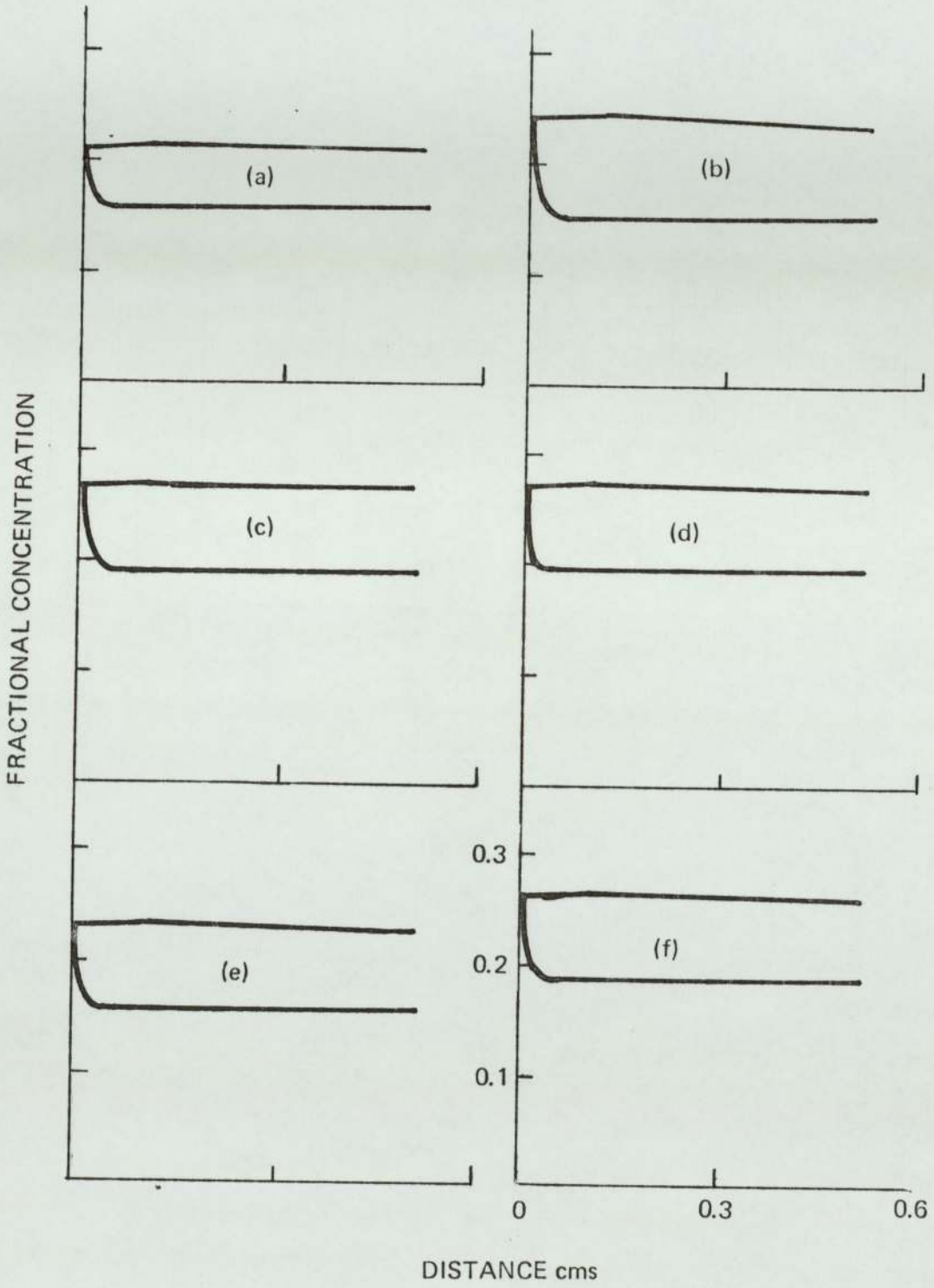


FIGURE 56

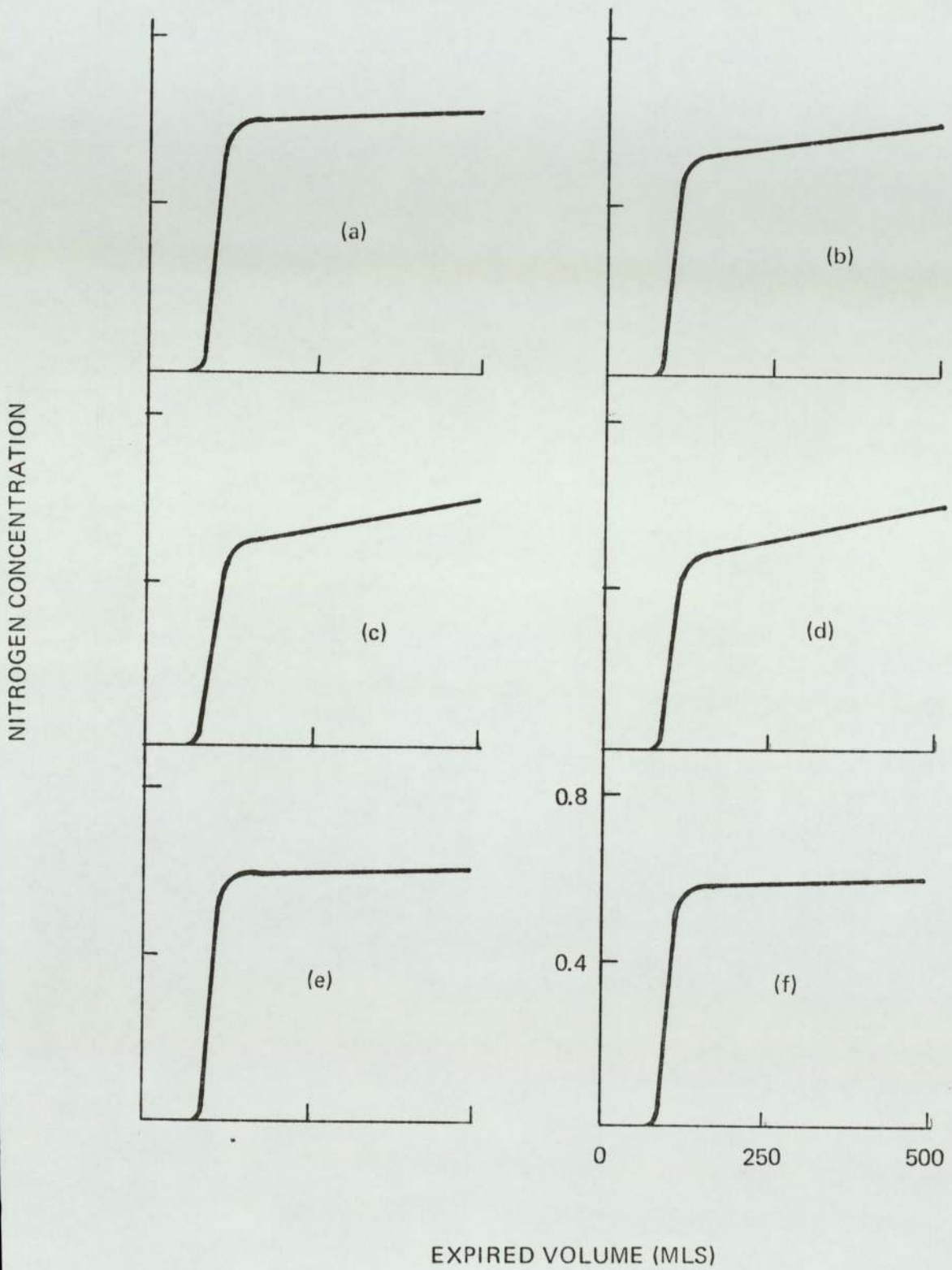
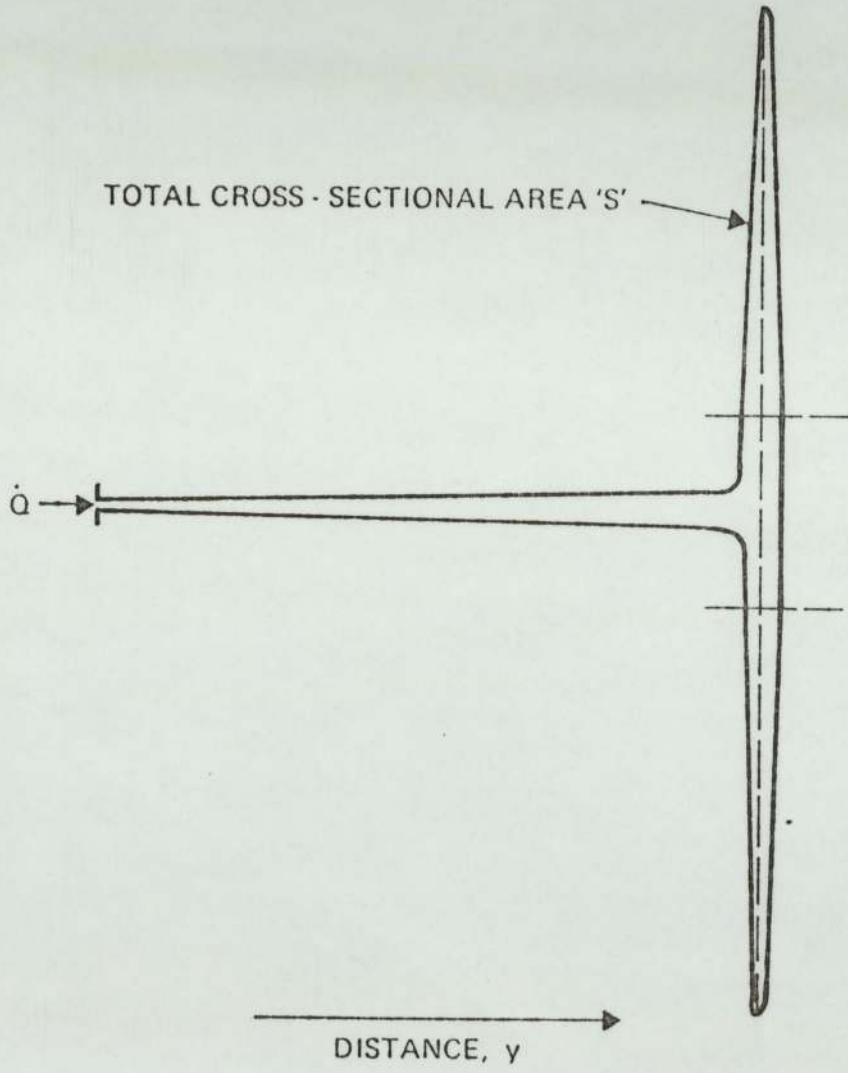


FIGURE 57



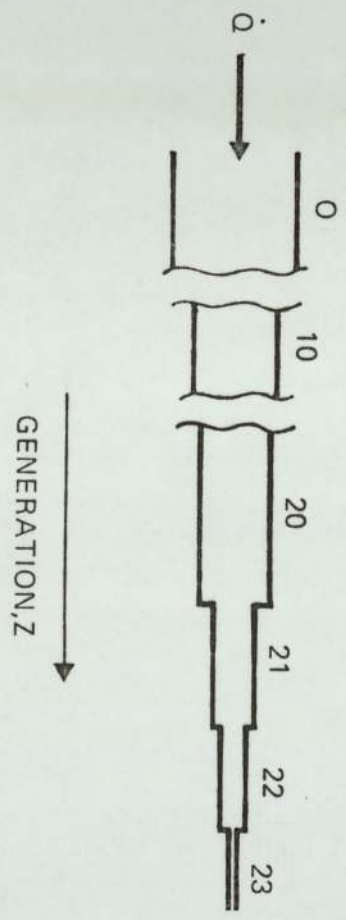


FIGURE 8

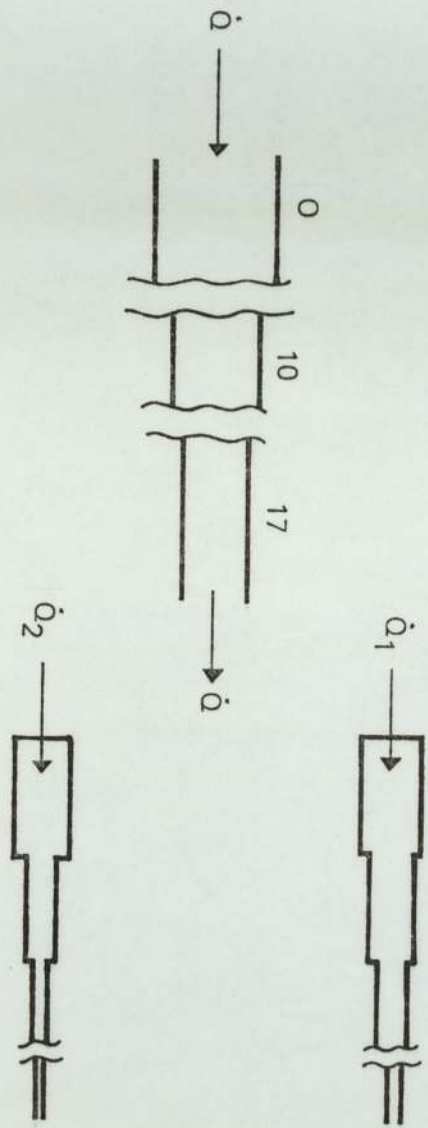
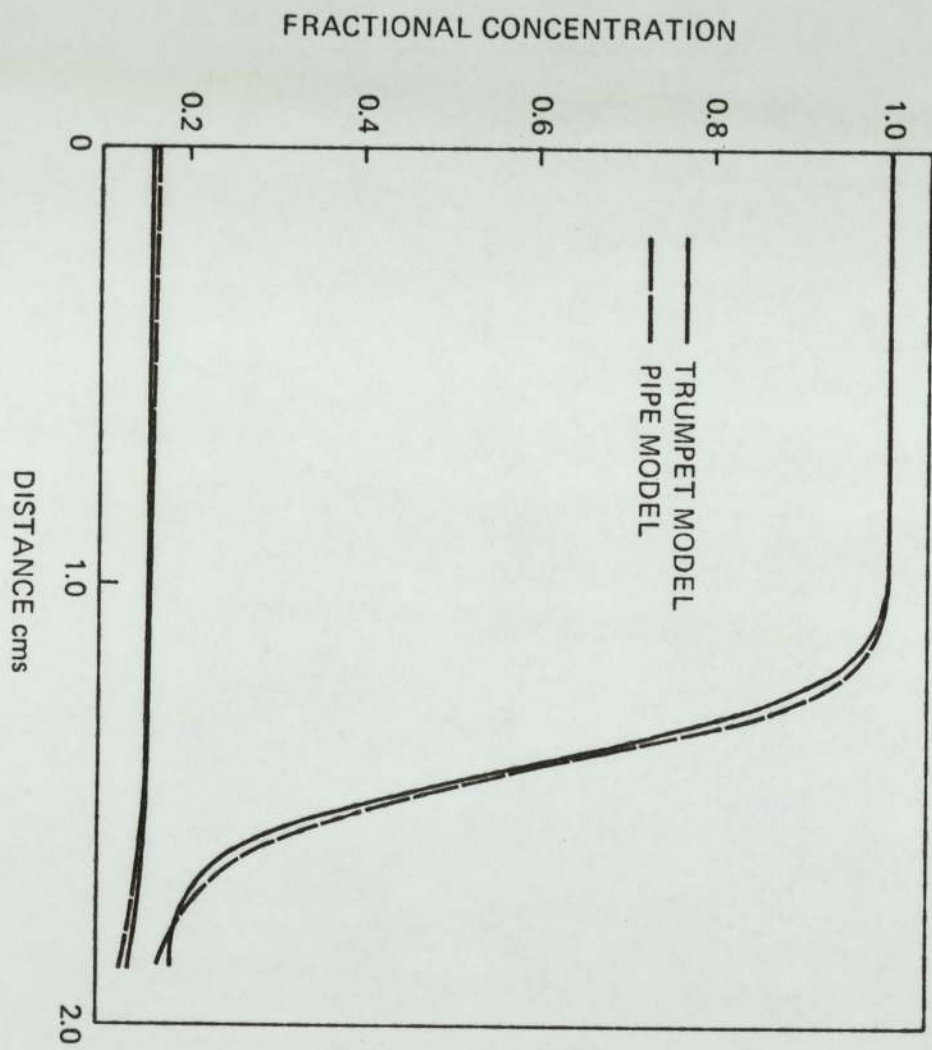


FIGURE 59

FIGURE 60



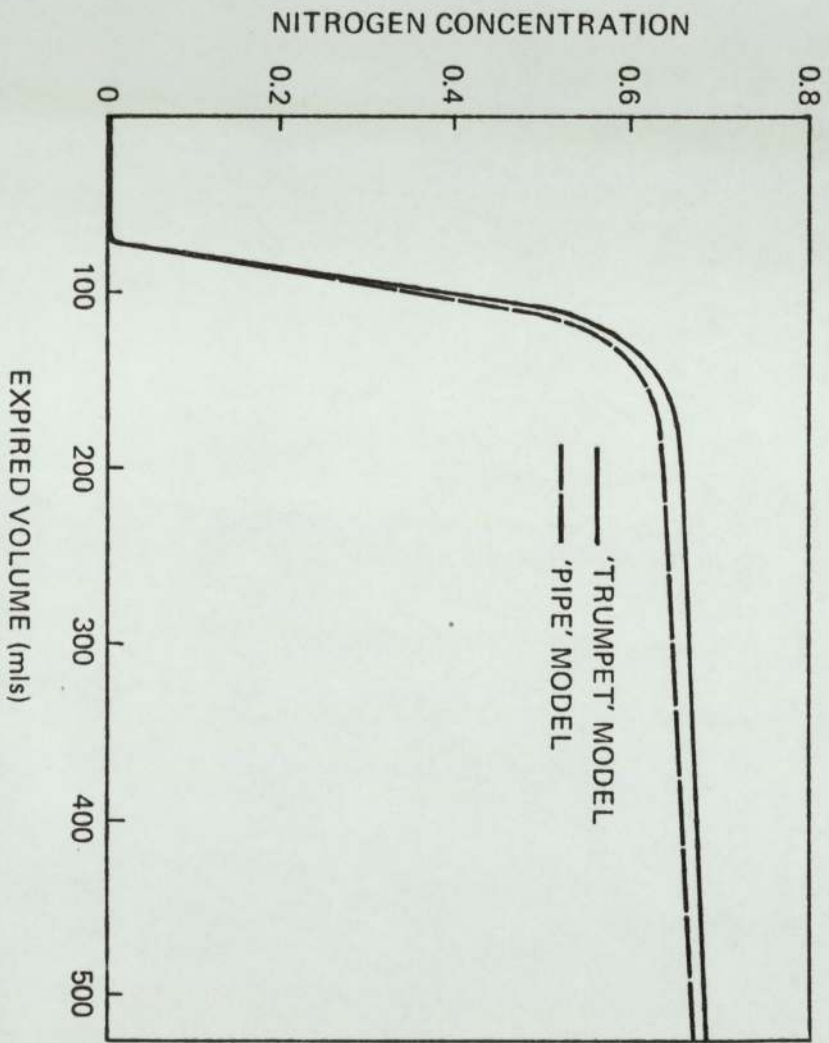
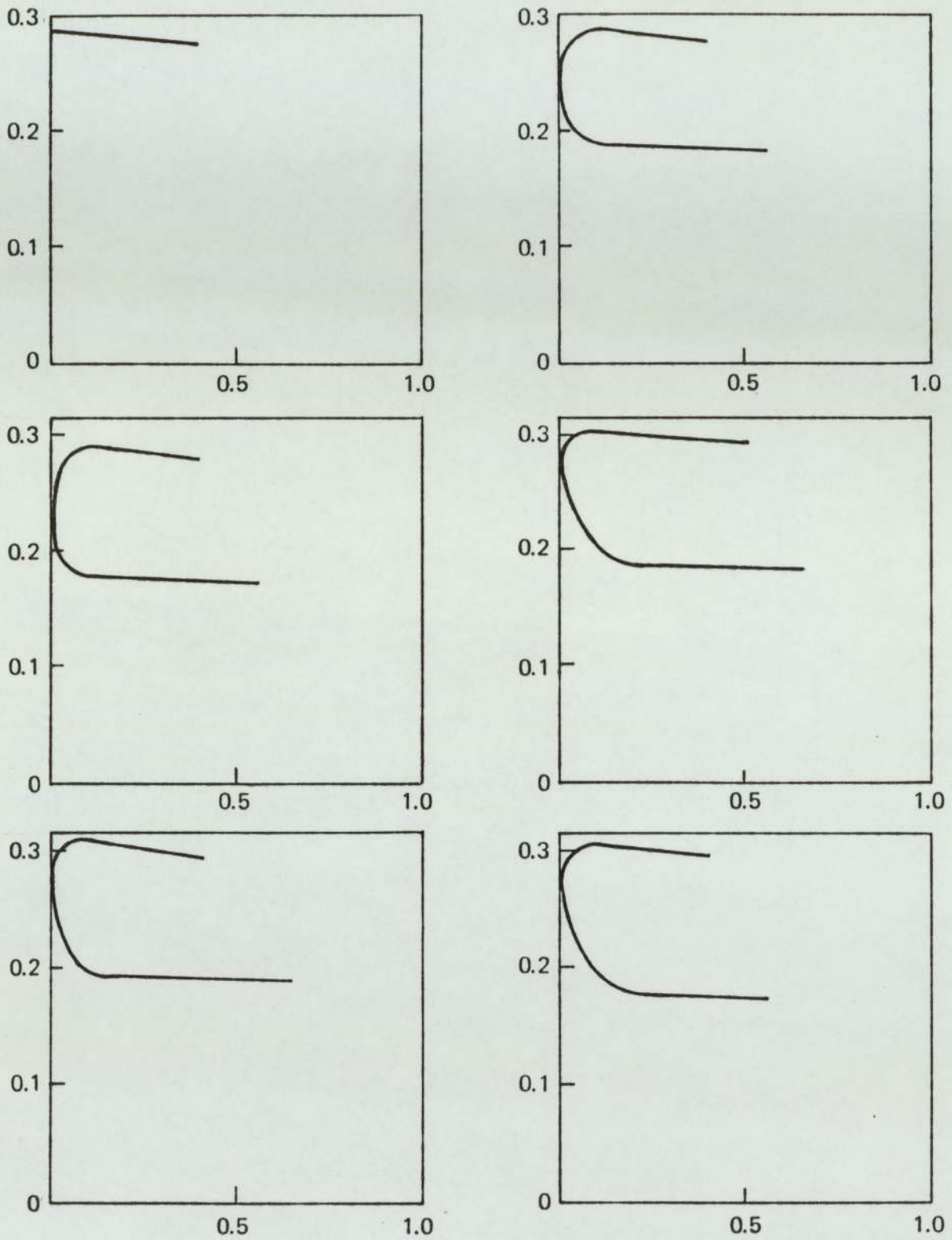


FIGURE 61

FIGURE 62



DISTANCE, CMS

FIGURE 63

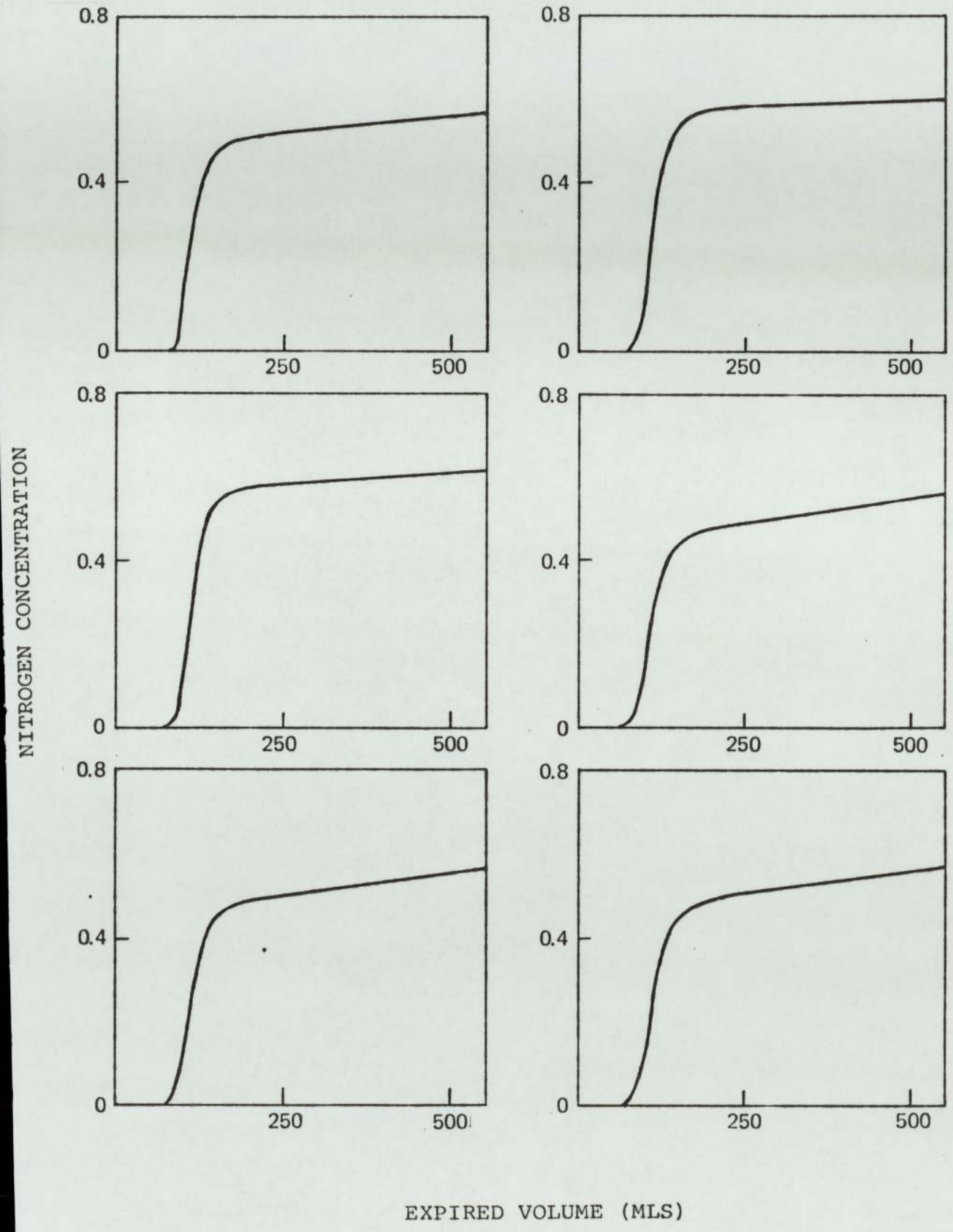


FIGURE 64

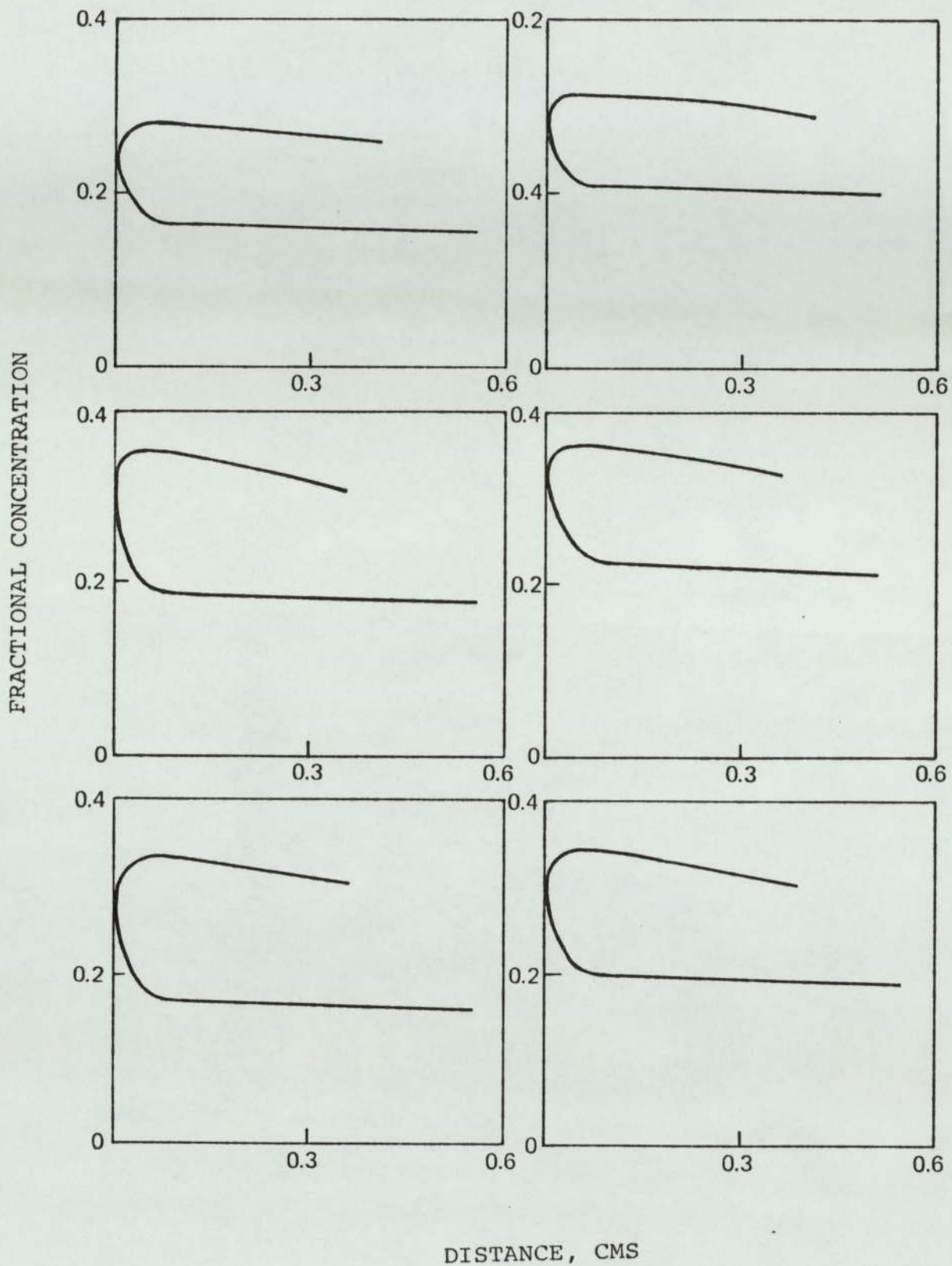


FIGURE 65

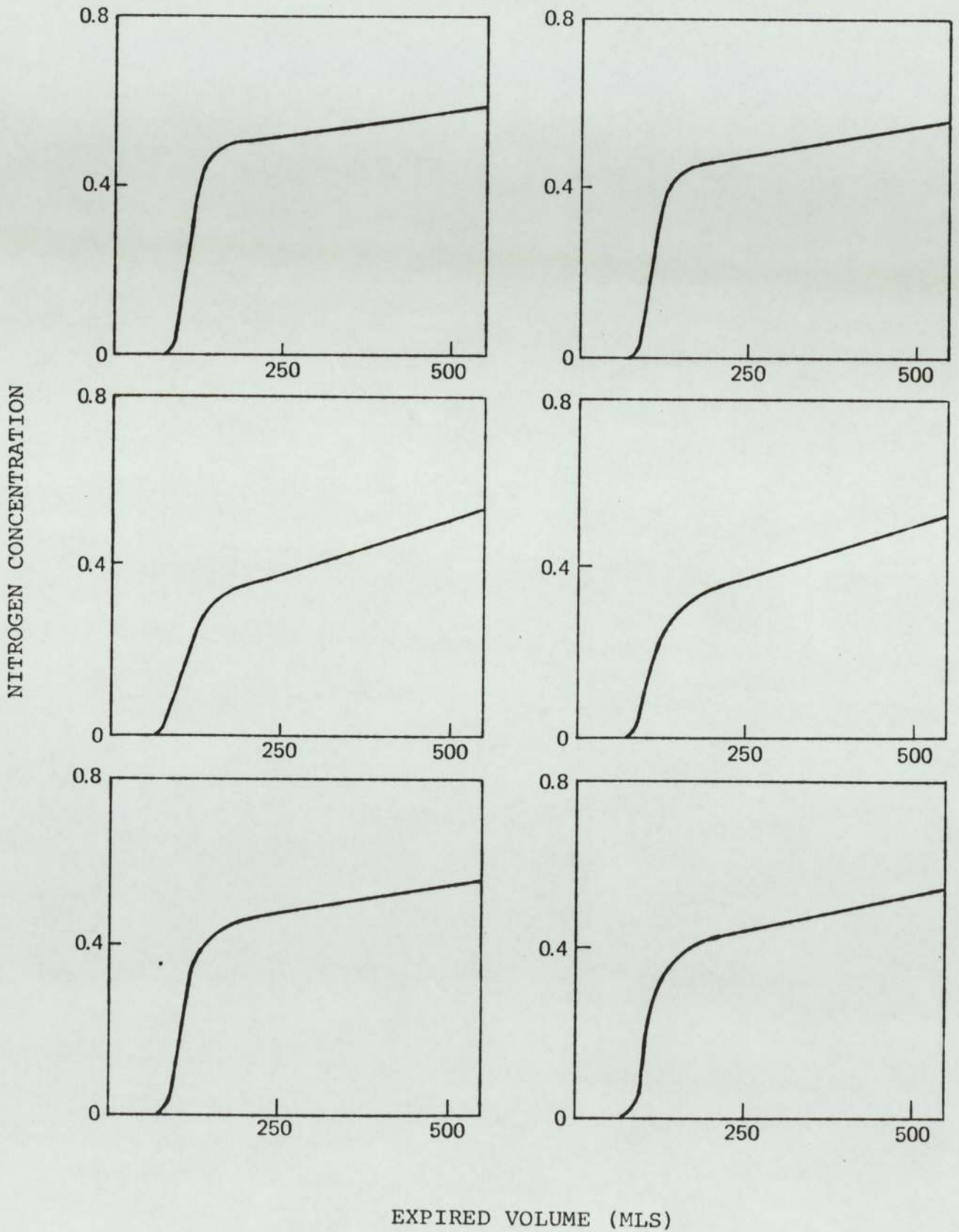


FIGURE 66

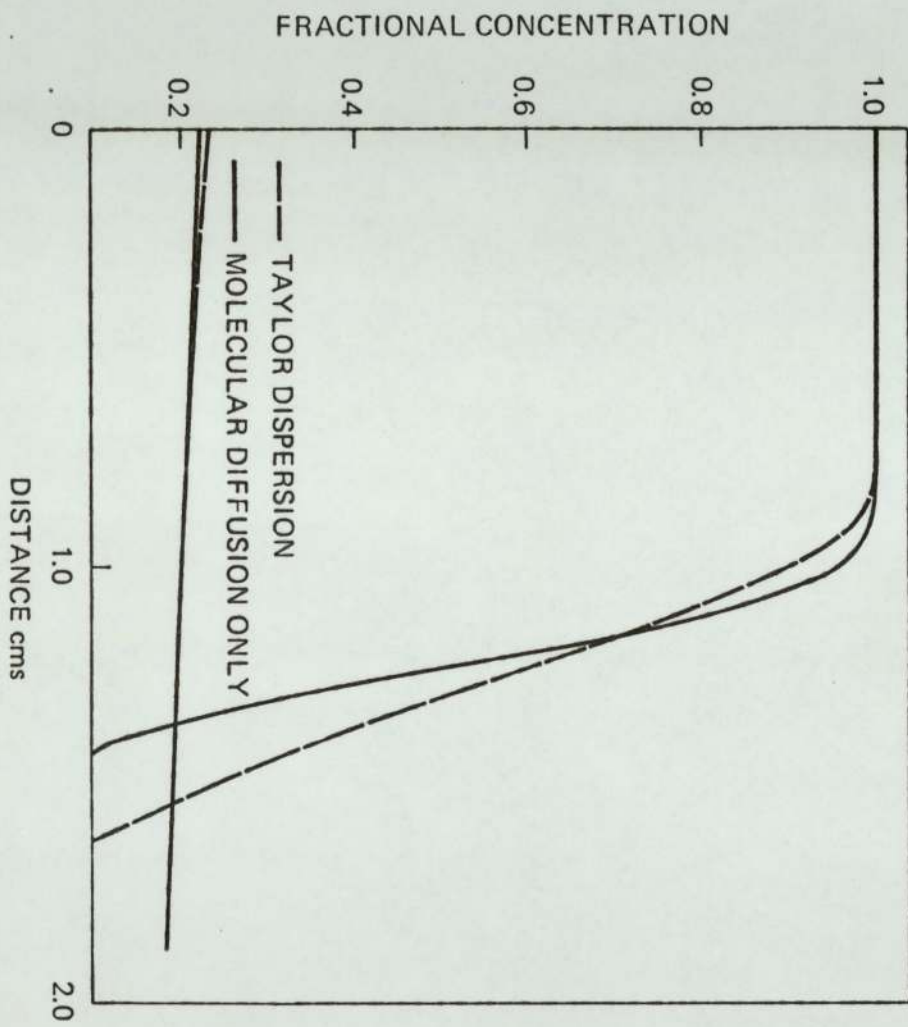
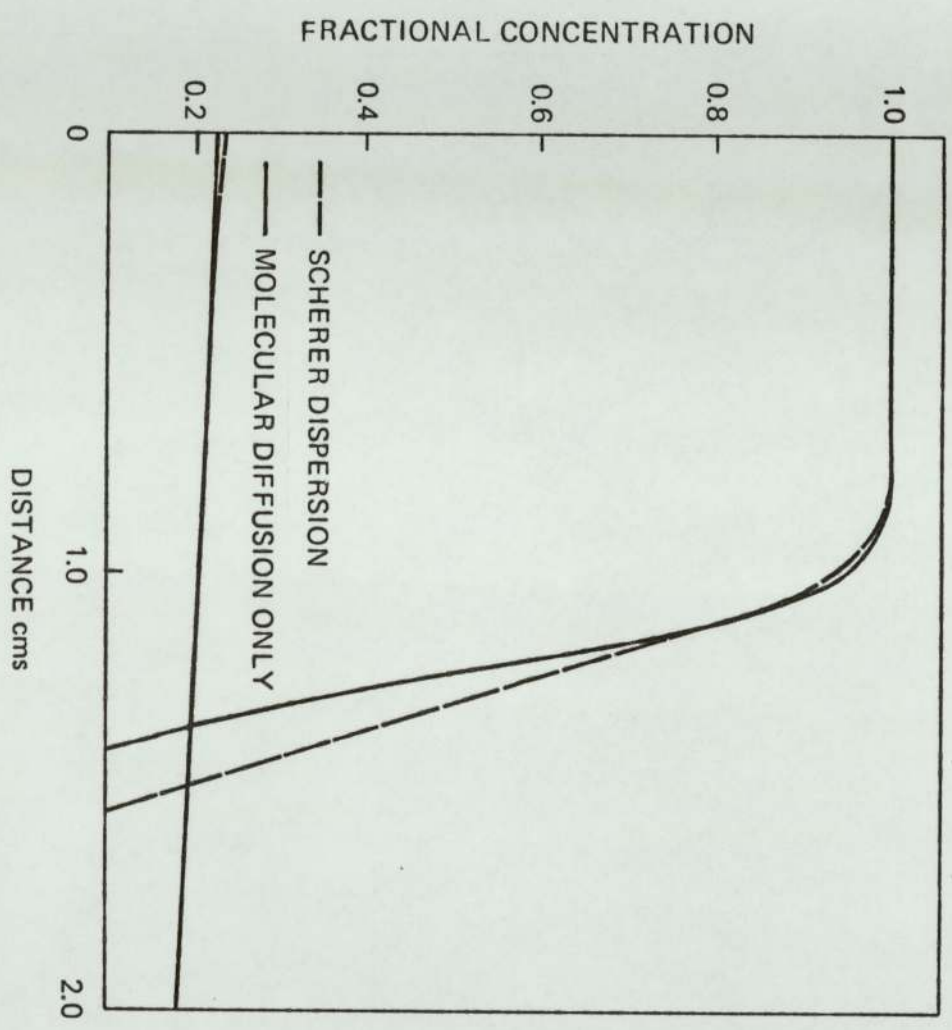


FIGURE 67



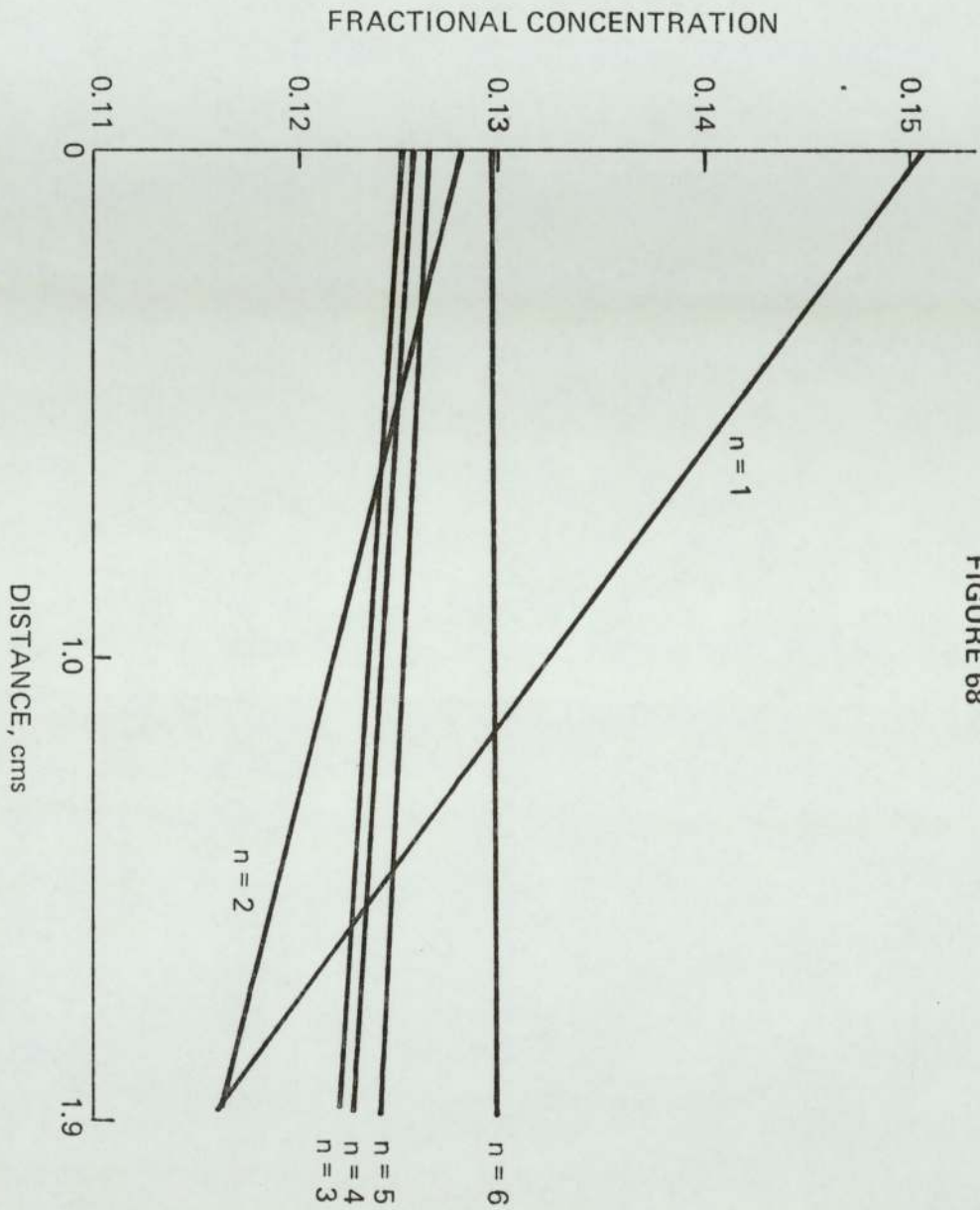


FIGURE 68

FIGURE 69

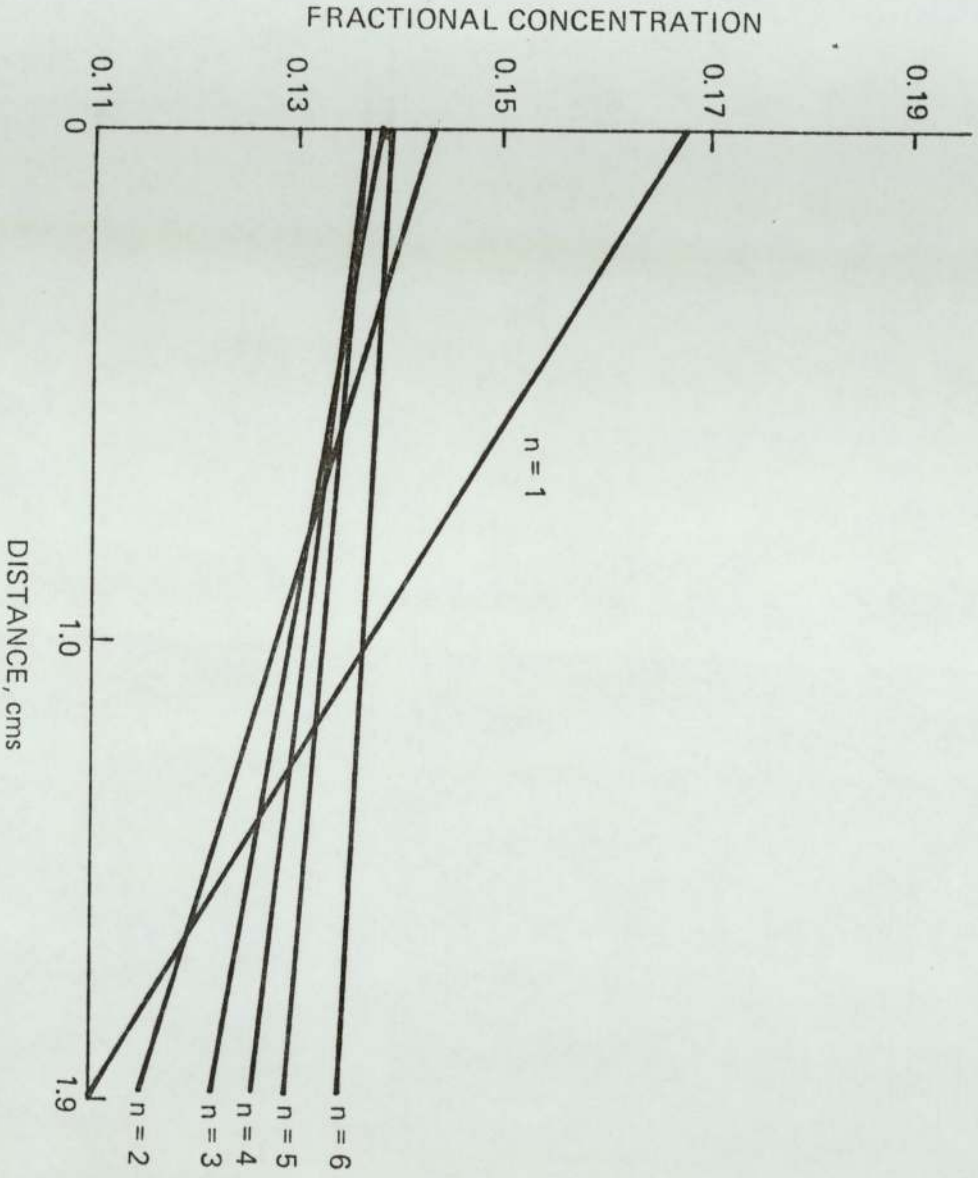
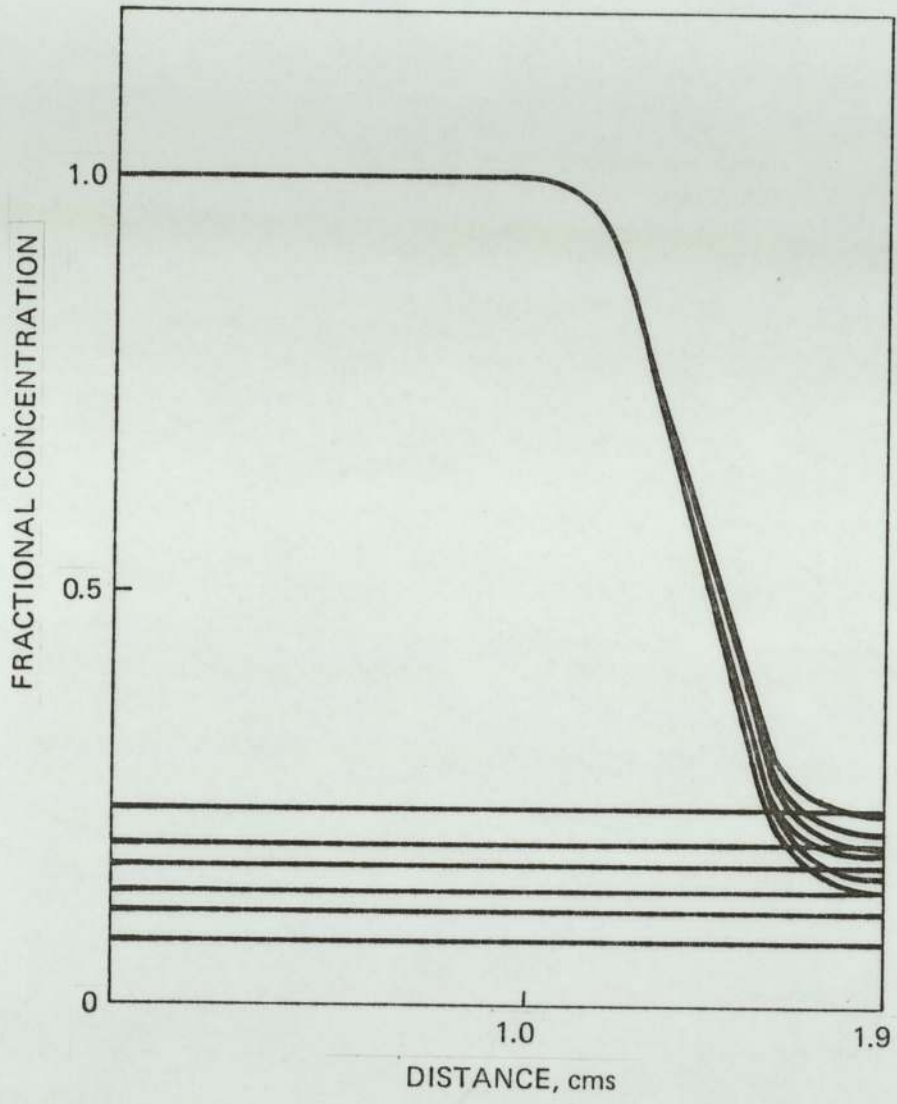


FIGURE 70



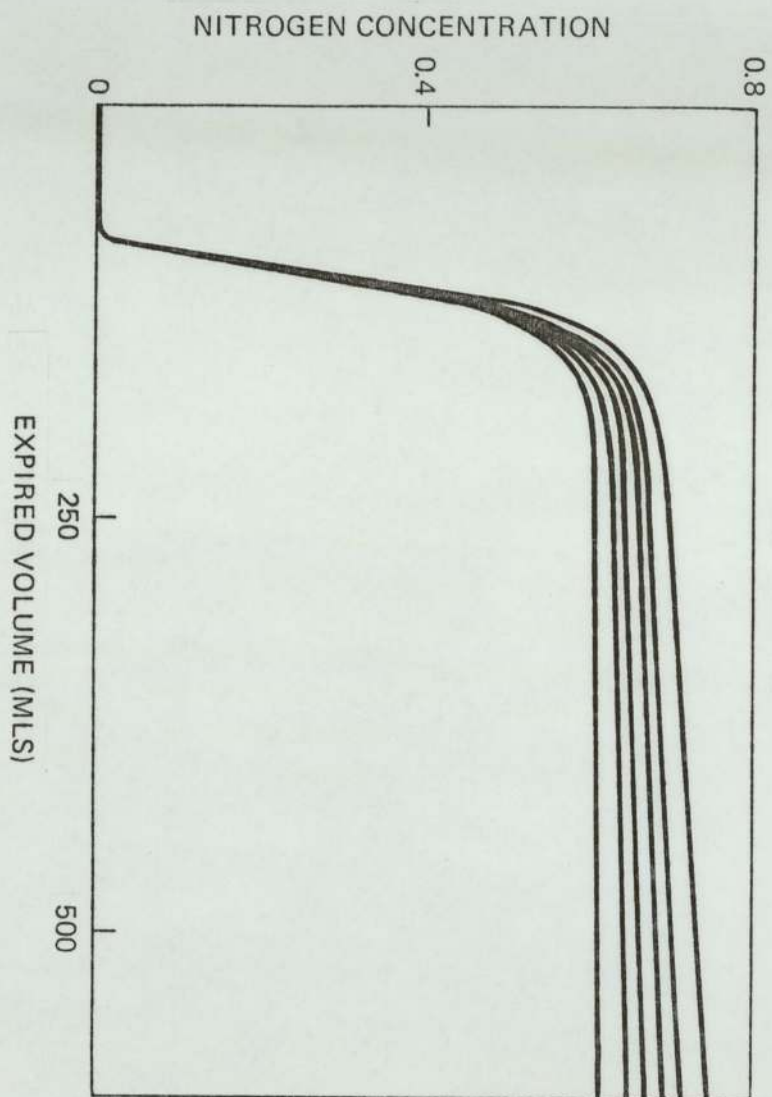


FIGURE 71

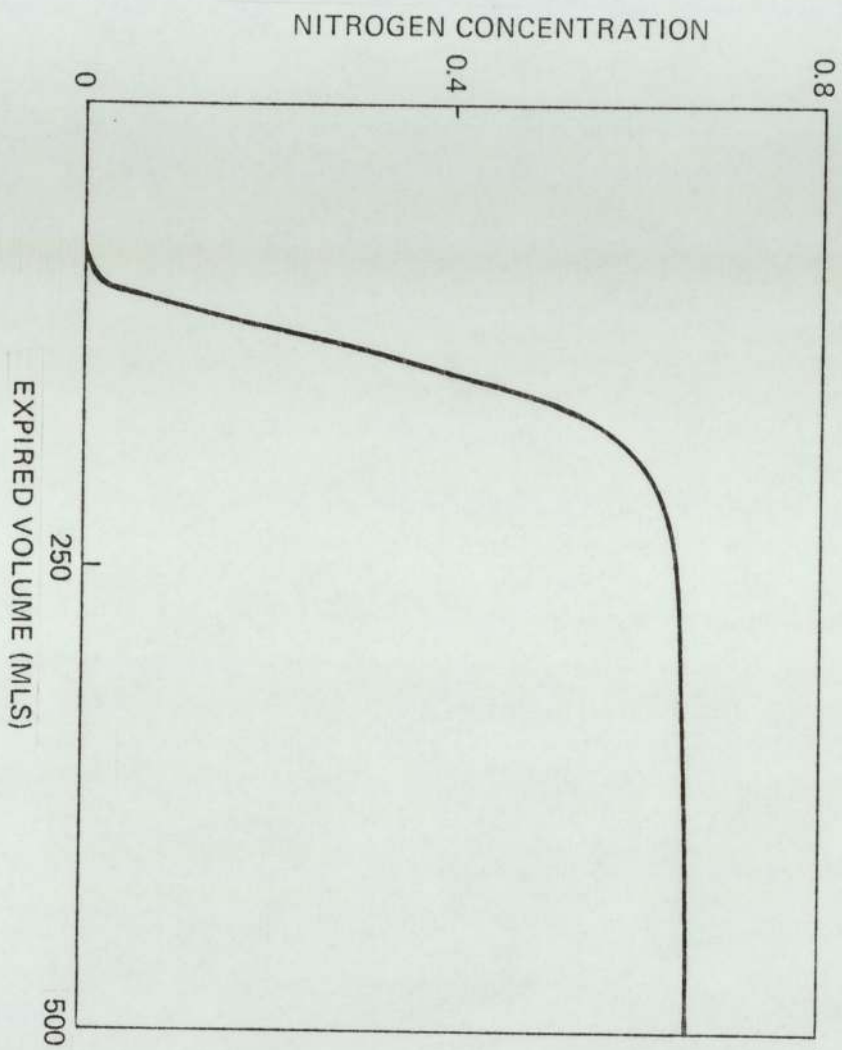


FIGURE 72

FIGURE 73

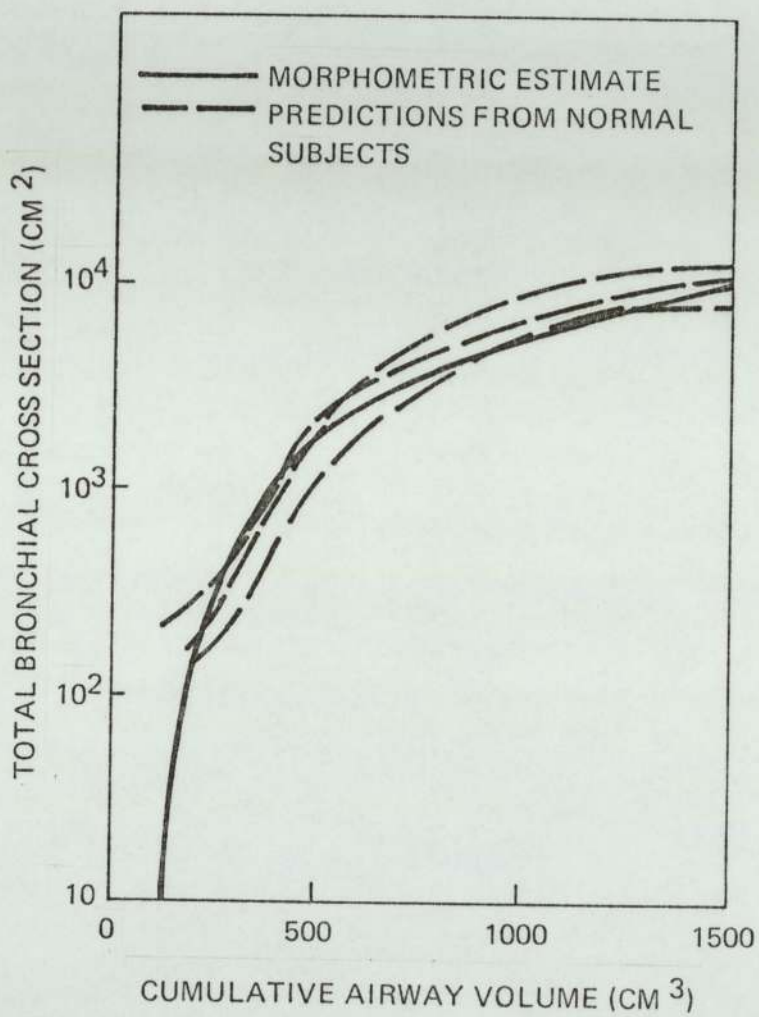


FIGURE 74

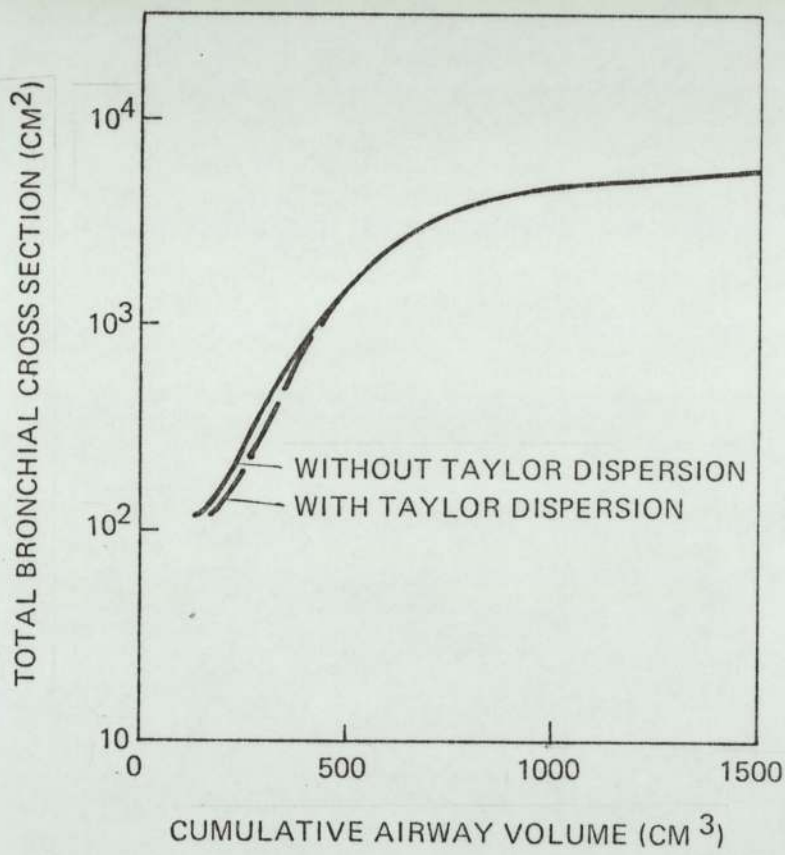


FIGURE 75  
N<sub>2</sub> RETENTION CURVE

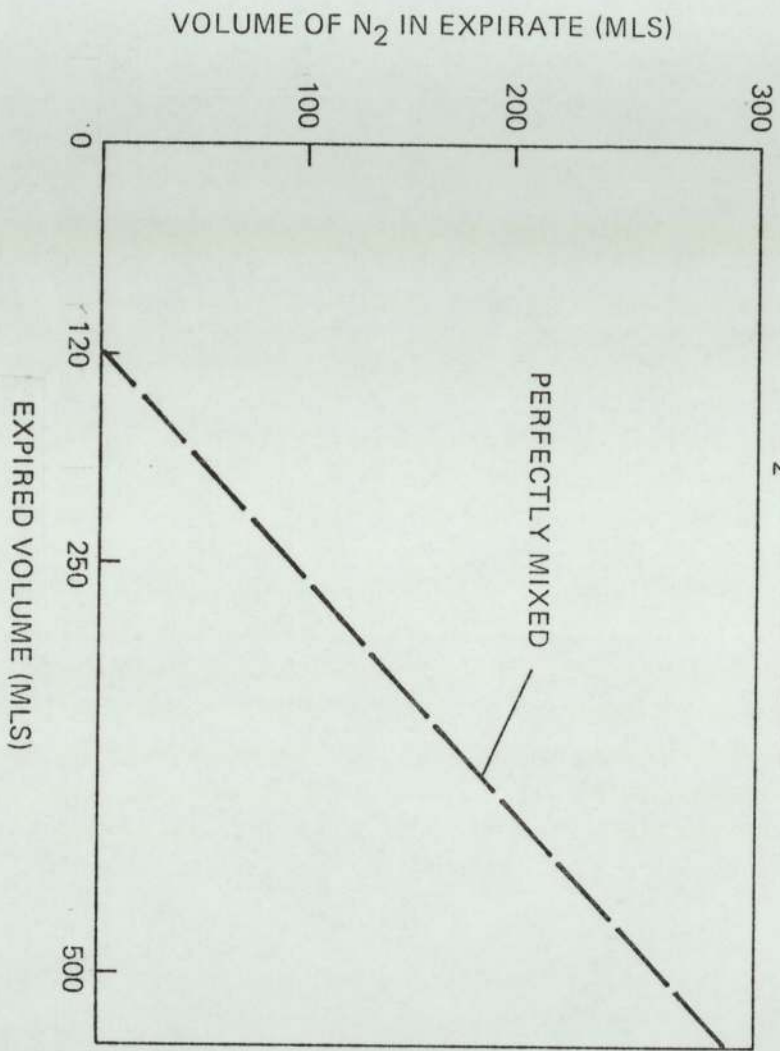
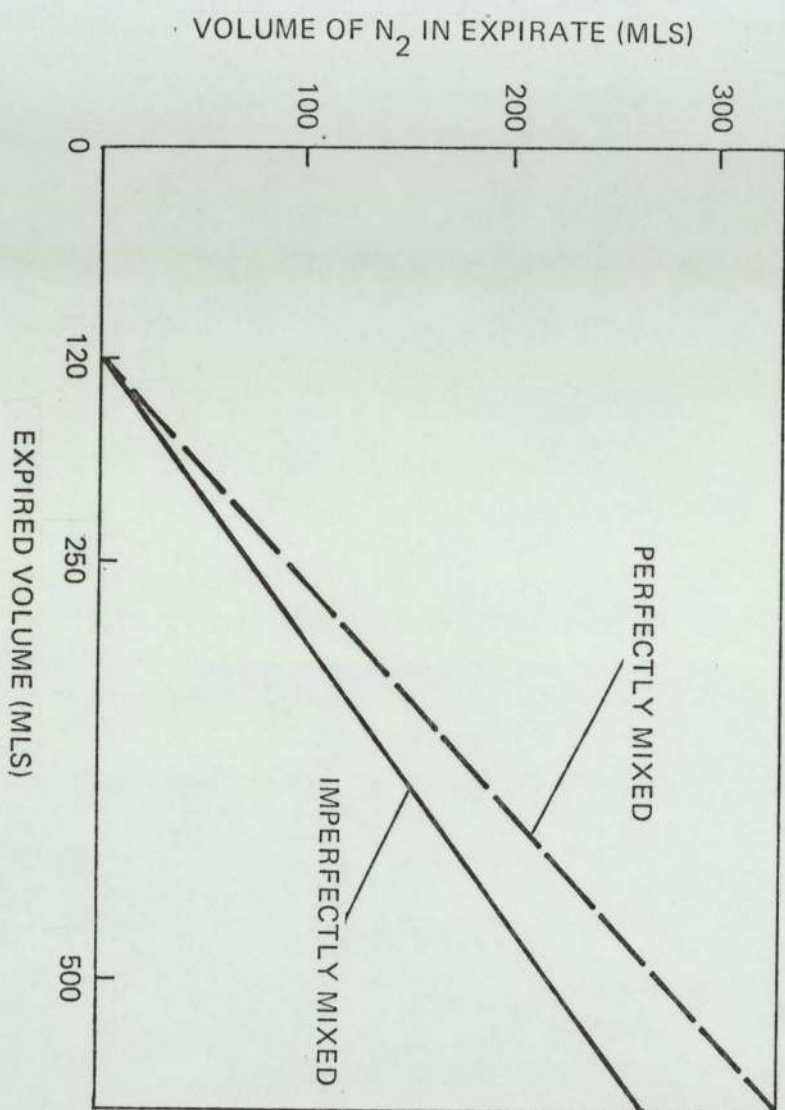


FIGURE 76  
N<sub>2</sub> RETENTION CURVES



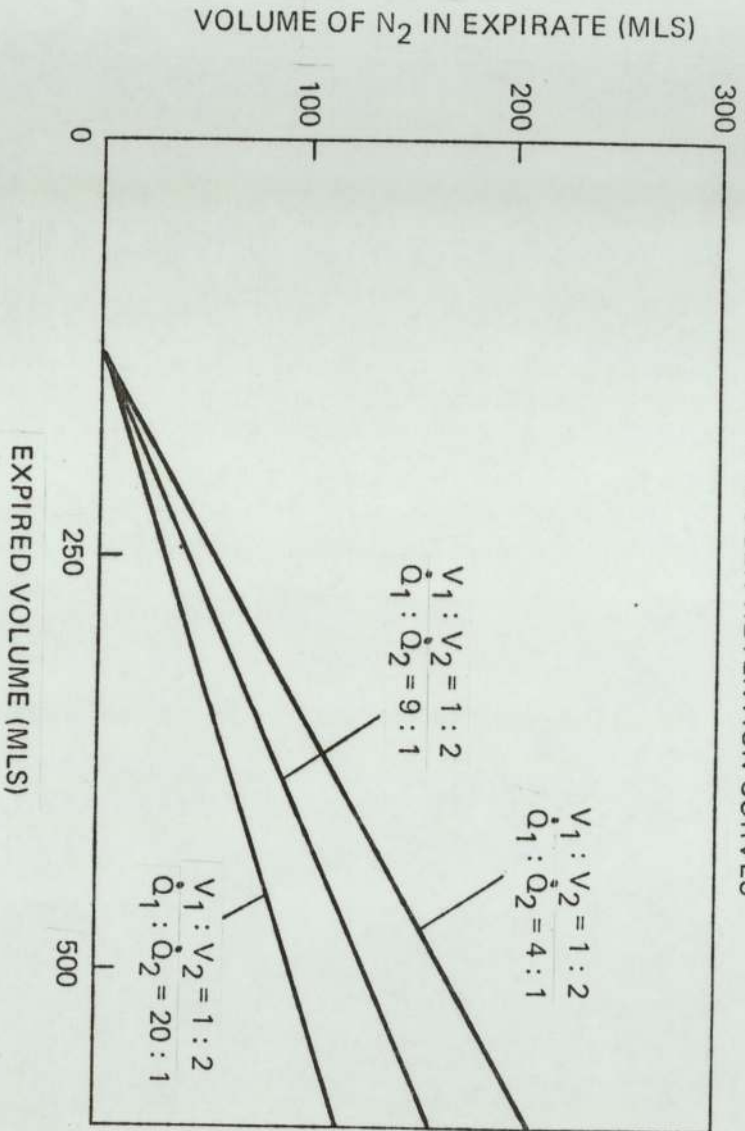


FIGURE 77  
NITROGEN RETENTION CURVES

*Reprinted from*



**ELSEVIER/NORTH-HOLLAND BIOMEDICAL PRESS, AMSTERDAM**

## A REAPPRAISAL OF BOUNDARY CONDITIONS ASSUMED IN PULMONARY GAS TRANSPORT MODELS\*

DAVID A. SCRIMSHIRE, ROBERT J. LOUGHNANE and TERENCE J. JONES

*Department of Production Technology and Production Management (Biomedical Engineering Section),  
University of Aston in Birmingham, Gosta Green, Birmingham B4 7ET, England*

**Abstract.** Solutions of the classic pulmonary gas transport equation are presented in which a true 'no-flux' boundary condition is specified throughout the respiratory cycle. For the particular models studied it is demonstrated that diffusive mixing is *incomplete* at end expiration, and that such stratified inhomogeneities give rise to a realistic alveolar plateau for a simulated N<sub>2</sub> washout test. The reasons for the disparity of the present findings with those obtained by contemporary workers are explained by critically examining the boundary conditions conventionally assumed at the alveolar wall.

|                                 |                                |
|---------------------------------|--------------------------------|
| Alveolar plateau                | Gas flux                       |
| Boundary conditions             | Pulmonary gas transport models |
| Diffusive and convective mixing | Stratified inhomogeneities     |

The application of modelling techniques to investigate gaseous transport in the human lung has attracted considerable attention from both physiologists and mathematicians during recent years. Whilst the representation of bronchial tree geometry has become progressively more realistic, and the techniques for solving the governing equations more accurate, the conclusions drawn by the various authors have not differed in essence from those presented over thirty years ago by Rauwerda (1946). Namely, that diffusional equilibrium is attained very rapidly, and no significant concentration gradients exist in the acinus at the end of the breathing cycle. Experimental findings, in contrast, suggest that gas mixing is incomplete at end expiration, hence series inequalities must be present to some extent, even in the normal lung. The work of Read (1966a,b), Cumming *et al.* (1967), Power (1969) and Kawashiro *et al.* (1976) for example, would be difficult to explain in terms other than stratified inhomogeneities. Moreover, the results obtained by

*Accepted for publication 1 July 1978*

\* The work was supported in part by the Science Research Council, United Kingdom.

Sikand *et al.* (1966, 1976) also point to the presence of incomplete diffusive mixing. In view of such incontrovertible experimental evidence it would appear cogent to re-examine the analytical work in an attempt to reconcile these apparently different views of pulmonary gas transport.

The physical model invariably used by workers to represent the bronchial tree is formulated by combining the dimensions of all airways of the same generation number, thereby producing the well-known 'trumpet' (Paiva, 1972) or 'thumbtack' (La Force and Lewis, 1970) shaped function of total cross-sectional area and distance. Actual data is either derived from the definitive morphometric studies of Weibel (1963) or the more recent work of Hansen and Ampaya (1975), scaled to an average FRC. Gaseous transport is then simulated by applying the governing partial differential equation, which describes the convection and diffusion of a tracer gas into an indigenous gaseous phase:

$$\frac{\partial F}{\partial t} = D \left[ \frac{\partial^2 F}{\partial y^2} + \frac{1}{S} \frac{\partial S}{\partial y} \frac{\partial F}{\partial y} \right] - \frac{\dot{Q}}{S} \frac{\partial F}{\partial y} \quad (1)$$

where  $F \equiv F(y,t)$  is the fractional concentration of inspired tracer gas at distance  $y$  from the beginning of the model and at time  $t$  after the start of the respiratory manoeuvre;  $S \equiv S(y)$  is the total cross-sectional area of the model at distance  $y$  from the portal end;  $D$  is the binary molecular diffusion coefficient between the inspired and residual gases; and  $\dot{Q}$  is the volumetric gas flow rate. The solution of equation (1) enables a plot of gas concentration against distance within the physical model to be given for the entire respiratory cycle.

Whilst several different numerical techniques have been employed to obtain such results (Scherer *et al.*, 1972; Paiva, 1973; Baker *et al.*, 1974; Davidson, 1975; Pack *et al.*, 1977), the boundary conditions assumed have always been identical, and are usually stated as follows:

$$F(0,t) = 1.0 \text{ for } t_1 \leq t \leq T/2 \quad (2)$$

$$\left. \frac{\partial F}{\partial y} \right|_{y=L} = 0.0 \text{ for } t_1 \leq t \leq T/2 \quad (3)$$

and for expiration:

$$\left. \frac{\partial F}{\partial y} \right|_{y=0} = 0.0 \text{ for } T/2 < t \leq T \quad (4)$$

$$\left. \frac{\partial F}{\partial y} \right|_{y=L} = 0.0 \text{ for } T/2 < t \leq T \quad (5)$$

where  $t_1$  is the time required for the inspired gases to traverse the upper 10 generations (approx. volume 60 ml) and  $T$  is the total duration of the respiratory cycle.

On applying these conditions to a typical model based on Weibel's Model A, and describing the airways from the end of generation 10 to the alveolar wall (see table 1), it is found that although there are significant concentration differences

TABLE I

| z  | l    | S        |
|----|------|----------|
| 10 | 0.39 | 9.80     |
| 11 | 0.33 | 14.33    |
| 12 | 0.28 | 21.05    |
| 13 | 0.23 | 32.53    |
| 14 | 0.20 | 50.73    |
| 15 | 0.17 | 82.60    |
| 16 | 0.14 | 131.60   |
| 17 | 0.12 | 242.18   |
| 18 | 0.10 | 522.00   |
| 19 | 0.08 | 1307.00  |
| 20 | 0.07 | 2946.00  |
| 21 | 0.06 | 5510.00  |
| 22 | 0.05 | 15328.00 |
| 23 | 0.04 | 26216.00 |

Weibel's Model A with the data scaled such that the FRC corresponds to that of an average normal lung (3.0 litres) where,

z = the generation number,

l = the generation length in cm,

S = the total cross-sectional area in  $\text{cm}^2$ .

in the acinar region at end inspiration, these stratifications are completely obliterated during early expiration. Bearing in mind that some measure of concentration gradient would be expected from the experimental work, it is evident that either the physical model is not a sufficiently accurate analogue of the pulmonary airways, or the prescribed boundary conditions do not represent the processes obtaining in the actual lung.

#### THE PHYSICAL MODEL

The influence of changes in the structural dimensions of the models has been extensively studied by several groups of investigators. Baker *et al.* (1974, 1975) found that the efficiency of gas mixing was insensitive to any single or multiple variation in airway size. Indirectly, Paiva *et al.* (1976) came to the same conclusion by utilising the data of Hansen and Ampaya (1975), and noting that the results did not differ significantly from those presented in an earlier study (Paiva, 1973) which assumed Weibel's Model A (Weibel, 1963). Furthermore, the work of Pack *et al.* (1974, 1977), which considers an expanding and contracting alveolar region, also demonstrates that diffusion equilibrium is unaffected by variable model dimensions.

## CONVENTIONAL BOUNDARY CONDITIONS

Whilst the boundary conditions conventionally assumed for the entry portal of all previously proposed models are easily understood, and represent a reasonable approximation to reality, those specified at the distal end are less obvious. The intention is to define a situation which ensures a zero flux of gas across the alveolar wall, thus mimicing the behaviour of an insoluble tracer.

In the work of authors assuming a 'rigid' physical model (for example Baker *et al.*, 1974; Paiva, 1973; Pedley, 1970) the actual effect of applying  $\left. \frac{\partial F}{\partial y} \right|_{y=L} = 0$  may best be mathematically interpreted by considering the functional form of the total flux equation,  $G(y,t)$ .

For inspiration we can write,

$$G(y,t) = \dot{Q}F - DS \frac{\partial F}{\partial y} \text{ for } t_1 \leq t \leq \frac{T}{2} \quad (6)$$

and for expiration,

$$G(y,t) = -\dot{Q}F - DS \frac{\partial F}{\partial y} \text{ for } \frac{T}{2} < t \leq T \quad (7)$$

In both equations (6) and (7) the total flux is defined to be the summation of convective and diffusive flux contributions. Now, at the alveolar wall,

$$G(L,t) = \dot{Q}F|_{y=L} - DS(L) \left. \frac{\partial F}{\partial y} \right|_{y=L} \text{ for } t_1 \leq t \leq \frac{T}{2} \quad (8)$$

and similarly,

$$G(L,t) = -\dot{Q}F|_{y=L} - DS(L) \left. \frac{\partial F}{\partial y} \right|_{y=L} \text{ for } \frac{T}{2} < t \leq T \quad (9)$$

Substituting from equation (3) into equation (8) yields

$$G(L,t) = +\dot{Q}F|_{y=L} \text{ for } t_1 \leq t \leq T/2 \quad (10)$$

and by a similar procedure equations (5) and (9) give,

$$G(L,t) = -\dot{Q}F|_{y=L} \text{ for } \frac{T}{2} < t \leq T \quad (11)$$

From a scrutiny of equation (10) it is clear that a finite flux of input gas is being continually drawn *out* of the model across the alveolar wall during inspiration, and from equation (11) it can be seen that gas is being similarly drawn *into* the model during expiration. When 'flux curves' (Pack *et al.*, 1977) are plotted for the entire respiratory cycle, as in fig. 1, these phenomena are readily apparent.

It should now be obvious why the conventional boundary conditions given in equations (3) and (5) fail to give a true no-flux condition at the distal end of

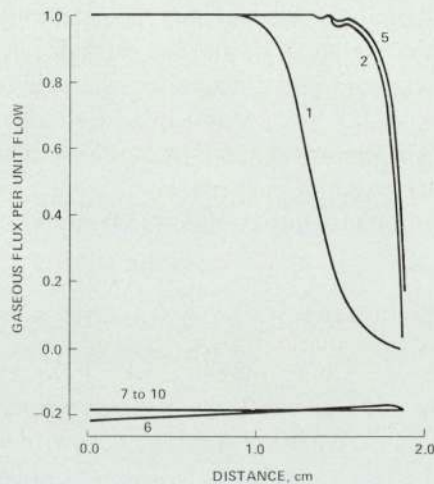


Fig. 1. Gaseous flux per unit flow existing in the model when using the conventional boundary conditions. Curve 1 is at 0.4 sec after the start of inspiration and curves 2 to 10 are at equivalent 0.14-sec time intervals thereafter. Note that a zero-flux condition at the distal end of the model is *not* specified.

rigid models, and why tracer gas concentrations fall too rapidly during inspiration. Thus during expiration the flux at the model entrance ( $y = 0$ ) is given by,

$$G(0,t) = -\dot{Q}F|_{y=0} \text{ for } \frac{T}{2} < t \leq T \quad (12)$$

Equations (11) and (12) state that eventually gas is leaving the model at the same rate at which it is being withdrawn through the alveolar wall; hence concentration gradients would not be expected to persist under such conditions. In other words, the artifact caused by the violation of the required no-flux condition at the alveolar wall would appear to be primarily responsible for the unrealistically rapid approach to gaseous equilibrium.

In contrast, the models of Scherer *et al.* (1972) and Pack *et al.* (1977) undergo volume changes during both inspiration and expiration in such a manner that convective gas flow is always zero at the alveolar wall. They assume that the amount of convection  $v(y,t)S(y,t)$  at any point  $y$  in the models are equal to the total volume change in the airways distal to that point, that is,

$$v(y,t) = \frac{1}{S(y,t)} \int_y^L \frac{\partial S}{\partial t} dy \quad (13)$$

The expansion and contraction of the models is represented by the functional relation,

$$S(y,t) = S(y)[1 - f(y)b(t)] \quad (14)$$

which defines the cross-sectional area at any point during the breathing cycle in terms of a 'flexibility function'  $f(y)$ , and an oscillatory function of time  $b(t)$ . Since there is a lack of experimental evidence on the precise distribution of lung volume changes (Hughes *et al.*, 1972; Marshall and Holden, 1963) the functional form of  $f(y)$  must remain empirical, and the authors assume it to be evenly distributed along the axial length of their models.

Substituting from equation (14) into equation (13) gives,

$$v(y,t) = -\frac{b(t)}{S(y,t)} \int_y^L S(y)f(y) dy \quad (15)$$

Putting  $y = L$  in equation (13) gives  $v(L,t) = 0$ , hence convective gas flow is always zero at the alveolar wall. Now, equation (13) may be rewritten in the form,

$$\dot{Q}(y,t) = S(y,t)v(y,t) = \int_y^L \frac{\partial S}{\partial t} dy \quad (16)$$

and therefore we know that  $\dot{Q}(L,t) = 0$ .

Substituting into equations (6) and (7) yields,

$$G(L,t) = DS \frac{\partial F}{\partial y} \quad t_1 \leq t \leq T \quad (17)$$

In order to ensure that the total flux is zero at the alveolar wall, it is further necessary to specify the boundary condition  $\left. \frac{\partial F}{\partial y} \right|_{y=L} = 0$ , as in the rigid models. Since some 95 per cent of lung volume is contained within the terminal generations of the bronchial tree (a linear distance of only 0.6 cm) it is hardly surprising that these models again fail to display any stratified inhomogeneities in the acinar region because of this explicit assumption. On reflection, it is clearly inappropriate to specify the boundary conditions in terms of a fixed concentration gradient at the alveolar wall, since it is the changes in concentration gradient immediately adjacent to this point that is the main purpose of the simulations.

#### REVISED BOUNDARY CONDITIONS

From the above discussion, it is evident that a better approximation to the actual conditions within the lungs could be made by ensuring a zero flux at the alveolar wall whilst simultaneously allowing the concentration gradient to be a variable. Applying the former condition, *i.e.*  $G(L,t) \equiv 0$  to equations (6) and (7) yields,

$$0 = \dot{Q}F|_{y=L} - DS(L) \left. \frac{\partial F}{\partial y} \right|_{y=L} \quad \text{for } t_1 \leq t \leq \frac{T}{2} \quad (18)$$

and,

$$0 = -\dot{Q}F|_{y=L} - DS(L) \left. \frac{\partial F}{\partial y} \right|_{y=L} \text{ for } \frac{T}{2} < t \leq T \quad (19)$$

rearranging, we obtain,

$$\left. \frac{\partial F}{\partial y} \right|_{y=L} = + \frac{\dot{Q}}{DS(L)} F|_{y=L} \text{ for } t_1 \leq t \leq \frac{T}{2} \quad (20)$$

and,

$$\left. \frac{\partial F}{\partial y} \right|_{y=L} = - \frac{\dot{Q}}{DS(L)} F|_{y=L} \text{ for } \frac{T}{2} < t \leq T \quad (21)$$

Equations (20) and (21) now represent a true no-flux condition. The conventional boundary conditions at the entrance to the model ( $y = 0$ ) are acceptable, for both inspiration and expiration, for the following reasons. During inspiration, we have from equation (6) that,

$$G(0,t) = \dot{Q}F|_{y=0} - DS(O) \left. \frac{\partial F}{\partial y} \right|_{y=0} \text{ for } t_1 \leq t \leq \frac{T}{2} \quad (22)$$

Since we are assuming that a uniform convective flux (that is uniform flow) of gas enters the model, we do not expect any concentration differences to exist near the model entrance. In other words, we require that  $G(0,t) = +\dot{Q}F|_{y=0}$  which implies, from equation (22) that,  $\left. \frac{\partial F}{\partial y} \right|_{y=0} = 0$ . It is thus intuitively obvious that the input gas concentrations at the model entrance must remain constant as defined in equation (2).

For the expiratory phase, equation (7) gives

$$G(0,t) = -\dot{Q}F|_{y=0} - DS(O) \left. \frac{\partial F}{\partial y} \right|_{y=0} \text{ for } \frac{T}{2} < t \leq T \quad (23)$$

Now, during expiration the contribution from diffusive mixing near the model entrance is negligible in comparison to the convective mixing (Paiva, 1972). As a result a relatively uniform convective flux of gas out of the model is anticipated, which may be stated mathematically as,

$$G(0,t) = -\dot{Q}F|_{y=0} \quad (24)$$

Substituting from equation (24) into equation (23) we obtain

$$\left. \frac{\partial F}{\partial y} \right|_{y=0} = 0, \text{ as given previously in equation (3).}$$

## Results

Having defined the true 'no-flux' boundary conditions, it is possible to obtain a solution to equation (1), by means of the explicit finite difference technique detailed in Appendix I. The resulting concentration/distance curves are shown in fig. 2, from which it will be noted that not only are there significant concentration differences in the acinus region at end inspiration, but more importantly, these stratifications persist during expiration. For example, a 0.7 per cent ( $\approx 5.32$  mm Hg) difference in tracer gas concentration exists between the ends of the model at end

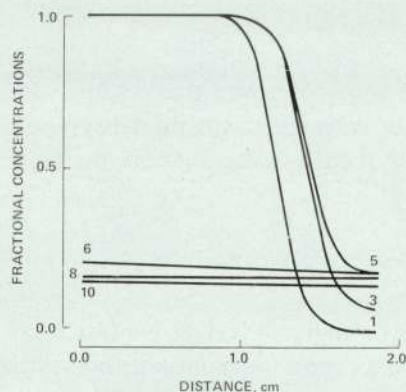


Fig. 2. Effect of the revised boundary conditions upon the input gas concentrations in the model at various times during the respiratory cycle. Curve 1 is at 0.4 sec after the start of inspiration and curves 2 to 10 are at equivalent 0.4-sec time intervals thereafter. In this case significant concentration differences do exist in the acinar region at end expiration (*i.e.* curve 10), which is more clearly evident from a scrutiny of the actual concentration values given in table 2.

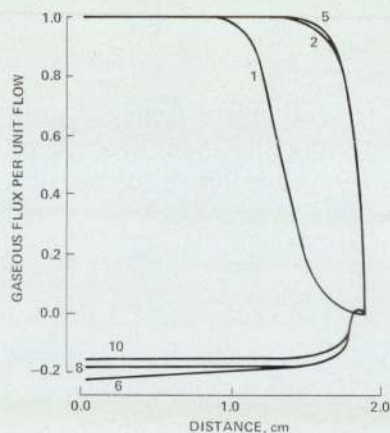


Fig. 3. Gaseous flux per unit flow existing in the model when using the revised boundary conditions. Curve 1 is at 0.4 sec after the start of inspiration and curves 2 to 10 are at equivalent 0.4-sec time intervals thereafter. Note that in this case a zero-flux condition at the distal end of the model is specified.

TABLE 2

|                       | Distance<br>y (cm) | Fractional gas concentration |             |
|-----------------------|--------------------|------------------------------|-------------|
|                       |                    | Conventional (a)             | Revised (b) |
| Conducting<br>airways | 0.00               | 0.178040                     | 0.155106    |
|                       | 0.33               | ..                           | 0.154794    |
|                       | 0.61               | ..                           | 0.154409    |
|                       | 0.84               | ..                           | 0.153931    |
|                       | 1.04               | ..                           | 0.153351    |
|                       | 1.22               | ..                           | 0.152709    |
| Acinar<br>region      | 1.36               | ..                           | 0.151825    |
|                       | 1.48               | ..                           | 0.151004    |
|                       | 1.58               | ..                           | 0.150414    |
|                       | 1.66               | ..                           | 0.149832    |
|                       | 1.73               | ..                           | 0.149280    |
|                       | 1.79               | ..                           | 0.148725    |
|                       | 1.84               | ..                           | 0.148510    |
| 1.88                  | 0.178040           | 0.148296                     |             |

The table gives the end expiration input gas concentration against distance down the model for (a) the conventional and (b) the revised boundary conditions. It will be noted that no concentration differences are apparent when the conventional boundary conditions apply, whereas with the revised boundary conditions significant gradients exist throughout the model. Specifically, a 0.42% difference in fractional gas concentration (representing 60% of the total predicted gradient) is evident in the acinar region.

expiration (see table 2); 60 per cent of this difference occurring in the acinus. The corresponding flux curves are shown in fig. 3, and as expected illustrate the required zero flux across the alveolar wall and, by implication, demonstrate that a balance must always exist between the convective and diffusive movements of gas molecules at the alveolar wall throughout the breathing cycle.

### Discussion

The main contribution of the present work has been to highlight the crucial role played by boundary conditions in providing a more realistic description of gaseous transport mechanisms in the bronchial tree.

Specifically, it has been demonstrated that diffusional equilibrium within the terminal airways is *incomplete* at end expiration, which further suggests that the stratified inhomogeneity thus produced may contribute to the alveolar plateau. In order to test this hypothesis it is necessary to modify our analysis to facilitate a simulation of the single breath nitrogen washout curve by taking,

$$F_{E_{N_2}}(t) = 0.8[1.0 - F(o, t - t_1)] \quad (25)$$

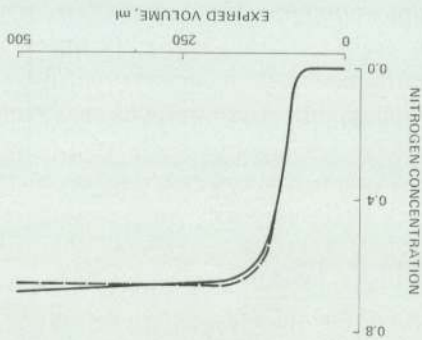


Fig. 4 Comparison of the predicted single-breath nitrogen washout curves corresponding to the conventional and revised boundary conditions. Dashed line: solution with the conventional boundary conditions showing no alveolar plateau slope; solid line: solution with the revised boundary conditions illustrating a significant alveolar plateau slope (3.42% on extrapolating to 500 ml expired).

where  $F_{N_2}(t)$  is the variation of the nitrogen concentration at the entry of the trachea during the first expiration following a single oxygen inspiration.

The resulting plot of expired nitrogen against volume is given in fig. 4 and clearly shows the expected alveolar 'plateau' slope (see table 3). On extrapolating the curve to 500 ml the observed slope is equivalent to 3.42 per cent, which is reminiscent of the average value for normals obtained experimentally by Mills and Harris (1965) and more recently, Jones (1967).

The only previous analytical work to show a similar finite alveolar plateau slope was that of Cumming *et al.* (1971), who produced a 1.1 per cent gradient between 750 ml and 1250 ml expired. These authors, however, did not attempt to simulate *simultaneous* convection and diffusion, but allowed successive quanta of flow to enter their model followed by a diffusion period. Although this 'relaxation' technique only provided a crude approximation to the actual process of pulmonary gas transport, it did guarantee that no gas was lost across the alveolar wall. Moreover, by controlling the way in which gas flowed out of their model, a continual fall in fractional concentration at the mouth was ensured, giving rise to the small alveolar slope.

When the physical structure of the present model was altered by taking into account the more recent data of Hansen and Ampaya (1975) we found that with the conventional boundary conditions, the input gas concentration attained equilibrium even more rapidly. The results obtained when employing the revised boundary conditions were similar to those shown in figs. 2 and 4, however, there were noticeable changes in the shape of the concentration transition (phase II) and the shape of the 'knee' of the ensuing nitrogen washout curve as illustrated in fig. 5. Over the last few years a great deal of experimental and theoretical work has been devoted to the study of 'effective diffusivity' in the upper airway generations. The idea is that the mixing produced by airway branching (turbulence and secondary flows) and the molecular diffusivity may be represented by an effective axial diffusion

TABLE 3

| Expired volume (ml) | Nitrogen concentration |             |
|---------------------|------------------------|-------------|
|                     | Conventional (a)       | Revised (b) |
| 25.0                | 0.000000               | 0.000000    |
| 50.0                | 0.000000               | 0.000000    |
| 60.0                | 0.000000               | 0.000000    |
| 75.0                | 0.041709               | 0.041047    |
| 100.0               | 0.385600               | 0.378557    |
| 125.0               | 0.572455               | 0.561785    |
| 150.0               | 0.632282               | 0.621552    |
| 175.0               | 0.650133               | 0.640789    |
| 200.0               | 0.655388               | 0.647882    |
| 225.0               | 0.656929               | 0.651382    |
| 250.0               | 0.657513               | 0.653808    |
| 275.0               | 0.657564               | 0.655901    |
| 300.0               | 0.657568               | 0.657879    |
| 325.0               | 0.657568               | 0.659804    |
| 350.0               | 0.657568               | 0.661695    |
| 375.0               | 0.657568               | 0.663559    |
| 400.0               | 0.657568               | 0.665397    |
| 425.0               | 0.657568               | 0.667210    |
| 450.0               | 0.657568               | 0.668999    |
| 475.0               | 0.657568               | 0.670763    |
| 500.0               | 0.657568               | 0.672504    |

The table gives the expired nitrogen concentrations at the beginning of the trachea for (a) the conventional and (b) the revised boundary conditions. It will be noted that the alveolar plateau has zero gradient when the conventional boundary conditions apply, whereas with the revised boundary conditions a significant plateau slope of the order of 1.87% over the terminal 250 ml expired, is apparent. On extrapolating the nitrogen washout curve to 500 ml, the slope rises to 3.42% which closely approximates to the experimentally observed value for normal subjects.

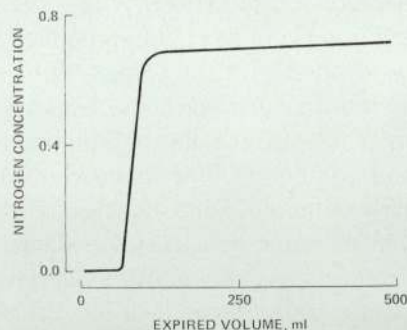


Fig. 5. Predicted single-breath nitrogen washout curve corresponding to the revised boundary conditions and when employing the data of Hansen and Ampaya (1975). Note that the slope of the concentration transition (phase II) and the shape of the 'knee' of this curve differ significantly from the curve shown in fig. 4 (solid line).

coefficient,  $De_{\text{eff}}$ , which is identically equal to the molecular diffusion coefficient,  $D_{\text{mol}}$ , in the alveolar region since the gas velocity is very small. At present there is no agreement on the actual functional form of  $De_{\text{eff}}$  to be used in the solution of the gas transport equation, however, the results obtained by Pack *et al.* (1977) illustrate that gas mixing efficiency is independent of the particular way in which the effective axial diffusion coefficient is employed. Moreover, the recent experimental results of Horsfield *et al.* (1977) and Worth *et al.* (1977) also suggest that the mechanism of Taylor Dispersion has a negligible effect on the mixing of the respiratory gases *in vivo*. Such results again emphasize the limited role that model parameters have upon gas mixing efficiency, compared to the significant influence of boundary conditions.

The physical model chosen in the present study is rigid, hence it has been necessary to mathematically impose a gaseous flow to simulate inspiration and expiration. In reality, breathing is brought about by the expansion and contraction of the respiratory regions of the lung, however, in order to follow these movements exactly it would be necessary to solve the appropriate hydrodynamic equations. Such additional complexity is considered unnecessary in view of the fact that the results obtained from variable volume models (for example, Pack *et al.*, 1977) do not differ significantly from those obtained from rigid models (for example Paiva, 1973) which are similar to that used in the present study. The only effect of considering rigid rather than variable volume models would appear to be that input gas concentrations will tend to be slightly underestimated (Paiva, 1978). As a corollary, it is interesting to observe that even when a 'compliant' model is assumed, it is clear from equation (15) that a convective flow must still be imposed in order to obtain a solution to the gas transport equation.

## Appendix 1

An explicit finite difference scheme (Bush *et al.*, 1977) was employed in the numerical solution of equation (1) rather than an implicit scheme due to the more rapid computing times associated with the former. It was found that due to the presence of the convective term in equation (1), the Gauss-Seidel iteration procedure (which is necessary in order to solve the appropriate implicit difference equations) required large amounts of computing time in order to attain a convergent and accurate solution. Similarly, a suitable one-dimensional finite element solution of equation (1) suffered from the same deficiencies as discussed above. The rationale for choosing central difference approximations of derivatives in favour of forward or backward differences was based solely on their properties of convergence. In fact, forward and backward differences are accurate to  $O(\Delta y)$ , whereas the central differences are accurate to  $O(\Delta y^2)$  as has been demonstrated in most standard texts on numerical methods (see Smith, 1965 for example). Thus, we have chosen to use central difference approximations of derivatives throughout the scheme, *i.e.*

$$\frac{\partial F}{\partial t} = \frac{(F_{i,j+1} - F_{i,j})}{\Delta t}$$

$$\frac{\partial F}{\partial y} = \frac{(F_{i+1,j} - F_{i-1,j})}{2(\Delta y)}$$

$$\frac{\partial^2 F}{\partial y^2} = \frac{(F_{i+1,j} - 2F_{i,j} + F_{i-1,j})}{(\Delta y)^2}$$

On substituting the above finite difference approximations into equation (1) we have, on simplifying

$$F_{i,j+1} = F_{i,j} + Dr(F_{i+1,j} - 2F_{i,j} + F_{i-1,j}) + \frac{1}{2} \left[ \frac{D}{S} \frac{\partial S}{\partial y} + \frac{\dot{Q}}{S} \right] (\Delta y)(F_{i+1,j} - F_{i-1,j}) \quad (i)$$

Equation (i) is the finite difference approximation to the gas transport equation. In order for the solution of equation (i) to converge to the true solution of the transport equation we require a stability criterion. By applying the Fourier series method of stability to equation (i) we found that convergence depended upon the value of  $r$  where; (Smith, 1965)

$$r \leq \frac{D}{2 \left[ D^2 \sin^2 \frac{\beta h}{2} + K_1^2 \cos^2 \frac{\beta h}{2} \right]} \quad (ii)$$

$$\text{and } K_1 = \frac{1}{2} (\Delta y) \left[ \frac{D}{S} \frac{\partial S}{\partial y} - \frac{\dot{Q}}{S} \right]$$

This expression for  $r$  assumes a minimum value for two particular cases, *i.e.*

*Case 1:*  $K < D$

When  $K < D$ ,  $r$  is minimum when  $\cos \left[ \frac{\beta h}{2} \right] = 0$  and thus

$$r \leq \frac{1}{2D}$$

*Case 2:*  $K > D$

When  $K > D$ ,  $r$  is minimum when  $\sin \left[ \frac{\beta h}{2} \right] = 0$  therefore,

$$r < \frac{D}{2K^2}$$

Thus, in order to obtain a stable and convergent solution to the numerical approximation of the gas transport equation, we require that, if  $K < D$ , then  $r \leq 1/2D$  and if  $K > D$ , then  $r < D/2K^2$ , we obtained a stable and convergent solution for  $D = 0.25$ ,  $\Delta y = 0.02$ ,  $r = 1$  and hence  $\Delta t = 0.0004$ . A detailed consideration of the stability of the proposed solution technique is given in Appendix 2 below.

## Appendix 2

### STABILITY OF SOLUTION TECHNIQUE

Consider the problem of solving the more general linear parabolic partial differential equation with variable coefficients, *i.e.*

$$\frac{\partial F}{\partial t} = a \frac{\partial^2 F}{\partial y^2} + b \frac{\partial F}{\partial y} + cF + d \quad (1)$$

where  $a$ ,  $b$ ,  $c$  and  $d$  are functions of  $t$  and  $y$  only, and with the more general boundary conditions

$$p \frac{\partial F}{\partial y} + qF = v \quad (2)$$

where  $p$ ,  $q$  and  $v$  are functions of  $t$  only.

Now, there is an important class of simulations to linear parabolic equations with variable coefficients for which rigorous sufficient conditions for stepwise stability are easily obtained (see Hildebrand, 1968). In illustration, let us suppose that a 'four-point' formulae has been obtained, for equations (1) and (2) above, in the form,

$$F_{i,j+1} = C_{-1}(i,j)F_{i-1,j} + C_0(i,j)F_{i,j} + C_1(i,j)F_{i+1,j} + d_{i,j} \quad (3)$$

as a consistent simulation, where the coefficients  $C_n(i,j)$  are known functions of  $i$  and  $j$ . We suppose that equation (3) holds for  $i = 1, 2, \dots, N$  and  $j = 1, 2, \dots$ . The propagated error  $\epsilon_{i,j}$  due to an initial error distribution  $g_i$  is then specified by the relations,

$$\epsilon_{i,j+1} = \sum_{n=-1}^1 C_n(i,j)\epsilon_{i+n,j} \quad (4)$$

and,

$$\epsilon_{i,1} = g_i \quad (5)$$

If the coefficients  $C_{-1}$ ,  $C_0$  and  $C_1$  are nonnegative for all relevant values of  $i$  and  $j$ , *i.e.*

$$C_n(i,j) \geq 0 \quad (n = -1, 0, 1) \quad (6)$$

and if their sum does not exceed unity,

$$\sum_{n=-1}^1 C_n(i,j) \leq 1 \quad (7)$$

then we may deduce from equation (4) the relation

$$|\epsilon_{i,j+1}| < \sum_{n=-1}^1 C_n(i,j) |\epsilon_{i+n,j}| < \max_n |\epsilon_{i+n,j}|$$

for  $i = 1, 2, \dots, N$  (8)

It thus follows that when the conditions (6) and (7) are satisfied for all relevant values of  $i$  and  $j$ , the errors propagated by a single line of initial errors can never exceed the largest initial error in magnitude, so that the formulation is stable in the stepwise sense. While the conditions (6), (7) and (8) are sufficient for stepwise stability, they may not be necessary, in the sense that the formulation may be stable even though one or more of these conditions is violated.

The finite difference approximation to the gas transport equation (*i.e.* equation (i) in Appendix 1) may be written in a form similar to that given in equation (1) above, *i.e.*

$$F_{i,j+1} = (D - K_i)rF_{i-1,j} + (1 - 2Dr)F_{i,j} + (D + K_i)rF_{i+1,j}$$

for  $2 \leq i \leq N - 1$  (9)

and similarly our revised boundary conditions may be expressed in finite difference form as,

$$F_{N,j+1} = 2DrF_{N-1,j} + \left[ 1 - 2Dr \pm \frac{2r(\Delta y)\dot{Q}}{S_N} \pm \frac{2K_N r(\Delta y)\dot{Q}}{DS_N} \right] F_{N,j}$$
(10)

where,

$$K_i = \frac{1}{2}(\Delta y) \left[ \frac{D}{S_i} \frac{\partial S_i}{\partial y} + \frac{\dot{Q}}{S_i} \right]$$
(11)

On equating coefficients of equation (3) with those of equations (9) and (10) we have that

$$r \leq \frac{1}{2D}, \quad |K_i| \leq D \text{ and } r \leq \frac{1}{2(D + A_N)}$$
(12)

where,

$$A_N = \frac{\dot{Q}(\Delta y)}{DS_N} (K_N + D)$$
(13)

In this particular case  $A_N \ll D$  and therefore the stability of our revised boundary conditions is guaranteed by the relations derived previously using the Fourier series method (See Appendix 1).

When the Fourier series method of stability was applied to equation (10) we found that stability depended on the value of  $r$  where

$$r = \frac{2 \left[ 4D \sin^2 \left[ \frac{\beta h}{2} \right] - B_N \right]}{\left[ 8D(2D - B_N) \sin^2 \left[ \frac{\beta h}{2} \right] + B_N^2 \right]}$$
(14)

and where,

$$B_N = \frac{2\dot{Q}(D + K_N)(\Delta y)}{DS_N}$$
(15)

The expression on the R.H.S. of equation (14) can be re-written in terms of partial fractions in the form,

$$r = \frac{1}{(2D - B_N)} - \frac{B_N(4D - B_N)}{(2D - B_N)} \frac{1}{\left[ 8D(2D - B_N) \sin^2 \left[ \frac{\beta h}{2} \right] + B_N^2 \right]} \quad (16)$$

For the particular solution that we derived, the values of the model parameters were as follows,

$$\Delta y = 0.02, \quad S_N = 26, 216.0 \quad (\text{see table 1})$$

$$D = 0.25, \quad \dot{Q} = 250$$

Substituting these values into the expression previously given for  $K$  we obtain,

$$K \approx 0.0125$$

and hence from equation (15) we know that

$$B_N \approx \frac{10.5}{26,216} \ll D \quad (16)$$

Since  $r > 0$ , the expression for  $r$  given in equation (14) will assume a minimum value when  $\sin \left[ \frac{\beta h}{2} \right] = 0$

*i.e.*

$$r_{\min} < \frac{1}{(2D - B_N)} - \frac{B_N(4D - B_N)}{(2D - B_N)} \frac{1}{(4D - B_N)^2} \quad (17)$$

$$r_{\min} < \frac{1}{\left[ 2D - \frac{B_N}{2} \right]}$$

When  $B_N$  is very small (as in the present case where  $B_N \approx 0.0004$ ), equation (17) becomes identical to the relationship found in Appendix 1 (Case 1). In order to test the validity of this stability criterion we have solved equation (9) with the revised no flux boundary conditions and for different values of  $r$  (in fact,  $r = 0.5$  and  $r = 1.0$ ) it was found that the solutions were identical to the sixth decimal place, thus indicating that both a convergent and stable solution was attained.

Hence it is concluded, that all of our model predictions are free from numerical artifacts arising from the use of a non-zero concentration gradient at the alveolar wall.

## References

- Baker, L. G., J.S. Ultman and R. A. Rhoades (1974). Simultaneous gas flow and diffusion in a symmetric airway system: a mathematical model. *Respir. Physiol.* 21: 119-138.

- Baker, L. G., J. S. Ultman and R. A. Rhoades (1975). Characterisation of lung geometry from the single-breath nitrogen washout test. *Comp. Biomed. Res.* 8: 254-266.
- Bush, A. W., M. A. Pinney and J. R. Wallis (1977). A mathematical model of the production of ammonium sulphate aerosol under an elevated temperature inversion in Cleveland County. In: Proceedings of the International Conference on Applied Numerical Modelling (University of Southampton), pp. 309-318.
- Cumming, G., J. Crank, K. Horsfield and I. Parker (1966). Gaseous diffusion in the airways of the human lung. *Respir. Physiol.* 1: 58-74.
- Cumming, G., K. Horsfield and S. B. Preston (1971). Diffusion equilibrium in the lung examined by nodal analysis. *Respir. Physiol.* 12: 329-345.
- Davidson, M. R. (1975). Lung gas mixing during expiration following an inspiration of air. *Bull. Math. Biol.* 37: 113-126.
- Hansen, J. E. and E. P. Ampaya (1975). Human air space shapes, sizes, areas and volumes. *J. Appl. Physiol.* 38: 990-995.
- Hildebrand, F. B. (1968). Finite-Difference Equations and Simulations. New Jersey, Prentice-Hall.
- Horsfield, K., A. Davies and G. Cumming (1977). Role of conducting airways in partial separation of inhaled gas mixtures. *J. Appl. Physiol.* 43: 391-396.
- Hughes, J. M. B., F. G. Hoppin and J. Mead (1972). Effect of lung inflation on bronchial length and diameter in excised lungs. *J. Appl. Physiol.* 32: 25-35.
- Jones, J. G. (1967). The effect of preinspiratory lung volume on the result of the single breath O<sub>2</sub> test. *Respir. Physiol.* 2: 375-385.
- Kawashiro, T., R. S. Sikand, F. Adaro, H. Takahashi and J. Piper (1976). Study of intrapulmonary gas mixing in man by simultaneous washout of helium and sulphur hexafluoride. *Respir. Physiol.* 28: 261-275.
- La Force, R. C. and B. M. Lewis (1970). Diffusional transport in the human lung. *J. Appl. Physiol.* 28: 291-298.
- Marshall, R. and W. S. Holden (1963). Changes in calibre of the smaller airways in man. *Thorax* 18: 54-58.
- Mills, R. J. and P. Harris (1965). Factors influencing the concentration of expired nitrogen after a single breath of oxygen. *J. Appl. Physiol.* 20: 103-109.
- Pack, A., D. Murray-Smith, R. J. Mills, M. Hooper and J. Taylor (1974). Application of Mathematical Models in Respiratory Medicine. In: Bulletin of the Institute of Mathematics and its Applications. Special Issue: *Math. Clin. Med.* 10: 20-26.
- Pack, A., M. B. Hooper, W. Nixon and J. C. Taylor (1977). A computational model of pulmonary gas transport incorporating effective diffusion. *Respir. Physiol.* 29: 101-124.
- Paiva, M. (1972). Computation of the boundary conditions for diffusion in the human lung. *Comp. Biomed. Res.* 5: 585-595.
- Paiva, M., L. M. Lacquet and L. P. van der Linden (1976). Gas transport in a model derived from Hansen-Ampaya anatomical data of the human lung. *J. Appl. Physiol.* 41: 115-119.
- Paiva, M. (1978). Hypothesis underlying a continuous analysis of gas transport in a lung model. *Bull. Inst. Math. Applications*, Vol. 14, pp. 17-21.
- Pedley, T. J. (1970). A theory for gas mixing in a simple model of the lung. AGARD Conference No. 65 (NATO).
- Power, G. (1969). Gaseous diffusion between airways and alveoli in the human lung. *J. Appl. Physiol.* 27: 701-709.
- Rauwerda, P. E. (1946). Unequal Ventilation of Different Parts of the Lung and the Determination of Cardiac Output (thesis). Groningen, The Netherlands, University of Groningen.
- Read, J. (1966a). Alveolar populations contributing to expired gas tension plateaus. *J. Appl. Physiol.* 21: 1511-1520.
- Read, J. (1966b). Stratification of ventilation and blood flow in the normal human lung. *J. Appl. Physiol.* 21: 1521-1531.

- Scherer, P. W., L. H. Shendalman and N. M. Greene (1972). Simultaneous diffusion and convection in single breath lung washout. *Bull. Math. Biophysics* 34: 393-412.
- Sikand, R., P. Cerretelli and L. E. Farhi (1966). Effects of  $\dot{V}_A$  and  $\dot{V}_A/\dot{Q}$  distribution and of time on the alveolar plateau. *J. Appl. Physiol.* 21: 1331-1337.
- Sikand, R., H. Magnussen, P. Scheid and J. Piper (1976). Convective and diffusive gas mixing in human lungs: experiments and model analysis. *J. Appl. Physiol.* 40: 362-371.
- Smith, G. D. (1965). Numerical Solution of Partial Differential Equations. Oxford University Press.
- Weibel, E. R. (1963). Morphometry of the Human Lung. New York, Academic Press.
- Worth, H., F. Adaro and J. Piper (1977). Penetration of inhaled He and SF<sub>6</sub> into alveolar space at low tidal volumes. *J. Appl. Physiol.* 43: 403-408.

THEORETICAL ANALYSIS OF DIFFUSIVITY  
ON PULMONARY GAS TRANSPORT AND MIXING

David A. Scrimshire

Robert J. Loughnane

(Biomedical Engineering Section)

Department of Production Technology and Production Management  
University of Aston in Birmingham  
Gosta Green, Birmingham, England.

Summary

The effects of different tracer gas diffusivities upon pulmonary gas transport and mixing have been examined by means of a new lung model. Specifically, it has been demonstrated how the expired alveolar plateau slope of a tracer gas gives an indication of the magnitude of the end expiratory concentration differences existing in the acinus. Further, by modifying our initial analysis slightly (to allow for a finite flux of gas across the alveolar wall) it has been indicated how more marked stratified inhomogeneities are associated with the transport of soluble rather than insoluble tracer gases.

Because of the practical difficulties of making direct measurements in the more distal regions of the bronchial tree it is at present only possible to infer what gas concentration differences exist in the acinus during the breathing cycle from expired data. Whilst Engel and his co-workers (1) have succeeded in sampling gas at terminal bronchiolar level in dogs, the experimental protocol requires open chest surgery and cannot be applied routinely in man. Moreover, as pointed out by the authors, the physical size of the catheter used may interfere significantly with local gas flows.

In order for a reasonably accurate *interpretation* of single breath wash-out (or washin) curves to be made, it is obviously necessary to employ a suitable quantitative model. In a recent paper we have proposed such a gas transport model, and have demonstrated that simulated results correspond closely to those observed in normal subjects (2). In the present study use is made of this new model to examine the effects of different tracer gas diffusivities on gaseous transport and mixing in human lungs, and specifically relate gaseous concentration differences in the acinar region to concentrations measurable at the mouth.

RUNNING TITLE

THEORETICAL ANALYSIS OF DIFFUSIVITY

KEY WORDS

Binary diffusion coefficients

Boundary Conditions

Stratified Inhomogeneities

Pulmonary Gas Transport Model

Gas Flux/Gas Exchange

Single Breath Washout Test

## Methods

The model is derived from a modified version of Weibel's 'Model A' and consists of the last 13 generations of the bronchial tree. The equations governing the transport of gases into and out of the model are written as:-

$$\frac{\partial F}{\partial t} = D \left[ \frac{\partial^2 F}{\partial y^2} + \frac{1}{S} \frac{\partial S}{\partial y} \frac{\partial F}{\partial y} \right] - \frac{\dot{Q}}{S} \frac{\partial F}{\partial y} \quad (\text{Eqn. 1})$$

where  $F \equiv F(y, t)$  is the fractional concentration of inspired tracer gas at distance  $y$  from the beginning of the model and at time  $t$  after the start of the respiratory manoeuvre;  $S \equiv S(y)$  is the total cross-sectional area of the model at distance  $y$  from the portal end;  $D$  is the binary molecular diffusion coefficient between the inspired and residual gases; and  $\dot{Q}$  is the volumetric gas flow rate.

In order to solve equation (1) suitable boundary conditions must be specified. At the mouth there is a constant flow of inspired tracer gas and this may be written as,

$$F(0, t) = 1.0 \quad \text{for } t_1 \leq t \leq \frac{T}{2} \quad (\text{Eqn. 2})$$

During expiration the contribution from diffusive mixing at the model entrance is considered negligible in comparison to the convective mixing and this implies that,

$$\left. \frac{\partial F}{\partial y} \right|_{y=0} = 0 \quad \text{for } \frac{T}{2} < t \leq T \quad (\text{Eqn. 3})$$

At the distal end of our model it is required that there is no flux of input tracer gas across the alveolar wall,  $y = L$ . Such a requirement may best be achieved by ensuring that the total contribution from both diffusive and convective gas fluxes is zero, implying that a balance exists between these two transport processes. In order to formulate this condition in mathematical terms we need to define the total flux function  $G(y, t)$ , that is,

$$G(y, t) = \dot{Q} F - D S \frac{\partial F}{\partial y} \quad (\text{Eqn. 4})$$

where  $G \equiv G(y, t)$  is the total flux (made up of both a diffusive and a convective contribution) at distance  $y$  from the beginning of the model and at time  $t$  after the start of the respiratory manoeuvre.

We require that  $G(L, t) = 0$  for all  $t$ , and from equation (4) the following *zero flux* boundary conditions may be derived,

$$\left. \frac{\partial F}{\partial y} \right|_{y=L} = + \frac{\dot{Q}}{D S(L)} F \Big|_{y=L} \quad \text{for } t_1 \leq t \leq \frac{T}{2} \quad (\text{Eqn. 5})$$

and,

$$\left. \frac{\partial F}{\partial y} \right|_{y=L} = - \frac{\dot{Q}}{D S (L)} F \Big|_{y=L} \quad \text{for } \frac{T}{2} < t \leq T \quad (\text{Eqn. 6})$$

In the above equations  $t_1$  is the time required for the inspired gases to traverse the upper 10 generations and  $T$  is the total duration of the respiratory cycle. The numerical technique used to solve the gas transport equation has been fully detailed elsewhere (2) along with an exhaustive examination of stability and convergence.

### RESULTS

Figures 1 and 2 show the input gas concentrations within the model at end inspiration and end expiration respectively for three tracers having molecular diffusion coefficients of 0.1 cm<sup>2</sup>/sec, 0.315 cm<sup>2</sup>/sec and 0.76 cm<sup>2</sup>/sec corresponding to SF<sub>6</sub>/N<sub>2</sub>, Ne/N<sub>2</sub> and He/N<sub>2</sub> mixtures. As intuitively expected, it can be seen that at end inspiration the heavier gas (SF<sub>6</sub>) has penetrated deeper into the model than that of the lighter gases (Ne or He), and hence it has a greater dead space volume. Furthermore, the heavier gas displays a more marked concentration stratification in the acinar regions. The actual concentration differences between the ends of the model at end expiration are 0.42% for He, 0.6% for Ne and 1.2% for SF<sub>6</sub>, with the greatest gradients occurring over the last 0.5 cms of the model length.

The resulting concentrations of the three tracer gases being expired through the "mouth" end of the model are given in Figure 3 and show that the heavier the gas, the greater the dead space volume and the greater the alveolar plateau slope. The plateau slopes for the three tracer gases were calculated on the basis of an extrapolation to 500 mls expired and were found to be 2.9% for He, 3.4% for Ne and 4.8% for SF<sub>6</sub>.

### DISCUSSION

The theoretical results presented show that the expired "alveolar plateau" slope of a tracer gas does indeed give an indication of end expiratory concentration differences in the acinus. Moreover, the magnitude of the slope, and the degree of stratified inhomogeneity, *increase* as the molecular weight of the input gas increases (that is  $D$  decreases). Such results concur with the experimental findings of previous workers (3, 4, 5, 6, 7, 8) who also concluded that gases having lower diffusivities should reach equilibrium more slowly, and that the observed expired concentration differences arose as a consequent of similar differences obtaining in the more distal regions of the bronchial tree.

Only two previous attempts have been made to simulate similar results. In 1969, Sasaki and Farhi (9) employing an algebraic lung model, concluded that the only effect of considering a heavy rather than a light tracer gas was that the dead space volume should be greater. A few years later Paiva (10) using a more detailed lung model analysis came to a similar conclusion, but could not demonstrate any concentration gradients in the acinar region at end expiration. We have indicated in a previous paper that a possible explanation for such a finding may well be traced to the boundary conditions assumed by these authors, a fact also suggested by Scherer and Pack (11). The particular boundary conditions applied in the present model ensure that none of the input

tracer gas escapes, or indeed is reabsorbed, through the alveolar wall. As the three gases studied have very low blood solubilities ( $SF_6 = 0.0067$ ,  $Ne = 0.011$ ,  $He = 0.0098$ ) such an assumption would appear to be a reasonably accurate representation. Nevertheless, it is interesting to speculate how a finite gas flux across the alveolar wall would affect concentration gradients. Chang and Farhi (12) have already considered such a case in qualitative terms, and have suggested that the gas exchange is likely to increase any stratified inhomogeneities existing in the acinus. The present model may readily be modified to accommodate a finite gas flux across the alveolar wall by slightly altering the boundary conditions (5) and (6). The necessary modification involves changing " $G = 0$ " to " $G = k$ ", where  $k$  is the amount of input tracer gas (mls/sec) being taken up by the blood flowing in the alveolar capillaries. In fact, equations (5) and (6) become,

$$\left. \frac{\partial F}{\partial y} \right|_{y=L} = + \frac{\dot{Q}}{D S (L)} F \Big|_{y=L} - \frac{G}{D S (L)} \quad (\text{Eqn. 7})$$

and,

$$\left. \frac{\partial F}{\partial y} \right|_{y=L} = - \frac{\dot{Q}}{D S (L)} F \Big|_{y=L} - \frac{G}{D S (L)} \quad (\text{Eqn. 8})$$

The effect of applying three values of  $G$  (10, 25 and 50 ml/sec) to a hypothetical gas having a diffusion coefficient of  $0.25 \text{ cm}^2/\text{sec}$  (equivalent to  $O_2/N_2$ ) is shown in Figure 4 for end inspiration. It can be seen that the higher the  $G$  value, the greater the concentration gradients for the input gas in the acinar region and the lower the alveolar gas concentration. The latter effect is to be expected since higher values of  $G$  are associated with tracers having a higher blood solubility hence they are being removed from alveolar space at a faster rate by capillary blood.

Figure 5 gives the ensuing end expiratory concentrations within the model. It will be noted that more marked stratified inhomogeneities are associated with tracers having higher blood solubilities, and that these concentration gradients are also reflected at the "mouth" end of the model as is evident from Figure 6.

A more realistic illustration of the independent effect of input gas solubility on stratified inhomogeneities may be given by considering the specific gases Argon and Nitrous Oxide because they have very similar diffusion coefficients ( $D = 0.192$  for Ar and  $D = 0.189$  for  $N_2O$ ). Because the solubility of Argon can be considered negligible, a value of zero is assumed for  $G$ . Nitrous Oxide in contrast has a much greater affinity for blood, having a solubility coefficient of 0.465. Using an earlier algebraic gas exchange model (13, 14) the value of  $G$  during a normal initial breath of 100%  $N_2O$  is estimated to be approximately 5.5 ml/sec. The results for the two tracer gases are given in Figures 7 and 8 and as anticipated, greater end inspiratory and end expiratory input gas concentration gradients exist in the acinus for Nitrous Oxide. Moreover, the actual alveolar concentration level for Nitrous Oxide is significantly lower than that of Argon for the reason previously discussed. The simulated single-breath input gas washout tests for these two tracer gases are given in Figure 9 and demonstrate a significantly greater alveolar plateau slope for Nitrous Oxide again reflecting conditions within the lung.

### References

1. L. A. Engel, L. Wood, G. Utz and P. T. Macklem, J. Appl. Physiol. 35 18-24 (1973).
2. D. A. Scrimshire, R. J. Loughnane and T. J. Jones, Resp. Physiol. 35 (1978).
3. J. Georg, N. A. Lassen, K. Mellemegaard and A. Vinther, Clin. Sci. 29 525-532 (1965)
4. G. Cumming, K. Horsfield, J. G. Jones and D. Muir, Resp. Physiol. 2 386-398 (1967)
5. J. Read, J. Appl. Physiol. 21 1521-1531 (1966)
6. G. Power, J. Appl. Physiol. 27 701-709 (1969)
7. R. S. Sikand, H. Magnussen, P. Scheid and J. Piper, J. Appl. Physiol. 40 362-371 (1976)
8. T. Kawashiro, R. S. Sikand, F. Adaro, H. Takahashi and J. Piper, Resp. Physiol. 28 261-275 (1976)
9. T. Sasaki and L. E. Farhi, In Circulatory and Respiratory Mass Transport (1969)
10. M. Paiva, J. Appl. Physiol. 35 401-410 (1973)
11. P. W. Scherer and A. I. Pack, J. Bioengineering 1 347-356 (1977)
12. H. K. Chang and L. E. Farhi, Resp. Physiol. 18 370-385 (1973)
13. D. A. Scrimshire, P. J. Tomlin and R. A. Etheridge, J. Appl. Physiol. 34 687-696 (1973)
14. D. A. Scrimshire and P. J. Tomlin, J. Appl. Physiol. 34 775-789 (1973)
15. A. W. Bush, M. A. Pinney and J. R. Wallis, In proceedings of the International Conference on applied Numerical Modelling (University of Southampton) 309-318 (1977)